University of Strathclyde Glasgow

Effects of modulating pontine astrocyte activity on REM sleep *in vivo*

Lucy Morton

September 2024

A thesis submitted to the University of Strathclyde in accordance with the requirements for award of the degree of Doctor of Philosophy

Sakata Lab Group, Strathclyde Institute of Pharmacy and Biomedical Sciences, University of Strathclyde, Glasgow G4 0RE

Declaration of authenticity and author's rights

This thesis is the result of the author's original research. It has been composed by the author and has not been previously submitted for examination which has led to the award of a degree.

The copyright of this thesis belongs to the author under the terms of the United Kingdom Copyright Acts as qualified by University of Strathclyde Regulation 3.50. Due acknowledgement must always be made of the use of any material contained in, or derived from, this thesis.

Signed: 

Date: 19th September 2024

Acknowledgments

Firstly, I would like to thank my supervisor, Dr Shuzo Sakata for giving me this opportunity, and for all of his invaluable support, advice, and expertise throughout my PhD. I would also like to thank our postdocs, Dr Mirna Merkler for her training and expertise in *in vivo* techniques and her continuous support throughout the years, and Dr Yuri Elias Rodrigues for his help and collaborations in fibre photometry techniques. I would also like to thank the rest of the Sakata lab for the support and encouragement throughout the past 3 years, as well as the technical staff in the BPU for all their help in caring for the animals used in this project. Also, to our collaborator Dr Jun Nagai for his advice and for supplying our chemogenetic virus.

I would also like to thank all of my friends and family for their patience and support throughout this project. Especially to my mum and dad who are the two pillars of my support system and have encouraged and supported me my whole life. I owe you both everything. Another special thanks must go to Jonny for being my head cheerleader and greatest motivation, and to Emma for her daily encouragement and words of wisdom.

Abstract

Sleep is an essential process for physical and cognitive health, and plays an important role in cognitive processes such as learning and memory. Impairments to the sleep-wake cycle, including reductions in rapid eye movement (REM) sleep occur alongside cognitive deficits in many neurodegenerative diseases, such as Alzheimer's Disease (AD). However, many aspects of sleep regulation, particularly for REM sleep remain to be fully characterised. Across the sleep-wake cycle, astrocytic intracellular Ca^{2+} levels fluctuate, with distinct changes occurring across different brain regions. Conflicting results have been reported regarding astrocytes in the pons, a region which is known to be involved in regulating REM sleep, with both reduced and relatively high Ca^{2+} signals upon REM sleep induction being reported. Thus, how pontine astrocytes contribute to REM sleep regulation remains unclear. Bridging the gap in this knowledge would benefit our understanding of REM sleep regulation, and provide valuable insight for disorders in which REM sleep is altered.

In this project, we hypothesised that manipulating pontine astrocyte activity would modulate REM sleep regulation. To test this, we virally induced hM3Dq receptor expression in pontine astrocytes, under the control of a $gfaABC_1D$ promotor, and monitored electroencephalography (EEG) and electromyography (EMG) activity to classify sleep states. We found that activating pontine astrocytes causes a significant reduction in the total percent of REM sleep and the number of REM sleep episodes across six hours in a dose-dependent manner (1, 5, and 10 mg/kg clozapine-N-oxide (CNO)) compared to controls. We also show that rebound REM sleep in the hours following this effect did not occur.

We next hypothesised that the reductions in REM sleep caused by chemogenetic manipulations of astrocytes would have a detrimental effect on spatial memory. We found a trend for reduced spatial memory, but not object recognition memory, in chemogenetically modified mice.

Finally, we conducted a pilot study to determine if astrocytic Ca^{2+} levels were increased following CNO administration. We observed some state-dependent changes in

exemplar data but were not able to confirm this trend across animals due to technical limitations.

Overall, our study shows that REM sleep is reduced following chemogenetic activation of pontine astrocytes. We included appropriate negative controls to validate our findings. For the first time, we show that this effect is dose dependent, does not induce rebound REM sleep, and has a tendency to impair spatial memory. Thus, in summary, our results suggest a causal role of pontine astrocytes in REM sleep induction, which is an important finding for our understanding of REM sleep regulation.

Table of Contents

List of figures and tables

Abbreviations

AAV – adeno-associated virus

AD – Alzheimer's disease

Aldh1L1 – aldehyde dehydrogenase 1 family member L1

AP – anterior/posterior

AQP4 – water channel aquaporin-4

ATP – adenosine triphosphate

AW - awake

Aβ – amyloid beta

BBB – blood-brain barrier

BF – basal forebrain

CalEx – Calcium extruder

CaM – calmodulin

CeA – central nucleus of the amygdala

CCFv3 – Common Coordinate Framework version 3

CFP – cyan fluorescent protein

ChR2 – channelrhodopsin2

CNO – clozapine-N-oxide

CNS – central nervous system

CRH – corticotropin-releasing hormone

CSF – cerebrospinal fluid

DCZ - deschloroclozapine

DMH – dorsomedial hypothalamus

dmM – dorsomedial medulla

DMSO – dimethyl sulfoxide

DpMe – dorsal mesencephalic nucleus

DREADDs – designer receptors exclusively activated by designer drugs

DRN – dorsal raphe nucleus

DV – dorsal/ventral

EAAT2 - excitatory amino-acid transporter type-2

ECM – extracellular matrix

EEG – electroencephalography

EMG – electromyography

ER – endoplasmic reticulum

eVLPO – extended part of the ventrolateral preoptic nucleus

fMRI BOLD – functional magnetic resonance imaging blood-oxygen-level-dependent

GABA – γ-aminobutric acid

GAD2 – glutamic acid decarboxylase 2

GAT3 – GABA transporter type 3

GATs – GABA transporters

GFAP – glial fibrillary acidic protein

GFP – green fluorescent protein

GiA – alpha paragigantocellular nucleus

GiV – ventral paragigantocellular nucleus

GLAST – glutamate aspartate transporter

GLT-1 – glutamate transporter type 1

GPCR – G-protein coupled receptor

GPe – external globus pallidus

GRAB – G-protein-coupled receptor activation-based

hPMCA2w/b – human plasma membrane Ca^{2+} ATPase isoform 2 splice variant w/b

IP_3 – inositol-1,4,5-trisphosphate

ISF – interstitial fluid

LC – locus coeruleus

LDT – laterodorsal tegmental nucleus

LED – light-emitting diode

LFP – local field potential

LGN – lateral geniculate nucleus

LH – lateral hypothalamus

Lhx6 – LIM homeodomain factor 6

LPGi – lateral paragigantocellular nucleus

LTP – long-term potentiation

MCH - melanin-concentrating hormone

mGluR – metabotropic glutamate receptor

ML – medial/lateral

MnPO – median preoptic nucleus

mPFC – medial prefrontal cortex

MS – medial septum

MS-DBB – medial septum-diagonal band of Broca

NAc – nucleus accumbens

NGS – normal goat serum

NI – national instruments

NMDA - N-methyl D-aspartate

NOLT – novel object location test

NORT – novel object recognition test

NP – nucleus papilio

NREM – non-rapid eye movement

NSAID – non-steroidal anti-inflammatory drug

OH – orexin/hypocretin

OPCs – oligodendrocyte precursor cells

OT – olfactory tubercle

PAG – periaqueductal grey

PBS – phosphate-buffered saline

PBST – Triton X in PBS

PC – precoeruleus area

periLCα – peri-locus coerulus alpha

PFA – paraformaldehyde

PGO – pontine-geniculo-occipital

PKA – protein kinase A

PLC – phospholipase C

POA – preoptic area

PPT – pedunculopontine tegmentum

PSD – power spectral density

PV – parvalbumin-positive

PZ – parafacial zone

REM – rapid eye movement

RMg – raphe magnus

RNA – ribonucleic acid

RPA – raphe pallidus

RSC – retrosplenial cortex

SCN – suprachiasmatic nucleus

SLD – sublateral dorsal nucleus

SNr – substantia nigra pars reticulata

SWR – sharp-wave ripple

SWS – slow-wave sleep

TMN – tuberomammillary nucleus

TNAP – tissue-nonspecific alkaline phosphatase

TRAP

TRN – thalamic reticular nucleus

vlPAG – ventrolateral periaqueductal grey

VLPO – ventrolateral preoptic nucleus

VP – ventral pallidum

VTA – ventrak regmental area

WT – wild-type

YFP – yellow fluorescent protein

ZI – zona incerta

ZT – zeitgeber

1. Introduction

1.1. Overview

In this chapter, I will introduce existing literature surrounding the key themes in this project, most importantly, the involvement of astrocytes in rapid eye movement (REM) sleep (section 1.3.4.3). Bettering our understanding of how astrocytes contribute to REM sleep regulation is important for sleep research, and may lead to advancements in treating disorders in which REM sleep is impaired, including neurodegenerative disorders, such as Alzheimer's disease (AD). To introduce the background for this study, initially, I will discuss the importance of sleep, and introduce each sleep state, describe the regulatory circuits and oscillatory components involved in sleep state, and the key functions of sleep (section 1.2). I will also discuss the role of the pons during sleep (1.2.2.5.1), specifically for induction and maintenance of rapid eye movement (REM) sleep, with a focus on the sublateral dorsal (SLD) nucleus, which is an important REM sleep-regulatory brain region. In the following section I will discuss the importance of sleep for various cognitive functions, with a focus on how REM sleep contributes to learning and memory, and how this can be altered in neurodegenerative disorders (section 1.2.3.3). Subsections describing sleep regulatory circuits are based on studies in rodents, unless stated otherwise. I will then discuss the structure and function of astrocytes in the brain (section 1.3) and outline important data implicating a role of astrocytes in the sleep-wake cycle, which this project aims to investigate further. Briefly, I will also talk about what tools are available for studying astrocytes, and the challenges these methods face, with a focus of the advantages and disadvantages of the methodology used in this project. Finally, I will outline the hypothesis and aims for this project (section 1.4).

1.2. Sleep

1.2.1. The importance of sleep

Sleep involves a shift in consciousness, changes in brain and bodily states and activities, and is universally important amongst higher vertebrate species, and quite possibly amongst all living animals (Anafi *et al.*, 2019; Bear *et al.*, 2020; Leung *et al.*, 2019). Sleep can generally be defined as "a readily reversible state of reduced

responsiveness to, and interaction with, the environment", and is essential for both physical and mental health. As humans, we spent around a third of our lives asleep, and just one night of sleep deprivation can alter brain activity and have detrimental effects on mood, memory, and attention (Venkatraman *et al.*, 2007; Krause *et al.*, 2017; Lewis, 2021). During sleep deprivation, sleep pressure increases accordingly, dissipating only with rebound sleep. This process is regulated by sleep homeostasis, and is influenced by several factors including genetics, cerebrospinal fluid (CSF) flow, and glial cells (Tobler and Borbely, 1986; Mander *et al.*, 2010; Tononi and Cirelli, 2003; Tononi and Cirelli, 2014; Vyazovskiy *et al.*, 2009; Huber *et al.*, 2004; Dopp *et al.*, 2024). The existence of sleep homeostasis regulation further emphasises how critical sleep is for our health. While we know that sleep is important, many aspects of sleep, including the complex mechanisms of regulation, remain incompletely understood. Developing this understanding will be important to improving general public health, cognitive performance, and potentially alleviate disorders in which sleep is affected.

1.2.2. The sleep-wake cycle

The sleep-wake cycle involves two distinct sleep states: non-rapid eye movement (NREM) sleep, and REM sleep. In mammals, birds, and reptiles, sleep states can be defined using electrophysiological changes in the frequency and amplitude of brain activity, which can be detected by electroencephalography (EEG), or local field potential (LFP) recordings (Grandner and Fernandez, 2021; Shein-Idelson *et al.*, 2016). Such sleep-related brain oscillations occur as a result of synchronised activity from large neural ensembles (Caton, 1875; Adamantidis *et al.*, 2019; Gent *et al.*, 2018). The oscillatory amplitude reflects the level of synchronisation of neural activity, and is heavily influenced by intrinsic cellular properties, feedback loops, synaptic inputs and interactions, as well as spontaneous activity such as background neural activity (Buzsaki *et al.*, 2012). In sleep research, changes in EEG or LFP are typically measured simultaneously to electromyography (EMG) which detects changes in muscle tone by measuring the electrical activity of musculature. Together, EEG/LFP and EMG are the "gold standard" method used to differentiate between the various sleep states across species.

In humans, NREM sleep can be further separated into several subcategories according to changes in oscillatory activity, representative of the depth of sleep (Franks and Wisden, 2021; Karna and Gupta, 2022; Girardeau and Lopes-Dos-Santos, 2021; Adamantidis *et al.*, 2019). Originally, NREM sleep was classified into 4 substages, according to the Rechtschaffen and Kales sleep scoring system (Rechtschaffen and Kales, 1968; Adamantidis *et al.*, 2019; Walker and Stickgold, 2004), but has since been updated in 2007 by the American Academy of Sleep Medicine guidelines, which combines stages 3-4 together to form NREM3, also known as slow-wave sleep (SWS) (**Fig. 1.1,** red circled) (Iber *et al.*, 2007b; Adamantidis *et al.*, 2019; Karna and Gupta, 2022; Blume *et al.*, 2015; Dutt *et al.*, 2023). Distinct brain oscillations can clearly classify the 3 NREM sleep substages, where NREM1 relates to the lightest form of sleep, occurring immediately following the transition from wakefulness to sleep, while NREM3, is the deepest stage of sleep (**Fig. 1.2**) (Franks and Wisden, 2021; Karna and Gupta, 2022; Girardeau and Lopes-Dos-Santos, 2021). Conversely, in rodents NREM is considered as a homogeneous state (**Fig. 1.3b**) (Mitler *et al.*, 1977; Le Bon *et al.*, 2007; Simasko and Mukherjee, 2009; Girardeau and Lopes-Dos-Santos, 2021).

During sleep, humans typically transition through the NREM-REM sleep cycle every 90 minutes (**Fig 1.1**) (Stickgold *et al.*, 2001; Walker and Stickgold, 2004), averaging 1-8 monophasic cycles per night (Le Bon, 2020). Throughout the night, proportions of the sleep states in humans can vary, with NREM3 predominating the initial period of sleep, and NREM2 and REM the latter sleep phases (**Fig. 1.1**) (Rasch and Born, 2013; Walker and Stickgold, 2004; Blume *et al.*, 2015; Karna and Gupta, 2022). In comparison, rodents transition through sleep in a polyphasic manner, with around 25% of NREM sleep periods transitioning into REM sleep (Luo *et al.*, 2013; Fritz *et al.*, 2021; Rayan *et al.*, 2024).

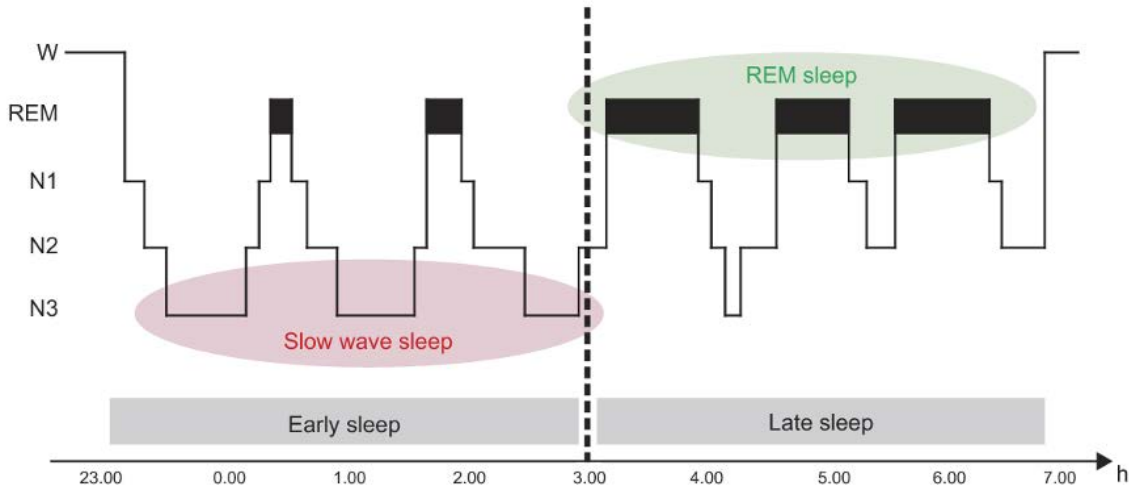

Figure 1.1. An example hypnogram of a healthy human sleep cycle over an 8-hour period of nocturnal sleep. During sleep, humans typically transition through the NREM-REM cycle every 90 minutes. Throughout sleep, the ratio of sleep stages changes. During the first half of sleep, NREM 3 predominates, while during the second half NREM2 and and REM sleep are more abundant.

Image from Rasch and Born 2013

1.2.2.1. NREM sleep

In mammals, NREM sleep is characterised by reduced muscular tone, decreased body temperature, and lowered response to sensory stimuli and the external environment (Adamantidis *et al.*, 2019). As previously described, NREM sleep in humans can be divided into 3 substages, NREM1-3, which can be distinguished based on differences in oscillations. Neural activity during NREM sleep typically consists of slow oscillations, delta waves, sleep spindles, K-complexes, and sharp-wave ripples (**Figs. 1.2-1.3**). Typically, the initial period of transitioning from wakefulness into NREM sleep can be characterised by reduced cortical alpha waves (8-11 Hz), followed by theta waves (4-7.5 Hz) during the later stages of transition into NREM1. In NREM2 intermittent sleep spindles (11-14 Hz), K-complexes, and sharp-wave ripples (SWRs) (150-200 Hz) are detected. In the deepest substage of NREM sleep, NREM3, also known as slow-wave sleep, delta waves (1-4 Hz) and large-amplitude slow-wave oscillations (<1 Hz) occur (**Fig. 1.2**) (Iber *et al.*, 2007a; Tarun *et al.*, 2021; Adamantidis *et al.*, 2019). These oscillations will be described in more detail in following subsections (sections 1.2.2.3.1-1.2.2.3.5).

In rodents, in which only one stage of NREM sleep is described, the onset of NREM sleep is characterised by slow-wave oscillations (0.5-4.5 Hz) and sporadic sleep spindles and K-complexes, comparable to substages 2-3 of NREM sleep in humans.

Despite extensive agreement that NREM sleep is a homogenous state in rodents, it has been suggested that classifying NREM sleep into 3 substages is also possible in mice. For such classifications in mice, like humans, the depth of sleep and slow-wave brain oscillatory activity increases concurrent to substage (Lacroix *et al.*, 2018) (available in pre-print form only).

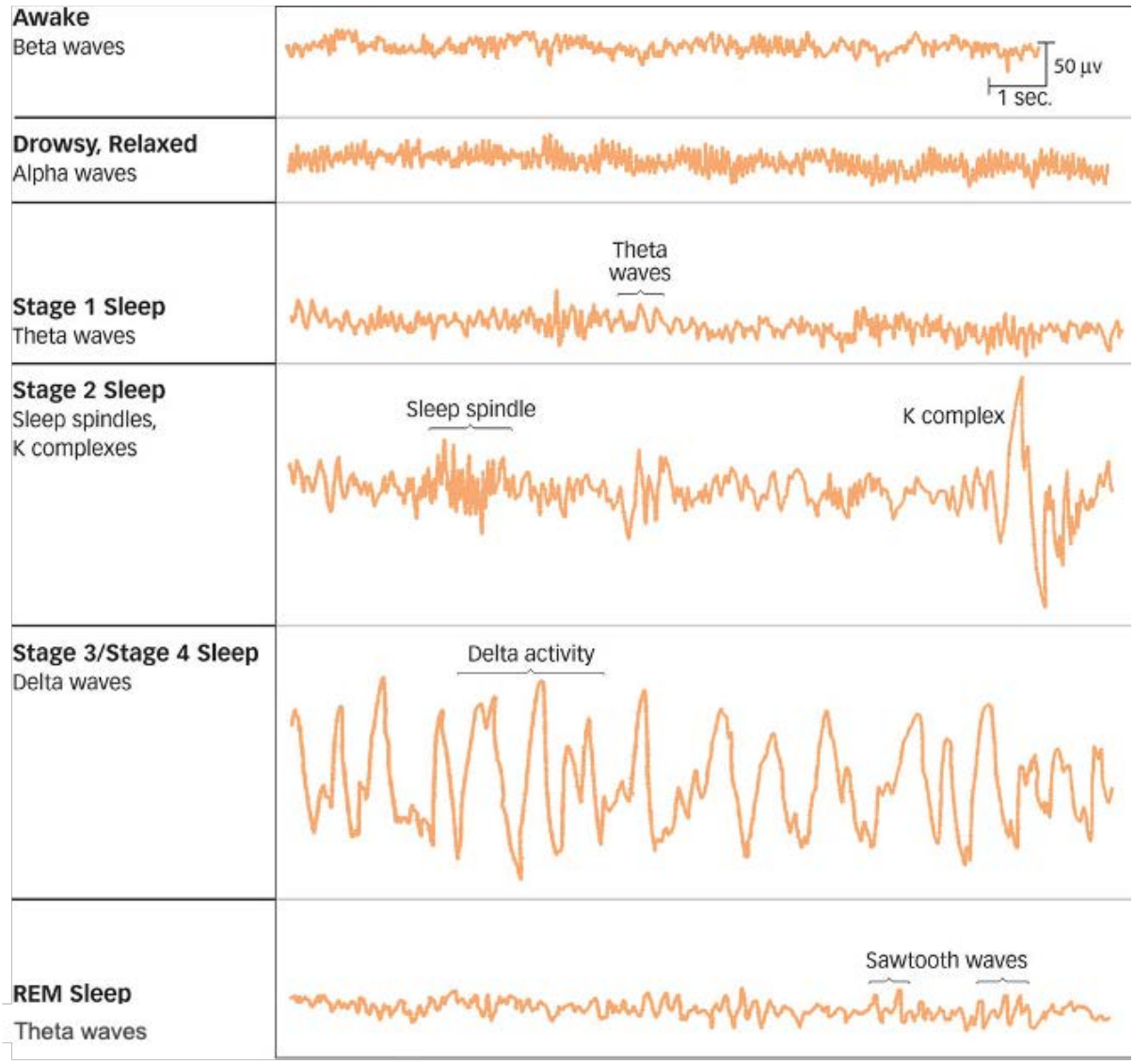

Figure 1.2. Representative images of brain waves during wakefulness, stages 1-3 NREM, and REM in humans captured by electroencephalogram (EEG). Beta waves (15-30 Hz) and alpha waves (8-11 HZ) are typical of wakefulness (alpha relating to quiet wakefulness/relaxed state), stage 1 NREM typically consists of theta waves (4-7 Hz), which coinsides with intermittent sleep spindles (11-15 Hz) and K-complexes in stage 2 NREM. Stage 3 NREM, the deepest form of NREM sleep, also known as slow-wave sleep, consists of delta waves (1-4.5 Hz) and slow-wave oscillations (0.5-2 Hz). REM consists of wake-like desynchronised activity and theta waves.

Image from Dutt et al. 2023.

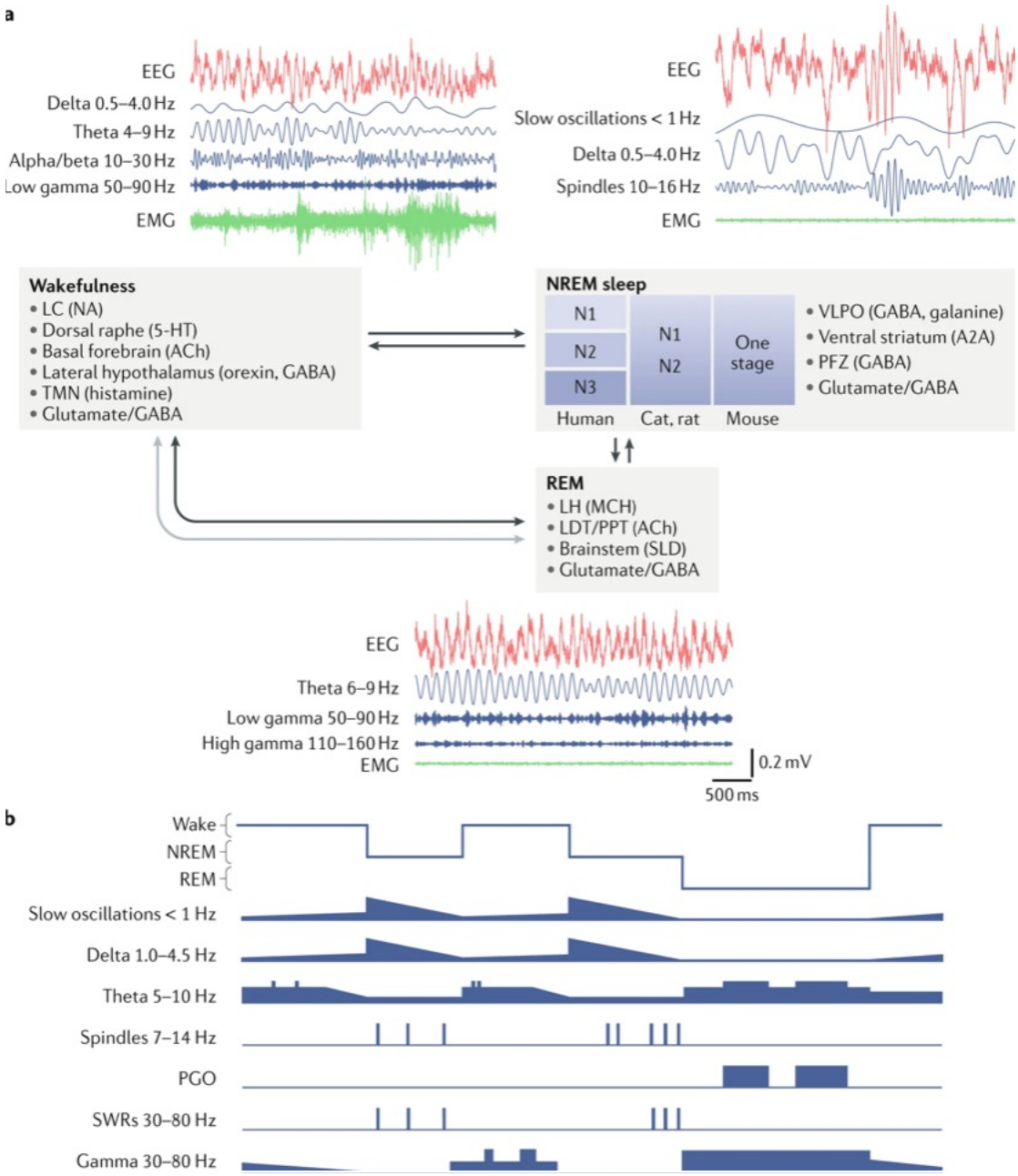

Figure 1.3. Specific sleep-state dependent oscillations and regulatory networks, and a representative hypnogram of a freely moving mouse sleep-wake cycle and state-associated oscillations. a) Summary of the main oscillatory patterns detected by EEG, muscle tone detected by EMG, brain regions, and neuromodulators involved in wakefulness, NREM, and REM sleep states. Black arrows indicate sleep state transitions, the grey arrow represents transition between wakefulness and REM sleep which is rare but can occur in some species. **b)** Representative hypnogram of mouse sleep-wake cycle and associated oscillations with each state.

Brain region abbreviations; LC - locus coeruleus, TMN - tuberomammilary nucleus, VLPO - ventrolateral preoptic area, PFZ - parafacial zone. LH - lateral hypothalamus, LDT - laterodorsal tegmentum, PPT - pedunculopontine tegmentum , SLD - sublaterodorsal nucleus.

Neurotransmitter abreviations; NA noradrenaline, 5-HT 5-hydroxytryptamine (serotonin), ACh acetylecholine, GABA γ-aminobutyric acid, A2A, adenosine A2A receptor, MCH melanin-concentration hormone.

Image from Adamantidis et al., 2019

Several conceptual theories have been proposed surrounding what brings about the transition from wakefulness into NREM sleep, including the “flip-flop” theory which proposes wake-promoting and sleep-promoting neurons inhibit each other to produce stable wake or sleep states (Saper *et al.*, 2001), and the “two-process” model, which proposes sleep is brought about by the interaction between two distinct processes, the circadian rhythm (Process C) and sleep homeostasis (Process S) (Borbely, 1982; Daan *et al.*, 1984; Borbely and Achermann, 1999; Borbely and Achermann, 1992). Process C is an internally generated 24-hour cycle which synchronises with time cues (zeitgebers) and external stimuli, and results in fluctuations in body temperature and levels of melatonin. The central drivers for Process C are circadian pacemaker neurons of the suprachiasmatic nucleus (SCN) (Borbely *et al.*, 2016; Sulaman *et al.*, 2023; Dopp *et al.*, 2024). Process S describes a sleep debt, or pressure, which increases with periods of wakefulness, and only decreases with sleep. Across species, prolonged periods of wake typically results in ”rebound sleep”, which characteristically has increased duration and intensity of sleep periods, and decreased latency to sleep (Borbely, 1982), a phenomena particularly obvious in sleep deprivation studies (Chowdhury *et al.*, 2023; Dispersyn *et al.*, 2017; Dijk and von Schantz, 2005; Krause *et al.*, 2017). While the circuitry drivers for Process S are poorly understood, several substances seem to accumulate with sleep pressure and are thought to induce sleep, such as adenosine and several cytokines and prostaglandins (first proposed by Legendre and Pieron in the early 1900s) (Mathis, 1995; Sulaman *et al.*, 2023). While these remain popular theories of sleep induction, they underestimate the complexity of sleep regulation and overlook several key components (Borbely *et al.*, 2016; Xu *et al.*, 2024), such as the role of glial cells, which seem to be involved in many different sleep components, including Process S and Process C (Dopp *et al.*, 2024). Sleep regulatory circuits and the involvement of glial cells will be expanded in following subsections.

1.2.2.2. NREM sleep regulatory circuits

Many oscillations that occur during NREM sleep arise from feedback loops in the thalamocortical network. A region of sleep-promoting neurons in the ventrolateral preoptic nucleus (VLPO) of the anterior hypothalamus was first identified in the 1990’s (Sherin *et al.*, 1996). Since then, the preoptic area (POA) is still considered to play a

central role in NREM sleep regulation, however, with new focus on the importance of sleep and advances in technology, NREM sleep regulatory circuits are now recognised to have brain-wide connections (**Fig. 1.4**) (Sulaman *et al.*, 2023).

1.2.2.2.1. The hypothalamus

Regarding the hypothalamus, lesion, immunohistochemistry, and electrophysiology studies initially implicated the POA as a central sleep-promoting area (Lu *et al.*, 2000; Sherin *et al.*, 1996; Alam *et al.*, 2014), which has been supported in recent studies using optogenetics and chemogenetics. Optogenetic activation and inhibition of a subpopulation of tuberomammillary nucleus (TMN)-projecting γ-aminobutric acid (GABA)ergic neurons in the POA promoted or suppressed NREM sleep, respectively (**Fig. 1.4**) (Chung *et al.*, 2017). NREM sleep-promoting GABAergic neurons in the medial POA, VLPO, and dorsal lateral POA also present increased activity in response to sleep deprivation, which continues to increase during initial periods of rebound sleep, before recovering to baseline during latter stages of rebound sleep (Alam *et al.*, 2014). Sleep-promoting neurons in the POA are linked to several populations of wake-promoting neurons. Wake-promoting GABAergic and noradrenergic neurons in the lateral hypothalamus (LH) directly inhibit sleep-promoting galaninergic neurons in the VLPO (Venner *et al.*, 2019; Liang *et al.*, 2021). A bidirectional sleep-promoting pathway has been implicated here, however has not been investigated. In addition, the POA also receives projections from NREM sleep-promoting dorsomedial hypothalamic (DMH) GABAergic neurons, and glutamatergic neurons in the ventrolateral periaqueductal grey (vlPAG), of which the latter also send NREM sleep-promoting projections to the medulla (**Fig. 1.4**) (Chen *et al.*, 2018; Zhang *et al.*, 2019).

A GABAergic subpopulation of neurons in the zona incerta (ZI), which express LIM homeodomain factor 6 (Lhx6), have increased activity when sleep pressure increases, and receive inputs from multiple sleep-wake regulating regions such as the vlPAG, LH, ventral tegmental area (VTA), and central nucleus of the amygdala (CeA) (**Fig.1.4**) (Liu *et al.*, 2017). Chemogenetic activation and inhibition of these neurons promotes and suppresses both NREM and REM sleep, respectively, demonstrating a role of these neurons in sleep regulation (Liu *et al.*, 2017).

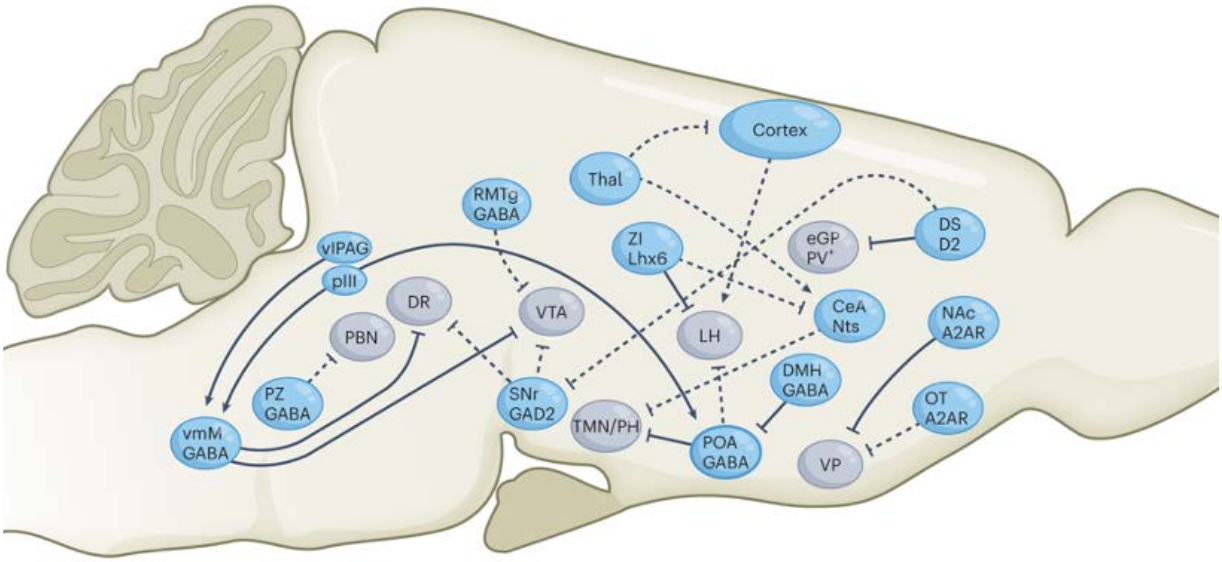

Figure 1.4. NREM sleep regulatory circuits. Neurons in the POA have a central role in NREM regulation. NREM-promoting regions have also been identified in the medulla, midbrain, ZI, amygdala, striatum and cortex. Blue, NREM-promoting neurons. Gray, wake-promoting regions which are inhibited by NREM-promoting neurons. Solid lines represent pathways which have been experimentally tested. Dashed lines represent pathways that have not been fully proven in the context of sleep–wake regulation. CeA, central nucleus of the amygdala; D2, dopamine type-D2 receptor; DMH, dorsomedial hypothalamus; DR, dorsal raphe; DS, dorsal striatum; eGP, external globus pallidus; LH, lateral hypothalamus; NAc, nucleus accumbens; OT, olfactory tubercle; PBN, parabrachial nucleus; pIII, perioculomotor midbrain; PH, posterior hypothalamus; POA, preoptic area; PZ, parafacial zone; RMTg, rostromedial tegmental nucleus; SNr, substantia nigra pars reticulata; TMN, tuberomammillaty nucleus; vlPAG, ventrolateral periaqueductal grey; vmM, ventromedial medulla; VTA, ventral tegmental area; VP, ventral pallidum; ZI, zona incerta.

Image from Sulamen et al., 2023.

1.2.2.2.2. The thalamus

GABAergic neurons in the thalamic reticular nucleus (TRN) receive GABAergic input from the LH (Herrera *et al.*, 2016). Optogenetic activation of this circuit induces arousal during NREM sleep, but not REM sleep, while optogenetic inhibition increased NREM sleep duration and amplitude of delta waves (Herrera *et al.*, 2016). This suggests GABAergic TRN neurons are involved in NREM sleep regulation and intensity. In agreement, optogenetically stimulating cholinergic projections to the TRN promoted NREM sleep, a finding which was reproduced by directly stimulating GABAergic TRN neurons, suggesting these neurons can be driven by cholinergic input to promote NREM sleep (Ni *et al.*, 2016). Optogenetic manipulation of glutamatergic neurotensin-expressing neurons in the posterior thalamus demonstrated that these neurons are also sleep-promoting, and project to sleep-promoting neurotensin-expressing GABAergic neurons in the central amygdala (Ma *et al.*, 2019), implicating this thalamo-amygdala pathway in promoting NREM sleep.

1.2.2.2.3. The cortex and hippocampus

The neocortex along with thalamocortical and hippocampal pathways are essential structures for generating and driving oscillatory components of NREM sleep (Sanchez-Vives and McCormick, 2000; Beltramo *et al.*, 2013; Krone *et al.*, 2021). Intracellular chloride influences inhibitory synaptic transmission via GABA type A receptors. In cortical pyramidal cells, this process reportedly contributes to sleep pressure (Alfonsa *et al.*, 2023). Chemogenetic activation of cortical somatostatin-positive and parvalbumin-positive interneurons increases NREM sleep duration (Funk *et al.*, 2017), suggesting inhibitory interneurons are also involved in NREM sleep regulation. Somatostatin-positive neurons in the pre-frontal cortex project to areas of the hypothalamus, with this pathway demonstrating enhanced activity during sleep and sleep-preparatory behaviour, such as nesting, elevated body temperature, and increased theta power (Tossell *et al.*, 2023). Cortical neurons which are immunoreactive for neuronal nitric oxide synthase and the neurokinin-1 receptor have also been found to be directly related to NREM sleep time, bout duration, and delta power (Morairty *et al.*, 2013). Together, these data implicate the cortex in NREM sleep initiation.

Evidence of hippocampal involvement for NREM sleep regulation is largely due to the generation of transient high frequency SWR oscillations (Buzsaki, 2015; Levenstein *et al.*, 2019). Hippocampal SWRs regulate synaptic depression and long-term potentiation (LTP), and silencing these events impairs learning of new memories (Norimoto *et al.*, 2018; Rasch and Born, 2013; Sadowski *et al.*, 2016). Cortico-hippocampal interplay is thought to drive memory consolidation during NREM sleep as a result of synchronised activity (Siapas and Wilson, 1998; Sirota *et al.*, 2003; Isomura *et al.*, 2006; Peyrache *et al.*, 2009; Girardeau *et al.*, 2009).

1.2.2.2.4. Basal ganglia

Several basal ganglia nuclei have recently been implicated in NREM sleep regulation. In the nucleus accumbens (NAc), neurons expressing excitatory adenosine A_{2A} receptors, which have inhibitory projections to the ventral pallidum (VP) have been implicated in NREM sleep regulation (**Fig. 1.4**) (Oishi *et al.*, 2017). Optogenetic and

chemogenetic activation of these cells induces sleep, increases total NREM sleep duration, and NREM sleep bout duration, while chemogenetic inhibition prevented sleep (Oishi *et al.*, 2017). Similarly, chemogenetic activation of adenosine A_{2A}-expressing D_2 dopaminergic neurons in the rostral and central striatum promoted NREM sleep, while chemogenetic inhibition reduced NREM sleep (Yuan *et al.*, 2017). The same study identified inhibitory projections from adenosine A_{2A}-expressing neurons in the striatum to the external globus pallidus (GPe) parvalbumin-positive neurons to be the source of NREM sleep regulation (**Fig. 1.4**) (Yuan *et al.*, 2017). Likewise, adenosine A_{2A}-expressing neurons in the olfactory tubercle (OT) promotes and suppresses NREM sleep under chemogenetic activation and inhibition, respectively (Li *et al.*, 2020a). These neurons have inhibitory projections to the VP and LH (Li *et al.*, 2020a), which may be involved in OT-dependent regulation of NREM sleep.

A subpopulation of somatostatin-positive GABAergic neurons in the basal forebrain (BF) also promotes NREM sleep, as optogenetic activation of these neurons promotes NREM sleep probability (Xu *et al.*, 2015). These neurons provide potent $GABA_A$-mediated inhibition to other populations of wake-promoting neurons in the BF (Xu *et al.*, 2015). In the medial substantia nigra pars reticulata (SNr), optogenetic activation and inhibition of glutamic acid decarboxylase 2 (GAD2)-expressing GABAergic neurons enhance and suppresses NREM sleep initiation, respectively (Liu *et al.*, 2020). As the basal ganglia is known to be essential for motor control and has numerous connections with wake-promoting and sleep-promoting regions (**Fig. 1.4**), its involvement in NREM sleep regulation seems essential.

1.2.2.2.5. The brainstem

Areas of the brainstem, such as the vlPAG, the pons, and the medulla are also involved in NREM sleep regulatory circuits. This was first reported by transection and lesion studies in the brainstem causing sleep disruption and/or prolonged states of insomnia (Batini *et al.*, 1958; Siegel *et al.*, 1984; Shouse and Siegel, 1992; Petitjean *et al.*, 1975; Lai *et al.*, 1999; Siegel, 2009; Takata *et al.*, 2018), suggesting the essential role of the brainstem in sleep. In the vlPAG, NREM-on glutamatergic neurotensin-expressing neurons promote NREM sleep when activated using optogenetics or chemogenetics,

while wake is promoted when these neurons are inhibited (Zhong *et al.*, 2019; Kashiwagi *et al.*, 2020). This effect seems to be in part due to excitatory projections to GABAergic neurons in the caudal ventromedial medulla, which induces NREM sleep by inhibiting many monoaminergic wake-promoting circuits (**Fig. 1.4**) (Zhong *et al.*, 2019). GABAergic neurons located in the vlPAG, as well as the dorsal part of the deep mesencephalic reticular nuclei are also involved in suppressing REM sleep and promoting NREM sleep, which is facilitated by the projections to the dorsolateral pons (Weber *et al.*, 2018; Li *et al.*, 2018). Chemogenetically activating neurotensin-expressing neurons in an area of the pons called the SLD increases total NREM sleep time (Kashiwagi *et al.*, 2020). This population of neurons in the SLD projects to other neurotensin-expressing neurons in the dorsal deep mesencephalic nucleus, the medial vestibular nucleus, and the previously mentioned vlPAG, which all demonstrated NREM sleep-promoting activity using chemogenetic activation (Kashiwagi *et al.*, 2020). The parafacial zone (PZ) of the medulla contains a population of GABAergic neurons which initiates NREM sleep and slow-wave activity, demonstrated by chemogenetic activation studies (Anaclet *et al.*, 2012; Anaclet *et al.*, 2014; Alam *et al.*, 2018; Li *et al.*, 2018). Optogenetic downstream circuitry mapping then found that these neurons sent inhibitory projections to parabrachial neurons (**Fig. 1.4**), which projected and released glutamate at magnocellular basal forebrain neurons, which innervated cortical neurons (Anaclet *et al.*, 2014), thus, identifying another NREM sleep-promoting circuit.

To summarise, numerous brain regions seem to contribute to the regulation of NREM sleep. In the following subsections, I will discuss how some of these circuits are involved in generating each type of oscillatory activity present in NREM sleep.

1.2.2.3. NREM sleep oscillations

1.2.2.3.1. Slow waves

Slow waves (<1 Hz) and delta waves (1-4.5 Hz) are two oscillatory components observed during deep substages of NREM sleep in humans, and in some forms of anaesthesia (Fellin *et al.*, 2009). Slow waves, which occur in the neocortex during NREM sleep, reflect synchronised activity and changes in the resting membrane potentials of neurons in the thalamocortical circuit, which alternate between UP states,

also known as active, where cells are depolarised causing intense burst firing of action potentials, and DOWN states, also known as inactive, in which the cells are hyperpolarised causing neural spiking quiescence (Steriade *et al.*, 1993b; Steriade *et al.*, 1993c; Steriade *et al.*, 1993d; Steriade and Timofeev, 2003; Bazhenov *et al.*, 2002; Gent *et al.*, 2018; Adamantidis *et al.*, 2019). UP state depolarisation is initiated in layer 5 pyramidal neurons in the neocortex, driven by input from various cortical and thalamic regions, and propagates to more superficial layers of the neocortex (Sheroziya and Timofeev, 2014; Sanchez-Vives and McCormick, 2000; Lorincz *et al.*, 2015; Sakata and Harris, 2009; Gent *et al.*, 2018), while astrocytes and cortical interneurons are involved in inhibiting UP states (Fellin *et al.*, 2009; Zucca *et al.*, 2017). Thus, this fluctuation between UP and DOWN states, with every state lasting tens to hundreds of milliseconds (Funk *et al.*, 2017), and can be observed in rodents (Vyazovskiy *et al.*, 2009; David *et al.*, 2013; Funk *et al.*, 2017; Honjoh *et al.*, 2018), cats (Contreras and Steriade, 1995; Lemieux *et al.*, 2014), non-human primates (Xu *et al.*, 2019), and humans (Csercsa *et al.*, 2010), is what generates slow waves (<1 Hz) that are detectable by EEG or LFP at thalamocortical structures.

Delta waves (1-4.5 Hz) are proposed to originate in thalamic and/or cortical layer 5 neurons. In the thalamus, hyperpolarisation, following a burst of action potentials or inhibitory input, causes activation of hyperpolarisation-activated currents (Lambert *et al.*, 2013), which are slowly activating currents which lead to a gradual depolarisation. This depolarisation causes neural firing, and induces activation of low-threshold calcium channels, which in turn leads to activation of a low-threshold calcium spikes, and a burst of action potentials (Brown *et al.*, 2012; Adamantidis *et al.*, 2019). Network synchronisation is thought to be subsequently generated by rhythmic excitation and hyperpolarisation in thalamocortical and corticothalamic neurons (Steriade *et al.*, 1991; Brown *et al.*, 2012). Delta oscillations observed in cortical layer 5 neurons are also dependent on stimulation by acetylcholine-sensitive potassium conductance (Steriade *et al.*, 1993b; Lorincz *et al.*, 2015; Adamantidis *et al.*, 2019).

1.2.2.3.2. K-complexes

K-complexes can occur spontaneously during NREM2 in humans or as a response to sensory stimuli during NREM sleep in humans, rodents, and cats. However, not every

internal or external stimulus will cause a K-complex and the frequency of K-complexes decreases as the depth of sleep increases, and cannot be elicited during REM sleep (De Gennaro *et al.*, 2017; Halasz, 2005; Adamantidis *et al.*, 2019). K-complexes (<1 Hz) have the highest amplitude of brain oscillations during normal, healthy sleep, and are characterised by a transient surface-positive peak followed by a larger, slower, surface-negative peak, and a final surface-positive peak which together generally lasts ~1 s (**Fig. 1.2**) (Contreras and Steriade, 1995; De Gennaro *et al.*, 2017). Spontaneous and evoked K-complexes can be detected across the cortex, proposed to be generated by outwardly flowing dendritic currents in middle and upper layers of the cortex (Cash *et al.*, 2009; De Gennaro *et al.*, 2017). It has also been proposed that K-complexes manifest from cortically-generated slow oscillations (Amzica and Steriade, 1997), however the exact mechanisms of how and why K-complex are initiated during NREM sleep are not fully understood.

1.2.2.3.3. Sleep spindles

Sleep spindles are transient oscillations (sigma band frequency 9-16 Hz) of varying amplitudes (peak ~100 μV) and durations (~500-2000 ms), which last ~6-15 cycles (**Fig. 1.2**) (Morison and Bassett, 1945). Sleep spindles, which often occur immediately following K-complexes, have been observed during NREM sleep in humans, sheep, cats, and rodents (Steriade *et al.*, 1993b; Steriade *et al.*, 1993a; Contreras *et al.*, 1997; Bandarabadi *et al.*, 2020). Increased rates of sleep spindles occur prior to the onset of REM sleep, but not wakefulness, while optogenetic stimulation of sleep spindles increases NREM to REM sleep transitions, suggesting that sleep spindles are involved in the onset of REM sleep (Bandarabadi *et al.*, 2020).

In humans, sleep spindles can be categorised into fast spindles (~14 Hz), which can be detected in centro-parietal neocortical areas, and slow (~12 Hz) spindles which are detected in frontal neocortical areas (Fernandez and Luthi, 2020; Contreras *et al.*, 1997; Bandarabadi *et al.*, 2020; Warby *et al.*, 2014). Sleep spindles are generated from the thalamic reticular nucleus from transient bursts of action potential firing of thalamic reticular neurons and thalamocortical relay cells (Steriade *et al.*, 1985; Steriade *et al.*, 1987; Contreras *et al.*, 1997; Bandarabadi *et al.*, 2020). Volleys of synaptic inhibitory input, in the frequency range of spindles, from the thalamic reticular

neurons to thalamocortical relay neurons causes a large hyperpolarisation. Subsequently, this hyperpolarisation activates the depolarising I_h current, which is closely followed by activation of an I_T current, a T-type calcium current, which causes rebound burst firing of thalamocortical neurons upon termination of inhibitory postsynaptic potential (Bartho *et al.*, 2014; Halassa *et al.*, 2011). This burst activity, and input from sensory thalamocortical cells, directly excites neurons in layer 4 of the neocortex, resulting in excitatory postsynaptic potentials and the characteristic spindle oscillations (Bonjean *et al.*, 2012; Bandarabadi *et al.*, 2020; Adamantidis *et al.*, 2019). Simultaneous bipolar stereoencephalography recordings of the thalamus and cortex have previously suggested that cortical DOWN states lead to thalamic DOWN states and hyperpolarisation of thalamic neurons, generating spindles which propagate back across the cortex during DOWN-to-UP state transitions, which is also thought to be an important process in memory replay and consolidation (Mak-McCully *et al.*, 2017). Therefore, interactions between the thalamus and the cortex are thought to influence the amplitude and duration of spindles, while spindle termination is thought to result from corticothalamic feedback and upregulation of I_h channels (Bonjean *et al.*, 2011).

1.2.2.3.4. Sharp wave-ripples

SWRs are composed of large-amplitude sharp waves which arise from excitatory activity in the hippocampal CA3 and brings about transient oscillatory ripples (140-200 Hz in rodents, 80-140 Hz in humans and non-human primates), occurring in the CA1 stratum radiatum layer (Buzsaki *et al.*, 1983; Buzsaki, 1986; Csicsvari *et al.*, 2000; Buzsaki, 2015; Norman *et al.*, 2019). SWR complexes are brief (<150 ms) and are predominantly detected in CA1 pyramidal layer but have been observed throughout hippocampal structures including CA1, CA2, CA3, subiculum, presubiculum, parasubiculum, and entorhinal cortex (Buzsaki, 2015; Oliva *et al.*, 2020; Norman *et al.*, 2019; Csicsvari *et al.*, 2000; Fernandez-Ruiz *et al.*, 2019). In reptiles, SWRs have been recorded in the dorsal ventricular ridge, where they have propagated to from the claustrum (Norimoto *et al.*, 2020; Shein-Idelson *et al.*, 2016). Sharp waves are thought to be generated by burst firing of CA3 neurons which depolarise CA1 neurons, whereas ripple generation is proposed to be caused by excitatory and inhibitory circuitry input between CA1 and CA3. Although the exact mechanisms driving ripple initiation are not fully understood, this is thought to involve preliminary pyramidal cell

firing, which drives tonic activity of parvalbumin-positive (PV+) interneurons, subsequently leading to simultaneous $GABA_A$ receptor-mediated inhibition and CA1-CA3 pyramidal cell firing, giving rise to fast ripple oscillations (140-200 Hz) (Csicsvari *et al.*, 2000; Stark *et al.*, 2014; Adamantidis *et al.*, 2019). During episodes of SWRs in the hippocampus, the cortex is selectively activated, with SWRs often following spindles or DOWN-to-UP transitions, whereas diencephalic, midbrain, and brainstem regions are strongly inhibited (Logothetis *et al.*, 2012).

As previously mentioned, hippocampal SWRs are known to be an integral component of memory. A two-stage model was proposed to underlie such hippocampal-memory formation (Buzsaki, 1989). This model proposes that hippocampal theta activity during waking exploratory behaviour leads to the formation of cell assemblies encoding the new information. Subsequently, during SWR events during NREM sleep, the cell assemblies are reactivated, and synaptic connections are strengthened, thus the memory is consolidated (Buzsaki, 1989; Girardeau and Lopes-Dos-Santos, 2021). In agreement, studies have since found through various methods the importance of SWRs and the hippocampus for spatial memory consolidation, with the replay of hippocampal place cell activity co-occurring with SWRs (O'Keefe and Dostrovsky, 1971; O'Keefe, 1976; Morris *et al.*, 1982; Girardeau *et al.*, 2009; Ego-Stengel and Wilson, 2010; van de Ven *et al.*, 2016; Wilson and McNaughton, 1994; Ormond and O'Keefe, 2022). Phase coupling between hippocampal SWRs, thalamo-cortical spindles, and cortical slow wave oscillations, and communication between the areas involved in these oscillations is also thought to promote and enhance such memory consolidation (Geva-Sagiv *et al.*, 2023; Maingret *et al.*, 2016; Latchoumane *et al.*, 2017; Binder *et al.*, 2019; Siapas and Wilson, 1998).

1.2.2.3.5. Infra-slow oscillations

Infra-slow oscillations (<0.1 Hz) have been recorded in human and animal brains during NREM sleep across various regions including visual and auditory cortices, hippocampus, basal ganglia, locus coeruleus (LC), dorsal raphe, and olivary pretectal nucleus, however, is most commonly documented in the thalamus (Lecci *et al.*, 2017; Osorio-Forero *et al.*, 2021; Hughes *et al.*, 2011; Blasiak *et al.*, 2013; Adamantidis *et al.*, 2019). Infra-slow oscillations have previously been used to define the resting state

in the human brain during functional magnetic resonance imaging, blood-oxygen-level-dependent (fMRI BOLD) signal studies, however, the importance, and maintenance of these specific brain oscillations remains unclear (Hughes *et al.*, 2011; Blasiak *et al.*, 2013). Astrocytes are thought to be involved in the generation of infra-slow oscillations due to the proposed role of adenosine A1 receptors, and positively coupled G-protein-coupled inwardly rectifying K^+ channels, causing characteristic prolonged periods of hyperpolarisation of thalamocortical neurons (Blasiak *et al.*, 2013).

1.2.2.4. REM sleep

Initially, REM sleep was considered as an intermittent behavioural state between sleep and wake, however, is now recognised as a complex and fundamental sleep state (Sulaman *et al.*, 2023). REM sleep is characterised by several biological features, including tonic features such as pupil constriction, fast low-amplitude theta oscillations, muscle atonia, and increased brain temperature, and phasic features, which include rapid eye movements and muscle twitches, irregular respiration and heart rate, and oscillatory activity called pontine-geniculo-occipital (PGO) waves in humans and cats, P-waves in rodents (**Fig. 1.2-1.3**) (Aserinsky and Kleitman, 1953; Henley and Morrison, 1974; Herice *et al.*, 2019; Kragel *et al.*, 2020; Jego *et al.*, 2013; Saper *et al.*, 2010).

REM sleep was described firstly in human infants, and then several years later in human adults, where rapid-eye activity during sleep was linked with vivid dreaming (Aserinsky and Kleitman, 1953; Dement and Kleitman, 1957). Subsequently, REM sleep, which was often referred to as paradoxical sleep, due to the 'active-like' fast oscillations, was identified in cats (Dement, 1958). This led to further research of REM sleep which highlighted the pons and other areas of the brainstem as central structures responsible for REM sleep onset and maintenance (Jouvet and Michel, 1959; Jouvet, 1962; Hobson *et al.*, 1975; McCarley and Hobson, 1971). Since then, many regions in the brainstem have been proposed to be important in the generation and control of REM sleep (Boissard *et al.*, 2002; Krenzer *et al.*, 2011; Lu *et al.*, 2006b; Luppi *et al.*, 2013; Weber *et al.*, 2018; Scammell *et al.*, 2017).

While the circuitry governing NREM sleep, as well as the functions of NREM sleep, are relatively well characterised, much less is known about REM sleep. Given the implicated importance of REM sleep in higher executive functions such as learning and memory, and as such the deficit in learning and memory following REM sleep deprivation (Sagales and Domino, 1973; Leconte *et al.*, 1973; Hennevin and Leconte, 1977; Shiromani *et al.*, 1979; Smith *et al.*, 1980; Hars and Hennevin, 1983; Beaulieu and Godbout, 2000; Rasch and Born, 2013), it is important we study and fully understand REM sleep circuitry and oscillatory activity to appreciate the importance of REM sleep in health and its possible implications in disease. In the following subsections, I will discuss our current understanding of these topics, and some recent advances in these areas.

1.2.2.5. REM sleep regulatory circuits

In comparison to NREM sleep, the regulatory circuity governing REM sleep is less extensively studied. In REM sleep, the brainstem has long been implicated as a critical region for initiating and maintaining REM sleep, first identified by Jouvet and colleagues (Jouvet and Michel, 1959; Jouvet, 1962). However, REM sleep is more recently emerging as a brain-wide activity (**Fig. 1.5**) (Hong *et al.*, 2023; Fraigne *et al.*, 2023; Sulaman *et al.*, 2023). REM sleep circuitry involves circuits which initiate and maintain REM sleep features, as well as those which suppress wake- and/or NREM sleep-promoting areas, and those that inhibit 'gatekeepers', where gatekeepers are regions that prevent REM sleep from occurring during wake or NREM sleep. In the following subsections, I will first discuss the role of the brainstem in REM sleep, which is of particular importance for this project, followed by other brain regions implicated in REM sleep circuitry.

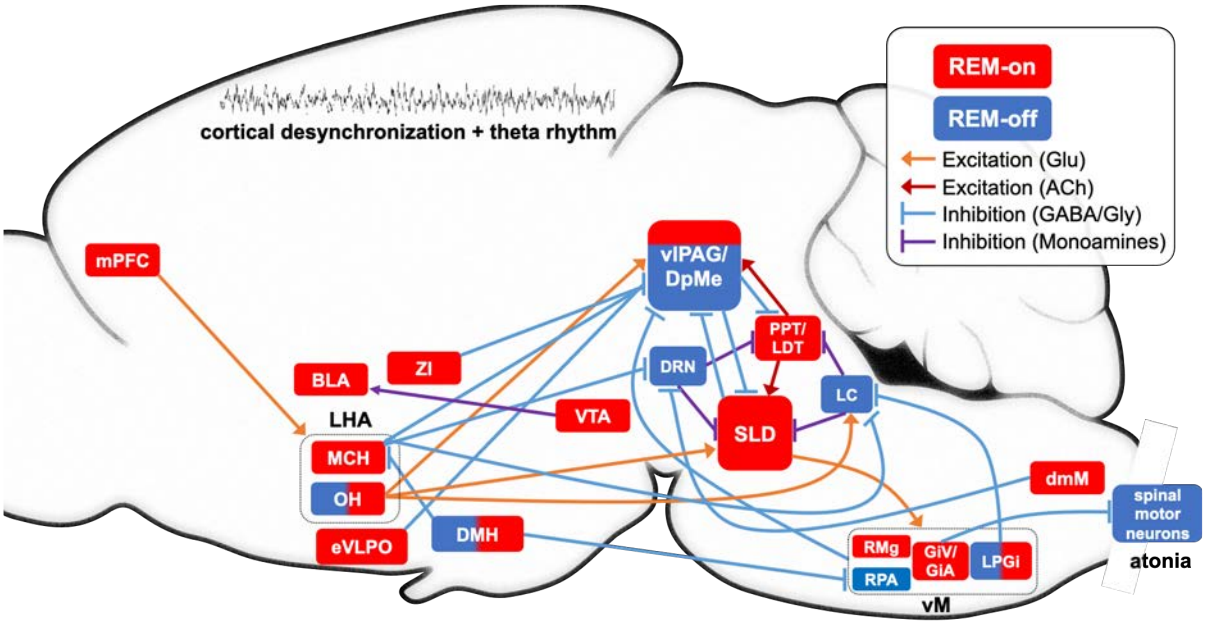

Figure 1.5. REM sleep regulatory circuits. The brainstem and hypothalamus contain key stuctures for regulating REM sleep. The SLD lies central to these pathways. The SLD generates muscle atonia during REM sleep by sending glutamatergic inputs to the vM, which in turn send inhibitory input to spinal motor neurons generating muscle atonia. The SLD recieves excitatory choinergic input from the hypothalamus, PPT and LDT, while cholinergic-producing neurons of the LC and serotonergic-producing neurons of the DRN promote arousal by inhibitory output to the SLD, PPT, and LDT. GABAergic input to these areas is thought to be important in promoting REM sleep. Hypothalamtic areas vlPAG and DpMe are thought to contain both REM-off and REM-on type neurons recieving both excitatory and inhibitory inputs from various brain structures such as the mPFC, vM, PPT, LDT, SLD, eVLPO, and OH.

BLA - basolateral amygdalar nucleus, DMH - dorsomedial hypothalamus, dmM - dorsal medial medulla, DpMe - dorsal part of the deep mesencephalic reticular nuclei, DRN - dorsal raphe nucleus, eVLPO - extended area of the ventrolateral preoptic area, GiA - alpha gigantocellular nucleus, GiV - ventral gigantocellular nucleus, LC - locus coeruleus, LDT - laterodorsal tegmental nucleus, LHA - lateral hypothalamus, LPGi - lateral paragigantocellular nucleus, MCH - melanin concentrating hormone neurons, mPFC - medial prefrontal cortex, OH - orexin/hypocretin neurons, PPT - pedunculopontine tegmental nucleus, RMg - raphe magnus, RPA - nucleus raphe pallidus, SLD - sublaterodorsal nucleus, vlPAG - ventrolateral periaqueductal grey, VTA - ventral tegmental area, ZI - zona incerta.

Glu - glutamate, ACh - acetylcholine, GABA - γ-aminobutyric acid, Gly - glycine

Modified from Héricé et al., 2019

1.2.2.5.1. The brainstem

Since transectional studies in cats by Jouvet, the pons has been known to be a key structure for REM sleep (Jouvet, 1965; Vanni-Mercier *et al.*, 1991). He identified an area of the dorsal pons, named the peri-locus coeruleus alpha (periLCα), as being critical in generating muscle atonia characteristic of REM sleep, as lesions to this area resulted in cats “acting out their dreams” during REM sleep, reflecting REM sleep behaviour disorder. It has since been reported in rodents that muscle atonia is controlled by glutamatergic inputs from the SLD, the equivalent of the cat periLCα, which project to GABAergic and glycinergic neurons of the ventromedial medulla

(Swanson, 1998; Luppi *et al.*, 2006; Luppi *et al.*, 2012; Scammell *et al.*, 2017; Luppi *et al.*, 2017). The ventromedial medulla is located in the ventrocaudal area of the brainstem, and collectively refers to areas such as the raphe magnus (RMg), lateral paragigantocellular nucleus (LPGi), and the ventral and alpha gigantocellular nuclei (GiV and GiA). Upon receiving glutamatergic input from the SLD, the ventromedial medulla then sends inhibitory signals to motor spinal neurons, resulting in muscle atonia (**Fig 1.5**) (Lu *et al.*, 2006b; Herice *et al.*, 2019). Silencing neurons in this pathway results in the generation of REM sleep-like states without atonia, closely mimicking symptoms of REM sleep behaviour disorder, and reduces total REM sleep time (Uchida *et al.*, 2021; Valencia Garcia *et al.*, 2018; Krenzer *et al.*, 2011). Retrograde tracing experiments also suggest that glutamatergic SLD neurons send direct input to interneurons located in the ventral horn of the spinal cord (Lu *et al.*, 2006b; Krenzer *et al.*, 2011), contributing to the generation of muscle atonia during REM sleep. Inhibitory projections from the LPGi to cardiac vagal neurons have also been implicated in reduced parasympathetic cardiac activity and elevated heart rate characteristic of REM sleep (Dergacheva *et al.*, 2010).

The medulla contains neurons which increase activity during REM sleep, and optogenetically stimulating GABAergic neurons in the ventral or dorsomedial medulla (dmM) induces and increases REM sleep, which is thought to be mediated by projections to the dorsal raphe nucleus (DRN) (Weber *et al.*, 2015; Stucynski *et al.*, 2022). Corticotropin-releasing hormone (CRH)-expressing excitatory neurons in the dmM are also active during REM sleep, with chemogenetic and optogenetic activation and inhibition of these neurons promoting and suppressing REM sleep, respectively (Schott *et al.*, 2023). In the medulla, certain structures have also been heavily implicated in controlling rapid eye movements during REM sleep. The dorsal medulla nucleus papilio (NP) contain a cluster of calbindin-D28K-expressing glutamatergic neurons which are highly active during REM sleep, and project to the contralateral nuclei of external eye muscles, including the oculomotor, trochlearis, and the abducens (Gutierrez Herrera *et al.*, 2019). Optogenetic activation of these neurons led to triggered eye movement during REM sleep while optogenetic inhibition suppressed eye movements without affecting REM sleep bout duration (Gutierrez Herrera *et al.*, 2019). These data suggest the medulla is involved in REM sleep induction as well as controlling eye movement during REM sleep.

The SLD lies ventral to the periaqueductal grey (PAG) and caudal laterodorsal tegmental nucleus (LDT)/pedunculopontine tegmentum (PPT), and anterior to the LC, and is made up of glutamatergic, cholinergic, and GABAergic neurons (Scammell *et al.*, 2017; Herice *et al.*, 2019). Glutamatergic neurons in the dorsal pons, likely to be the SLD, display highest activity during REM sleep and increase activity prior to REM sleep transitions (Cox *et al.*, 2016). Damage to the SLD or connections to or from the SLD results in REM sleep-like states without atonia (Lu *et al.*, 2006b), while pharmacological activation, or disinhibition, of the SLD increases REM sleep duration, and pharmacological inhibition of the SLD promotes wakefulness (Boissard *et al.*, 2002). This suggests that the SLD has a key role in generating and maintaining REM sleep, which is further implied by the numerous projections and innervations with REM-on and REM-off structures.

The SLD receives inhibitory projections from the vlPAG, a connection which is essential for REM sleep control (**Fig. 1.5**) (Krenzer *et al.*, 2011; Feng *et al.*, 2020). The vlPAG, as well as the deep dorsal mesencephalic nucleus (DpMe), act as gatekeepers of REM sleep, are maximally active during wake, and mostly inactive during REM sleep, with a subpopulation showing high activity during REM sleep (Lu *et al.*, 2006b; Weber *et al.*, 2018). These structures send GABAergic projections to many REM-on structures such as the SLD, LDT/PPT, LC, and DRN, and in turn receive various input from the SLD, LDT/PPT, LH, ZI, CeA, NAc, the median preoptic nucleus (MnPO), the extended part of the ventrolateral preoptic nucleus (eVLPO),and medulla (**Fig. 1.5**) (Lu *et al.*, 2006b; Clement *et al.*, 2012; Weber *et al.*, 2018; Herice *et al.*, 2019). Optogenetic and chemogenetic activation of the vlPAG/DpMe suppresses REM sleep, and reducing inhibitory input from melanin-concentrating hormone (MCH)-expressing LH neurons in the vlPAG using optogenetics reduces total REM sleep and number of REM sleep episodes (Hayashi *et al.*, 2015; Kroeger *et al.*, 2019). Inactivating the vlPAG/DpMe using chemogenetics, lesions, or pharmacology increases REM sleep (Hayashi *et al.*, 2015; Sapin *et al.*, 2009; Lu *et al.*, 2006b). Similarly, optogenetically activating GABAergic input from the ventral medulla in the vlPAG also promotes REM sleep (Weber *et al.*, 2015), implicating these structures as important REM-off areas. Dopaminergic wake-promoting neurons of the vlPAG project to the midline and intralaminar thalamus, and cholinergic basal forebrain neurons, and

have bidirectional connections with many sleep-wake regulatory structures such as LH orexin/hypocretin (OH) neurons, the VLPO, medial prefrontal cortex, cholinergic LDT/PPT neurons and noradrenergic LC neurons (Lu *et al.*, 2006a). However, despite clear REM sleep suppressing activity, it has been suggested that the vlPAG and DpMe exert both REM-on and REM-off activity, reflecting the complex nature of excitatory and inhibitory pathways involving these areas.

The SLD also receives cholinergic input from the LDT and PPT, which is thought to influence the promotion of transitions into REM sleep, as activity of these neurons is at its highest during and immediately before this state, and optogenetic activation of cholinergic neurons in the PPT and LDT increases REM sleep initiations (Scammell *et al.*, 2017; Van Dort *et al.*, 2015). The PPT/LDT receive inputs from many areas of the brain such as the cortex, thalamus, pons, basal ganglia, hypothalamus, and other areas of the brainstem such as the DRN and LC (**Fig 1.5**) (Semba and Fibiger, 1992; Martinez-Gonzalez *et al.*, 2011; Jones and Yang, 1985; Vertes, 1991). However, the exact role of the PPT and LDT on initiating and maintaining REM sleep is unknown, as studies have found various contradictory results. On the one hand, application of cholinergic agonists into the PPT/LDT, electrical, and optogenetic stimulation of the PPT/LDT has shown increased REM sleep onset and/or duration (Huitron-Resendiz *et al.*, 2005; George *et al.*, 1964; Thakkar *et al.*, 1996; Van Dort *et al.*, 2015). On the other hand, chemogenetic activation of cholinergic PPT/LDT neurons has shown increased light NREM sleep and no alteration of REM sleep (Kroeger *et al.*, 2017).

Noradrenergic neurons of the LC, and serotonergic neurons of the DRN are REM sleep suppressing areas of the brainstem which also receive inputs and project to many areas of the brain including the medulla, SLD and PPT/LDT (**Fig. 1.5**) (Ennis and Aston-Jones, 1989; Sirieix *et al.*, 2012; Luppi *et al.*, 1995; Weber *et al.*, 2018; Jones and Yang, 1985; Schwarz *et al.*, 2015). These neurons are most active during wakefulness, and least active during REM sleep (Gervasoni *et al.*, 2000). Inhibitory inputs to the DRN are thought to be important in the generation of REM sleep (Gervasoni *et al.*, 2000).

1.2.2.5.2. The hypothalamus

Areas in the hypothalamus heavily influence activity of both REM-on and REM-off neurons within the brainstem and other areas (**Fig 1.5**). GABAergic neurons in the LH and ZI increase firing activity immediately prior to REM sleep initiation, while suppression of the LH completely inhibits REM sleep (Blanco-Centurion *et al.*, 2021; Hassani *et al.*, 2010; Clement *et al.*, 2012), suggesting the hypothalamus plays an important role in REM sleep regulation. However, different populations of neurons in these areas seem to exert distinct REM-on and REM-off activities. Hypothalamic OH neurons are generally REM-off and are most active during active wakefulness and quiet during sleep (Lee *et al.*, 2005; Mileykovskiy *et al.*, 2005; Hassani *et al.*, 2009). They innervate and receive input from regions of the brainstem which promote wakefulness such as LC, DRN, and vlPAG (Peyron *et al.*, 1998; Yoshida *et al.*, 2006; Sakurai *et al.*, 2005). Surprisingly, a population of hypothalamic OH neurons innervate and excite the SLD and exhibit synchronised firing activity (**Fig. 1.5**). Optogenetic activation of this connection increases REM sleep bout duration and theta activity, while optogenetic and chemogenetic inhibition achieve opposite effects (Feng *et al.*, 2020). While OH neurons in the hypothalamus are generally known to be REM-off, MCH neurons are REM-on and are most active during REM sleep (Verret *et al.*, 2003; Hassani *et al.*, 2009; Herice *et al.*, 2019). MCH neurons are primarily located in the LH and ZI, and innervate and inhibit wake-promoting areas such as the LH, TMN, LC, and DRN. Optogenetic and chemogenetic activation of these neurons promotes transitions into REM sleep and bout duration (Verret *et al.*, 2003; Kroeger *et al.*, 2019; Jego *et al.*, 2013; Tsunematsu *et al.*, 2014; Varin *et al.*, 2018; Vetrivelan *et al.*, 2016). Hypothalamic MCH neurons send inhibitory projections to the vlPAG and LC, with optogenetic inhibition of MCH terminals in these regions causing reduced transitions into REM sleep (Kroeger *et al.*, 2019). Galanin-expressing GABAergic neurons in the DMH can be separated into two distinct subpopulations, which promote or inhibit REM sleep by projecting to the raphe pallidus (RPA), or POA, respectively (Chen *et al.*, 2018). Galanin-expressing neurons in the eVLPO have also been implicated in REM sleep regulation (Lu *et al.*, 2000; Lu *et al.*, 2002). Interestingly, these areas in the hypothalamus are involved in thermoregulation, with studies suggesting these circuits may be involved in the elevated brain temperature associated with REM sleep (Kawamura and Sawyer, 1965; Chen *et al.*, 2018).

1.2.2.5.3. The cortex and hippocampus

Traditionally, it was thought that the brainstem and hypothalamus were the two primary structures responsible for REM sleep generation, with these structures activating areas of the forebrain and cortex and resulting in characteristic "wake-like" EEG during REM sleep (Nofzinger *et al.*, 1997; Renouard *et al.*, 2015; Peever and Fuller, 2017). More recently, research has implied a direct role for the cortex in REM sleep generation and maintenance. Pyramidal cells in the medial prefrontal cortex (mPFC) display high activity during REM sleep compared to wake and NREM sleep, with gradual increases occurring prior to transitioning into REM sleep, and high activity persisting throughout REM sleep bouts (Hong *et al.*, 2023). Optogenetic activation of mPFC pyramidal cells increases total REM sleep, and probability of REM sleep transitions, while optogenetically activating GABAergic neurons in the same area reduces REM sleep episode duration and frequency, and maintains NREM sleep (Hong *et al.*, 2023). Similarly, chemogenetically and optogenetically stimulating somatostatin-expressing GABAergic neurons in the PFC induced sleep nesting behaviour and sleep (Tossell *et al.*, 2023). These effects were thought to be mediated by projections from the mPFC to the LH (**Fig. 1.5**) (Hong *et al.*, 2023; Tossell *et al.*, 2023). During REM sleep, the occipital cortex also displays high activity while low activity occurs in the somatic sensorimotor cortex, a pattern which begins to gradually appear during NREM to REM sleep transitions (Wang *et al.*, 2022). Optogenetically exciting GABAergic neurons in the occipital cortex, to suppress activity, reduces the probability of REM sleep and increases NREM sleep, while exciting all neurons in a small area of the occipital cortex, the retrosplenial cortex (RSC), increases REM sleep and reduces NREM sleep (Wang *et al.*, 2022). In agreement, two-photon imaging shows pyramidal cells in layer 2/3 of the RSC are activated during REM sleep, and optogenetic inhibition of such neurons reduced REM sleep (Dong *et al.*, 2022). The RSC also displays enhanced spiking activity which is synchronised with hippocampal theta during REM sleep (Koike *et al.*, 2017), which may contribute to REM sleep-dependent memory consolidation. Activity in the RSC precedes activity in other areas of the cortex during REM sleep and initiates cortical Ca^{2+} waves in the primary visual cortex, and anterior cingulate cortex (Dong *et al.*, 2022). Such changes in excitatory/inhibitory balance within microcircuits of the PFC occurs specifically during REM sleep and is thought to cause a somatodendritic decoupling to pyramidal

neurons. This decoupling leads to increased excitability of pyramidal cells, which is thought to be involved in fear-motivated memory consolidation (Aime *et al.*, 2022).

The hippocampus is responsible for theta generation, the primary oscillatory component of REM sleep. Hippocampal generation of theta oscillations will be discussed in further detail in the following section. However, in addition, the hippocampus has been implicated in REM sleep-dependent memory formation. Disrupting GABAergic signalling in the medial septum during REM sleep impairs spatial and fear-conditioned contextual memory (Boyce *et al.*, 2016), supporting this theory. Within the limbic system and adjacent to the hippocampus, in the basolateral amygdala an increase in dopamine occurs in NREM sleep prior to transitions into REM sleep (Hasegawa *et al.*, 2022). Dopaminergic neurons in the VTA send projections to dopaminergic neurons in the amygdala, and also demonstrate increased activity during REM sleep (Dahan *et al.*, 2007), suggesting a role for these connections in REM sleep generation.

1.2.2.6. REM sleep oscillations

1.2.2.6.1. Theta oscillations

Theta oscillations (~7 Hz) are a principle component of REM sleep, but also occur during locomotor activity and other wakefulness-related states in humans and other mammals, including rabbits, cats, monkeys, bats, and rodents (Colgin, 2016; Cantero *et al.*, 2003). They can be measured throughout hippocampal structures as well as the subicular complex, entorhinal cortex, perirhinal cortex, cingulate cortex, and amygdala (Mitchell and Ranck, 1980; Alonso and Garcia-Austt, 1987; Leung and Borst, 1987; Buzsaki, 2002), but occur most frequently and at the highest amplitude in the hippocampal CA1 and CA3 (Bullock *et al.*, 1990; Buzsaki, 2002; Montgomery *et al.*, 2008). Theta activity occurs in a phasic nature during REM sleep in humans and monkeys, while is observed in a tonic manner in rodents, suggesting there may be differences in the neuronal circuitry involved in the generation of theta oscillations between species (Cantero *et al.*, 2003).

Theta oscillations are generated by GABAergic projections from PV+ neurons from the medial septum-diagonal band of Broca (MS-DBB), which target the dentate gyrus,

CA1 and CA3 (Winson, 1978; Petersen and Buzsaki, 2020; Roland *et al.*, 2014). As such, optogenetically silencing MS GABAergic neurons, which innervate the hippocampus, reduces theta power (Boyce *et al.*, 2016). GABAergic MS neurons rhythmically fire phase-locked to hippocampal theta, and post-synaptically inhibit hippocampal interneurons, ultimately causing a rhythmic disinhibition of hippocampal pyramidal cells. MS interneurons express hyperpolarisation-activated cyclic nucleotide-gated non-selective cation channels, which promotes such rhythmic intrinsic properties (Petersen and Buzsaki, 2020; Huh *et al.*, 2010; Buzsaki, 2002; Colgin, 2016).

Cholinergic and glutamatergic neurons of the MS are also thought to be involved in promoting hippocampal theta rhythms, as chemogenetically activating glutamatergic and cholinergic neurons in the BF increases theta power (Anaclet *et al.*, 2015). Cholinergic MS neurons may influence theta activity by providing excitatory input to the hippocampus, and by suppressing other oscillatory patterns, such as SWRs (Montgomery *et al.*, 2008; Vandecasteele *et al.*, 2014; Colgin, 2016; Zhang *et al.*, 2021b). Administering acetylcholine antagonists disrupts theta rhythm generation, and interestingly, perturbs memory, while agonists induce theta oscillations (Gedankien *et al.*, 2023; Teitelbaum *et al.*, 1975; Huerta and Lisman, 1993; Konopacki *et al.*, 1987; Asaka *et al.*, 2000), implicating cholinergic neurons in theta oscillation generation, and theta-dependent memory formation. MS-DBB glutamatergic neurons, which primarily project locally to GABAergic and cholinergic neurons in septal regions, as well as distally to interneurons and pyramidal cells in the hippocampus, fire at theta rhythms seemingly spontaneously, and influence the firing theta power and rhythmicity of hippocampal neurons (Huh *et al.*, 2010; Robinson *et al.*, 2016). Further input from the brainstem, entorhinal cortex, and hypothalamus may also influence theta oscillations during REM sleep (Zutshi *et al.*, 2022; Buzsaki, 2002; Adamantidis *et al.*, 2019). In particular, in the brainstem, lesions to the precoeruleus area (PC) have been reported to abolish theta rhythms during REM sleep (Lu *et al.*, 2006b).

1.2.2.6.2. P-waves

Pontine waves (P-waves), also known as PGO waves, are large amplitude (>300 μV), phasic oscillations which occur for ~100 ms, and are observed in humans, non-human

primates, cats, and rodents (Aserinsky and Kleitman, 1953; Callaway *et al.*, 1987; Jouvet and Michel, 1959; Jouvet, 1962; Brooks and Bizzi, 1963; Datta, 1997; Datta, 2000; Karashima *et al.*, 2002; Tsunematsu *et al.*, 2020; Fernandez-Mendoza *et al.*, 2009). P-waves were initially recorded in the pons, lateral geniculate nucleus (LGN) of the thalamus, and occipital cortex, as well as the visual and sensorimotor systems of the forebrain, and can be divided into single, or cluster events (two or more successfully generated single P-waves within a burst), with the latter occurring most frequently during REM sleep (Callaway *et al.*, 1987; Datta, 1997; Karashima *et al.*, 2002; Hobson, 2009). It is worth noting that while P-waves primarily occur during REM sleep, they can also be observed during NREM sleep, generally in a phase-locked manner with certain cortical oscillations, particularly hippocampal SWRs, implying a role in memory replay and consolidation (Tsunematsu *et al.*, 2020; Ramirez-Villegas *et al.*, 2021; Tsunematsu *et al.*, 2023). During REM sleep, P-waves precede CA1 neuron firing and are generally phase-locked with theta oscillations in the hippocampus and neocortex, in which acceleration of theta wave activity correlates with P-wave activity, suggesting common activatory systems (Karashima *et al.*, 2002; Tsunematsu *et al.*, 2020). P-waves are thought to originate by synchronous firing in the pontine reticulum, activating cholinergic neurons of the PPT/LDT of the mesopontine tegmentum (Fernandez-Mendoza *et al.*, 2009; Adamantidis *et al.*, 2019; Patel *et al.*, 2020; Tsunematsu *et al.*, 2023). Optogenetic stimulation of dmM neurons expressing CRH can elicit P-waves, with high levels of activity of such neurons and P-waves naturally co-occurring during REM sleep, suggesting a role of these dmM neurons in the initiation of P-waves (Schott *et al.*, 2023).

1.2.2.6.3. Gamma Oscillations

Gamma oscillations can be observed in wakefulness and both sleep states, however during REM sleep, gamma oscillations can be recorded in multiple brain regions including the neocortex, entorhinal cortex, amygdala, hippocampus, striatum, olfactory bulb, and thalamus (Buzsaki and Wang, 2012). Gamma oscillations are generally reported in the frequency band 30-100 Hz, and can be categorised into low gamma or high gamma, however ranges of gamma frequency bands vary between study, species, and brain region (Scheffzuk *et al.*, 2011; Buzsaki and Wang, 2012; Tiesinga and Sejnowski, 2009). Gamma oscillations, particularly fast gamma, is coupled with

theta oscillations in neocortex of mice, and this theta-high gamma coupling is strongly enhanced during REM sleep (Scheffzuk *et al.*, 2011). Theta-gamma coupling in the dentate gyrus and CA3 is also highly increased in REM sleep, in which theta-gamma synchrony was increased during phasic REM sleep periods, in comparison to tonic REM sleep, in the dentate gyrus, CA1 and CA3, suggesting a role of the hippocampus in contributing to gamma oscillations during REM sleep (Montgomery *et al.*, 2008).

Overall, while more research has been done in recent years, our understanding of REM sleep regulatory circuits, and the circuits with govern REM sleep specific oscillations is still lacking in comparison to NREM. It is important we continue to learn more about how these regions communicate with each other during both sleep states, due to critical nature of sleep. In the following section, I will justify how important the continuation of sleep research is, by outlining some key functions sleep exerts on our cognitive health.

1.2.3. Functions of sleep

Sleep is essential for both physical and mental wellbeing, and is known to be important for cardiovascular health, metabolic functioning including roles in insulin and glucose homeostasis, and immunological health, where sleep deprivation results in proinflammatory states and increased risk of infection and illness (Grandner and Fernandez, 2021). While sleep is known to be important for the entire body, in the following sections I will focus on the role of sleep on several cognitive functions, specifically highlighting evidence for REM sleep in each subsection.

1.2.3.1. Development

Across species such as humans, rats, cats, and invertebrate, the amount of sleep required changes throughout the lifespan. Generally, total sleep requirement in mammals is highest during early postnatal life, which is particularly evident for REM sleep in mammals and birds (Roffwarg *et al.*, 1966; Jouvet-Mounier *et al.*, 1970; McGinty *et al.*, 1977; Shaw *et al.*, 2000; Szymczak, 1987; Kirov and Moyanova, 2002). This is also reflected in developmental sleep changes in the number of sleep bouts required, where younger infants and children typically nap during the day, which can exert cognitive benefits (Kurdziel *et al.*, 2013; Friedrich *et al.*, 2015; Seehagen *et al.*,

2015; Friedrich *et al.*, 2020). In humans, REM sleep is even more prevalent during prenatal stages (Knoop *et al.*, 2021). Together, this led to scientific investigation into the importance of REM sleep during development. Studies later found a direct link of REM sleep and the reorganisation of the brain, including plasticity, synaptogenesis, myelination, and energy consumption between the ages of 2 and 3 (Cao *et al.*, 2020). During REM sleep, selective pruning of newly-formed post-synaptic dendritic spines of layer 5 pyramidal neurons occurs in the motor cortex during development in mice. This facilitates new spine formation, which can also be strengthened during REM sleep (Li *et al.*, 2017). Similarly, ocular dominance plasticity, which is induced by monocular deprivation during critical development periods, is enhanced in cats after sleep, with opposite effects observed following sleep deprivation (Frank *et al.*, 2001). This effect during sleep appears to be mediated by protein synthesis and glutamate N-methyl D-aspartate (NMDA)-type receptor- and/or protein kinase A (PKA)-mediated synaptic strengthening in the cortex (Aton *et al.*, 2009; Seibt *et al.*, 2012). Specifically, this sleep-dependent enhancement of ocular dominance plasticity is lost when cats are selectively deprived of REM sleep (Dumoulin Bridi *et al.*, 2015). Together, these data implicate a role of sleep, and specifically REM sleep, in brain plasticity and early brain development.

1.2.3.2. Waste clearance

Sleep is also essential for the clearance of wasteful metabolites, proteins, and oxidative stress which accumulate during wakefulness, via the glymphatic system, which is most active during sleep (Xie *et al.*, 2013; Nedergaard and Goldman, 2020). During sleep in humans and rodents, CSF from the subarachnoid space is exchanged with interstitial fluid (ISF), facilitated by water channel aquaporin-4 (AQP4) located on astrocytic endfeet (Iliff *et al.*, 2013; Iliff *et al.*, 2012). The glymphatic process results in clearance of waste proteins such as amyloid beta (Aβ), a protein in which abnormal accumulation is implicated in the pathology of AD (Jack *et al.*, 2018). Studies mimicking sleep fragmentation in AD models, as well as studies with AQP4 knock-out mice models, show reduced performance in memory tests (Vasciaveo *et al.*, 2023; Skucas *et al.*, 2011). Thus, stimulating the glymphatic system has become an interesting potential therapeutic strategy for AD research (Murdock *et al.*, 2024). However, a recent study which used the diffusion coefficient of fluorescent dyes to

examine waste clearance found that clearance was reduced during sleep and anaesthesia in mice, the opposite of previously described opinions (Miao *et al.*, 2024). While this is an interesting finding in this field, some technical constraints have been highlighted. This study injects tracer dyes directly into the brain, where previous studies have primarily injected markers into the CSF, which can damage the brain tissue and increase intracranial pressure. Similarly, the projection of dyes from injection site to cortex is less descriptive of hypothesised glymphatic pathways in comparison to studies injecting into the CSF. The reported sleep condition group also involved animals in recovery sleep following 5 hours of sleep deprivation, and not natural sleep. More control groups, and refined methodology, are needed to strengthen this opposing argument.

1.2.3.3. Learning and memory

For over a century, sleep has been implicated in memory formation and consolidation (Heine, 1914; Rasch and Born, 2013; Klinzing *et al.*, 2019; Girardeau and Lopes-Dos-Santos, 2021). Briefly, memory formation can be described as encoding information from a new experience by a brain-wide network of neurons and glial cells to regulate future behaviour to related contexts (Brodt *et al.*, 2023). Memory consolidation can then be explained as the strengthening of synaptic connections between neurons encoding a memory (Müller and Pilzecker, 1900; Brodt *et al.*, 2023). The reactivation of engram sub-ensembles, thus the strengthening of acquired memories, has been detected during sleep (Ghandour *et al.*, 2019). NREM sleep specific oscillations such as sharp-wave ripples, sleep spindles, and slow wave activity, as well as the coupling between these oscillations, have been particularly associated with memory performance (Schabus *et al.*, 2004; Girardeau *et al.*, 2009; Ego-Stengel and Wilson, 2010; Girardeau and Lopes-Dos-Santos, 2021; Peyrache and Seibt, 2020). As such, reduced sleep and slow wave activity result in lower memory scores and increased brain atrophy, and sleep disturbances are a prominent characteristic of memory disorders, such as dementia (Sabia *et al.*, 2021; Lewis, 2021; Girardeau and Lopes-Dos-Santos, 2021).

During REM sleep, theta activity is involved in place cell strengthening after encoding during prior wakefulness, and is thus thought to contribute towards spatial memory

consolidation (Poe *et al.*, 2000; Louie and Wilson, 2001; Drieu *et al.*, 2018). In agreement, attenuating theta activity during REM sleep impairs spatial and emotional learning (Boyce *et al.*, 2016). Theta coherence between the hippocampus, the amygdala, and prefrontal cortex is enhanced after fear-conditioned memory tasks, in which such theta coordination correlates with task performance (Popa *et al.*, 2010), suggesting interactions of these regions during REM sleep are involved in aversive learning and memory consolidation. Optogenetically silencing adult-born neurons in the dentate gyrus during REM sleep impairs memory consolidation, thought to be mediated by impaired synaptic plasticity (Kumar *et al.*, 2020). Similarly, REM sleep plays an important role in pruning and strengthening postsynaptic dendritic spines of layer 5 pyramidal neurons in the mouse motor cortex following motor learning tasks, a process which involves NMDA receptor-dependent dendritic Ca^{2+} spikes during REM sleep (Li *et al.*, 2017). In addition, cortical activity during REM sleep, specifically somatodendritic decoupling in pyramidal neurons in the prefrontal cortex, has been implicated in memory consolidation in response to biological stressors (Aime *et al.*, 2022).

Brain activity which suggests that memory reactivation occurs during REM sleep has also been observed in humans (Abdellahi *et al.*, 2023). Furthermore, REM sleep behaviour disorder, characterised by a loss of muscle atonia during REM sleep, is an early clinical marker of neurodegenerative disorders in which memory is impaired, such as Parkinson's disease, AD, and dementias (Postuma *et al.*, 2009; Dauvilliers *et al.*, 2018; Postuma *et al.*, 2019; Krohn *et al.*, 2022). Specifically, in patients with AD, spectral changes in EEG and increased power of slower frequency oscillations (delta/theta) over faster frequency (alpha/gamma) occurs during REM sleep, which is absent in healthy controls. Such changes in EEG during REM sleep are indicative of AD status (Prinz *et al.*, 1992; Petit *et al.*, 1992; Hassainia *et al.*, 1997). In addition, meta-analysis has demonstrated that changes in the sleep-wake cycle occur in AD, which includes reduced total sleep time, increased awakenings and sleep fragmentations, and reduced SWS, and REM sleep. Importantly, the reductions in SWS and REM sleep both appear to correlate with disease progression in AD(Zhang *et al.*, 2022b). Most significantly for our project, a recent study linked both lower REM sleep percentage and increased latency to REM sleep with predictive risk of incidence dementia, while changes in NREM sleep were not associated predictive risk.

Specifically, each percentage of reduction in REM sleep was associated with an approximate 9% increase in predictive risk of dementia (Pase *et al.*, 2017). It is thought that a loss of cholinergic activity, which is typical of AD, may drive such a reduction in REM sleep, as cholinergic activity is relatively high during REM sleep in comparison to NREM sleep in healthy individuals (Andre *et al.*, 2023).

The outlined data demonstrates the importance REM sleep plays in memory consolidation, and the implications of reduced REM sleep in neurodegenerative disorders such as AD. However, more research needs to be done to fully understand REM sleep regulation, and how REM sleep exerts such an effect on memory. Current evidence is largely correlative, with studies showing causal evidence beginning to emerge over the last few years. This is a difficult task for REM sleep due to several methodology constraints. Firstly, attempts for selective REM sleep deprivation typically inadvertently affect NREM sleep and wake states, thus making it hard to relate changes in memory with REM sleep alone. Secondly, *in vivo* tests for spatial memory, which is of particular interest given the strong role of hippocampal theta during REM sleep, can often induce stress and anxiety (Harrison *et al.*, 2009), while sensitivity and variation can vary between different memory tasks, and involves numerous contributing parameters in test environments and data analysis.

1.2.3.3.1. Spatial memory tests in vivo

Common tests for spatial memory include the novel object location test (NOLT), Morris water maze, maze tests, and fear conditioned place avoidance. NOLT is a modified version of the novel object recognition test (NORT). NORT tests object recognition memory, and was previously assumed to be hippocampus-independent, but is now considered to be modulated by hippocampal activity (Sawangjit *et al.*, 2018). On the other hand, NOLT is hippocampal-dependent and assesses spatial memory and consists of monitoring behaviour in three separate sessions; habituation, encoding and retention (Ennaceur and Delacour, 1988; Vogel-Ciernia and Wood, 2014). After being habituated to test environment, during encoding mice explore two identical objects. In the retention session, one of these objects is moved to a novel location (**Fig. 1.6A**). If spatial memory consolidation occurred between these sessions, animals should explore the object in novel location more during retention, thus

demonstrating a higher discrimination for this object (**Fig. 1.6A**). If memory consolidation is perturbed between encoding and retention sessions, this discrimination preference will not occur, and animals will explore objects in familiar and novel locations equally (**Fig. 1.6A**). While this is a common approach for investigating spatial memory, it relies on innate exploratory behaviour.

Alternatively, the Morris water maze utilises a pool filled with water, made opaque with dyes, paints, or milk, where animals learn to locate an elevated platform to escape swimming (Morris, 1981; Morris, 1984). Over a number of trials, animals should learn where the platform is located using spatial cues, and spatial memory can be tested by determining differences in the latency or distance used to find platform (**Fig. 1.6B**). However, due to the nature of this test, excessive stress can affect results (Othman *et al.*, 2022). The Morris water maze was originally designed as an alternative to the radial arm maze (Morris, 1981). The radial arm maze, as well as other mazes such as the Y maze, consist of a central chamber, and multiple arms extending from the central chamber (Olton and Samuelson, 1976). At the end of one arm, or in radial arm maze in each arm, a food reward is placed. After several trials, the time taken to retrieve rewards, or number of re-entries into arms where reward have already been collected, can be measured to assess learning and memory of reward locations (**Fig. 1.6C**). Some limitations of these tests include that strategy is often used in radial arm maze tests, collecting rewards from each arm sequentially, rather than using spatial cues, while Y mazes have less arms and are therefore less complex, leading to a higher probability of chance success (Sharma *et al.*, 2010; Othman *et al.*, 2022).

The Barnes maze test was subsequently designed as a dry-based alternative to the Morris water maze (Barnes, 1979), and has a similar concept to other maze-based tests. In the test platform, multiple holes are spaced around the edge, with one hole leading to an escape tunnel. After a period of learning, animals should use spatial cues to locate the correct escape location, thus latency and trajectory can be used to assess spatial learning (**Fig. 1.6C**). Alternatively, fear conditioned spatial leaning consists of using aversive stimuli, such as foot shocking, in a particular location within test environment to assess place avoidance behaviour (**Fig. 1.6D**) (Cimadevilla *et al.*, 2000), however, this arguably tests contextual and emotional learning and memory,

instead of specifically spatial, and may be affected by the stress this causes for the animals.

Overall, of these commonly used spatial memory tests, no “gold-standard” approach has been identified, with each of these commonly used tests offering different sets of advantages and disadvantages. Thus, when looking at the relationship between sleep and spatial memory, it is important to choose the most appropriate test for specific experimental designs.

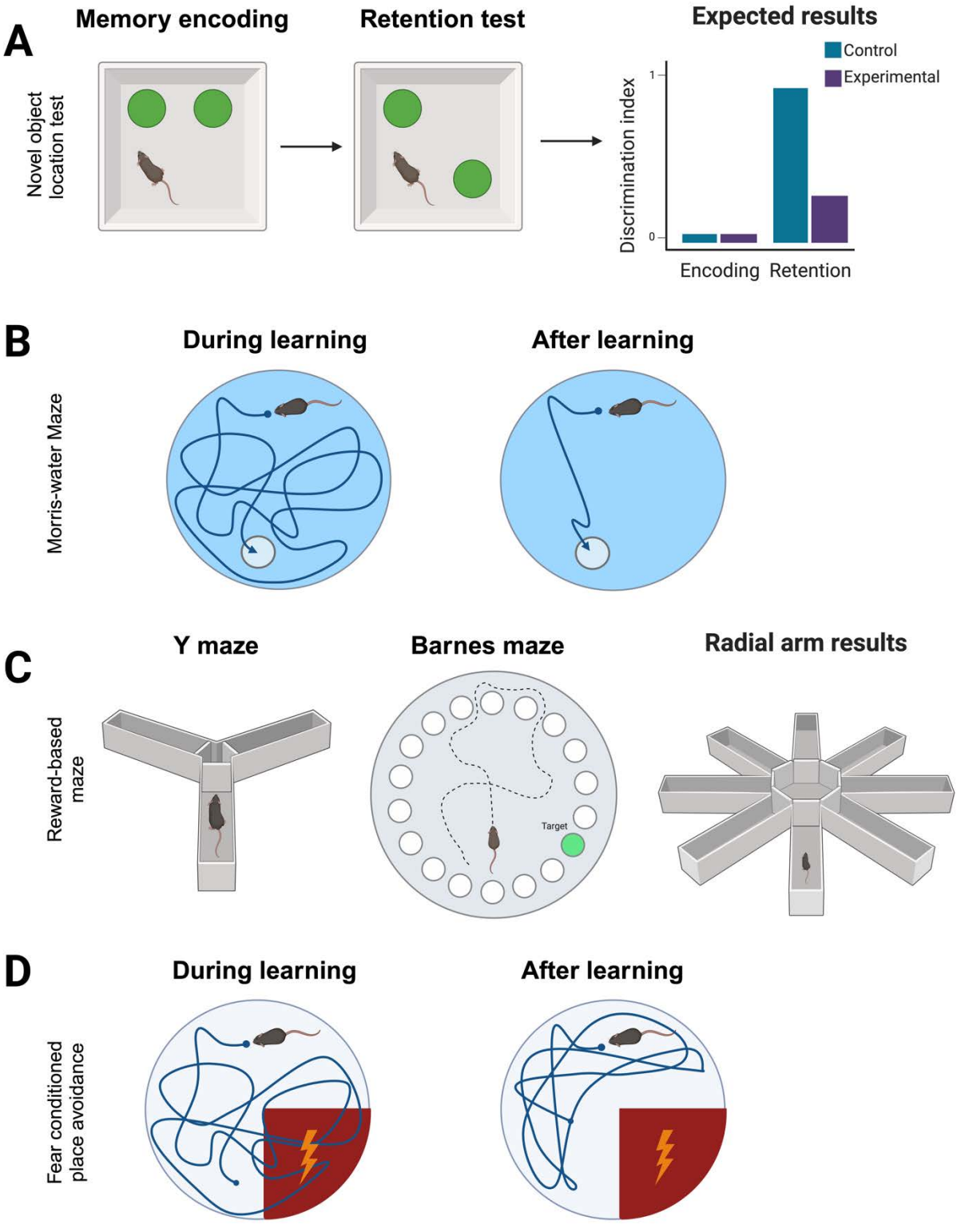

Figure 1.6. Schematics of techniques for testing spatial memory. **A**. Novel object location test, after exploring two objects during encoding one object is moved to a novel location. Animals should remember encoding and explore the object at novel object more thus increasing discrimination index, unless memory was impaired during experimental paradigm. **B.** Morris water maze, after being placed in water, mice learn where an elevated platform is located, thus taking less time to reach this location over time. **C.** Reward-motivated mazes can be used to determine how long if takes to find reward after a period of learning. **D.** Fear-conditioned place avoidance, an area of testing box has adverse stimuli such as foot shock, mouse learns to avoid this area.

Image created using BioRender.com

1.2.4. Interim summary

So far in this chapter we discussed in depth the regulatory circuits and oscillations involved in both NREM and REM sleep. We also discussed sleep functions, in particular, the role for sleep in memory. A major caveat for the data described in these sections is that it solely reports on neural circuitry. As well as neurons, the mammalian brain is made up of glial cells including astrocytes, microglia, oligodendrocytes, and oligodendrocyte precursor cells (OPCs) (**Fig. 1.7**). In particular, astrocytes envelop synapses, and are involved in influencing synaptic transmissions between neurons, thus regulate neuronal activity (**Fig. 1.7**) (Parpura and Verkhratsky, 2012a; Corkrum *et al.*, 2020; Lezmy *et al.*, 2021; Liu *et al.*, 2023). In addition, they are known to exert roles in various sleep functions, such as waste clearance. This puts astrocytes in a prime position to exert effects on neuronal communication during sleep. As such, in the following sections, I will describe the structure, functions, and activity of astrocytes before linking these topics and discussing existing evidence for a role of astrocyte activity in sleep regulation, and thus provide the context and motivation for this project.

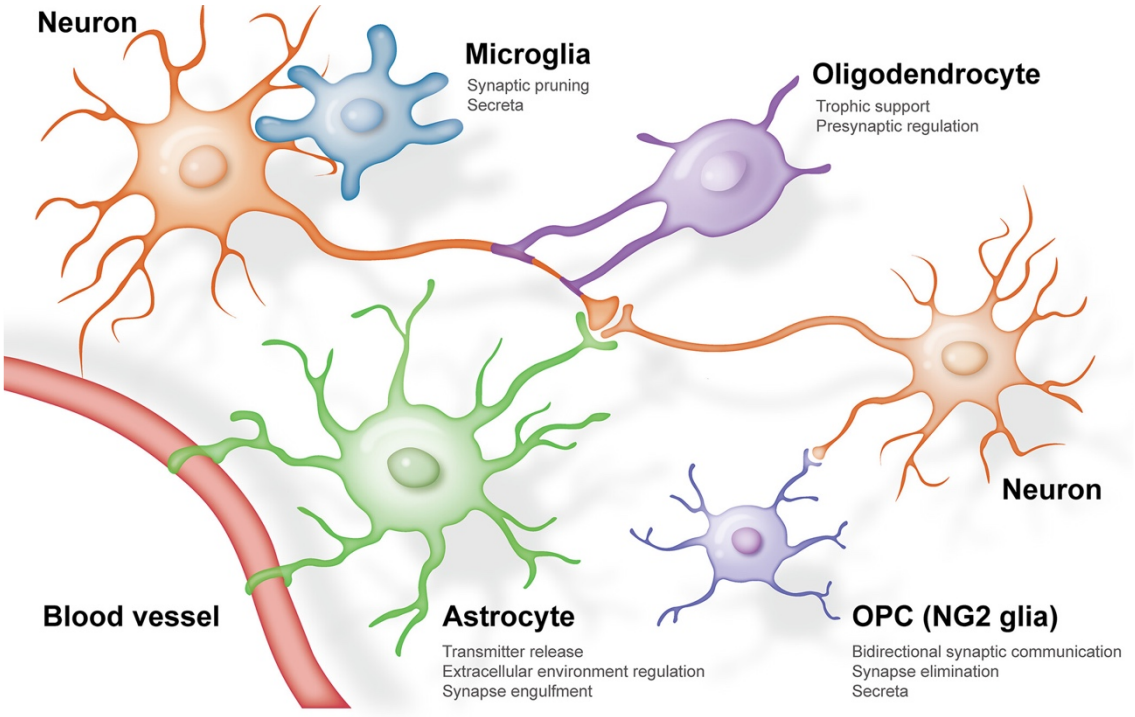

Figure 1.7. Interaction of neurons and glia cells in the brain. The brain is made up of neurons and glial cells. Glial cells include astrocytes, microglia, oligodendrocytes, and oligodenrocyte precursor cells (OPC) also known as neurons-glial antigen 2 (NG2). The main functions of glial cells are listed.

Image from Liu et al. 2023.

https://creativecommons.org/licenses/by-nc/4.0/

1.3. Astrocytes

1.3.1. Discovery and history

Astrocytes are the most abundant type of glial cell in the mammalian brain. The existence of neuroglia was first described by Rudolf Virchow in 1856, who considered these cells as connective substances in the central nervous system (CNS), in which nervous system elements were embedded (Virchow, 1856; Parpura and Verkhratsky, 2012b). Later in the 19th century, Camillo Golgi discovered glia-vascular contacts, now known as 'endfeet', and proposed that certain glial cells have functions in metabolic support and substance exchange (Golgi, 1873; Golgi, 1903). Such cells were later named astrocytes (von Lenhossék, 1891) and categorised into two morphologically distinct groups; protoplasmic and fibrous astrocytes (Andriezen, 1893; y Cajal, 1913). The characterisation of astrocytes was furthered by Ramón y Cajal, who developed staining techniques for the study of astrocytes, such as the gold chloride-sublimate staining method which allowed for the visualisation of the nucleus and other intracellular structures and found close proximity of astrocytes to neurons. He proposed this was due to astrocytic involvement in the flow of information between neurons, in which he suggested astrocytes act as insulators (y Cajal, 1913; Somjen, 1988; Garcia-Marin *et al.*, 2007). Ramón y Cajal was the first to hypothesise the involvement of astrocytes in more complex interactions with neurons, other glia, and blood vessels. He proposed that astrocytes could be involved in executive functions such as attention via movements of their endfeet structures to induce vasodilation or vasoconstriction in arterioles which supplied nutrients to specific regions of the brain (Garcia-Marin *et al.*, 2007). He also proposed, in a theoretical article, an involvement of astrocytes in the sleep-wake-cycle, suggesting that during sleep astrocytes extend their processes to prevent neural contact and stop nervous current, to act as a 'circuit breaker' (y Cajal, 1895; Garcia-Marin *et al.*, 2007), a theory which will be expanded on in later sections. In agreement with Ramón y Cajal's concepts of astrocytic interactions, electron microscopy techniques later developed identified contact between protoplasmic astrocyte processes and neural synapses, and fibrous astrocyte processes and the nodes of Ranvier (Sofroniew and Vinters, 2010). By mid-20th century, several distinct morphologies, and various functions, of astrocytes had been identified (Somjen, 1988; Zeisel *et al.*, 2018).

1.3.2. Astrocyte structure

The morphological and physiological diversity of astrocytes which was identified over a century ago remains fundamentally similar, albeit less complex, to our current understanding. The major categories of astrocytes include the widely distributed protoplasmic and fibrous astrocytes, typical of grey and white matter respectively, as well as various types of specialised astroglia such as retinal Müller cells and cerebellar Bergmann glia (**Fig. 1.8**) (Rakic, 2003; Ben Haim and Rowitch, 2017). Protoplasmic astrocytes have 'bushy' star-shaped structures with fine perisynaptic processes emerging from secondary and tertiary branches. These delicate processes ensheath neuronal synapses, in which some branches feature specialised and polarised distal compartments called 'end-feet', which directly contact blood vessels (**Fig. 1.8**) (Allen and Eroglu, 2017; Khakh and Sofroniew, 2015). Fibrous astrocytes have a more elongated structure and are in close proximity to myelinated axonal tracts and oligodendrocytes, and contact the nodes of Ranvier (**Fig. 1.8**) (Allen and Eroglu, 2017; Ben Haim and Rowitch, 2017). Bergmann glia and velate astrocytes are two subtypes of astrocytes found in the cerebellum, which have distinct positioning, molecular profiles, and morphological features (Farmer *et al.*, 2016). Primates, including humans, also exhibit several morphologically distinct types of cortical astrocytes, while adult rodent brains display several astrocyte-like neural stem cells in the subventricular zone (**Fig. 1.8**) (Merkle *et al.*, 2014; Oberheim *et al.*, 2009; Merkle *et al.*, 2007).

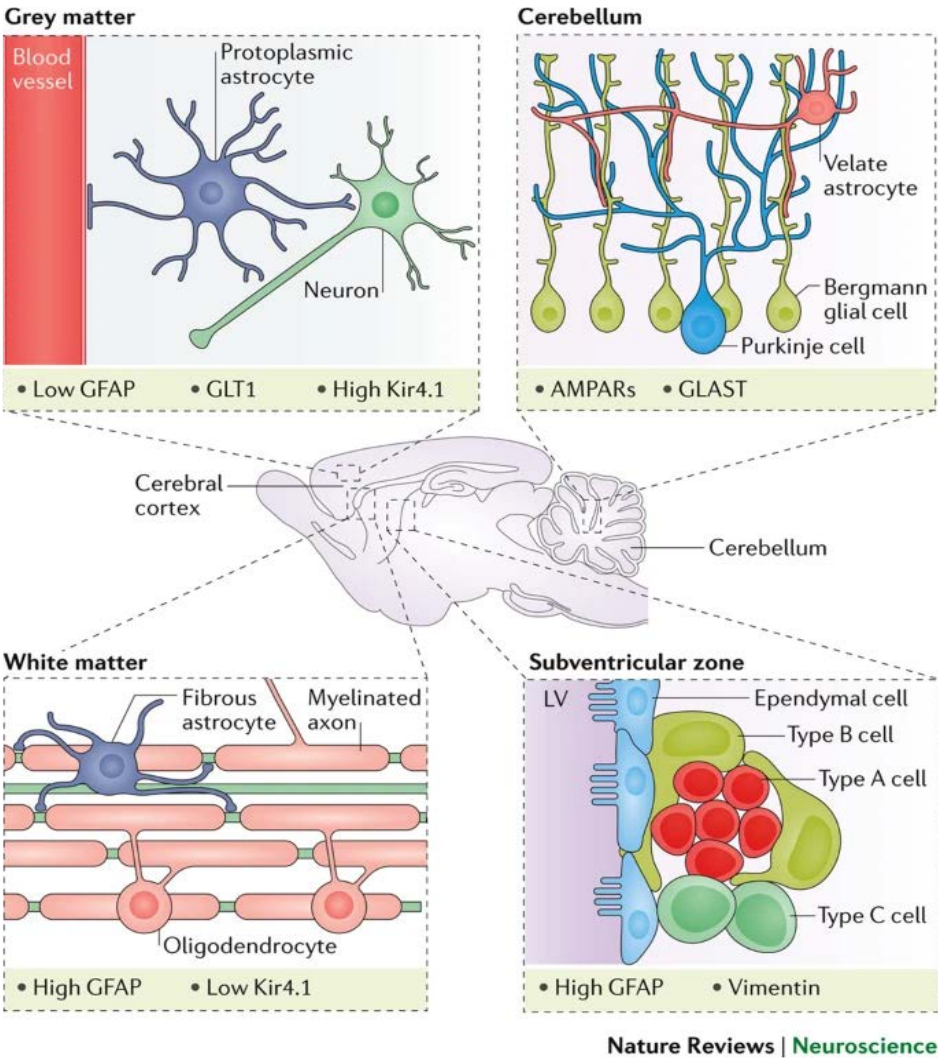

Figure 1.8. Morphological and molecular diversity of astrocytes in various brain regions. Schematics illustrating the mophology and characteristics of astrocytes in different brain regions. Protoplasmic astrocytes, located in grey matter, contact neurons and blood vessels, have a more radial morphology, and express markers glutamate transporter 1 (GLT1) and inward rectifying potassium channel (Kir4.1) while having low glial fibrillary acidic protein (GFAP) expression (top left panel). In the cerebellum, velate astrocytes are found in the molecular layer and closely relate to protoplasmic astrocytes. Bergmann glia in the cerebellum have long processes, which extend to the molecular layer, and express Ca^{2+}-permeable AMPA receptors on these processes which enwrap Purkinje cell dendrites. Bergmann glia also express glutamate aspartate transporter (GLAST) and Kir4.1 (top right panel). Fibrous astrocytes, found in white matter, closely contactoligodendrocytes and myelinated axon tracts. They have a more enlongated morphology and highly express GFAP while having low Kir4.1 expression (bottom left panel). Stem cells with astocyte-like features are also found in the rodent subventricular zone, in which astrocyte-like type B cells line the lateral ventricles (LV). These cells differentially express markers such as GFAP and vimentin (bottom right panel)

Image from Ben Haim and Rowitch, 2017.

More recently, improved techniques to study astrocytes across several species has led to the understanding that astrocytes have complex morphological and molecular profiles, which depend on specific CNS area, circuit, and/or disease incidence (Huang *et al.*, 2020; John Lin *et al.*, 2017; Batiuk *et al.*, 2020; Ben Haim and Rowitch, 2017; Nagai *et al.*, 2021). For example, in the mouse cortex, single-cell ribonucleic acid

(RNA) sequencing and spatial reconstruction studies show that like neurons, astrocytes display layer specific gene expression patterns, which also differed depending on cortical region (Bayraktar *et al.*, 2020). Similarly, multi-technique studies show distinct differences in morphology, Ca^{2+} signalling, proximity to astrocytes, electrophysiological properties, and RNA and proteomic expression between striatal and hippocampal astrocytes (Chai *et al.*, 2017). Less than a decade ago, 7 types of distinct molecular expression profiles amongst astrocytes were identified, in which *Aqp4* was universally expressed (Zeisel *et al.*, 2018). More recently, a highly impactful study on this topic looked at 13 distinct regions in the adult mouse brain, and found a range of region-specific differences (Endo *et al.*, 2022). Firstly, they found neuron-to-astrocyte ratios were varied depending on brain region, this was largely driven by differences in neuron density, however, may suggest differences in neuron-astrocyte communications between regions (Endo *et al.*, 2022). Next, using astrocyte-specific RNA sequencing from the 13 regions they identified over 4,000 astrocyte-enriched genes, of which ~20% were expressed across all regions, ~22% were uniquely expressed, and the remaining were shared across 2-12 regions which generally followed an expression pattern to three broader regions; the cerebrum, the brainstem and spinal cord, and the cerebellum. In addition, using confocal imaging, several morphological differences were found between the 13 regions, including territory size, shape, and complexity (Endo *et al.*, 2022). Similarly to RNA sequencing data, similarities were found between closely related-regions. By identifying different genetic profiles and morphology, this study suggests region-specific functions, and emphasises the complexity of astrocytes.

1.3.3. Functions of astrocytes

Consistent with the diverse profile of astrocyte morphology and molecular expression profiles, astrocytes have a wide variety of functions in the CNS. Astrocytes are derived from progenitor cells in the subventricular zone, or from radial glia in the ventricular zone, and migrate to the CNS along radial glia processes (Ge *et al.*, 2012; Lee *et al.*, 2022). A single astrocyte typically contacts several thousand neuronal synapses through astrocytic processes, with studies recording as many as 140,000 synapses contacted by single hippocampal astrocytes in adult rats (Bushong *et al.*, 2002; Allen, 2014), placing them in a central location for communicating information between

neurons. In addition to dense contact with neurons, astrocytes make contact with blood vessels via endfeet, by which they regulate cerebral blood flow, provide blood vessels with nutrition, and help maintain the blood-brain barrier (BBB) (Foo *et al.*, 2011; Allen, 2014). Astrocytes are essential in the formation of neuronal development, particularly in synaptic formation and plasticity, neurotransmitter and ion uptake, balance, and recycling, phagocytosis, and importantly, synaptic transmission regulation (Ullian *et al.*, 2001; Perez-Alvarez *et al.*, 2014; Allen and Eroglu, 2017; Abbott *et al.*, 2006; Oliveira and Araque, 2022). The essentiality of astrocytes to neuronal survival is obvious by ablating astrocytes in *in vivo* research, which leads to an imbalance of neurotransmitters and eventual excitotoxicity and death of neurons (Cui *et al.*, 2001; Wagner *et al.*, 2006).

Unlike neurons, astrocytes do not fire action potentials along their processes. Instead, increased intracellular calcium concentrations can represent astrocytic excitability (Charles *et al.*, 1991; Volterra and Meldolesi, 2005; Oliveira and Araque, 2022). Such activity can be spontaneous or evoked by neurotransmitters such as glutamate, noradrenaline, GABA, dopamine, acetylcholine, histamine, adenosine triphosphate (ATP), and endocannabinoids (Pasti *et al.*, 1997; Porter and McCarthy, 1995b; Porter and McCarthy, 1996; Kang *et al.*, 1998; Duffy and MacVicar, 1995; Shelton and McCarthy, 2000; Porter and McCarthy, 1995a; Bowser and Khakh, 2004; Araque *et al.*, 2014; Haydon and Carmignoto, 2006). Astrocytes express a wide range of ionotropic, transporters, and metabotropic receptors (**Fig. 1.9**), which, upon stimulation, leads to inositol-1,4,5-trisphosphate (IP_3) production, Ca^{2+} release from the endoplasmic reticulum (ER), and multiple Ca^{2+} oscillatory events (Volterra *et al.*, 2014; Kofuji and Araque, 2021; Liu *et al.*, 2023). Astrocytic calcium activity was initially described in the cell soma, with astrocytes displaying large, slow, global Ca^{2+} events (seconds to minutes) following G-protein coupled receptor (GPCR) stimulation (Hirase *et al.*, 2004; Di Castro *et al.*, 2011; Araque *et al.*, 2014). However, improved imaging techniques led to the discovery that small, fast, and localised Ca^{2+} events occur in astrocyte processes, more frequently than those involving the cell soma (Di Castro *et al.*, 2011; Panatier *et al.*, 2011). Once activated, astrocytes release gliotransmitters such as ATP, glutamate, GABA, and $_D$-serine, which bind to neuronal receptors and influence synaptic transmission and neuronal excitability (**Fig. 1.9**) (Volterra and Meldolesi, 2005; Savtchouk and Volterra, 2018).

Following activation of astrocytes, astrocytic release of ATP, which is extracellularly converted to adenosine, binds to presynaptic adenosine A1 receptors, purinergic P2Y or P2X receptors, and/or postsynaptic purinergic P2X receptors (**Fig. 1.9**) (Chen *et al.*, 2013a; Cho *et al.*, 2022; Li *et al.*, 2020b; Liu *et al.*, 2023). Astrocyte-derived adenosine modulates synaptic transmission and has been implicated in various behaviours such as anxiety and fear-induced memory (Cho *et al.*, 2022; Li *et al.*, 2020b). Astrocyte glutamate promotes excitatory synaptic transmission and synaptic plasticity, and is thought to be crucial for a developmental switch from spike timing-dependent long-term depression to timing-dependent long-term potentiation at hippocampal neuronal synapses (Schwarz *et al.*, 2017; Yang *et al.*, 2019; Falcon-Moya *et al.*, 2020). Excessive release of glutamate by astrocytes has been implicated in excitotoxicity, suggesting targeting astrocytes in excitotoxicity-associated neurological disorders, such as stroke (Yang *et al.*, 2019). On the other hand, release of GABA by astrocytes, largely via Best1 anion channel, is essential for tonic inhibition at synapses (**Fig. 1.9**) (Kwak *et al.*, 2020; Lee *et al.*, 2010; Woo *et al.*, 2018; Liu *et al.*, 2023). Reactive astrocytes can overproduce GABA, impairing spike probability and synaptic plasticity, and reducing learning and memory in mice. Brain tissue from patients with AD have shown increased levels of astrocytic GABA, while reducing synthesis of astrocytic GABA seems to rescue synaptic transmission and memory in AD mice models (Jo *et al.*, 2014; Park *et al.*, 2019). D-serine released from astrocytes acts as a co-agonist at NMDA receptors and is involved in regulation of synaptic transmission via promotion of excitatory postsynaptic potentials and is thought to be important for dendritic spine maturation (Henneberger *et al.*, 2010; Yang *et al.*, 2003; Sultan *et al.*, 2015). Overall, astrocyte signalling is extremely complex, in both down- and upstream events. Due to the large number and variety of channels and receptors expressed on an astrocyte, and the activities of astrocytic derived gliotransmitters, it is clear that astrocytes play an important role in synaptic transmission.

In addition, astrocytes are also involved in regulating synaptic transmission via clearance of neurotransmitters, regulating ion balance, generating extracellular matrix molecules, and phagocytosis. The uptake of glutamate, via glutamate transporters glutamate aspartate transporter (GLAST) or glutamate transporter type 1 (GLT-1) or excitatory amino-acid transporter type-2 (EAAT2), and GABA, through GABA

transporters (GATs), by astrocytes contributes to strength and timing of synaptic input, regulates the inhibitory/excitatory balance, and is essential for neuronal signalling and correct information transfer (**Fig. 1.9**) (Goubard *et al.*, 2011; Muthukumar *et al.*, 2014; Shigetomi *et al.*, 2011; Valtcheva and Venance, 2016; Voutsinos-Porche *et al.*, 2003). In addition to Ca^{2+} signalling, astrocytes also express various K^+, Na^{2+}, H^+, and Cl^- transporters and are involved in regulating ion balance (Verkhratsky and Nedergaard, 2018; Verkhratsky *et al.*, 2020). For instance, astrocytes express potassium channels such as Kir4.1, and homeostatically control levels of extracellular K^+, which influences neuronal firing (Ballanyi *et al.*, 1987; Kofuji and Newman, 2004; Olsen *et al.*, 2015; Tong *et al.*, 2014). The uptake of extracellular neurotransmitters and ions is mediated by the inward transmembrane gradient of Na^{2+}, thus is an important contributor to astrocyte-mediate homeostasis functions (Rose and Verkhratsky, 2016; Verkhratsky *et al.*, 2020). Cl^- fluxes, via astrocytic Cl^- transporters, mediates inhibitory GABAergic transmission, a signalling pathway which has been implicated to play an important role in neuronal signalling during sleep and brain state activity (Untiet *et al.*, 2023). Astrocytes also secrete components of the extracellular matrix (ECM) such as thrombospondins, glypican, chondroitin sulfate proteoglycans, chordin-like 1, Hevin, and secreted protein acidic and rich in cysteine (**Fig. 1.9**). Astrocyte-derived ECM are responsible for regulating cellular and synaptic functions, such as synaptic strength and formations, cellular growth, migration, differentiation and survival (Hughes *et al.*, 2010; Kucukdereli *et al.*, 2011; Allen *et al.*, 2012; Blanco-Suarez *et al.*, 2018; Nagai *et al.*, 2019; Xie *et al.*, 2022; Liu *et al.*, 2023). In addition, astrocytes are now known to also play a role in phagocytosis, where astrocytes can clear excessive and functionally impaired synapses (Chung *et al.*, 2013; Gomez-Arboledas *et al.*, 2018; Lee *et al.*, 2022). Overall, these data show that in addition to a supportive role of astrocytes, they also play a direct role in synaptic transmission.

In pathological situations, astrocytes become reactive and undergo various functional, morphological and molecular changes, which can result in both protective and/or detrimental effects (Escartin *et al.*, 2021). Specifically, in pathological conditions such as in AD, astrocytes can undergo reactive astrogliosis in which they become hypertrophic and upregulate GFAP, and cluster around amyloid-beta (Aβ) plaques (Simpson *et al.*, 2010). They also overexpress BACE1, which can promote Aβ aggregation, and are involved in signalling of inflammatory cytokines which can also

promote Aβ aggregation (Cole and Vassar, 2007). Reduced expression of glutamate transporters EAAT1 and EAAT2 leads to increased extracellular glutamate and neurotoxicity in AD (Hefendehl *et al.*, 2016).

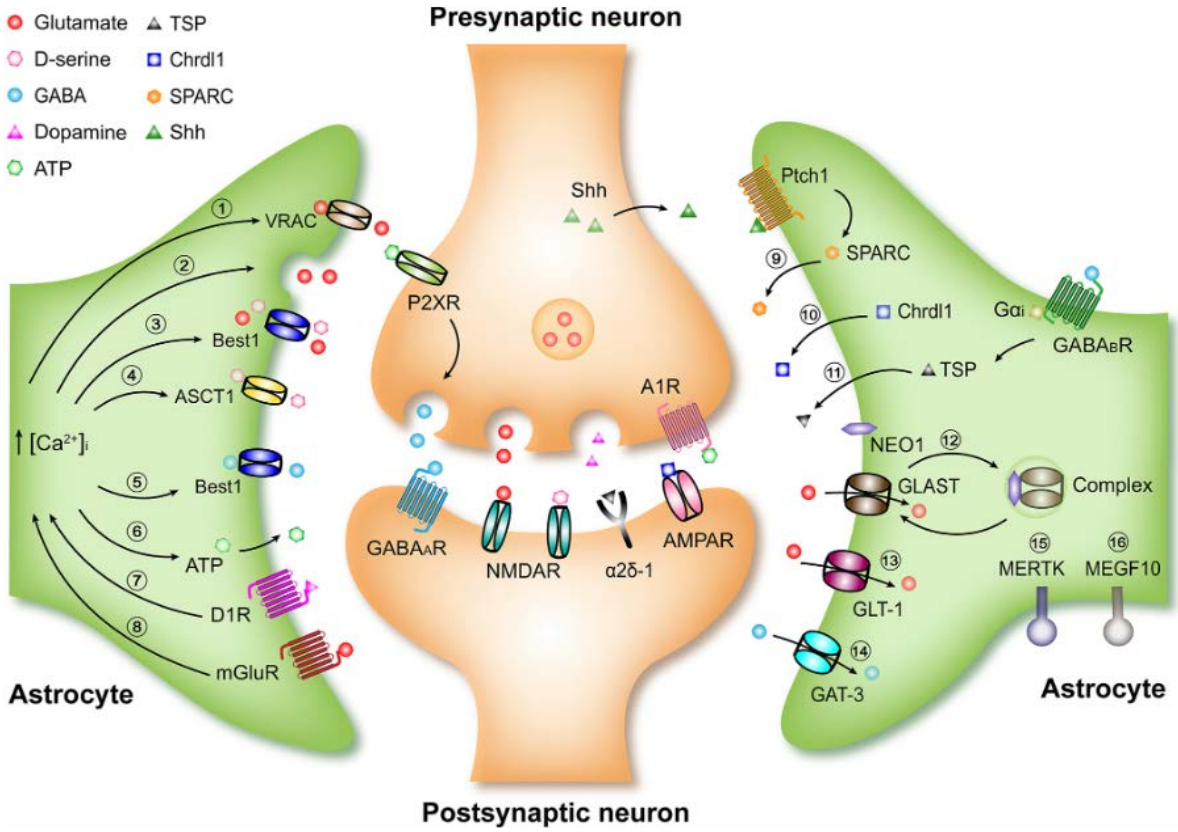

Figure 1.9. Astrocyte-neuron synapse interactions. Upon neuronal stimulation, astrocytes increase intracellular Ca^{2+} and release various transmitters to modulate synaptic transmission. Glutamate is released from astrocytes via VRAC (1), vesicles (2), or the Best1 channel (3), which activates NMDARs on postsynaptic membranes and triggers LTP. D-serine, which is released via the Best1 channel (3) or ASCT1 (4), binds to NMDARs and induces LTP and EPSPs. Astrocytic GABA, released through the Best1 anion channel (5), acts on the postsynaptic $GABA_AR$, which inhibits synaptic transmission. Dopamine and glutamate can activate astrocytic D1R (7) and mGluR (8), respectively, to induce a Ca^{2+}-dependent ATP increase (6), which in turn acts on the presynaptic A1Rs and P2XRs to modulate vesicular release and synaptic plasticity, modulating excitatory or inhibitory circuitry in different brain regions. Additionally, secreted proteins from astrocytes constitute the extracellular matrix molecules, which contribute to synaptic structure formation and stabilization. Astrocyte-derived extracellular matrix molecules includes SPARC (9), Chrdl1 (10), and TSP (11). The clearance of glutamate in the synaptic cleft involves two major glutamate transporters, GLAST (12) and GLT-1 (13). Binding of NEO1 to GLAST increases the astrocytic membrane distribution of GLAST and facilitates glutamate uptake. GABA clearance mainly depends on Ca^{2+}-dependent GAT-3 (14). Through the phagocytic receptors MERTK (15) and MEGF10 (16), astrocytes directly engulf excessive synapses in the developing and adult mouse brain.

VRAC, volume-regulated anion channel; Best1, Bestrophin-1; NMDAR, N-methyl-D-aspartate receptors; LTP, long-term potentiation; ASCT1, alanine/serine/cysteine/threonine transporter 1; D1R, dopamine-1 receptor; mGluR, metabotropic glutamate receptors; ATP, adenosine triphosphate; A1R, adenosine A1 receptors; P2XR, presynaptic purinergic P2X receptor; SPARC, secreted protein acidic and rich in cysteine; Chrdl1, chordin-like 1; TSP, thrombospondins; GLAST, glutamate–aspartate transporter; GLT-1, glutamate transporter-1; NEO1, Neogenin 1; GAT-3, GABA transporter 3 ; MERTK, MER proto-oncogene, tyrosine kinase; MEGF10, multiple EGF-like domains 10.

Image from Lui et al., 2023

https://creativecommons.org/licenses/by-nc/4.0/

1.3.3.1. Function of astrocytes in the brainstem

In rodents, astrocytes within the brainstem have been shown to play important roles in regulation of the microenvironment. In response to changes in pH, CO_2, O_2, astrocytes increase intracellular Ca^{2+} and release ATP to influence neuronal firing (Gourine and Kasparov, 2011; Teschemacher *et al.*, 2015). In the brainstem, astrocytes are also involved in regulating food intake and nutritional/energy balance, mechanosensory signalling, cardiovascular control of blood pressure and heart rate, respiratory control and regulation, oxygen sensing, and motor rhythms, including that of the preBötzinger complex which controls the rhythm of breathing (MacDonald *et al.*, 2020; Marina *et al.*, 2020; Turovsky *et al.*, 2020; Kohro *et al.*, 2020; Sheikhbahaei *et al.*, 2018; Angelova *et al.*, 2015; Caravagna *et al.*, 2013; Eugenin Leon *et al.*, 2016). Brainstem astrocytes have also been implicated in changes in brain state, which will be expanded on in the following sections.

1.3.4. Astrocytes and sleep

Ramón y Cajal first proposed a theory for a role of astrocytes in sleep in 1895. As previously mentioned, he claimed that astrocytes act as a 'circuit breaker' during sleep, in which astrocytic processes extend in order for astrocyte endfeet to invade the synaptic cleft, stopping synaptic transmission and thus inducing sleep. During waking he suggested astrocytes retract their processes, allowing for synaptic transmission (y Cajal, 1895; Garcia-Marin *et al.*, 2007; Tso and Herzog, 2015). Subsequent theories of astrocytic involvement in sleep included Frank's model, which proposed astrocytes act as integrators of neuronal signalling during the sleep-wake cycle, increasing their activity with sleep pressure, and driving wake-to-sleep transitions (**Fig. 1.10**) (Frank, 2019).

Given that both astrocyte activity and REM sleep are altered in many neurodegenerative disorders such as AD, understanding how astrocytes are involved in REM sleep regulation would provide us with vital information that could benefit our understanding of such disorders. In the following subsections, I will discuss the role of astrocytes in sleep according to current understanding, first describing astrocytic changes during various oscillatory activities and brain states, and then specifically astrocyte activity during sleep, in which my project is based on.

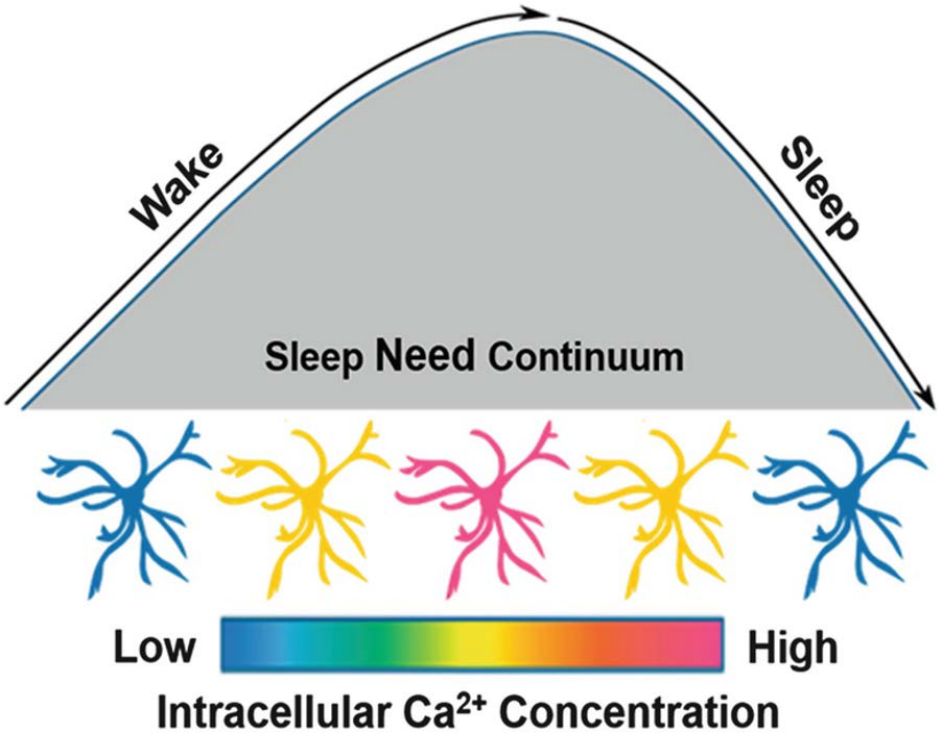

Figure 1.10. Frank's model of astrocytes as wakefulness integrators. Astrocytes respond to surrounding activity such as neurontransmitters with slow changes in intracellular Ca^{2+} concentrations to integrate with neuronal activity during wakefulness. Astrocytic responses may then contribute to negative feedback to dampen wake signalling and promote sleep. Such signalling activities may be proportionate to sleep pressure, therefore are most active during the wake-to-sleep transition and lowest at the end of the sleep period.

Image from Frank, 2019.

1.3.4.1. Neuron-astrocyte interactions during oscillatory activity

Transient increases in intracellular astrocytic Ca^{2+} precedes the onset of oscillatory activity, while perturbing astrocytic activity, without affecting neural activity, shortened gamma oscillatory activity, and reduced EEG gamma power across all behavioural states (wakefulness, NREM sleep and REM sleep), in *in vitro* and *in vivo* studies (Lee *et al.*, 2014). *In vitro* studies have demonstrated that astrocyte stimulation can trigger UP states, while inhibiting astrocytic activity has the opposite affect (Poskanzer and Yuste, 2011). In anaesthetic models of slow-wave sleep, synchronised recurrent astrocytic activity occurs during UP states, which also precedes neuronal synchronised activity (Poskanzer and Yuste, 2016; Szabo *et al.*, 2017). Astrocytic K^+ clearance, S100β gliotransmission, glutamate gliotransmission/regulation, and GABAergic signalling have all been shown to have various effects of oscillatory activity and synchronicity (Bellot-Saez *et al.*, 2018; Brockett *et al.*, 2018; Sakatani *et al.*, 2008; Poskanzer and Yuste, 2016; Mederos *et al.*, 2021), highlighting the versatile roles of

astrocytes in regulating cortical rhythms. Blockade of astrocytic gap junction communication and Ca^{2+} transients reduces the number of active astrocytes and neurons during slow-wave oscillations (Szabo *et al.*, 2017), while optogenetic activation of astrocytes induces slow-wave activity, which co-occurs with astrocyte-generated glutamate transients (Poskanzer and Yuste, 2016). In addition, astrocytic Ca^{2+} signalling also occurs following sensory stimulus-evoked oscillations and directly modulates such neural evoked activity (Wang *et al.*, 2006; Lines *et al.*, 2020). Together these studies suggest astrocytes are highly involved in initiating and/or regulating neuronal oscillatory activity, however studies manipulating astrocytes during specific states are required to convincingly implicate a role of astrocytes during sleep.

1.3.4.2. Astrocytic responsiveness to brain state

Locomotion is followed by astrocytic activity in multiple brain regions in mice (Slezak *et al.*, 2019; Paukert *et al.*, 2014; Nimmerjahn *et al.*, 2009; Ingiosi and Frank, 2023), via noradrenergic signalling (Paukert *et al.*, 2014). Noradrenergic activity has been shown to stimulate brainstem radial astrocytes to drive behavioural state changes, in which astrocyte activity suppressed swimming and induced 'passive' states in larval zebrafish via signalling to GABAergic neurons (Mu *et al.*, 2019). Similar results were found in awake behaving mice, where aversive stimuli induced transient increases in noradrenaline activity and subsequently Ca^{2+} elevations in astrocytes (Oe *et al.*, 2020). Elevated astrocyte Ca^{2+} activity co-occurring with arousal in mice follows phasic increases in noradrenaline, which has been shown to be independent of local neuronal activity (Reitman *et al.*, 2023). Such noradrenaline-dependent astrocyte activity occurs via astrocyte Adra1a receptor activation alongside reduced arousal-associated neuronal activity. This process acts as a feedback mechanism for cortical synchrony, thus astrocytes are thought to act as sensors of noradrenaline changes and synchronise the cortex in response to arousal (Reitman *et al.*, 2023).

Optogenetic and noradrenaline-induced activation of astrocytes has also been linked to astrocytic release of ATP, decreased excitability of pyramidal neurons, and increased excitability of interneurons via modulation of various potassium channels (Tan *et al.*, 2017; Chen *et al.*, 2019), in agreement with previous statements suggesting astrocytes induce GABAergic activity. Astrocytic modulation of glutamatergic activity

has also been thought to vary depending on brain state. Acetylcholine tone is at its highest during wakefulness and lowest during NREM sleep, which is also the case for astrocytic a_7-nicotinic acetylcholine activation as well as synthesis and release of $_D$-serine, an astrocyte-derived gliotransmitter and co-agonist of glutamate NMDA-type receptors (Papouin *et al.*, 2017). It has been shown *in vitro* and in mice that wakefulness-dependent increases of acetylcholine binds to a_7-nicotinic acetylcholine receptors to directly modulate astrocytic release of $_D$-serine, subsequently responsible for NMDA receptor activity relative to brain state (Papouin *et al.*, 2017). Intracellular chloride concentration is also higher during immobile states compared to mobile states in mice, with such concentrations decreasing upon movement and sensory stimulation (Untiet *et al.*, 2023). Optogenetic increases in intracellular astrocytic chlorine shortened neural activity in a similar means as pharmacological application of $GABA_A$ receptor agonists, while optogenetic depletion of intracellular chloride extended excitatory activity, suggesting that astrocytic gliotransmission of chloride may serve as a source of chloride for GABAergic transmission (Untiet *et al.*, 2023).

Astrocyte morphology also changes according to brain state. During sleep, astrocytic processes retract, and coverage of synapses reduces, which causes decreased gliotransmission, and affects astrocytic clearance of neurotransmitters and ions (Panatier *et al.*, 2006; Bellesi *et al.*, 2015). Reduced astrocytic coverage of synapses, and lower noradrenaline levels, during sleep are also thought to facilitate microglia surveillance (Stowell *et al.*, 2019; Van Horn *et al.*, 2021). Brain state dependent changes in astrocyte signalling and morphology is summarised in **Figure 1.11**.

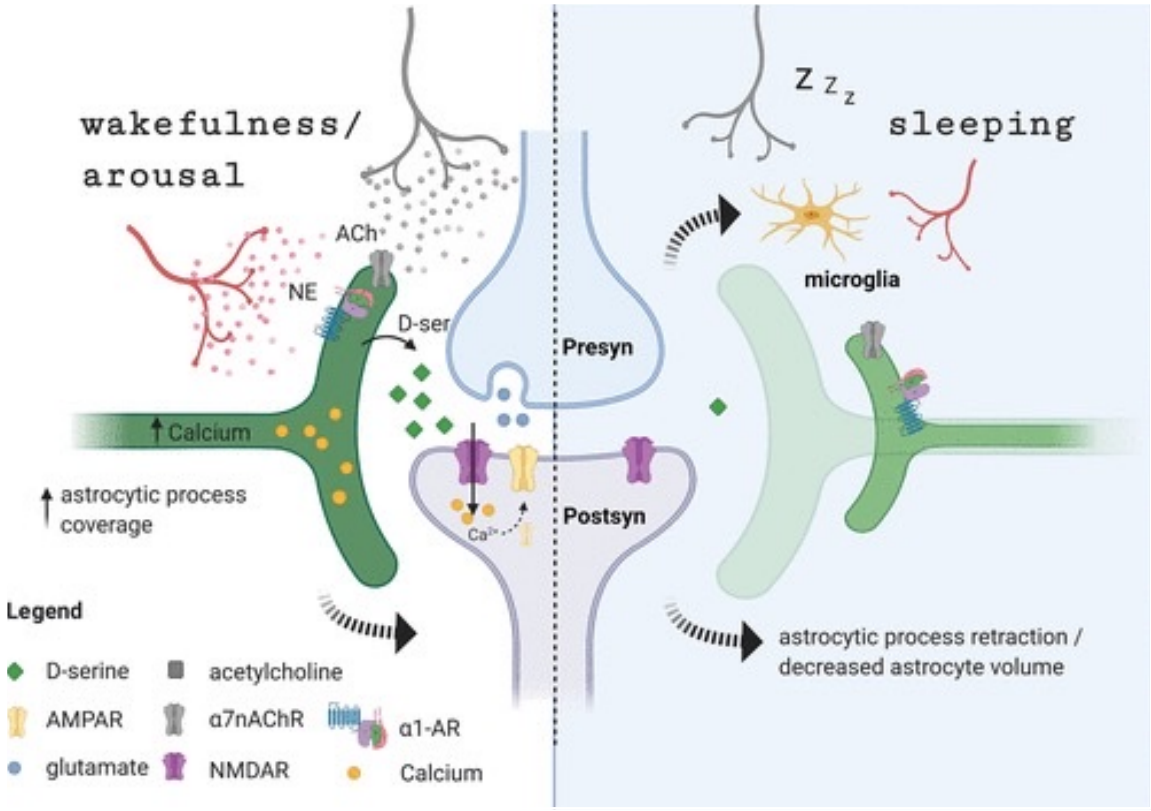

Figure 1.11. Changes in astrocytic signalling and morphology according to brain state. Increased cholinergic tone during wakefulness/arousal is sensed by astrocytes via a7-nicotinic acetylecholine receptors (a7nAChRs), leading to increased astrocytic D-serine release. This in turn leads to increased NMDA receptor activtion on postsynaptic neurons. Reduced astrocytic Ca2+ activity and retracted astroctyic process from neural synapses occurs during sleeping.

Image from Van Horn et al 2021.

1.3.4.3. Neuron-astrocyte interactions in sleep regulation

In awake-behaving animals, astrocytic activity has been studied in more detail across the sleep-wake cycle. Convincing, simplistic evidence for an involvement of astrocytes in sleep was first found in mice, which found the highest levels of intracellular astrocytic Ca^{2+} during periods of wakefulness and the lowest during REM sleep, and peak Ca^{2+} signalling occurring during sleep-to-wake transitions (Ingiosi *et al.*, 2020; Bojarskaite *et al.*, 2020a). In addition, longer durations of individual Ca^{2+} events occur during wakefulness compared to NREM and REM sleep (Vaidyanathan *et al.*, 2021; Ingiosi *et al.*, 2020; Bojarskaite *et al.*, 2020b; Ingiosi and Frank, 2022). Such Ca^{2+} event characteristics also differ within different structures of an individual astrocyte, with the amplitude and frequency of Ca^{2+} signalling being found to be more dynamic in the processes compared to the soma across the sleep-wake cycle (Ingiosi *et al.*, 2020; Bojarskaite *et al.*, 2020a).

In *Drosophila* models, sleep deprivation studies show increased intracellular concentrations of astrocytic Ca^{2+} in the soma and processes, dependent on a specific L-type Ca^{2+} channel. Astrocytic Ca^{2+} transients further increase with intensity of sleep deprivation (Blum *et al.*, 2021). And while fundamental differences in astrocyte complexity, morphology, and functions occur in *Drosophila,* similar findings were also found in mice. Such findings also observed fluctuations in astrocytic Ca^{2+} signals according to sleep pressure, particularly in NREM sleep, where changes in Ca^{2+} were largest following sleep deprivation (Ingiosi *et al.*, 2020), suggesting that, in agreement with Frank's model, astrocytic activity is involved in sleep homeostasis. Attenuating Ca^{2+} signalling using *Itpr2*$^{-/-}$ mice (genetic ablation of IP_3R2) resulted in fragmented sleep with reduced length of sleep periods, increased number of microarousals, and reduced delta power, suggesting that astrocytes regulate sleep, particularly NREM sleep, and sleep pressure via IP_3-mediated Ca^{2+} signalling (Bojarskaite *et al.*, 2020a).

In a study in *ex vivo* rabbit tissue, it was discovered that the enzyme activity of glial cells in the caudal reticular formation of the brainstem was lower for rabbits killed during sleep compared to those killed during wakefulness, the opposite to that of neurons (Hyden and Lange, 1965). Following these results, studies identified close coherence of neuron-glia activities during slow-wave sleep oscillations in cats, in which glial cells actively modulated neuronal activity via ion buffering of K^+ and Ca^{2+} (Amzica and Neckelmann, 1999; Amzica and Massimini, 2002). SNARE-dependent inhibition of astrocytic gliotransmission reduced NREM sleep in mice and reduced the accumulation of slow-wave activity following sleep deprivation with a particular importance highlighted on adenosine acting on A1 receptors (Halassa *et al.*, 2009), suggesting astrocytes contribute to sleep homeostasis via gliotransmission. Further evidence of astrocytic gliotransmission influencing the sleep-wake cycle followed this work, with studies using optogenetic manipulation in various brain regions in rodents. Optogenetic activation of astrocytes in the VLPO increased total sleep time, in which extracellular ATP levels were correspondingly elevated following optogenetic activation. In addition, infusion of a tissue-nonspecific alkaline phosphatase (TNAP) inhibitor, in which TNAP is responsible for hydrolysis of ATP into adenosine, increased wakefulness and decreased sleep duration, implicating a sleep-promoting role of TNAP-mediated ATP hydrolysis, which is released by VLPO astrocytes (Kim *et al.*, 2020; Ingiosi and Frank, 2022). Similarly, optogenetic activation of astrocytes in the

posterior hypothalamus, which are known to envelop wake-promoting histaminergic neurons, also resulted in increased sleep duration, particularly slow-wave NREM sleep, thought to be caused by the influence of gliotransmission by astrocytes, however, gliotransmitter concentrations were not directly measured (Pelluru *et al.*, 2016; Ingiosi and Frank, 2022). These data led to Frank's theory that astrocytes act as a 'wakefulness integrator', in which astrocytes exert slow, cumulative activities via gliotransmission, particularly of ATP and adenosine, which influence neuronal activity throughout the sleep-wake cycle (**Fig. 1.10**) (Frank, 2013; Frank, 2019; Ingiosi and Frank, 2022; Ingiosi and Frank, 2023).

Due to the convincing link between astrocytes and sleep, in which astrocytic Ca^{2+} activity seems to peak during sleep-to-wake transitions, many studies are beginning to explore the exact role of astrocytes in sleep regulation in various brain regions. Tsunematsu *et al.* (2021) investigated levels of astrocytic Ca^{2+} in the cortex, hippocampus, hypothalamus, and pons during the sleep-wake cycle using fibre photometry. In this study they use a Mlc1-tTA; TetO-YCnano50 mouse model to monitor astrocytic intracellular Ca^{2+} dynamics. YCnano50 is a genetically encoded calcium indicator consisting of a yellow fluorescent protein (YFP) and a cyan fluorescent protein (CFP), in the presence of calcium, a conformational change between YFP and CFP occurs, and the fluorescence emission is altered, thus the ratio between fluorescence is representative of Ca^{2+} changes (Horikawa *et al.*, 2010). Tsunematsu *et al.,* found that astrocytic Ca^{2+} was consistently at its lowest during REM sleep in all brain regions, while activity was lowered during NREM sleep compared to wakefulness in the cortex and hippocampus, and no significant difference was found in the hypothalamus and pons (**Fig. 1.12**) (Tsunematsu *et al.*, 2021). Conversely, studies in areas such as the basal forebrain have found that Ca^{2+} activity of astrocytes was relatively high during REM sleep and at its lowest during NREM sleep (Peng *et al.*, 2023).

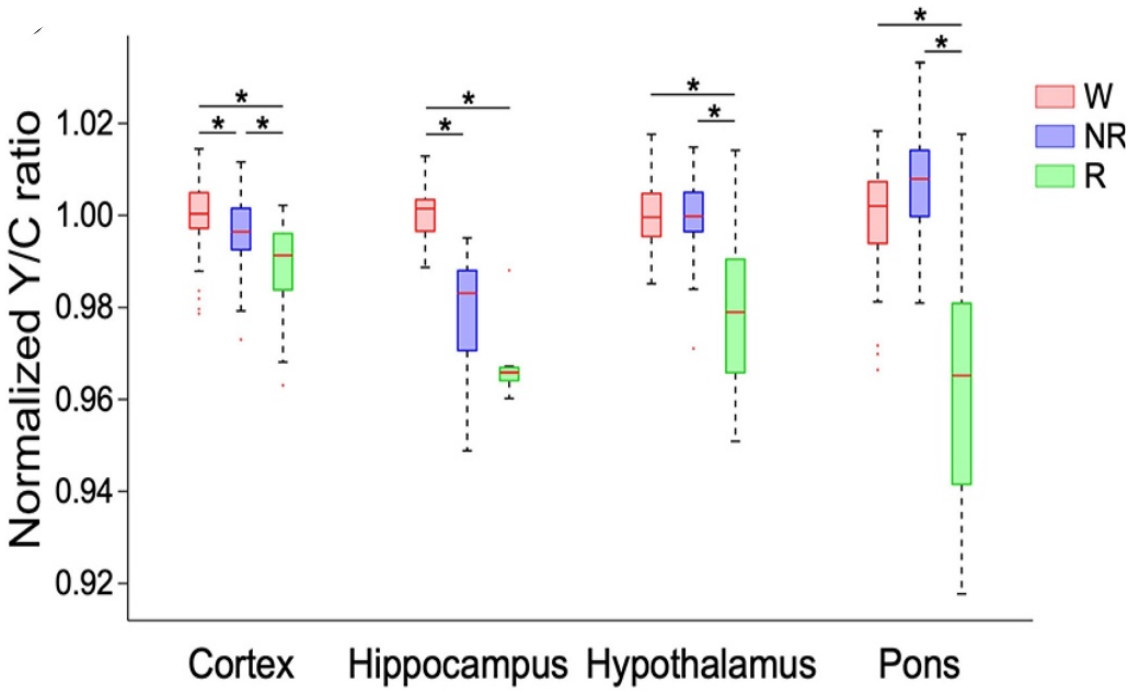

Figure 1.12. State-dependent astrocyte Ca^{2+} activity in different brain regions. Box plots obtained from normalised yellow fluorescence protein to cyan fluorescence protein (Y/C) ratios in various brain regions in wake (W), NREM sleep (NR) and REM sleep (R); p *<0.05

Image from Tsunematsu *et al.* 2021.

Recent studies which have modulated astrocyte activity have highly contributed to our understanding of the effects of astrocyte activity on the sleep-wake cycle (**Table 1.1**). Chemogenetic activation of astrocytes in the basal forebrain of mice produced long, continuous periods of wakefulness, without leading to rebound sleep in some studies (Ingiosi *et al.*, 2023), while other investigations within the basal forebrain showed no effect of stimulating astrocytic Ca^{2+} on wakefulness or NREM sleep, but significantly reduced REM sleep (Peng *et al.*, 2023). Chemogenetic stimulation of astrocytes in the LH increases wake and promotes long-term arousal, while chemogenetic inhibition of these astrocytes reduced wakefulness and promoted NREM sleep (Cai *et al.*, 2022). Chemogenetic activation of LH astrocytes also caused activation of GABAergic neurons in the LH, suggesting astrocytes may drive wakefulness via GABAergic neuron activation (Cai *et al.*, 2022). Interestingly, and most significantly for this project, Peng *et al.* recently looked at the LC/SLD region in the brainstem and found elevated astrocytic Ca^{2+} during wakefulness and REM sleep (**Fig. 1.13a-b**), which surprisingly opposes previously reported results found in the pons by Tsunematsu *et al.* However, they found contradicting results following chemogenetic activation of astrocytes in the LC/SLD, which reduced total REM sleep and number of REM sleep transitions over a

4-hour period following CNO injections (**Fig. 1.13c-f**) (Peng *et al.*, 2023). Chemogenetic activation of LC/SLD astrocytes also modulated EEG power, in particular increased delta power during NREM sleep, and theta during REM sleep (**Fig. 1.13g-j**). Such results were mirrored in CD73-KO mice (a model that lacks the key enzyme CD73 that converts AMP to adenosine), demonstrating this REM sleep suppression by LC/SLD astrocyte activity is independent of adenosine (Peng *et al.*, 2023). Due to conflicting reports by Tsunematsu *et al.* 2021, and Peng *et al*., 2023, astrocyte activity in the pons during the sleep-wake cycle needs to be further investigated.

Table 1.1. Astrocyte activity and effects of modulating activity on the sleep-wake cycle.

Reference	Technique	Brain region	Ca^{2+} Activity/ Effect
Tsunematsu et al. 2021	Fibre Photometry	Cortex	Lowest during REM sleep, highest during wake
		Hippocampus	Lowest during REM sleep, highest during wake
		Hypothalamus	Lowest during REM sleep
		Pons	Lowest during REM sleep
Ingiosi et al. 2023	Chemogenetic activation	Basal forebrain	↑ wakefulness
Peng et al. 2023	Fibre Photometry	Basal Forebrain	Lowest during NREM sleep, high during wake and REM sleep
	Chemogenetic activation	Basal forebrain	↓ REM sleep
	Fibre Photometry	LC/SLD	Lowest during NREM sleep, high during wake and REM sleep
	Chemogenetic activation	LC/SLD	↓ REM sleep
Cai et al. 2022	Chemogenetic activation	Lateral hypothalamus	↑ wakefulness
	Chemogenetic inhibition		↓ wakefulness ↑ NREM sleep

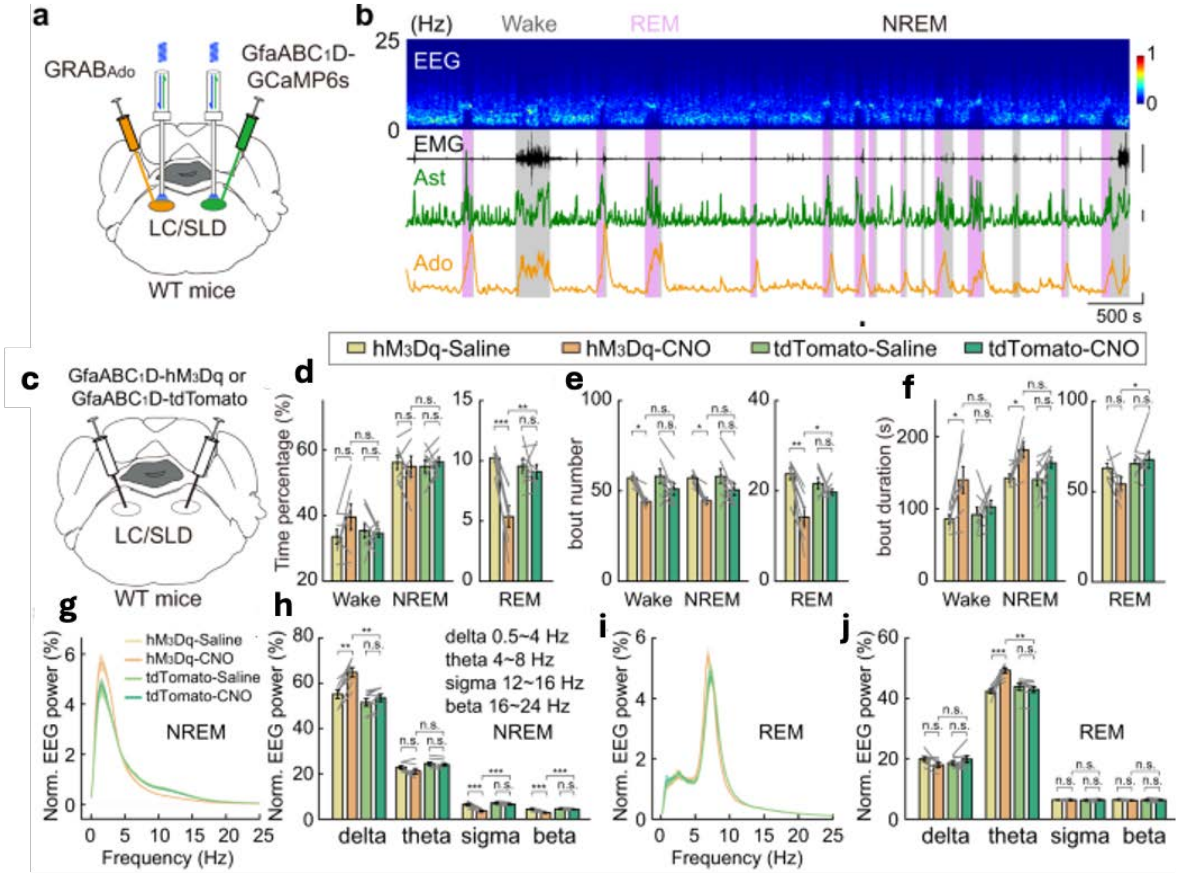

Figure 1.13. Sleep regulation by brainstem astrocytes. **a)** Schematic diagram of fiber photometry recording of astrocyte population Ca2+ signal and extracellular adenosine level in LC/SLD region of the brainstem. **b)** Top to bottom, EEG power spectrogram, EMG (scale, 1 mV), GCaMP fluorescence (scale, 1 z-score), and $GRAB_{Ado}$ fluorescence (scale, 1 z-score). **c)** Schematic diagram of chemogenetic activation of astrocytes in the LC/SLD. **d-j)** Chemogenetic activation of LC/SLD astrocytes in WT mice significantly changed sleep–wake behaviour, including total percent time in state **(d)**, bout number **(e)**, bout duration **(f),** EEG power in NREM **(g-h)** and REM sleep **(i-j)**, within 4 hours after CNO injection. hM3Dq group, n = 7 mice; tdTomato group, n = 8 mice. The statistical method used was two-way repeated measures ANOVA, followed by Tukey's post hoc multiple comparison test. ns, p>0.05, *p<0.05, **p<0.005, ***p<0.001.

Adapted from Peng, et al., 2023.

1.3.5. Tools for studying astrocytes

Over the past several decades, important progress in understanding the diverse functions of astrocytes has been made. However, due to the complexity of astrocytic signalling, studies can be challenging, and therefore the characterisation of astrocytes remains incompletely understood. Recent advances in genetic manipulation and *in vivo* imaging techniques have furthered the knowledge of astrocytic activity, but some issues remain. In the following subsections, I will discuss the techniques used to study astrocyte activity, with a focus on *in vivo* methods.

1.3.5.1. *Molecular markers and visualising astrocytes*

Molecular profiling of astrocytes has identified several useful molecular markers. The first to be associated with astrocytes was intermediate filament glial fibrillary acidic protein (GFAP), which is important for astrocyte motility and structure (Eng *et al.*, 2000). Despite GFAP being expressed in many of mature astrocytes, particularly during astrogliosis where GFAP is upregulated, not all astrocytes express detectable levels of GFAP, particularly in certain brain regions such as the thalamus. Other limitations of GFAP include lack of expression in astrocytic fine processes and therefore display simplified structure in immunohistochemistry, (Endo *et al.*, 2022; Bushong *et al.*, 2002; Reeves *et al.*, 2011; Khakh and Sofroniew, 2015; Sofroniew and Vinters, 2010), however, GFAP remains one of the most widely used marker for astrocyte studies. Other popular astrocytic markers include cytosolic protein S100β, glutamate synthetase, and folate enzyme aldehyde dehydrogenase 1 family member L1 (Aldh1L1), however, these molecules are not exclusively expressed by astrocytes and each offer different advantages and disadvantages (Endo *et al.*, 2022; Escartin *et al.*, 2021; Sofroniew and Vinters, 2010; Khakh and Sofroniew, 2015; Yu *et al.*, 2020). Due to the molecular and genetic diversity of astrocytes across distinct brain regions, which has recently been further characterised (Endo *et al.*, 2022), it would be advantageous to develop several different markers which are optimal for specific brain regions, and could be selected according to the needs of individual studies.

1.3.5.2. *Transgenic and viral approaches*

These molecular markers have been utilised to construct several Cre-dependent or tetracycline-controllable transgenic mouse lines (Yu *et al.*, 2020). Mouse lines *Aldh1l1*-CreERT2 and *Gfap*-Cre are the most common mouse lines used to target astrocytes and display high expression in astrocytes in adult mice, however they display some expression in other cell types such as oligodendrocytes (Srinivasan *et al.*, 2016; Winchenbach *et al.*, 2016; Sofroniew, 2012; Yu *et al.*, 2020). In addition, transgenic techniques are not specific to brain region, making circuit-specific investigations challenging.

Using viral vectors with astrocytic promotors is one way to overcome this issue. Lentiviruses and adeno-associated viruses (AAVs) are the most widely used methods of viral delivery methods. While lentiviruses can carry larger viral loads, AAVs can be concentrated to higher titre concentrations as they do not integrate into the genome, giving them higher efficiency (Nagai *et al.*, 2019). Recent advances in AAV-microRNA targeting sequences, as well as developing new AAV serotypes, have shown improvements in cell specificity and potency, with minimal off-target expression (Gleichman *et al.*, 2023; Han *et al.*, 2023). Astrocyte-specific promotors can be used to introduce cell-specificity. The *GfaABC$_1$D* (681bp) promotor is derived from the previously developed human *GFAP* promotor gfa2 (2210 bp). *GfaABC$_1$D* has twofold greater activity than gfa2, and its smaller size makes it highly efficient for viral vector delivery (Lee *et al.*, 2008). AAVs under the control of the *GfaABC$_1$D* promotor have been successfully used with very high astrocyte specificity in various brain regions in mice, rats, and macaque monkeys (Zhang *et al.*, 2022a; Heffernan *et al.*, 2022; Du *et al.*, 2021; Nagai *et al.*, 2019; Yu *et al.*, 2018; Dvorzhak *et al.*, 2016; Adamsky *et al.*, 2018; Testen *et al.*, 2020; Huntington and Srinivasan, 2021). *GfaABC$_1$D* has also been used in combination with a newly developed type of AAV variant, PHP.eB. It causes widespread astrocyte expression with high specificity delivered via intravenous injection (Chan *et al.*, 2017). This provides a relatively non-invasive alternative to mouse lines but lacks the region specificity of other viral methods. Other promotors such as *Aldh1l1* have shown little astrocyte-specificity and actually show higher expression in neurons when used in combination with viral vectors (Koh *et al.*, 2017; Mudannayake *et al.*, 2016). For this reason, *GfaABC$_1$D*-containing viral vectors are an optimal option for targeting astrocytes.

1.3.5.3. Measuring astrocyte activity

As astrocytes are not electrically excitable, unlike neurons, their natural activity was previously hard to characterise. Most studies examined astrocytes using *ex vivo,* or *in vitro* studies, and largely focused on morphological changes and gene/ protein expression (Ingiosi and Frank, 2022). Only recently, technology advances have allowed studies to measure *in vivo* astrocyte activity, represented by intracellular Ca^{2+} levels, largely using techniques such as one- and two-photon microscopy and fibre photometry. Microscopy techniques, specifically two-photon imaging, can measure

detailed changes in astrocytic Ca^{2+}, including in finer structures such as astrocytic processes (Ingiosi *et al.*, 2020; Vaidyanathan *et al.*, 2021; Bojarskaite *et al.*, 2020a). Imaging studies traditionally meant that animals would have to be head-restrained in order to prevent movement of the imaging plane, thus affecting natural behaviour (Bojarskaite *et al.*, 2020a; Vaidyanathan *et al.*, 2021). However, recent advances in miniaturised microscopes has allowed application for freely moving animals and deep brain imaging (Sekiguchi *et al.*, 2016; Ingiosi *et al.*, 2020), while advances in genetically encoded sensors has improved resolution of imaging techniques (Zheng *et al.*, 2015; Srinivasan *et al.*, 2015; Bindocci *et al.*, 2017; Stobart *et al.*, 2018). However, a major caveat for traditional imaging studies is that they cannot be applied to deep brain structures, and while techniques such as miniaturised microscopes can overcome this issue, they tend to be more invasive and have lower resolution.

Alternatively, fibre photometry can be used to measure population astrocyte activity in freely moving animals, without strict limitation of target brain regions (Tsunematsu *et al.*, 2021; Suthard *et al.*, 2023; Cai *et al.*, 2022; Han *et al.*, 2023; Reitman *et al.*, 2023; Noh *et al.*, 2023). Fibre photometry is a technique that consists of expressing genetically-encoded indicators/sensors to measure cell-type specific population activity, or extracellular ligands activity, using optic fibres (**Fig.1.14**) (Byron and Sakata, 2024; Simpson *et al.*, 2024). By delivering light at a specific wavelength to the expressed biosensor through an implanted optic fibre, a conformational change in biosensor occurs, which emits fluorescence. The intensity of the emitted fluorescence is collected using a photodetector, and this signal can be processed and analysed to depict cell activity (**Fig. 1.14**) (Simpson *et al.*, 2024). The pioneering study of fibre photometry used a chemical calcium-sensitive dye (Adelsberger *et al.*, 2005), however, currently GCaMPs are the most popular sensors. GCaMPs were first developed in 2001, and are composed of a single green fluorescent protein fused with calmodulin (CaM) and CaM-interacting peptide M13 (Nakai *et al.*, 2001; Chen *et al.*, 2013b). Over the past few decades, several types of GCaMPs have been developed, with varying characteristics, such as fast and slow kinetics, high contrast with low baseline fluorescence, and various sensitivity (Zhang *et al.*, 2023; Dana *et al.*, 2019; Yang *et al.*, 2018; Akerboom *et al.*, 2012). Thus, the unique requirements for an experimental design should be considered to select the most appropriate genetically-encoded sensor (Wu *et al.*, 2022b; Simpson *et al.*, 2024). In line with the previous

section, sensors can be expressed using transgenic mouse lines or using viral vectors (Simpson *et al.*, 2024). Growing interesting has also developed in modifying conventional multimode fibres to offer certain benefits, such as wireless technologies which improve freely-moving conditions or tapered fibres that are less invasive and delivery depth-resolved light (Pisano *et al.*, 2019; Burton *et al.*, 2020).

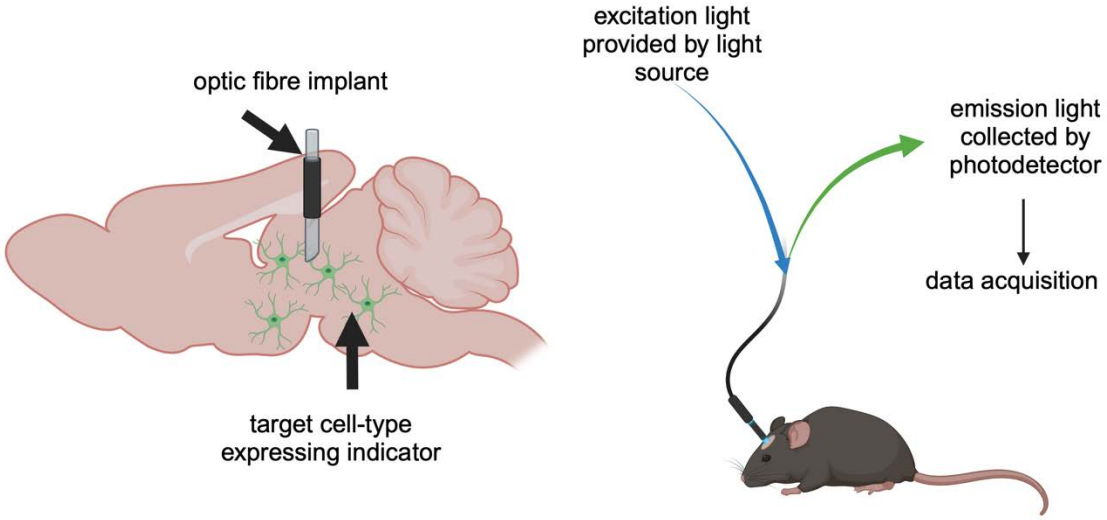

Figure 1.14. Simplified schematic of fibre photometry principles. Left, fibre photometry has two main requirements, expression of indicators, and implantation of optic fibre. Right, fibre photometry consists of an excitation light to stimulate a conformational change in the expressed indicator, giving rise to an emission light which can be collected and processed to reflect cell/ligand activity.

Created using BioRender.com

A major consideration in fibre photometry systems is that the collected signal can often be contaminated with background noise. Therefore, it is important to select appropriate controls which are not expected to elicit any physiological processes and can selectively measure background noise. For this, the most common approach is to use an 'isosbestic' light. An isosbestic light would be chosen at a wavelength that does not cause conformational changes to the expressed sensor, and thus any fluorescence collected at this wavelength could be used as a reference to correct against background noise and movement artifact (Simpson *et al.*, 2024). Another consideration for fibre photometry experiments is autofluorescence, which can occur from the optic fibre, brain tissue, or patch cable. To overcome this issue, low-autofluorescence patch cables can be used, additionally, photobleaching of patch

cables is recommended prior to beginning experiments (Pisanello *et al.*, 2014; Byron and Sakata, 2024; Simpson *et al.*, 2024). Overall, fibre photometry has been successfully used to measure astrocyte activity in multiple brain regions (Tsunematsu *et al.*, 2021; Zhang *et al.*, 2021a; Cai *et al.*, 2022; Suthard *et al.*, 2023; Noh *et al.*, 2023; Peng *et al.*, 2023), and is a key technique to measure Ca^{2+} activity in astrocytes.

1.3.5.4. Manipulating astrocyte activity

As astrocytes do not fire action potentials, manipulating their activity was largely overlooked until recent progress in technology. Intracellular astrocytic Ca^{2+} activity was first discovered in astrocyte cultures (Cornell-Bell *et al.*, 1990; Charles *et al.*, 1991), followed by slice experiments (Duffy and MacVicar, 1995), in anaesthetised animals (Hirase *et al.*, 2004), behaving animals (Wang *et al.*, 2006), and finally human cells (Oberheim *et al.*, 2009). Following these studies classifying astrocytic activity, the challenge remained of modulating astrocyte activity to further classify their activity.

Progress with astrocyte promoters has allowed for improvements in manipulating astrocytic activity using optogenetic and chemogenetic techniques. Optogenetic stimulation using channelrhodopsin2 (ChR2) has been used to excite astrocytes *in vivo* (**Fig. 1.15A**) (Gourine *et al.*, 2010; Perea *et al.*, 2014; Masamoto *et al.*, 2015; Pelluru *et al.*, 2016; Yamashita *et al.*, 2014; Sasaki *et al.*, 2012). However, ChR2-induced astrocytic activation causes increases in extracellular K^+ which affects neuronal firing (Octeau *et al.*, 2019; Yu *et al.*, 2020), making them generally undesirable for studying astrocyte activity. Furthermore, as astrocytes do not elicit action potentials, longer optogenetic stimulation is required (Octeau *et al.*, 2019).

Chemogenetic manipulation has become the most popular technique for manipulating astrocytic activity. Chemogenetic technology involves engineering macromolecules such as GPCRs to interact with previously unrecognised small molecules for the specific manipulation of a target cell population, a technique often referred to as designer receptors exclusively activated by designer drugs (DREADDs) (Shen *et al.*, 2021; Urban and Roth, 2015). Modified muscarinic, adrenergic, serotonergic, and k-opioid chimeric receptors are amongst the most commonly used. Of these, modified human M3 muscarinic G_q-PCR (G_q-coupled hM3D) and the human M4 muscarinic G_i-

PCR (G_i-coupled hM4D), are the most popular choices for activating and inhibiting neuronal/glial activity, respectively (Armbruster *et al.*, 2007; Roth, 2016; Urban and Roth, 2015). In terms of inducing astrocytic Ca^{2+} signalling, the G_q/phospholipase C cascade is activated intrinsically by noradrenergic α1 and muscarinic acetylcholine receptors, which triggers ATP release, phospholipase C (PLC) activation and IP_3-mediated release of intracellular Ca^{2+} from the endoplasmic reticulum (**Fig. 1.15B**). Following modifications to hM3D, it responds solely to synthetic designer activating ligands, such as clozapine N-oxide (CNO). Activating astrocytes using chemogenetics has successfully been used in many studies across brain regions (Adamsky *et al.*, 2018; Agulhon *et al.*, 2013; Van Den Herrewegen *et al.*, 2021; Martin-Fernandez *et al.*, 2017; Wahis and Holt, 2021; Durkee *et al.*, 2019; Chai *et al.*, 2017; Ding *et al.*, 2013; Peng *et al.*, 2023; Cai *et al.*, 2022; Ingiosi *et al.*, 2023). Inhibiting astrocytic Ca^{2+} signalling using chemogenetics, on the other hand, is more challenging. While the exact G_i pathway in astrocytes remains unclear, G_i activation also seems to lead to increased IP_3-mediated intracellular Ca^{2+} concentration and triggers gliotransmission (**Fig. 1.15B**) (Yu *et al.*, 2020; Durkee *et al.*, 2019; Chai *et al.*, 2017; Nagai *et al.*, 2019).

A major consideration when using chemogenetics is the activity of DREADDs agonists. CNO is most commonly used and was originally reported to be pharmacologically inert and have no off-target binding (Armbruster *et al.*, 2007). However, CNO can be reverse-metabolised into parent compound clozapine, with both clozapine and CNO being reported to bind at several off-target receptors (Jendryka *et al.*, 2019; Gomez *et al.*, 2017). Application of CNO alone, without expression of DREADDs, has been shown to alter the sleep-wake cycle, particularly at high doses, reducing proportion of REM sleep in total sleep time, and REM sleep episode number, increasing REM sleep episode duration and latency to REM sleep, as well as increasing NREM sleep time, episode duration, and reducing NREM sleep latency and episode number (Traut *et al.*, 2023). This puts a large emphasis on the importance of having multiple control groups for chemogenetic studies, particularly for studies investigating sleep. Alternatively, new DREADDs agonists have been developed which are not reverse metabolised to clozapine and avoid off-target effects (Chen *et al.*, 2015; Thompson *et al.*, 2018; Nagai *et al.*, 2020). In particular deschloroclozapine (DCZ) displays high potency and selectivity, and has no reported off-target binding (Nagai *et al.*, 2020)

Inhibiting astrocytic activity using other methods are possible, but the efficacy of such techniques is debatable. Targeting IP_3, which is highly involved in one of the major pathways giving rise to astrocytic Ca^{2+} release, is one of these methods. Mice lacking IP_3 receptor-2 (IP_3R2), the primary IP_3 receptor found in rodents, lack spontaneous and evoked astrocytic Ca^{2+} signalling, without knock-on effects on neuronal signalling, however, this reduction was only found in the soma, not in astrocytic processes (Srinivasan *et al.*, 2015; Fiacco and McCarthy, 2018; Agarwal *et al.*, 2017). Using the Tet system with GLT1 promoter in transgenic mouse lines can create "IP_3 sponges", which compete with IP_3 for endogenous IP_3R2 binding, reduced metabotropic glutamate receptor (mGluR)-mediated astrocytic Ca^{2+} responses and reduced astrocytic coverage of neurons (Uchiyama *et al.*, 2002; Tanaka *et al.*, 2013), however also resulted in altered behaviours and detection of transgene expression in some neurons (Tanaka *et al.*, 2013; de Vivo *et al.*, 2010). Combining AAVs under the astrocyte promotor *GfaABC$_1$D* along with protein p130 (p130PH), which acts as a mobile cytosolic IP_3 buffer, reduces cortical astrocyte activity by ~70% (Xie *et al.*, 2010), however the mechanisms of how this occurs are unclear. Alternatively, a genetic approach was developed which utilises a human Ca^{2+} pump called plasma membrane Ca^{2+} ATPase isoform 2 splice variant w/b (hPMCA2w/b), which is not endogenously expressed in murine astrocytes and extrudes Ca^{2+} from cells, thus named 'calcium extruder' (CalEx) technique (**Fig. 1.15C**) (Yu *et al.*, 2018). AAVs under the control of *GfaABC$_1$D* overexpressing hPMCA2w/b can induce expression in astrocytes and therefore attenuate astrocyte signalling regardless of Ca^{2+} source. Using this methods, reduced astrocytic Ca^{2+} was found in the soma, branches and processes and reduced tonic inhibition of striatal medial spiny neurons via blocking astrocyte GABA transporter 3 (GAT3) (Yu *et al.*, 2018; Yu *et al.*, 2021). However, this calcium attenuation technique has relatively slower dynamics in comparison to chemogenetics or optogenetics.

Overall, chemogenetic activation of astrocytes by activating G_q-coupled hM3D, delivered via an AAV under *GfaABC1D* promotor is currently the most accurate way of inducing astrocyte activity, and provides flexibility in terms of target region. On the other hand, 'CalEx' appears to be the most promising method to diminish astrocyte activity.

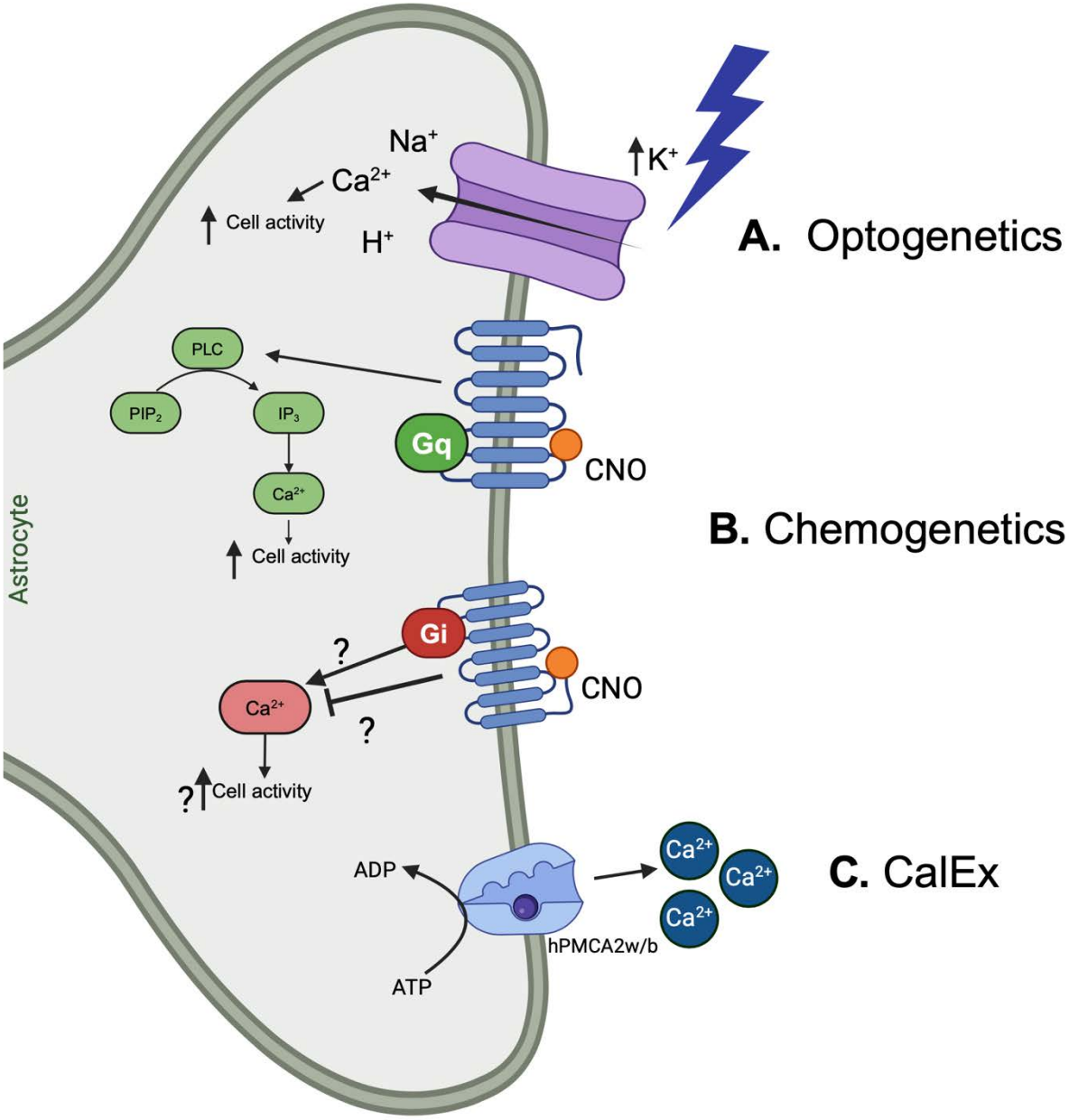

Figure 1.15. Techniques for modulating astrocyte activity. **A.** Optogenetic light stimulation of Chr2 causes it to open allowing for an influx of Ca^{2+}, Na^{+} and H^{+} leading to increased intracellular Ca^{2+}, but also results in increased extracellular K^{+}. **B.** Top, Gq-couple GPCR activation leads to PLC activation and cleavage of PIP_2 into IP_3 which mediates intracellular Ca^{2+} realease. Bottom, Gi-couple GPCR activation has unknown consequences which has been mostly reported to cause increases in Ca^{2+} signalling. **C.** CalEx involves over expressing hPMCA2w/b which pumps Ca^{2+} outwards from cell.

GPCR = G-protein couple-receptor, PLC = phospholipase C, PIP_2 = phosphatidylinositol 4,5-biphosphate, IP_3 = inositol 1,4,5-triphosphate.

Image created using BioRender.com

1.4. Hypothesis and aims

In summary, growing interest in astrocyte function has developed over the last several decades. Given the robust functions of astrocytes, their role in executive functions has become of particular interest, including their impact on sleep. As initially outlined in this chapter, sleep is essential for our health and is highly involved in regulating memory and learning, and is altered during neurodegenerative disorders such as AD. In comparison to NREM sleep, REM sleep is relatively understudied but is thought to contribute to learning and memory consolidation, and reductions in REM sleep occur in patients with AD. Interestingly, in such disease pathology, astrocytes are also altered and can undergo reactive astrogliosis. Thus, understanding if, and how, astrocytes are involved in REM sleep regulation could contribute towards our understanding of disease pathology.

While convincing evidence for changes in astrocyte activity throughout the sleep-wake cycle has been outlined in studies so far, the effects of modulating astrocyte activity is relatively unstudied, particularly in hindbrain regions such as the pons, which are known to be a central regulatory region for REM sleep. Tsunematsu *et al.* recently showed that pontine astrocytic Ca^{2+} levels were lowest throughout the sleep-wake cycle during REM sleep. However, a conflicting study by Peng *et al*. showed that pontine astrocyte activity was increased during REM sleep compared to NREM sleep. Contradictingly, they subsequently showed a reduction in REM sleep following chemogenetic astrocytic stimulation. Further investigations which modulate pontine astrocyte activity would develop our understanding of their contribution to sleep. This information will provide insight for the possibility of modulating such astrocyte activity to manipulate sleep outcomes, and sleep-mediated functions such as memory. If such a link is found, this could lead to advancements in therapeutic strategies for various disease states in which REM sleep and memory are both altered, such as neurodegenerative diseases including AD.

This project is based upon the hypothesis that pontine astrocytes will play a regulatory role in REM sleep generation, thus increasing astrocytic activity will reduce REM sleep incidence. We also hypothesised that, given the implicated involvement of

hippocampal theta for spatial memory, if REM sleep could be reduced by activating pontine astrocytes, spatial memory would be impaired. To investigate this, we aimed to chemogenetically activate pontine astrocytes using various concentrations of CNO and monitor changes to the sleep-wake cycle. Given previous research finding changes in the sleep-wake cycle dur to CNO alone, we carefully designed our experiments to include several control groups. We then aimed to determine such astrocytic modulation would affect memory *in vivo* using a spatial memory test.

In the following chapter, I will describe the techniques we used to address our hypotheses and aims.

2. Material and Methods

In this chapter, I will describe the methods and materials that were used throughout this project. First, I will provide a brief summary about the animals used (section 2.1), and which type of experiments they were used in, which will be expanded on in the relevant results chapters. Next, I will clarify how implants for surgeries were fabricated (section 2.2), followed by detailed descriptions of all types of surgeries that were done throughout this project (section 2.3). I will then outline the different types of experiments that were carried out. Firstly, this will involve details about chemogenetic experiments, including how drug treatments were prepared, the electrophysiology system which was used for experiments, and finally explain how habituations and recordings were done, with reference to timelines of the entire experiment (section 2.4 and section 2.5). Details regarding the methods and materials used in behavioural experiments will then be reported (section 2.6). Next, fibre photometry experiments will be described by outlining the system used, and how recordings were completed, with reference to experimental timelines (section 2.7). I will then provide details about histology procedures and the materials used (section 2.8). Finally, approaches for data analysis and statistical analysis for all experiments will be described (section 2.9 and section 2.10).

2.1. Animals

All experiments were performed in accordance with the UK Animals (Scientific Procedures) Act of 1986 Home Office regulations (PP0688944), and with the consent of the University of Strathclyde's Ethical Committee. A total of 94 wild-type (WT) C57BL/6 mice (consisting of 55 males and 39 females aged 8-24 weeks upon time of surgery) have been used in this project. In this project, 4 of these mice were used for surgical technique training and optimisation of surgical procedures. 43 mice were used during chemogenetic studies (Chapter 3), of which 11, and an additional 33 mice were used for memory tests (Chapter 4). Finally, 14 mice were used for pilot fibre photometry studies (Chapter 5) (**Fig. 2.1A**). A detailed breakdown of the animals used in different experiments and the inclusion criteria for experiments will be described in the relevant results chapters. Animals were provided with *ad libitum* access to food and water and were housed with sex-matched littermates where possible, or otherwise

housed individually, in a 12:12 hour light/dark cycle. All experiments were performed during the light-on period (7:00-19:00 zeitgeber time (ZT) 0-12).

An overview of each workflow can be seen in **Figure 2.1B**. Briefly, animals used in chemogenetic studies underwent virus injection surgeries (see section 2.3.2.2), and EEG/EMG headcap implantation surgery (see section 2.3.3) which required fabrication of EEG/EMG headcaps to be completed prior to surgery (see section 2.2.1). The methodology for chemogenetic experiments for these animals is explained in section 2.5 (for CNO preparation see section 2.4). After completing experiments these animals were perfused and their brain tissue extracted (see section 2.8.1-2.8.2) and used for immunohistochemistry (see section 2.8.2.1). Data analysis for histology (see section 2.9.1) and sleep scoring data (see section 2.9.2) and statistical analysis was applied (see section 2.10). The results from these animals are reported in **Chapter 3**. Animals used in memory tests underwent the same virus injection surgery protocol (see section 2.3.2.2) prior to behaviour experiments (see section 2.6) in which CNO preparation was also necessary (section 2.4). Brain extraction and histology was also done using the same protocols (see sections 2.8.1-2.8.2 and section 2.8.2.1, respectively) prior to data analysis which involved histological analysis (see section 2.9.1), behaviour analysis (see section 2.9.3), and statistical analysis (see section 2.10). The results from this subgroup of animals are reported in **Chapter 4**. Animals that were used in combined fibre photometry and chemogenetic experiments first underwent a unilateral virus injection surgery (see section 2.3.2.3), and then a joint EEG/EMG headcap implantation and fibre implantation surgery (see section 2.3.4). Prior to implantation surgeries, fabrication of EEG/EMG headcaps and fibres had to be completed (see section 2.2.1 and section 2.2.2, respectively). Experimental protocols for this animal group are outlined in section 2.7, in which CNO preparation was again necessary (see section 2.4). Following completion of experiments the brain tissue was extracted for these mice (see section 2.8.1-2.8.2) and immunohistochemistry was undertaken using a separate protocol to other animal groups (see section 2.8.2.2). Data analysis was done for histological data (see section 2.9.1), sleep scoring (see section 2.9.2) and fibre photometry data was processed (see section 2.9.4). The results from this subgroup of animals are reported in **Chapter 5**.

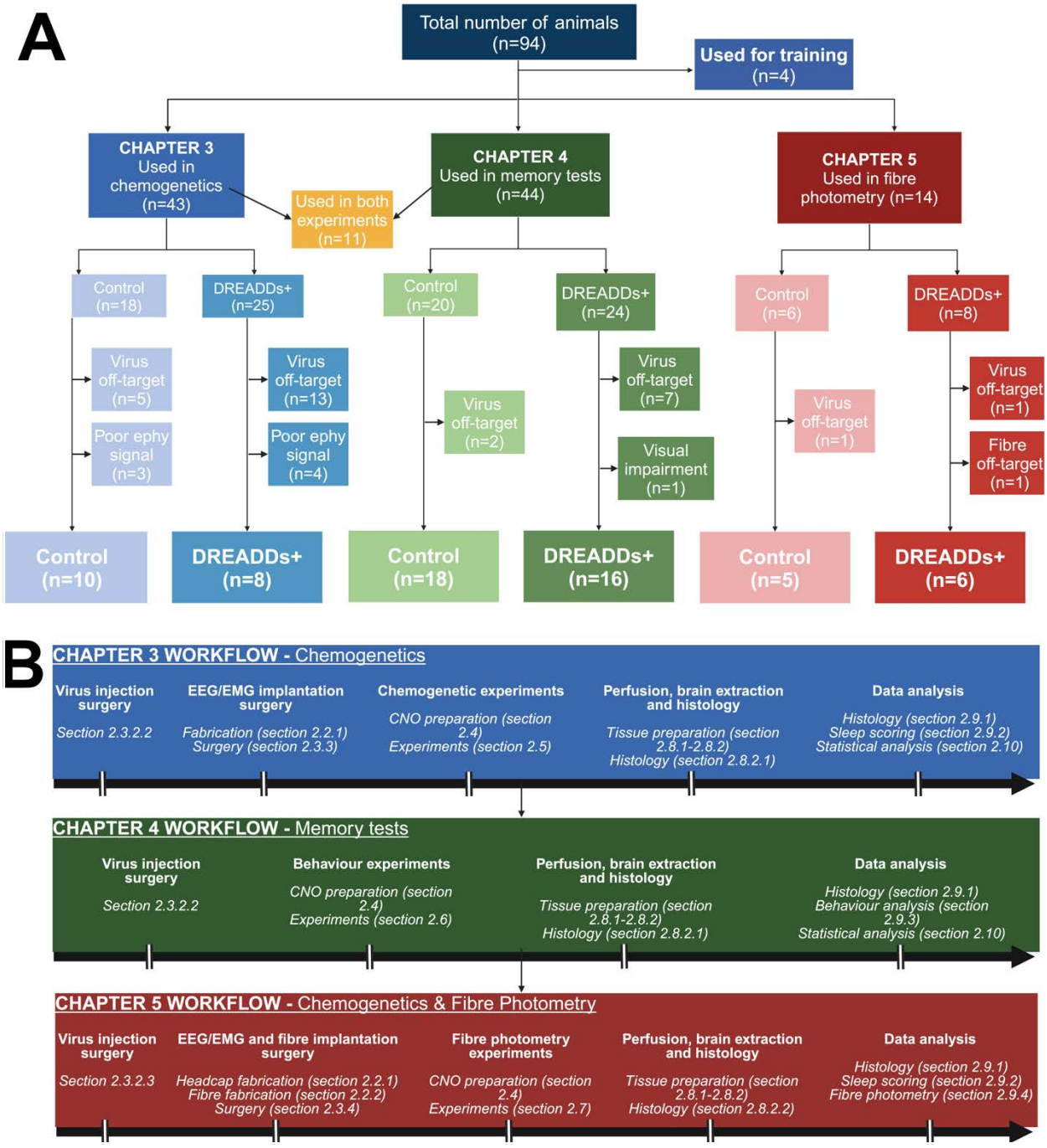

Figure 2.1. Flowchart of animals used in all experiments. A. From a total of 94 mice, 4 were used for training purposes, 43 were used for chemogenetic experiments, and 44 for memory tests. 11 of these animal were used in both experiments. 14 mice were used for fibre photometry experiments. **B**. Workflow of experimental methodology in each chapter, with reference to relevant sections for descriptions of methods.

2.2. Implant fabrication

2.2.1. Soldering EEG/EMG headcaps

Insulation was removed from either side of ~1cm sections of copper wires (Farnell, 357-918) for EEG and ground connections and red wires (Farnell, 2840/7) for EMG connections, and soldered to pins of 2x3 PCB sockets (RS components, 767-8944). Connections were tested using a voltmeter and secured using dental cement (Kemdent, Simplex rapid powder ACR803; Simplex rapid liquid ACR920) (**Fig. 2.2A-B**).

2.2.2. Fibre fabrication

Insulation from a section of 400 µm fibre patch cable (Thorlabs, FP400URT) was removed using a microstripper (Thorlabs, T21S31), and the fibre was cut into ~1.5 cm segments using a fibre optic scribe (Thorlabs, S90R). Fibres were inspected under a microscope to ensure edges were flat and undamaged. One side of the fibre was inserted into a ferrule (Thorlabs, CF230-10) and secured using epoxy (Opti-tec, OPT5053-F-B450G parts A and B). Once dried and solidified, the excess fibre was removed from the top of the ferrule, leaving only ~5mm of fibre exposed from the bottom side of ferrule. For polishing, the top side of the fibre was placed into a polishing disk (Thorlabs, D50-F), and several diamond lapping polishing sheets (Thorlabs, LF30D, LF6D, LF3D, LF1D, LFCF) were laid on a glass polishing plate. Using distilled water, the top of the ferrule and fibre were polished starting with the coarsest grit size polishing sheet, working down to the finest grit size polishing sheet (30, 6, 3, 1, 0.2 µm) (**Fig. 2.2C-D**).

To test the efficacy of the fibres, a baseline power output was first calculated using an analogue handheld laser power metre console (Thorlabs, PM100A), and attached photodiode power sensors (Thorlabs, S120C), by measuring the optical power of the 400 μm fibre cable alone at an LED output power of 5V. The baseline optical power was calculated for both LED laser wavelengths (405 nm and 470 nm). The fibres for testing were then connected to the fibre cable using a mating sleeve, and the optical power was measured at the same output powers for both wavelengths. For *in vivo* experiments using GCaMP6f, light powers in the range of 10-60 $\mu W/mm^2$ at the tip of optic fibre were used (Chen *et al.*, 2013b; Sylantyev and Rusakov, 2013).

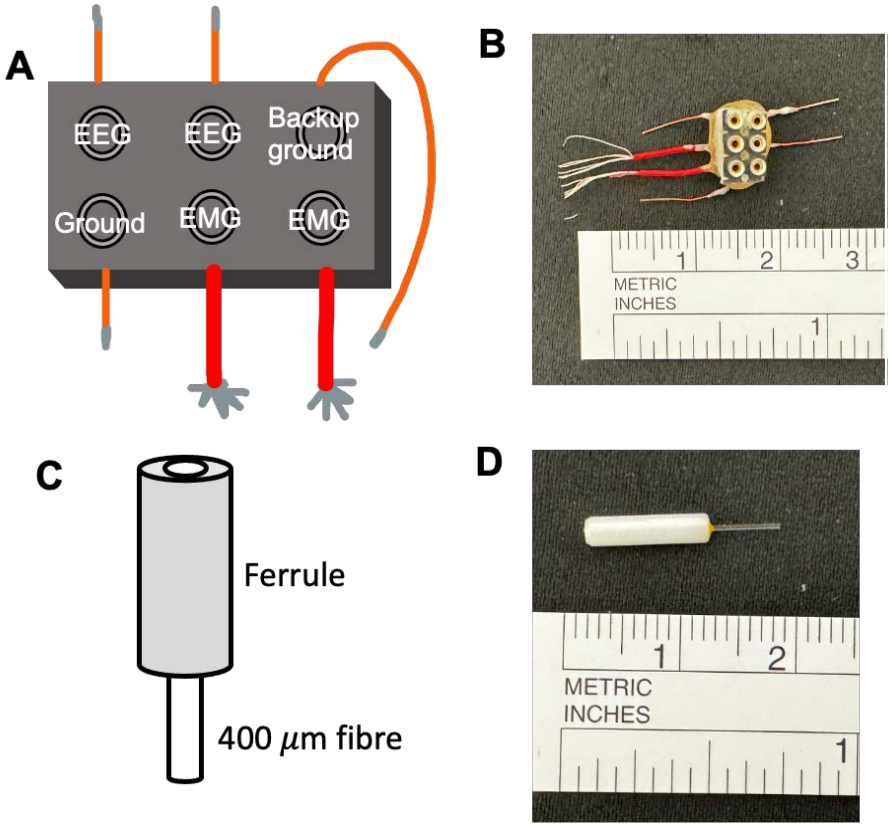

Figure 2.2. Schematic and images of headcaps and fibres. Layout and final construct of headcap (A-B), and fibre (C-D).

2.3. Surgeries

2.3.1. Anaesthesia and analgesia

Anaesthesia was induced by 5% isoflurane and 0.8 L/min oxygen airflow and lowered to 3% following loss of consciousness (**Fig. 2.3**). The head was shaved and then mice were moved to a stereotaxic frame (Narishige, SR-5M-HT) with teeth fitted into the incisor bar (**Fig. 2.3**). Heat was provided by placing animal on a heat pad (which was kept at 37°C throughout surgeries) to maintain body temperature throughout the surgery, and anaesthesia was maintained between 1-2% isoflurane and 0.8 L/min air flow, delivered via a nose cone (**Fig. 2.3**). The head was stabilised by fitting ear barring cones in the ear canals, and eye gel was applied on the eyes throughout the surgery to prevent drying. Breathing and lack of reflexes were monitored throughout surgery.

Analgesia was given prior to commencing surgery as 8 mg/kg local analgesia (Lidocaine or Naropin) subcutaneously at the head, and 20 mg/kg non-steroidal anti-inflammatory drug (NSAID) (Carprofen) and 0.1 mg/kg opioid (Buprenorphine)

subcutaneously at the lower back, sites were cleaned with ethanol prior to injections. 0.3-0.4 ml of saline was injected subcutaneously following surgery to support recovery, and a second oral dose of 20 mg/kg Carprofen was administered 24 hours following surgery. All surfaces were disinfected prior to surgery, and aseptic techniques were maintained during surgery by using sterile surgery gloves, and autoclaving gowns, surgical equipment, and drapes to cover the surgical environment.

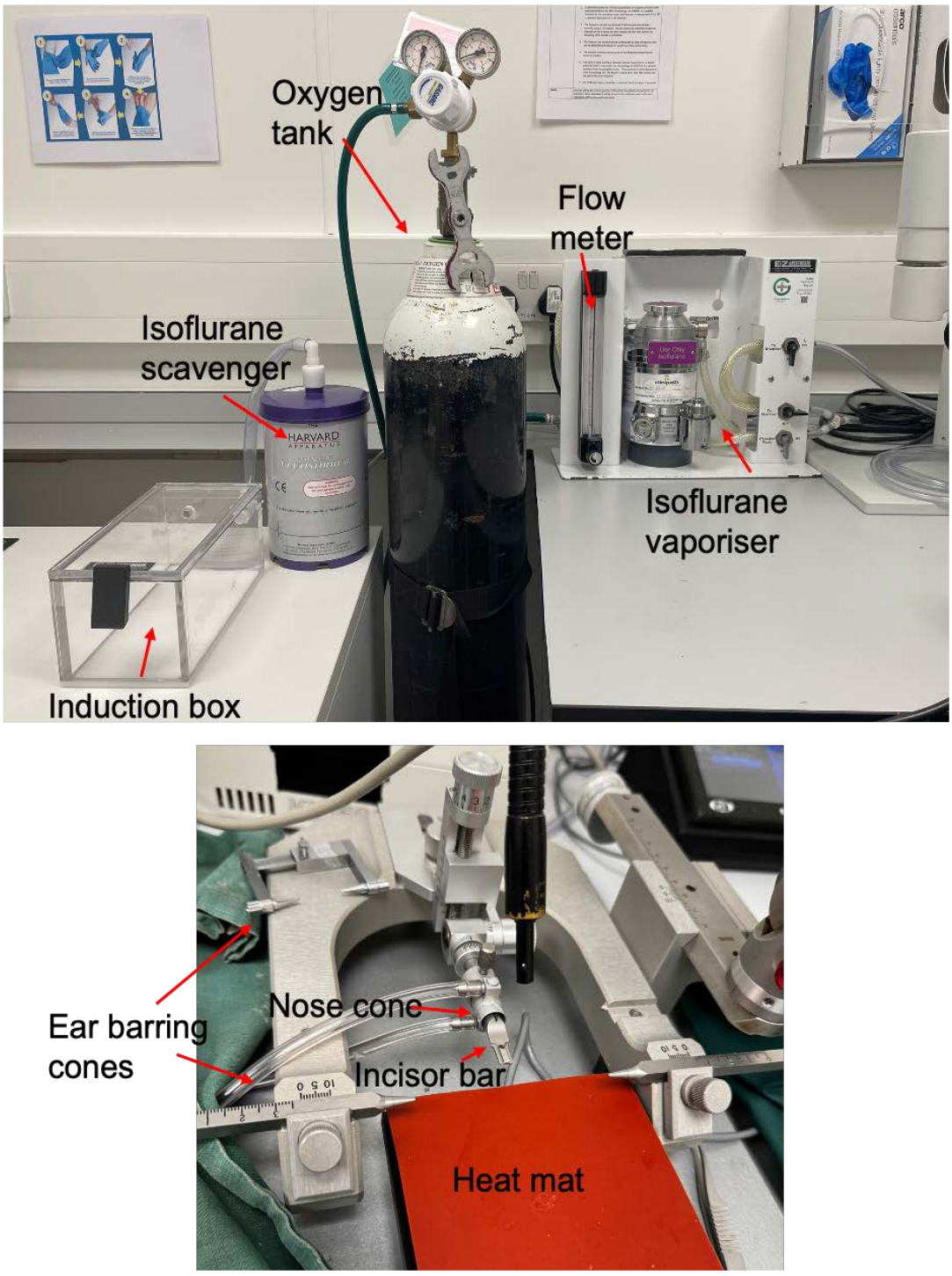

Figure 2.3. Anaesthesia set up. Anaesthesia induction begins in the induction box (top), before animals are moved onto a stereotaxic frame where anaesthesia is delivered via the nose cone (bottom).

2.3.2. Viral injections

2.3.2.1. General start of viral injection surgery

After mice were anaesthetised and prepped for surgery, the head was covered in betadine to promote healing and prevent infection, and an incision was made down the midline of head. The periosteum was then dissolved using hydrogen peroxide and removed using surgical scissors. Using bregma and lambda (**Fig. 2.4**), the head was levelled to a difference of less than 100 μm, ideally >50 μm, for precise and accurate targeting of stereotactic coordinates. Burr holes were drilled over the site(s) of interest at a 90° angle. Sterile phosphate-buffered saline (PBS) was then used to clean the scull surface from scull fragments and blood.

2.3.2.2. Animals used in chemogenetic-only and memory testing experiments

For animals used in chemogenetic-only experiments or memory testing, 200-300 nl of either AAV5-gfaABC$_1$D-tdTomato (Addgene, 44332-AAV5; ≥ 7×10^{12} gc/mL) or AAV5-gfaABC$_1$D-hM3D-mCherry (provided by Dr. Jun Nagai, 3x10^{12} gc/mL) was ejected bilaterally into the region of the SLD (from bregma; -5.1 mm anterior/posterior (AP), ± 0.8 mm medial/lateral (ML), from brain surface; -3.2 mm dorsal/ventral (DV)) at a rate of 50 nl/min (**Fig. 2.4** & **Fig. 2.5**). Such co-ordinates were chosen based on previous publications (Tsunematsu *et al.*, 2020; Uchida *et al.*, 2021; Patel *et al.*, 2020; Feng *et al.*, 2020; Krenzer *et al.*, 2011). Volumes of viral injections were originally 300 nl, which were reduced to 250 nl and eventually reduced to 200 nl to minimise viral spread, based on histological data. Several animals included in memory tests only were injected with a second batch of AAV5-gfaABC$_1$D-hM3D-mCherry (provided by Dr. Jun Nagai, 1x10^{13} gc/mL) at a dilution of 1:2 hM3D:saline.

2.3.2.3. Animals used in combined fibre photometry and chemogenetic experiments

For animals used in combined fibre photometry and chemogenetic experiments, equal volumes of AAV5-gfaABC$_1$D-GCaMP6f (Addgene, 52925-AAV5; ≥ 7×10^{12} vg/mL) and either AAV5-gfaABC$_1$D-tdTomato or AAV5-gfaABC$_1$D-hM3D-mCherry were mixed together and 200 nl of the final combination was injected unilaterally into the SLD (from

bregma; -5.1 mm AP, + 0.8 mm ML, from brain surface; -3.2 mm DV) at a rate of 50 nl/min (**Fig. 2.4**).

2.3.2.4. General end of viral injection surgery

As per the “pocket” technique, the pipette was initially slowly lowered an extra 20 μm depth than the area of interest for 1-2 minutes before returning to the correct position to create a pocket, in hope that this would prevent upwards leakage along the injection pathway and result in a more accurate delivery of virus to correct position. The “sandwich” technique, layering virus between layers of mineral oil, was originally used to minimise viral leakage along injection pathway, but due to damage caused from air bubbles, this technique was discontinued.

After the injection was complete, brain tissue was left to settle for at least 10 minutes before the pipette was removed. For animals used in chemogenetic and memory test experiments this process was repeated for the other hemisphere. Injection sites were covered with a biocompatible silicone adhesive (Kwik-Sil or Kwik-Cast, World Precision Instruments) to seal the skull, and sutures were used to close the incision (Ethicon Ethilon 1865H Black 5-0 suture PC-3 45cm). Mice were given post-operation fluids, and analgesia as previously described, and closely monitored for the following 4 days.

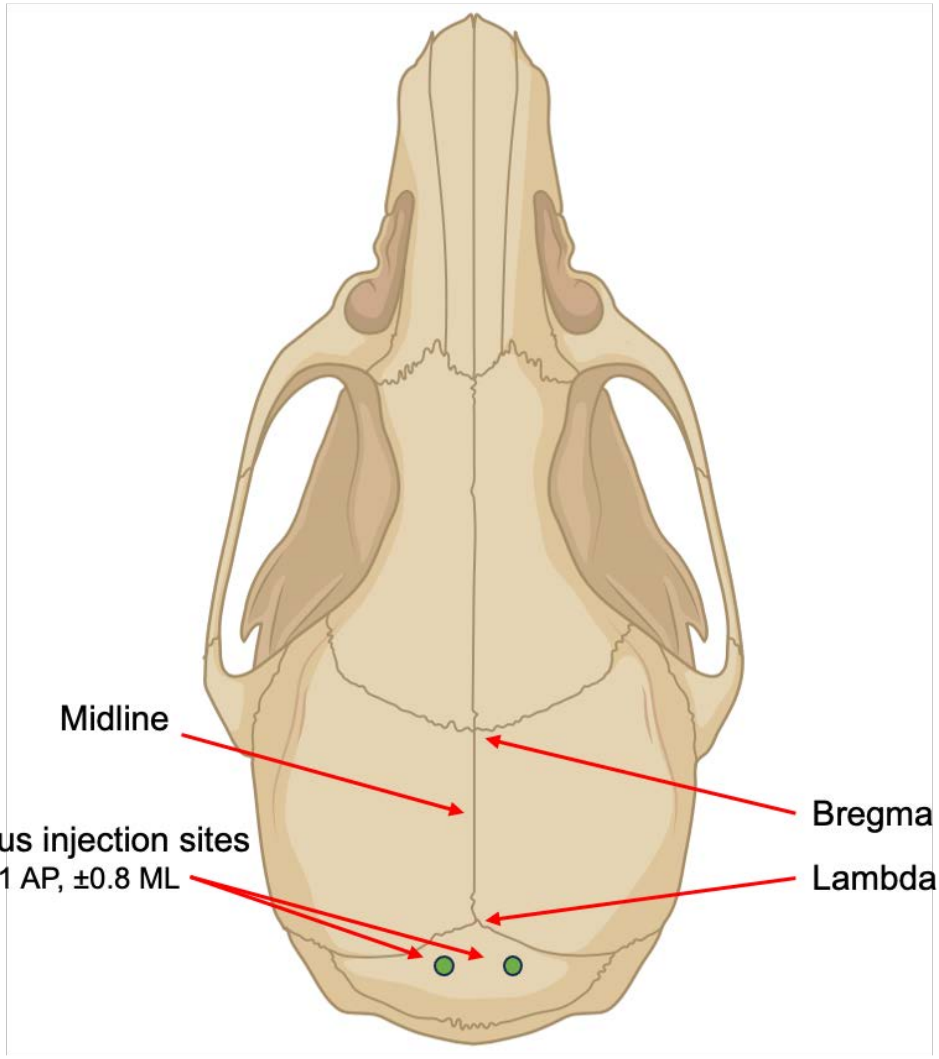

Figure 2.4. Skull markings and injection site.

Image created using BioRender.

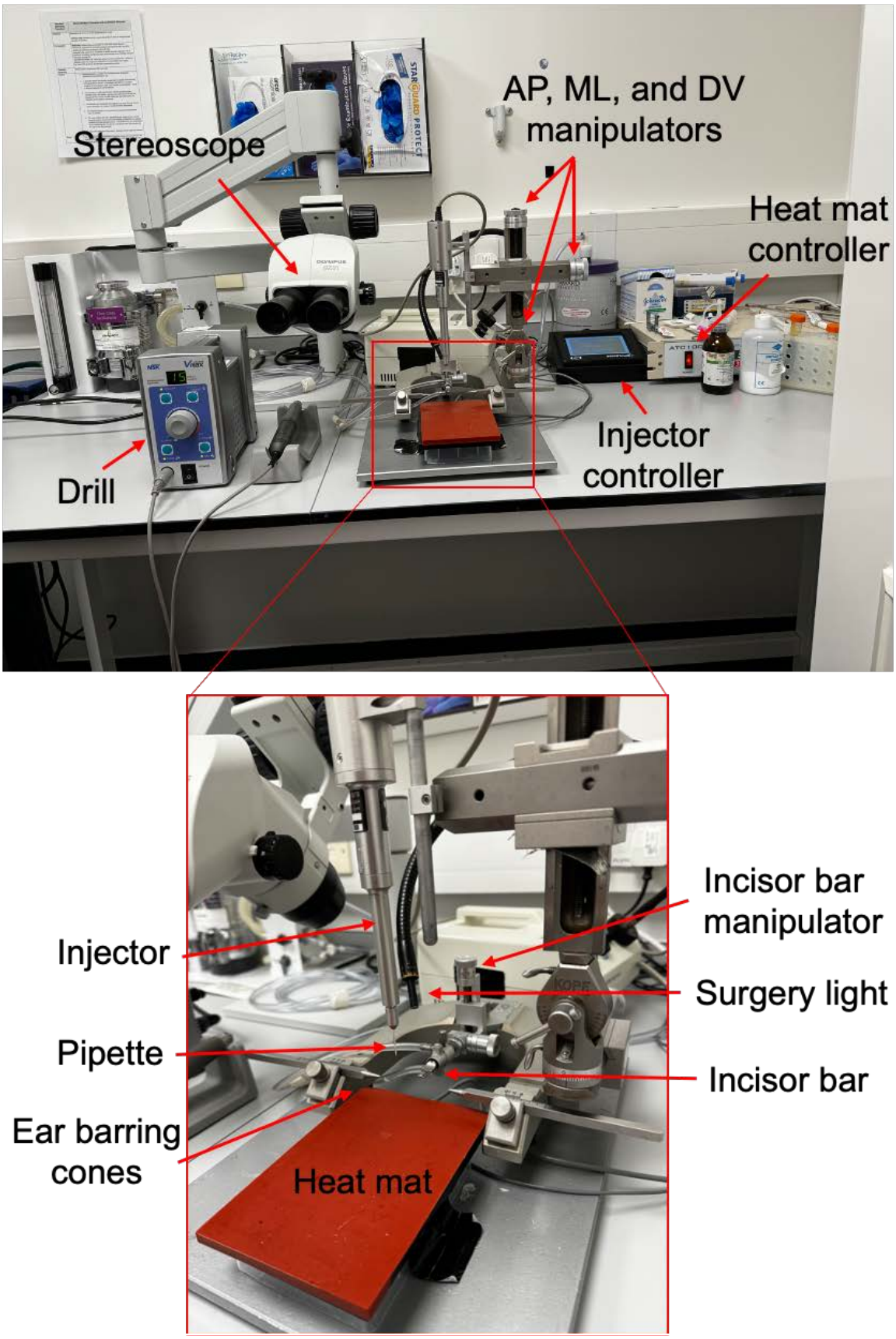

Figure 2.5. Surgical set up for virus injections.

2.3.3. EEG and EMG headcap implantation

As described previously, the head was shaved and covered in betadine to promote healing and prevent infection, and an incision was made down the midline of the head. The incision was then expanded, and excess skin was removed using forceps and surgical scissors, and periosteum was dissolved using hydrogen peroxide and removed. Skull screws were fitted into burr holes over the pre-frontal cortex for EEG connections (bilaterally from bregma; +1.5 mm AP, ±1.0 ML) and over the cerebellum for ground connections (bilaterally from lambda; -2 mm AP, ±2 mm ML) and the uninsulated part of relevant EEG and ground wires were twisted and tightened around screws (**Fig. 2.6,** without fibre). A voltmeter was used to ensure firm connections between wires and screws. EMG wires were placed under the skin at the back of the neck for contact with the neck muscle. The head cap was secured with dental cement, and the skin was sealed using dental cement. In some animals, EEG implants were made over the hippocampus (from bregma; -2 mm AP, ±1.5 ML) on one hemisphere to test the difference in the quality of EEG signals between the pre-frontal cortex and hippocampus. Such difference in quality was minor, so the pre-frontal cortex was used for the majority of mice due to ease of positioning the headcap. Mice were given post-operation fluids, and analgesia as previously described, and closely monitored for the following 4 days. To allow for recovery, habituations and experiments begun at least one week after headcap surgery.

2.3.4. Fibre implantation

An incision was made and expanded as described above. The skull was levelled by measuring bregma and lambda (<50 μm) using a 'dummy' fibre fitted into a custom-made attachment to the stereotaxic frame. If the previous site from virus injection surgery was not visible, the fibre-implant site was measured and marked. Skull screws for EEG and ground connections were fitted as described above and the wires from the headcap were attached and secured, and the EMG wires were placed under the skin at the neck (**Fig. 2.6**). A burr hole was made over the fibre implant location and any remaining Kwik-Cast from the previous surgery was removed. Craniotomy tweezers were used to ensure the bone was properly removed, and to pierce the dura. The fibre was slowly lowered into the target location using the manipulator (from bregma; -5.1 AP, +0.8ML, from brain surface; -3.1 DV) (**Fig 2.5**) slightly dorsal from

virus injection to receive optimal fluorescent signal. During insertion, the fibre was retracted slightly every ~1000 nm to allow the brain tissue to adjust and avoid damage. The brain was left to settle for 10 minutes and the burr hole around the fibre was covered using Kwik-Cast. The exposed fibre and bottom of the ferrule were covered in superglue (RS Components, 918-6872), which was then covered in a layer of dental cement. Alternating layers of superglue and dental cement were applied until the fibre, and headcap were secured. Once the fibre was secure, the stereotaxic frame attachment was removed, and a ceramic cap was placed over the fibre for protection (**Fig. 2.6,** insert). Mice were given post-operation fluids, and analgesia as previously described, and closely monitored for the following 4 days. To allow for recovery, habituations and experiments begun at least one week after implantation surgery.

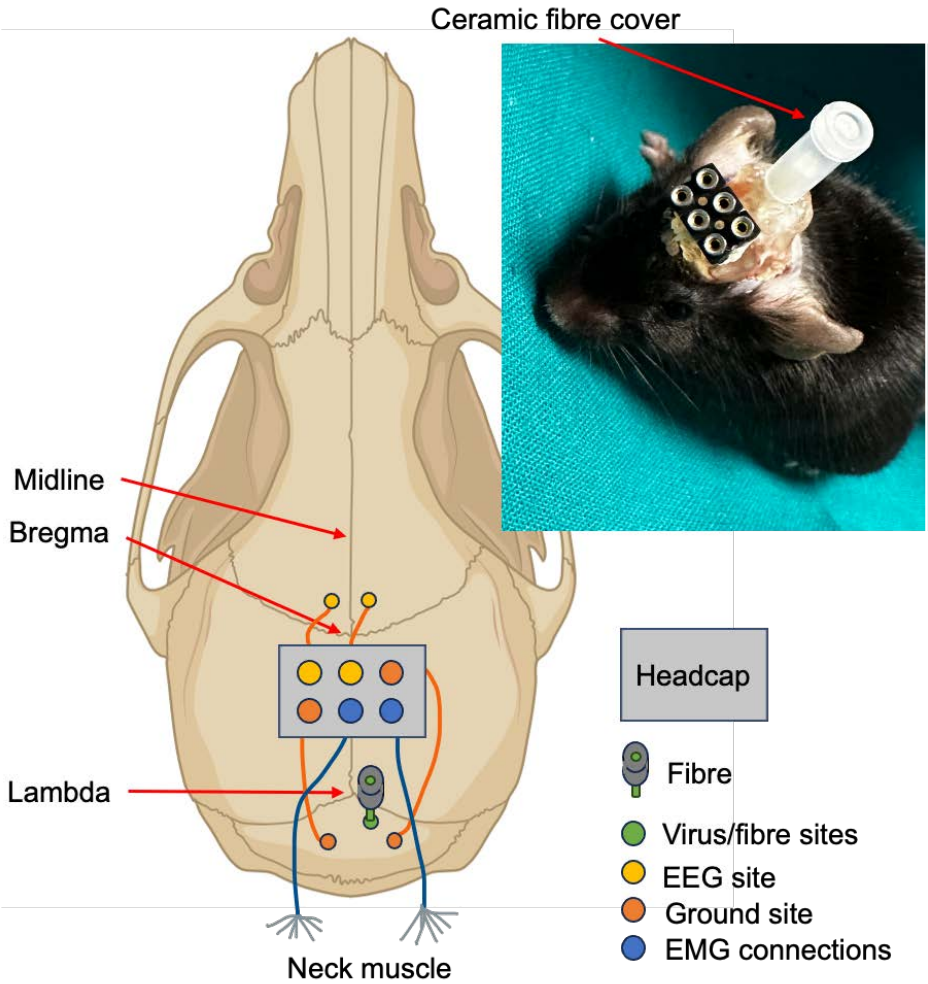

Figure 2.6. Arrangement of headcap and fibre after fibre implantation surgery.

Image created using BioRender.

2.4. CNO preparation

2.4.1. Drug preparation

Clozapine-N-oxide (CNO) (Tocris, 4936) was diluted in a 0.5% DMSO in PBS to a final dose of 1, 5, or 10 mg/kg. The following equation was used to calculate injection volumes in ml:

$$injection\ volume\ (ml) = \frac{weight\ (kg) \times\ drug\ dose\ (\frac{mg}{kg})}{drug\ concentration\ (\frac{mg}{ml})}$$

Vehicle solutions consisted of 0.5% DMSO in PBS.

2.4.2. Drug delivery

All drug treatments were delivered via *i.p.* injections using the above equation. Animals were habituated to injections 1-2 days prior to commencing experiments by scruffing and touching the lower left and right quadrants of the abdomen prior to experiments.

2.5. Chemogenetic experiments

In this subsection, I will first describe how we fabricate connectors, which, for electrophysiology experiments, are fitted into the mouse's headcap and are used to transmit the initial signal to the rest of the system (**Fig. 2.7,** bottom right insert). I will then explain in detail the electrophysiology set-up that was used in chemogenetic experiments, which are explained in the final part of this section (see section 2.5.3).

2.5.1. Soldering the connectors

The relevant wires of connectors (Omnetics, A79044-001) were cut roughly 2-3 cm from the base, and the insulation was removed from the ends of these wires. 2 sections of 3 pins were cut from one-row PBC sockets (RS components, 767-9751), and the uninsulated ends of wires were soldered to their relevant socket. Connections were secured using dental cement. Exposed wires were secured using either dental cement or heat shrink tubing (**Fig 2.7,** bottom right).

2.5.2. Electrophysiology set-up

The connector (Omnetics, A79044-001, configuration described above) was attached to a 16Ch headstage (Intan, #C3334), responsible for amplifying and digitalising electrophysiology signals. From the headstage, the signal was then passed through a blue RHD serial peripheral interface (SPI) cable (Intan, #C3203), to a RHD SPI cable adapter board (Intan, #C3430) (**Fig. 2.7**). Following the first cable adapter board, the signal was passed through a slip ring (Moflon, MC330) to a second SPI cable adapter board. From here, the signal passed through a second SPI cable to a RHD USB interface board (Intan, C3100), and then directly to the computer. Electrophysiology signals were displayed and recorded on the computer using Intan RHX Data Acquisition Software, version 3.1.0 (**Fig. 2.7**).

Four set-ups could be connected to the single USB interface board using the four SPI ports A-D. Copper wire mesh was placed underneath the box and connected to a ground for Faraday cage connection on the USB Intan board using a copper wire to ground the recorded signals (**Fig. 2.7**).

For each set-up, lids of transparent acrylic boxes (30 cm x 30 cm x 40 cm height) were fitted with a slip ring (Moflon, MC330) (**Fig 2.7**). The wires emerging from each end of the slip ring were soldered to relevant pins on the SPI cable adapter board. The configuration of wires and pins had to be carefully mapped so that signals could pass through the entire system, and then the correct corresponding channels on Intan RHX Data Acquisition Software were selected.

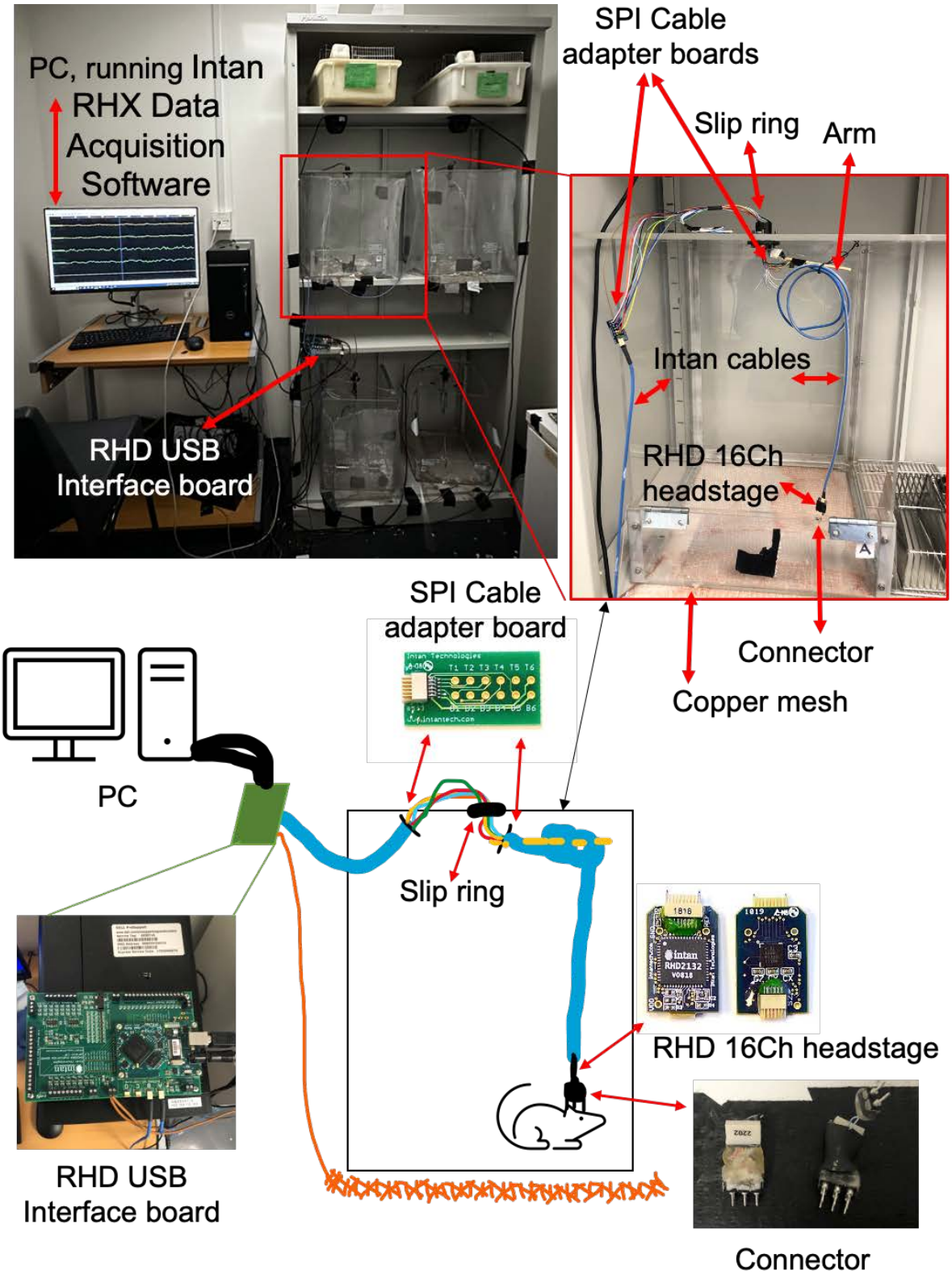

Figure 2.7. Sleep recording set-up. Schematic of set up equipment including acrylic box, lid with slip ring attached, two blue intan wires, both connected to slip ring wires using RHD adapter boards - one then is attached to an arm and fitted with a 16Ch headstage and adapter which is plugged into mouse's headcap, and the other is plugged into the RHD USB interface board which is connected to the computer. A grounding cable is also connected to the RHD USB interface board which is also connected to a copper mesh fitted underneath the box to ground electrophysiological signals.

2.5.3. *Habituations and recordings*

To allow an adequate recovery period, mice were allowed to recover for at least 1 week following headcap surgery, which took place at least 3 weeks after viral injection surgeries, to allow for optimal virus expression (**Fig. 2.8**). Habituations were then performed for 2-3 days prior to commencing experiments by increased handling of the mouse and introducing the mouse into the acrylic box, untethered, and then tethered for an increasing amount of time. Following habituations, 1-2 days of 6-hour baseline recordings were done where mice received no drug treatment (**Fig. 2.8**). Mice were connected to the recording set-up by head-fixing the mouse and attaching the connector to the mouse's headcap. For baseline recordings and chemogenetic studies, signals were recorded for 6 hours during the light-on phase (zeitgeber (ZT) 1-12) (**Fig. 2.8**). For studies also looking at rebound sleep following chemogenetic drug manipulation, signals were recorded for 10 hours during the light-on phase (ZT 0-12). CNO injections were delivered immediately before commencing recordings, and each treatment was repeated at least twice before brain extraction and histological analysis (**Fig. 2.8**). Electrophysiological signals from relevant channels were recorded using Intan software at a 1 kHz sampling rate with a bandwidth range above 0.1 Hz.

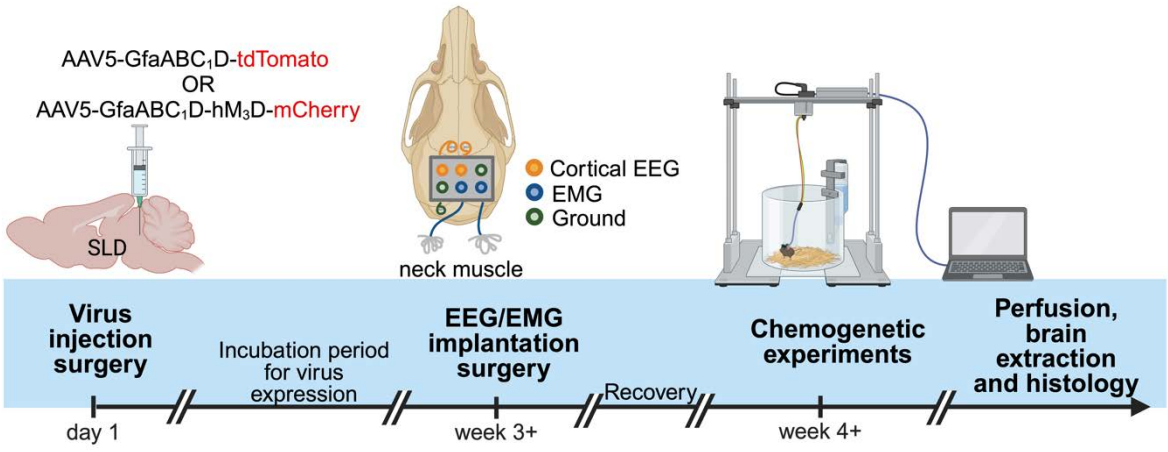

Figure 2.8. Timeline of chemogenetic experiments. Experimental process begins at day 1 on the day of surgery undergoing bilateral viral injections, followed by EEG/EMG headcap implantation. The animal was left to recover for at least 1 week prior to habituations to recording chambers. To allow for virus incubation, chemogenetic experiments began 4 weeks onwards. Once experiments were complete the animal was perfused for histological analysis.

Created using BioRender.com

2.6. Behavioural tests

Behaviour testing was completed at least 4 weeks after virus injection surgery to allow sufficient viral expression. For behavioural testing, mice first completed the novel object location test, a modified version of the novel object recognition test (Antunes and Biala, 2012; Boyce *et al.*, 2016), followed by the novel object recognition test (Ennaceur and Delacour, 1988; Ennaceur, 2010; Silvers *et al.*, 2007). The experimental design was largely based on the study by Boyce *et al.* which examined memory deficits following optogenetic inhibition of theta oscillations during REM sleep (Boyce *et al.*, 2016).

The test boxes were open-topped 40 x 40 x 40 cm white opaque square containers with obvious markings on one wall, for spatial cues (**Fig. 2.9**). Behavioural tests were run between ZT 0-2 (first two hours of the light-on phase) over 5 consecutive days (**Fig. 2.10**). On day 1 mice were habituated to the empty test box and allowed to freely explore for 20 minutes. On day 2, two identical objects (**Fig. 2.9**, left) were each placed in a random quadrant of the test box, and mice were exposed to this environment for 10 minutes. Before being returned to their home cage, mice received an *i.p.* injection of either Veh or CNO (1 mg/kg). On day 3, one of these objects was moved to a different quadrant and mice were allowed to explore this environment for 10 minutes. On day 4, the same two objects were each randomly assigned to a quadrant and mice were allowed to explore for 10 minutes. Again, before being returned to the home cage, mice received *i.p.* injections of either veh or CNO (1 mg/kg). On day 5, objects were placed in the same location as on day 4, but one object was replaced by a distinctively different object (**Fig. 2.9** & **Fig. 2.10**). To prioritise spatial memory tests, NOLT was consistently performed first, followed by NORT. Objects used, and locations of said objects where randomised for each animal. An overhead camera (Nulaxy HD, 1080p) was attached to the ceiling directly above the centre of test boxes and videos were recorded using a custom written LABVIEW code at 25 frames per second.

Figure 2.9. Objects and test boxes used in memory testing. Example of two pairs of distinct objects used in memory testing, including plastic cylinders, and falcon tubes filled with sand. Other objects of similar size were also used (left). Layout of the 4 test boxes with wall markings on one side (right).

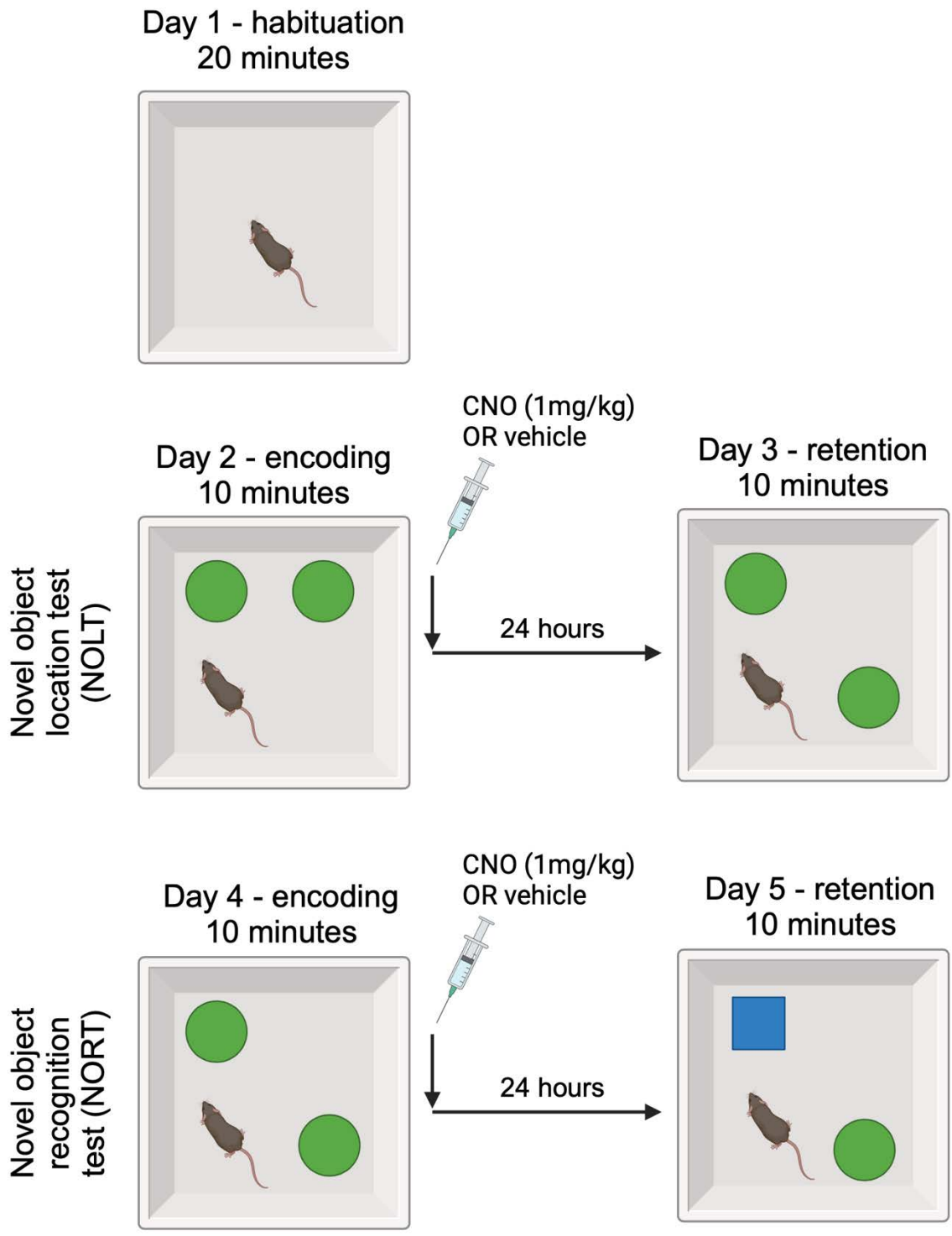

Figure 2.10. Schematic of behavioural test experimental design. Day 1 includes habituation to the empty box (20 mins). Day 2 includes encoding phases of novel object location test (NOLT) to two identical objects each placed in a random quadrant (10 mins). Day 3 is retrieval of NOLT, where one object is moved to a distinct location (10 mins). Day 4 is the encoding phase of the novel object recognition test (NORT) where two objects are each placed in a random quadrant (10 mins). Day 5 is the retrieval phase of NORT where one object os changed to a distinct object (10 mins). Injections of either vehicle or CNO (1 mg/kg) are given immediately after encoding phases on day 2 and 4.

Created using BioRender.com

2.7. Fibre photometry

2.7.1. Set up

The fibre photometry system was set up and characterised by Dr. Shuzo Sakata and Dr. Yuri Elias Rodrigues (**Fig. 2.11** & **Fig. 2.12**). This system was based on established illumination protocols using two wavelengths, a 470 nm LED (Thorlabs, M470F3) used to excite GCaMP6f (**Fig. 2.13**), and a 405 nm LED (Thorlabs, M405F1) used to obtain a Ca^{2+}-independent isosbestic signal (Patel *et al.*, 2020; Kim *et al.*, 2016; Simpson *et al.*, 2023). LEDs were each connected to an LED driver (Thorlabs, LEDD1B) and were independently controlled by a National Instruments (NI)-DAQ (NI, USB-6343) (**Fig. 2.11**), using a custom-written LABVIEW code. Light from each LED was passed to the first dichroic mirror using an FC/PC to SMA patch cable (Thorlabs, M91L01). Light from the 470 nm LED was transmitted through both dichroic mirrors (Thorlabs, MD416 and DMSP490R), while light from the 405 nm LED was reflected through the first dichroic mirror and transmitted through the second. At the four optical entry points of the dichroic mirrors, a collinator (Thorlabs, F950FC-A) was used to direct the beam of light (**Fig. 2.11**).

Light from both LEDs was carried along a low autofluorescence patch cable to ferrule (Thorlabs, MAF3L1) and connected to the implantable optic fibre using a 2.5 mm ceramic mating sleeve (Thorlabs, ADAF1) (**Fig 2.11,** bottom right). After GCaMP6f was excited by the 470 nm LED, emitted fluorescence (~520 nm) (**Fig. 2.13**) was collected from the fibre and carried back along the autofluorescence patch cable and reflected through the dichroic mirror (DMSP490R) (**Fig. 2.11-2.12**). It was then filtered using a bandpass filter (Thorlabs, FBH520-10) and carried along a low autofluorescence patch cable (Thorlabs, MAF1L1) and collected at a Femtowatt photodetector (Newport, 2151), where the signal was sent back to the NI-DAQ and recorded using the previously mentioned custom-written LABVIEW code (**Fig. 2.11**).

Simultaneously, EEG and EMG signals from the implanted headcap were connected to an Omnetics adapter (Omnetics, A79044-001) and 16Ch headstage to amplify signals (Intan, #C3334). EEG/EMG signals were carried along an Intan wire (Intan, #C3203) to a USB interface board (Intan, C3100). Finally, EEM/EMG signals were carried to the NI-DAQ, and recorded using the LABVIEW code (**Fig. 2.11**).

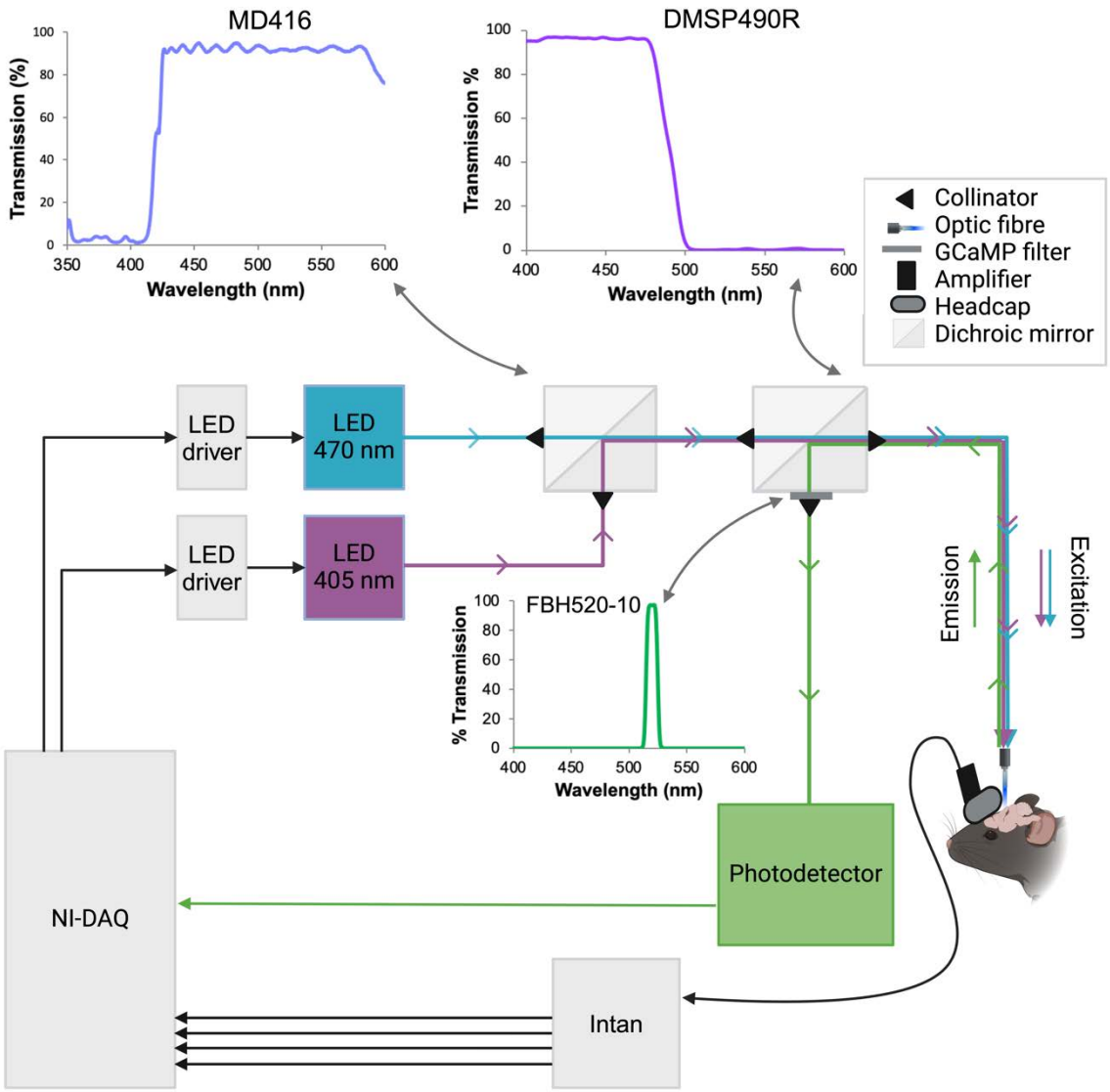

Figure 2.11. Schematic of fibre photomtry set up. 470 nm and 405 nm LEDs were driven by LED drivers and controlled by an NI-DAQ. Light was directed through two dichroic mirrors and delivered to animal. When GCaMP6f was excited, emitted light was reflected through a dichroic mirror and filtered by a GCaMP bandpass filter to be collected by a photodetector and recorded by the NI-DAQ. EEG/EMG signals were simultaneously meaured using Intan equipment.

Top inserts, MD416, reflective band = 360-407 nm, transmission band 425-575 nm (left). DMSP490R, reflective band = 505-800 nm, tranmission band 380-475 nm (right). Centre insert, FBH520-10, blocking regions 200-500 nm, 540-1200 nm.

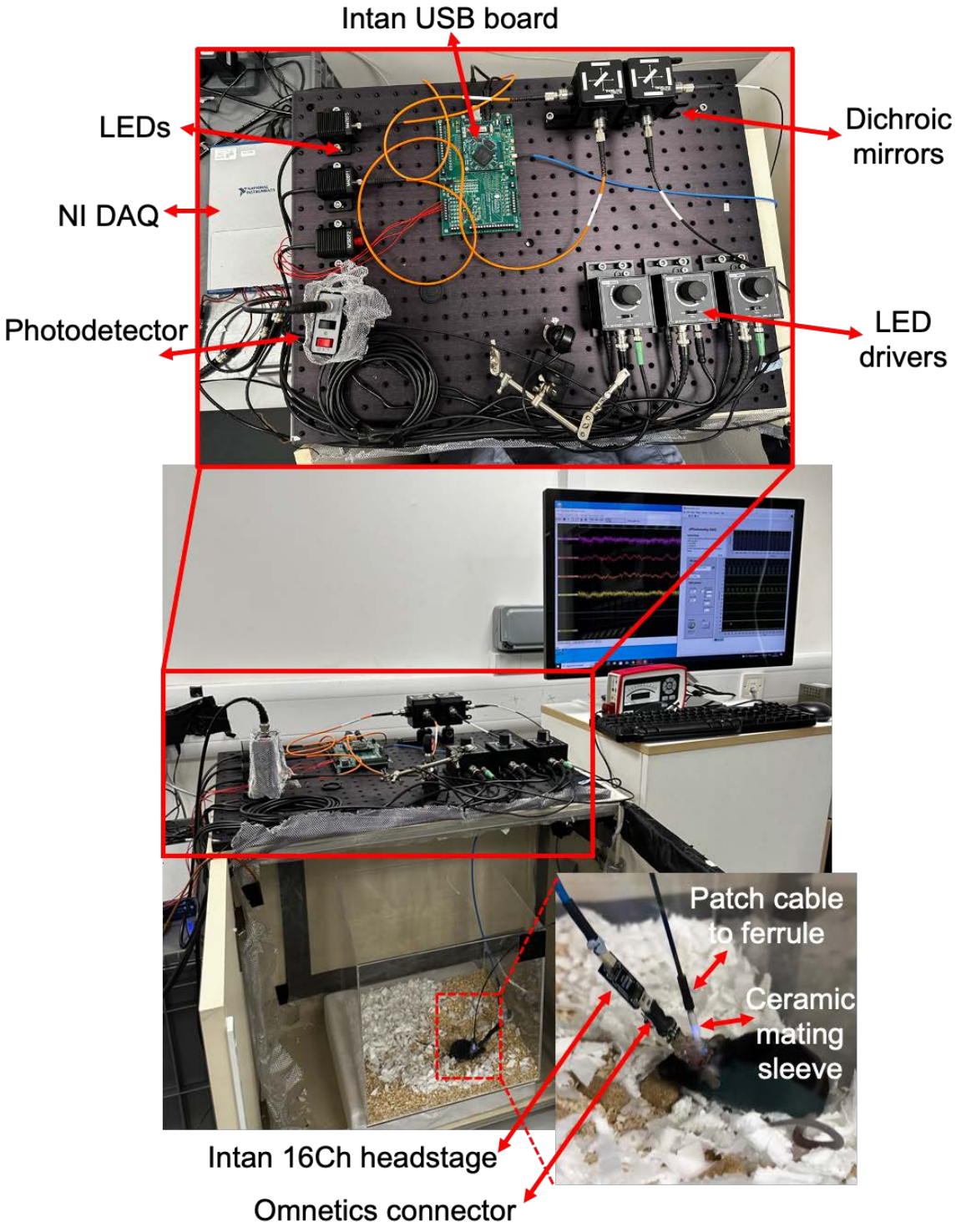

Figure 2.12. Fibre photometry set up. Fibre photometry set up including zoomed in pictures of the LED-Fibre-Photodetector system (top), and tethered mouse (bottom).

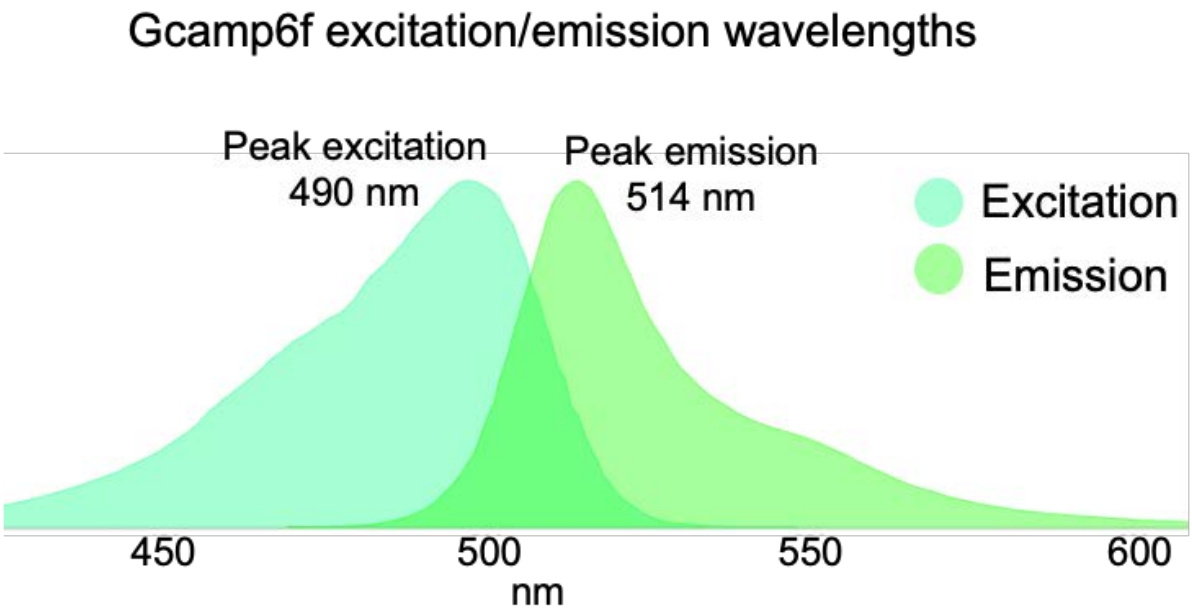

Figure 2.13. Excitation/emission wavelengths of GCaMP6f.
Spectrum image from fpbase.org

2.7.2. Habituations and recordings

Habituations occurred several days prior to experiments by tethering the mouse to the patch cable and connector. On habituation days different laser powers were tested for 10-30 minutes for both 405 nm and 470 nm (output power 3-5V) to achieve maximum effects at minimum voltage. As autofluorescence of the patch cable can interfere with the collected signal, photobleaching of the patch cable was done for at least several hours before each experiment using a custom-written LABVIEW code. Ultimately this meant the LEDs were left on at full power to reduce autofluorescence within the system. Experiments begun at least 4 weeks after virus injection, and at least one week after fibre implantation to allow sufficient virus expression and recovery, respectively (**Fig. 2.14**). For experiments, mice were tethered to the Omnetics connector, and the patch cable using a ceramic mating sleeve (**Fig. 2.12, bottom**). Light was delivered with a pulse frequency of 40 Hz and a 30% duty cycle. Baseline recordings of fluorescence output and EEG/EMG signals were measured for

1 hour before mice were administered an *i.p.* injection of vehicle or CNO (1-10 mg/kg). Signals were recorded for a further 3 hours after CNO or vehicle injection before animals were returned to homecage, thus recordings lasted a total of 4 hours (ZT 5-10). Both electrophysiology and fluorescence data were collected at a sampling rate of 10 kHz. After untethering mice, the mating sleeve was removed, and a protective ceramic cap was used to protect the fibre (**Fig 2.5**).

It is worth noting that due to time constraints, only such short baseline activity (1-hour) was measured prior to vehicle or CNO administration. Ideally, baseline recordings of 4 hours would be done prior to commencing experiments, to measure natural changes in brain activity cause by circadian fluctuations.

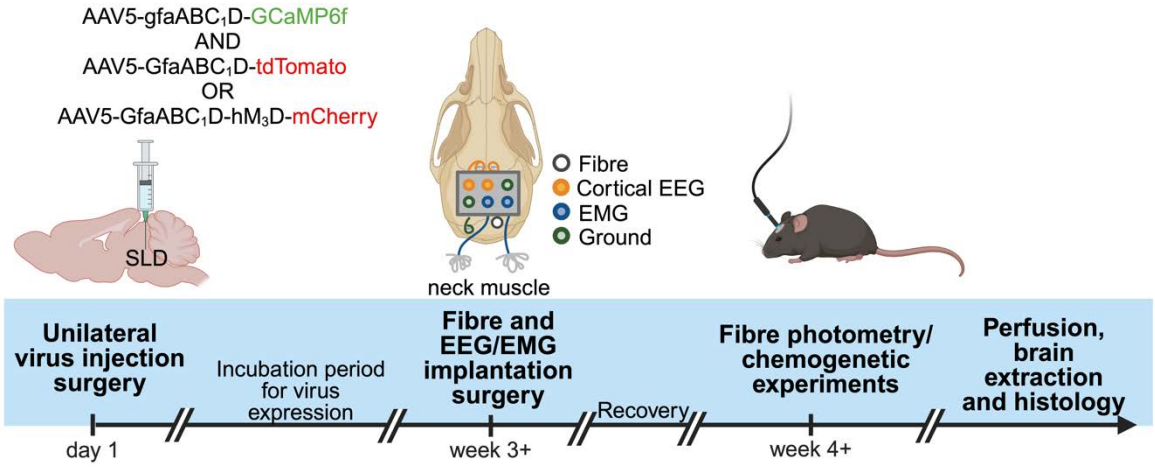

Figure 2.14. Fibre photometry and chemogenetic experiment timeline. Virus injections occur on day 1 and around 3 weeks later fibre and headcap implantation occurs. At least 4 weeks after virus injection and one week after fibre implantation experiments can begin. Once all conditions have been tested the animal is perfused and histology is done.

Created using BioRender.com

2.8. Histology

2.8.1. Tissue removal

Following injections with 0.1 ml (i.p.) lidocaine and 0.1 ml (i.p.) pentobarbital, a transcardial perfusion with 20 mls PBS (0.1 M) and 20 mls 4% paraformaldehyde

(PFA) in PBS was performed. The brain tissue was extracted and post-fixated in 4% PFA at 4°C overnight, and finally transferred into 30% sucrose/ 0.1 M PBS solution for several days at 4°C prior to immunostaining.

2.8.2. Immunostaining and imaging

60-80 μm coronal slices were obtained using a microtome (SM2010R, Leica) from the posterior brain regions to include areas of the hindbrain, and midbrain, specifically the pons.

2.8.2.1. Staining for chemogenetic-only and behavioural experiments

For post-experimental histological analysis for animals used in chemogenetic-only and behavioural tests, 80 μm slices underwent blocking using a 10% normal goat serum (NGS) (Invitrogen - Thermo Fisher)-0.5% Triton X (Merck, 648462) in PBS (PBST) solution for 1 hour at room temperature. Slices were then incubated with primary antibodies rabbit anti-dsRed (1/1000) (clontech, 632496), or mouse anti-mCherry (1/1000) (Abcam, ab125096), and rabbit anti-GFAP (1/1000) (Abcam, ab7260), rabbit anti-S100b (1/200) (Abcam, ab52642), or rabbit anti-NeuN (1/1000) (Abcam, ab177487) in a 3% NGS-PBST solution overnight at 4°C. 3% NGS in PBST was used as a negative control.

The following day, slices were washed with PBS for 5 minutes 3 times prior to an incubation with secondary antibodies goat anti-rabbit AlexaFluor 594 (Invitrogen, A11012), or goat anti-rabbit AlexaFluor 488 (1/1000) (Life Technologies, A11034) and goat anti-mouse AlexaFluor 594 (1/1000) (Life Technologies, A21145) in a 3% NGS-PBST solution for 2 hours at room temperature. Slices were washed as previously described and counterstained with DAPI (1/1000) (ThermoSci, 62248) for 5 minutes at room temperature. Slices were washed for a third time as previously described and mounted onto microscope slides using 0.3% gelatine solution. Finally, the slides were sealed with coverslips using flouromount (Invitrogen, 00-4958-02) and imaged on an epifluorescent upright microscope (Nikon, Eclipse E600) or a confocal microscope (Leica SP8).

2.8.2.2. Staining for combined fibre photometry and chemogenetic experiments

For animals used in combined fibre photometry and chemogenetic studies, immunostaining was similar to that described in the previous section, with some alterations. Briefly, 60 μm slices first underwent blocking with 10% goat serum-PBST as previously described, and were incubated with primary antibodies rabbit anti-dsRed (1/1000) (clontech, 632496), or mouse anti-mCherry (1/1000) (Abcam, ab125096), and chicken anti-GFP (1/1000) (Abcam, ab13970) in a 3% NGS-PBST solution overnight at 4°C. A proportion of slices were also stained with rabbit anti-GFAP (1/1000) or rabbit anti-NeuN (1/1000). Again, 3% NGS in PBST was used as a negative control.

The following day sections were washed as previously described before the secondary antibody incubation. Secondary antibodies goat anti-rabbit AlexaFluor 594 (Invitrogen, A11012), or goat anti-mouse AlexaFluor 594 (1/1000) (Life Technologies, A21145) and goat anti-chicken AlexaFluor 488 (1/1000) (Abcam, ab150169) in a 3% NGS-PBST solution were left to incubate for 2 hours at room temperature. Slices that were exposed to rabbit anti-GFAP or rabbit anti-NeuN were also stained with goat anti-rabbit AlexaFluor 405 (1/500) (Abcam, 175652). Slices were washed as previously described, and those that were not stained for rabbit anti-GFAP or rabbit anti-NeuN and goat anti-rabbit 405 were counterstained with DAPI (1/1000) for 5 minutes at room temperature and washed for a third time. Slices were then mounted and imaged as previously described.

Individual images taken with a 4x objective lens on the epifluorescent microscope were stitched together using a custom-written MATLAB script to create full-brain slice images. Fiji (ImageJ) was used to process images and to add the relevant colour to all images captured on the epifluorescent or confocal microscopes.

2.9. Data analysis

2.9.1. Histology mapping

Virus expression was mapped partly using the QUINT workflow (Puchades *et al.*, 2019; Berg *et al.*, 2019), and Adobe Illustrator 2024. Once images were prepared

using Fiji (**Fig. 2.15A**), each image was registered to the Allen Mouse Brain Common Coordinate Framework version 3 (CCFv3) (Wang *et al.*, 2020), by matching identifiable landmarks using QuickNII software (**Fig. 2.15B**). Next, sections underwent non-linear refinement and were corrected for deformations using VisuAlign software (**Fig. 2.15C**), which gave output atlas maps corresponding to input sections (**Fig. 2.15D**). Next, the ilastik software was trained to detect virus expression and/or damage from fibre from input images, and was used to extract segmentations of virus expression and/or fibre location (**Fig. 2.15E**). Atlas maps and segmentations were overlayed (**Fig. 2.15F**). Atlas maps from multiple animals in the same experimental group, which were of similar regions (in terms of AP axis) were then aligned on Adobe Illustrator, and the corresponding segmentation was matched. Transparency of segmentations were then altered to visualise several segmentations of a singular atlas map to show expression patterns in specific regions across multiple animals (**Fig. 2.15G**).

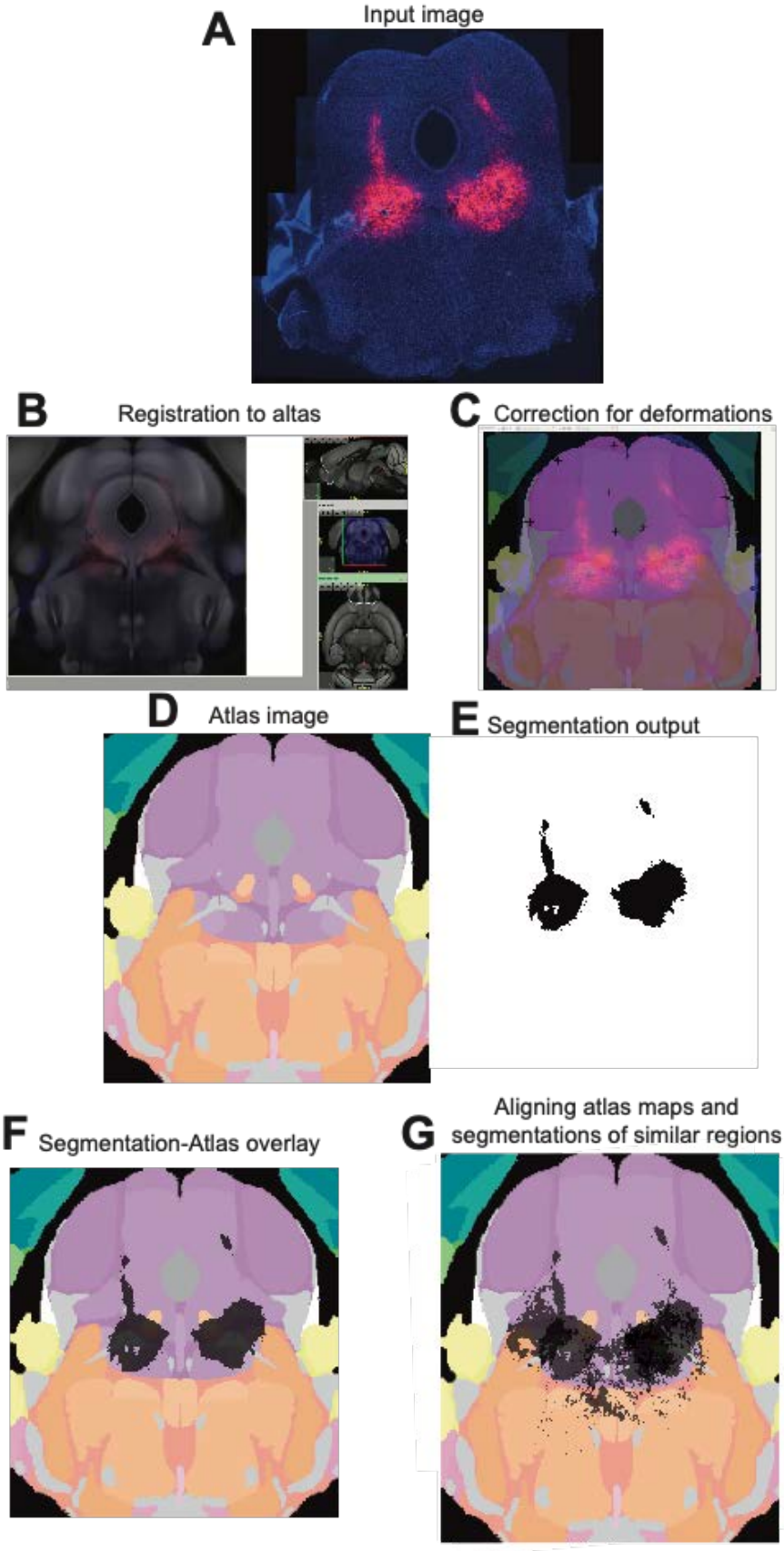

Figure 2.15. Histology using QuickNII workflow. Input images (**A**), were registered to the Allen Mouse Brain atlas CCFv3 (2017) using QuickNII (**B**) and corrected for deformations using VisuAlign (**C**) which produced output atlas maps (**D**). The ilastik software was trained to detect virus expression and produce segmentation outputs (**E**). Altas maps from visualign and segmentation from ilastik were overlayed (**F**). Altlas maps from the same brain regions were aligned and the corresponding segmentation was overlayed, transparency was used to demostrate quantity of animals expressing virus in specific regions (**G**).

2.9.2. Sleep scoring

RHD files from Intan were converted into a singular .dat file using a custom-written MATLAB script. For fibre photometry experiments, electrophysiology data was down sampled from 10 kHz to 1 kHz, for ease of sleep scoring. For all sleep scoring, the EEG and EMG signals were then extracted and processed using a MATLAB function (SleepScoring_Auto, https://github.com/Sakata-Lab/SleepScore), and then manually curated using a custom-written Manual Sleep Scoring code (SleepScoring_Manual_ver2, https://github.com/Sakata-Lab/SleepScore). For manual curation, 4-second epochs of EEG and EMG signals were used to determine awake, NREM sleep, or REM sleep states in accordance with the standard criteria (Radulovacki *et al.*, 1984; Tobler *et al.*, 1997). NREM sleep consists of high amplitude EEG activity, delta activity (1-5 Hz), and low EMG power (**Fig. 2.16,** top), and REM sleep consists of low amplitude EEG, theta activity (6-10 Hz), and the lowest form of EMG power demonstrating muscle atonia (**Fig. 2.16,** bottom). Episodes of active wake are typical of very active EMG traces and very low EEG trace amplitude, with frequent artefacts caused by excessive movement (**Fig. 2.17,** top), while quiet wakefulness is characteristic of low EEG amplitude and larger EMG amplitude than both sleep states but visibly lower than active wakefulness (**Fig. 2.17,** bottom). Both active and quiet wakefulness have little to no delta or theta activity, and were classified together as awake (**Fig. 2.17**). Specific data such as spectrograms and hypnograms, percentage of time in each sleep state, number of sleep transitions, and length of state episodes were extracted from individual data sets following sleep scoring and was used for group analysis using custom-written MATLAB codes.

Spectral analysis was done following manual sleep scoring. Oscillatory frequencies were extracted from all recordings and sorted depending on animal group, drug treatment, and state classification. Data was the normalised to the sum of all power spectral density (PSD) data, thus converting PSD data into a proportion where the sum of all PSD data in a given state within a given recording was equal to 1, allowing for comparable data.

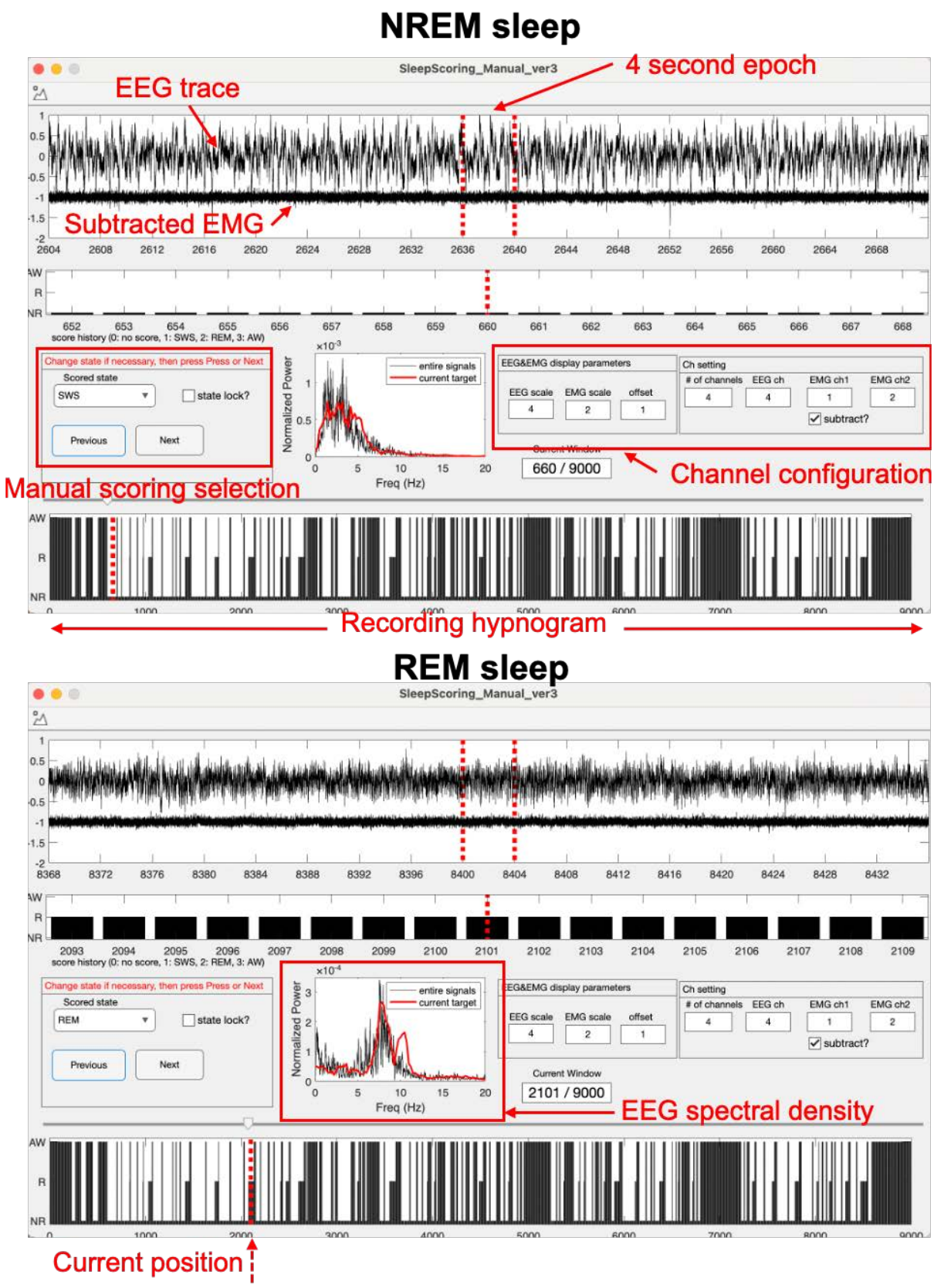

Figure. 2.16. Manual curation identification of NREM and REM sleep. Custom toolbox for manual scoring where each 4 second epoch is scoring to NREM or REM. NREM sleep criteria consists of high amplitude EEG, delta oscillations, and low EMG power (top). REM sleep consists of low frequency EEG, theta activity, and very low EMG power (bottom). Examples of NREM and REM sleep are taken from the same individual recording.

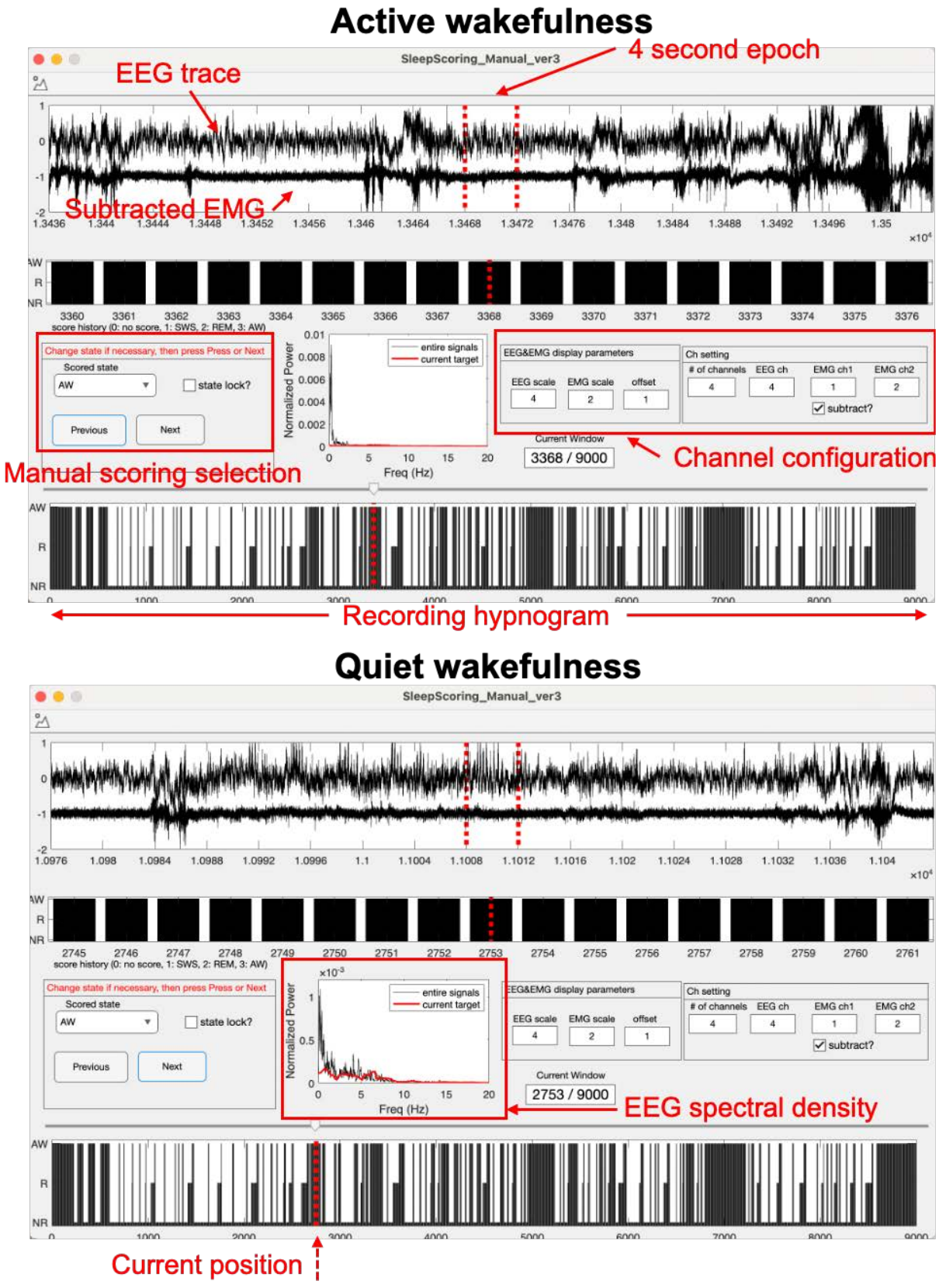

Figure. 2.17. Manual curation identification of awake. Custom toolbox for manual scoring where each 4 second epoch is scoring to AW, or QW. Wakefulness consists of low amplitude EEG, and high EMG power. Wakefulness can consist of periods of very high EMG activity (top), and quieter, but still present bursts of EMG activity (bottom)

2.9.3. Behavioural analysis

10-minute AVI videos were obtained using a custom-written LABVIEW code and analysed using DeepLabCut software (Mathis *et al.*, 2018). We trained a deep convolutional network by first extracting 50 frames from 3 videos (150 frames in total), and labelling 8 body parts, the nose, centre of head, left ear, right ear, midpoint, right hip, left hip, and tail base manually on each frame. After this network was trained, we could automatically detect all body parts across the frames of all experimental videos. The accuracy of our trained network was visually inspected for every experiment by superimposing raw videos with labelled body parts (**Fig. 2.18**). Subsequently, we used the position of the nose to extract trajectories and body position to determine exploration of objects and discrimination indices using custom-written MATLAB scripts. Exploration threshold was set at 4 cm from the centre of objects, as objects were 44 mm wide, this threshold was ~2 cm from the edge of objects.

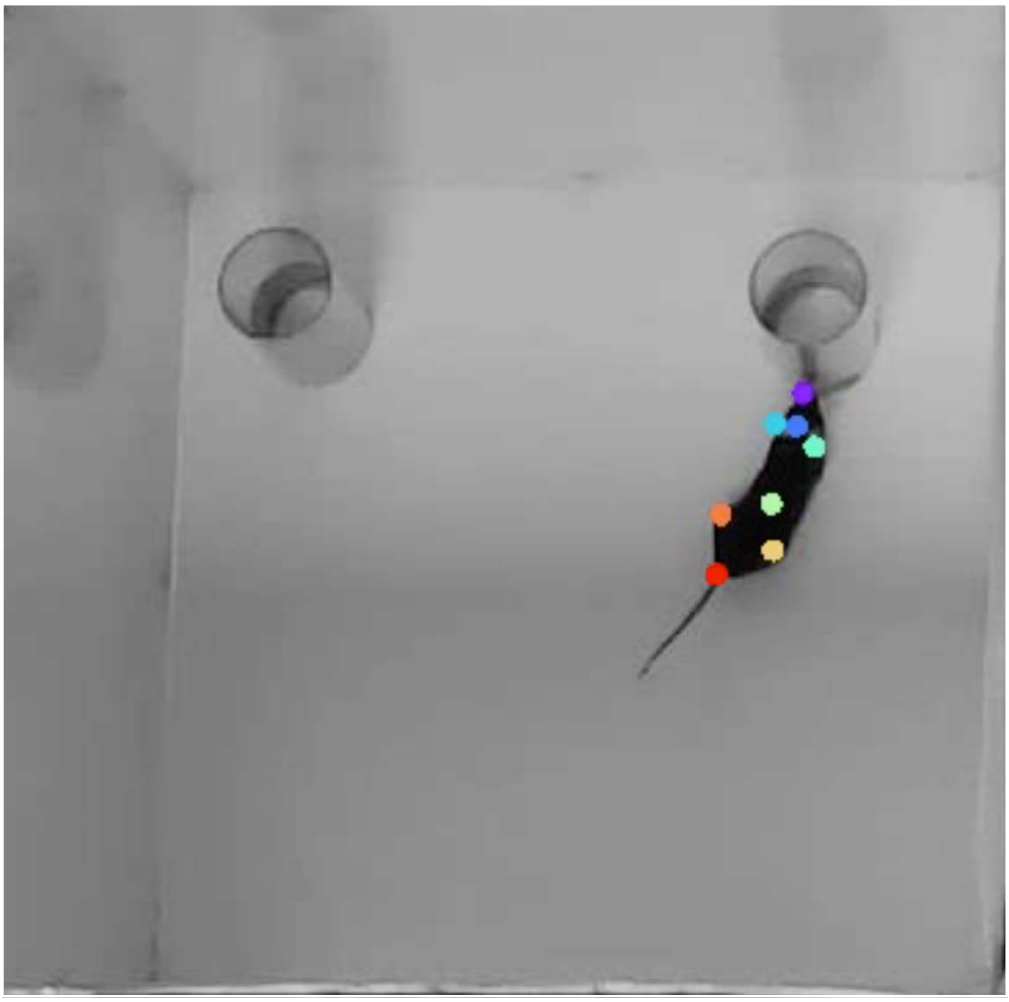

Figure 2.18. Example of labelled body parts by DeepLabCut.

2.9.4. Fibre photometry

To extract data that was collected only while LEDs were on, data was extracted if LED sync/output channels were above a threshold of 0.05V. Signals from photodetector data corresponding to LED-on events were extracted and averaged using the median to reconstruct fluorescent signals from 405 nm and 470 nm LEDs (**Fig. 2.19,** top).

Fluorescence signals were then smoothed by passing them through a 3rd-order Butterworth low-pass filter with a 10 Hz cut-off frequency to reduce noise. This filter was applied using a zero-phase filter to avoid phase distortion (**Fig. 2.19**). A double exponential model was then fitted to 405 nm and 470 nm to correct for photobleaching. Following this, the 405 nm signal was linearly scaled to match the 470 nm signal and subtracted to isolate the calcium-dependent change in fluorescence (**Fig. 2.19**). The resulting signal was then normalised by dividing it by the scaled 405 nm signal (fitted

with the double exponential model). Finally, the signal was Z-scored, which standardises data by subtracting the mean and dividing by the standard deviation (**Fig. 2.19**). Z-scoring transforms fluorescence into a distribution with a mean of 0 and standard deviation of 1 to allow for easier interpretation.

To visualise changes across animals according to different treatment conditions, we extracted data for specific time periods before and after the injection of vehicle or CNO. The time of injection was identified using high-frequency artifacts observed in the EMG and/or EEG which occurred when the mouse was removed from the cage for the injection. We then cropped, extracted, and plotted raw data from relevant recordings. For visualisation, we then overlaid raw fluorescence data with a smoothed, average trace to highlight trends and changes relative to drug treatments.

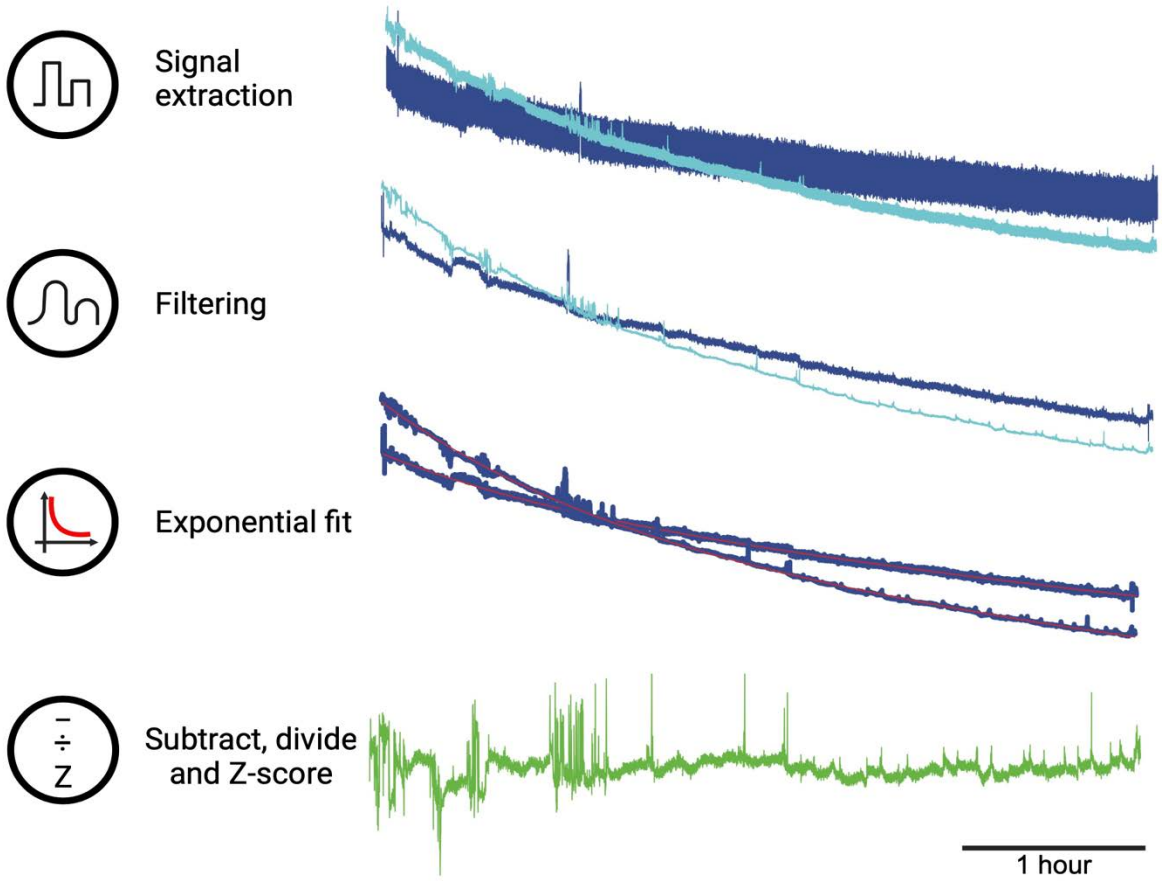

Figure 2.19. Signal processing for fibre photometry. Fluorescent data for 405 nm (dark blue) and 470 nm (light blue) during LED-on events are extracted, filtered, and fitted with a double-exponential fit model. Following linear scaling, isobestic fluorescence (405 nm) is subracted from GCaMP fluorescence (470 nm), normalised, and Z-scored, to produce calcium-dependent change in fluorescence trace.

2.10. Statistical analysis

MATLAB was used for all statistical analysis. Data is expressed as mean ± standard error unless stated otherwise. Shapiro-Wilk tests were used to test the normality of data, all data was normally distributed unless stated otherwise.

Comparisons between animal groups and treatment type in chemogenetic experiments (chapter 3) were performed using two-way ANOVA on MATLAB. In these studies, some groups of data did not follow normal distribution ($p < 0.05$), however, two-way ANOVA way still used. This was due to the need for determining significant interactions between animal groups and drug treatments, and a lack of compatible non-parametric tests to study two independent factors. Post-hoc analysis to determine differences between individual groups was then done by applying pairwise comparisons using the Tukey-Kramer test on MATLAB, in which $p < 0.05$ was considered as significant. For behavioural experiments (chapter 4), comparisons were made between encoding and retention sessions per animal/treatment group using paired t-tests.

3. Chemogenetic activation of pontine astrocytes reduces REM sleep

The primary objective in this project was to modulate astrocyte activity in the pons and determine the effects on REM sleep and the sleep-wake cycle. Thus, in this chapter I will firstly briefly introduce the literature, rationale, and hypothesis surrounding this topic (section 3.1), followed by a description of the dataset and animals used in these experiments, including the exclusion criteria (section 3.2.1 & 3.2.2). I will then show histology results obtained from the animals used (section 3.2.3 & 3.2.4), and the effects of chemogenetically activating astrocytes in the pons on the sleep-wake cycle (section 3.2.5). Subsequently, I will report of any modifications to the sleep-wake cycle in the hours following chemogenetic modifications (section 3.2.6). Overall, in this chapter we show that activating pontine astrocytes using chemogenetics reduces REM sleep in a dose dependent manner. We also show evidence for sedative effects of NREM sleep caused by CNO alone, but no effects of CNO alone on REM sleep. Finally, we show that the effects of our chemogenetic manipulations on REM sleep are diminished 10 hours after CNO administration, but no significant rebound REM sleep occurs.

3.1. Introduction

As previously described, conflicting results regarding pontine astrocyte activity during the sleep-wake cycle have been reported. Tsunematsu *et al.* demonstrated that astrocyte activity was lowest during REM sleep in multiple brain regions, with the most pronounced reduction occuring in the pons (Tsunematsu *et al.*, 2021). On the other hand, Peng *et al.* showed relatively high astrocyte activity in the pons during REM sleep, while chemogenetically activating such activity seemed to reduce REM sleep (Peng *et al.*, 2023). Modulating astrocyte activity and measuring changes to the sleep wake cycle is an important strategy to gain more information about the relationship between astrocytes and sleep.

3.1.1. Hypothesis and aims

Due to the outlined previous studies, the results in this chapter were based on the hypothesis that manipulating astrocyte activity in the pons using G_q-coupled

DREADDs would reduce REM sleep incidence. We also hypothesised that following chemogenetic manipulation, rebound REM sleep would occur in the case of increased number of REM sleep episodes, or increased length of REM sleep episodes. To test these hypotheses, we aimed to chemogenetically activate pontine astrocytes and monitor the sleep wake cycle for an extended period of time, which firstly would assess any direct effects of chemogenetic modifications, and then rebound sleep occurrence. To do this, we used a virus-based delivery of hM3D receptors to be exclusively expressed in pontine astrocytes, and delivered vehicle or CNO drug treatments immediately before recording sessions via *i.p*. injections. During experimental sessions we recorded intracranial cortical EEG and EMG from the neck muscle to monitor the sleep-wake cycle. Due to our known effects of CNO alone on the sleep-wake cycle in which CNO alone modulated both NREM sleep and REM sleep (Traut *et al.*, 2023), we carefully designed our experiments to include multiple control groups.

3.2. Results

3.2.1. Animal groups and database

As briefly outlined (see section 2.1), a total of 43 mice aged 8-24 weeks upon time of surgery were used for the experiments described in this chapter (**Fig. 3.1A**). Of these 43, 18 mice were bilaterally injected with a control virus while 25 were injected with the activatory chemogenetic receptor (hM3D). Of these, a total of 10 mice were used as a final control group (5 males and 5 females), and 8 were used as the DREADDs group (5 males and 3 females) for chemogenetic studies. Some of these animals were recorded for 6 hours only, leaving 7 control animals (2 males and 5 females) and 5 DREADDs animals (2 males and 3 females) used for rebound sleep studies, reported later in this chapter (**Fig. 3.1A**).

3.2.2. Establishing inclusion and exclusion criteria

Based on images obtained from immunohistochemistry, we excluded animals that did not have satisfactory bilateral virus expression in the pons (n=5 control, n=13 DREADDs). In excluded animals this included virus expression that was off-target, for example too dorsal (**Fig. 3.1B,** top), too lateral (**Fig. 3.1B,** middle), only unilaterally expressed (**Fig. 1.3B,** middle and bottom), or had excessive leakage along the injection pathway (**Fig. 3.1B,** middle and bottom). In some cases, which occurred only

in DREADDs animals, we found a complete lack of expression (n=10). Upon further investigation into this issue, we hypothesised that this may have been due to histological error, rather than error during virus injection surgeries. The two viruses used in control and DREADDs animals had different titres as well as different fluorescent tags (AAV5-gfaABC$_1$D-tdTomato, 7×10^{12} gc/mL, vs AAV5-gfaABC$_1$D-hM3D-mCherry, $3x10^{12}$ gc/mL, respectively). Therefore, we hypothesised that the lack of expression in DREADDs animals may be in part due to a dimmer fluorescence.

To amplify the signal of the red fluorescent proteins conjugated to our viral constructs, we used primary and secondary antibodies raised in a mouse, mouse anti-mCherry and anti-mouse AlexaFluor 594. Due to the mouse strain of these antibodies, it is possible that they bound to endogenous IgG and FC receptors, leading to high background fluorescence and non-specific staining, which may also have contributed to the dim fluorescence of staining the DREADDs virus (Goodpaster and Randolph-Habecker, 2014; Mascadri *et al.*, 2021). To test this, we compared our histology techniques with staining using antibodies which were raised in a rabbit, for this we chose rabbit anti-dsRed and anti-rabbit AlexoFlour 594 antibodies. An example of two adjacent 80 μm slices from the same DREADDs animal using the different stains is shown in **Figure 3.2**. Images captured on an epifluorescent microscope show that rabbit anti-dsRed signals are much brighter than mouse anti-mCherry signals, with strong background fluorescence being detected across the brain slice in the latter (**Fig. 3.2**). Without images captured of such anti-dsRed signals, it would be difficult to determine true virus expression, and thus this animal would have been considered to have no virus expression. Before developing and testing our hypothesis, a total of 10 DREADDs animals were excluded from our dataset due to displaying no virus expression, which may have occurred due to the outlined histological error.

The other reason for exclusion was poor electrophysiology signals (n = 3 control, n = 4 DREADDs), which was detected during sleep scoring. The reasons that this occurred was lack of grounding of the signals, either in the set-up or poor connections of grounding within the headcap of animals, which led to high levels of noise, artifacts, and electrical interference. This caused difficulty in extracting or reading true EEG and EMG traces (**Fig. 3.1C**). To avoid this issue, we added a 'back-up' ground

intracranial connection (see **Fig. 2.6**) which allowed monitoring of signals with a different orientation of connector, if the first failed.

Overall, with the outlined exclusion criteria, results from a total of 10 control animals and 8 DREADDs animals are reported for chemogenetic studies in this chapter. As a subset of animals were used for 6-hour sleep recordings only, this dataset reduced to 7 control animals and 5 DREADDs animals for rebound sleep studies.

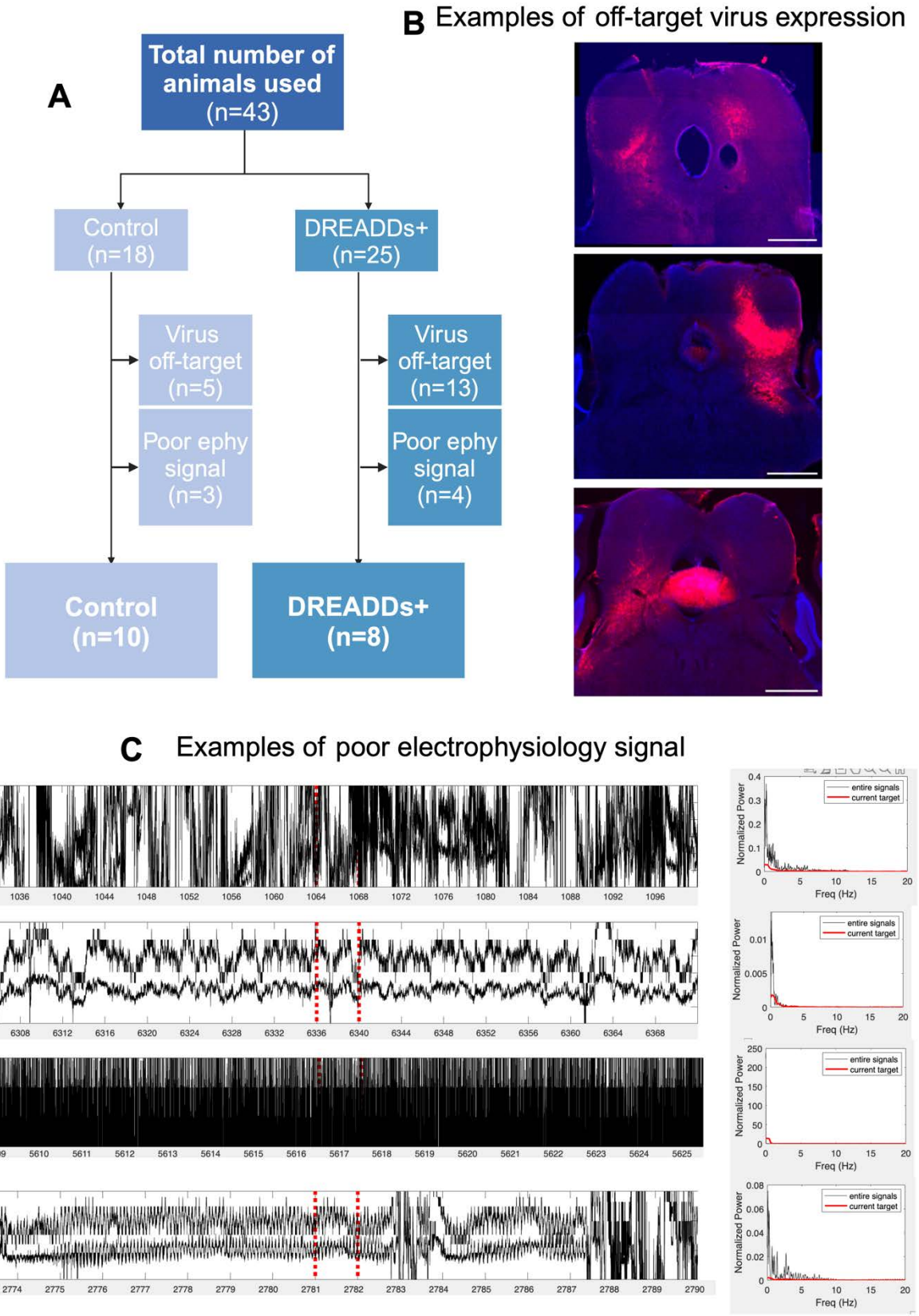

Figure 3.1. Schematic of animals used and examples of excluded animals. **A.** Schematic of animals used in chemogenetic studies. **B.** Examples of excluded animals due to poor virus expression. Scale bars = 1000 μm. **C.** Examples of animals excluded due to bad electrophysiolgy quality. 4 second ephochs of EEG and EMG traces (right), EEG spectral density for entire signal and current 4 second window, red dotted (right).

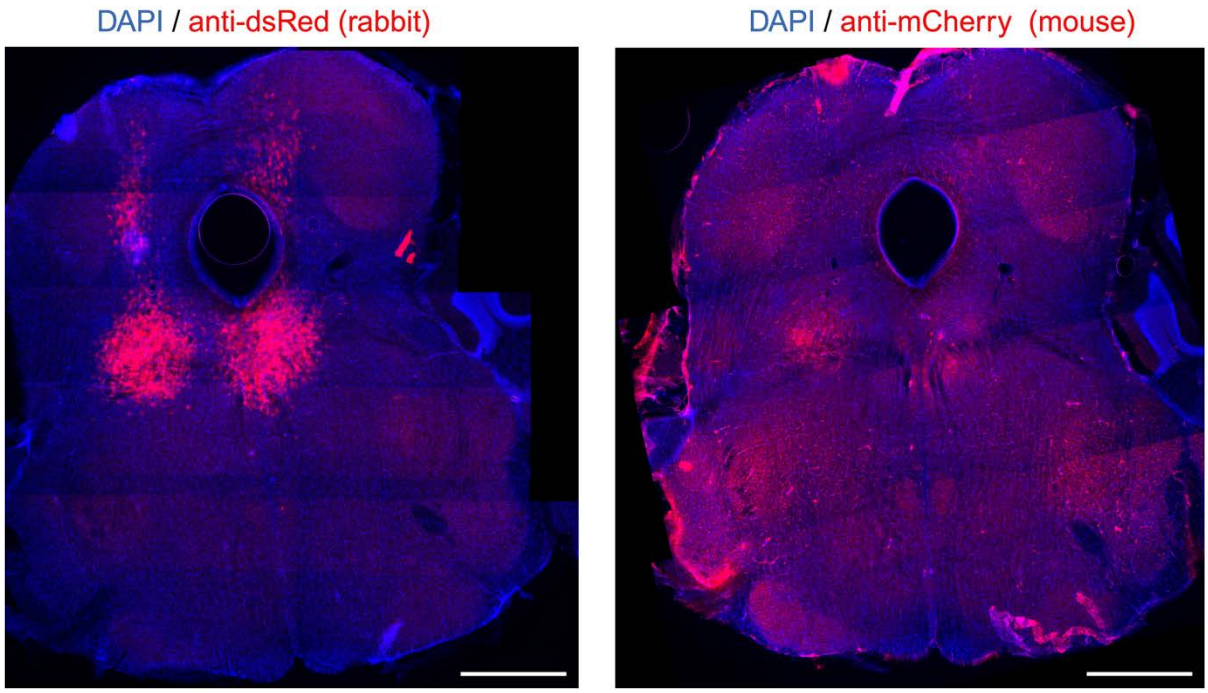

Figure 3.2. Difference of the same DREADDs animal stained with anti-mCherry and anti-dsRed one 80 μm section apart. Scale bar = 1000 μm.

3.2.3. Bilateral virus expression in the pons

To confirm that virus expression was contained in the pons, immunohistochemistry was carried out on all mice. As viruses were conjugated with fluorescent tags mCherry, or tdTomato, bilateral virus expression was confirmed using anti-DsRed or anti-mCherry staining (shown in red) and DAPI counterstaining (**Fig. 3.3A**). Expression could generally be observed across 3-5 80 μm sections, suggesting viral spread was relatively well contained. To better visualise expression, we took histological images from all animals used in this chapter, registered each to the Allen Mouse Brain atlas CCFv3, and extracted virus expression for each image. Atlas maps were grouped according to AP axis position and aligned, and the matching virus expression segmentation was overlayed to the corresponding atlas. This visualisation suggests that in control animals, virus expression occurred mostly in the pons, however some expression did occur in midbrain and medullar regions (n = 30 histological images from 10 control animals, n = 3 images per animal) (**Fig. 3.3B**). This was also the case in DREADDs animals, with most overlay of virus expression occurring in the pons (n = 16 histological images from 8 DREADDs animals, n = 1-3

images per animal) (**Fig. 3.3C**) and some expression being observed in midbrain, cerebellar, and medullar regions. However, in DREADDs animals, expression was much harder to visualise, and cerebellar signals appear to largely be caused by autofluorescence. This was due to the problems we encountered during histology as previously discussed (**Fig. 3.2**), leading to autofluorescence also being extracted. Overall, after visualising expression across animals used in chemogenetic we observed virus was expressed largely in pontine regions, with some expression occurring in midbrain and other hindbrain regions (**Fig. 3.3**).

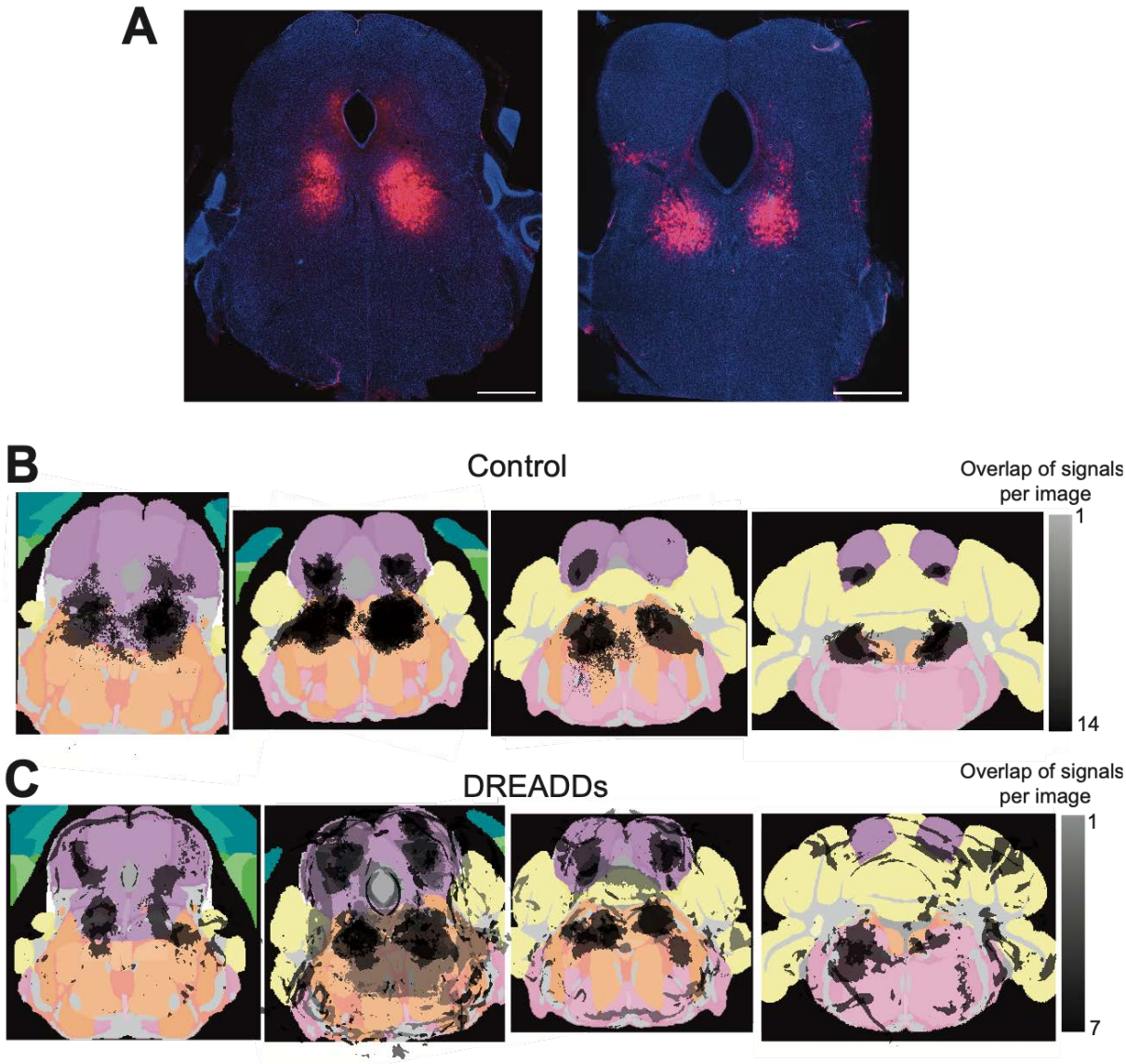

Figure 3.3. Virus expressed in pontine regions and some midbrain and cerebellar regions across animals used in chemogenetic studies. A. Examples of bilateral expression in the pons in two seperate animals (blue = DAPI, red = anti-DsRed). Scale bar = 1000 μm. **B.** Virus expression in control animals across anterior-posterior axis. Histological images were registered to the Allen Mouse Brain atlas CCFv3, where colours indicate wider regions. Blue/green = cortex, purple = midbrain, orange = pons, pink = medulla, yellow = cerebellum. Black indicates the virus where darker colour indicates overlayed expression in multiple sections (demonstrated in colourbar). n = 30 histological slice images for 10 animals, 3 images per animal. **C.** Same as in (B) but for DREADDs animals, n = 16 histologcial slice images for 8 animals, 1-3 per animal.

3.2.4. Virus expression in pontine astrocytes

To confirm that each virus was specifically expressed in astrocytes, sections were also co-stained with either an astrocyte specific marker, anti-GFAP, or a neuron-specific marker anti-NeuN. Using epifluorescent imaging we observed in mice injected with the control virus, many cells co-expressed both anti-mCherry and anti-GFAP (**Fig. 3.4**), while little-to-no co-expression with anti-NeuN occurred (**Fig. 3.5**). It is worth noting that no quantification analysis was performed for these results, as astrocytes are large with complex morphology, and their processes can extend up to 120 μm, thus making it extremely difficult to identify and count individual astrocytes.

Using epifluorescent imaging on sections obtained from animals injected with the DREADDs virus, we again observed cells stained with anti-mCherry also co-expressed anti-GFAP (**Fig. 3.6**), while little-to-no cells co-expressed anti-NeuN (**Fig. 3.7**). Due to the complex nature of astrocyte morphology and the lack of Z-axis control in epifluorescent imaging, we wanted to look at co-localisation of anti-mCherry and anti-GFAP staining in more depth. For this, we next utilised confocal microscopy to further explore co-expression in both animal groups.

Confocal imaging has superior axial resolution and has the ability to control the depth of focal field, thus removing background signals. Confocal imaging of animals injected with the control virus show extensive co-expression of anti-mCherry and anti-GFAP in cells with astrocyte-like morphology (**Fig. 3.8**). In animals expressing the DREADDs virus, we again observed overlay of anti-mCherry and anti-GFAP in cells with astrocyte-like morphology (**Fig. 3.9**). In DREADDs animals, while overlay did occur, morphology of cells stained with anti-GFAP did not exactly match that of anti-mCherry, unlike what we observed in control animals. We noticed that in comparison to expected morphology observed in control animals (**Fig. 3.8**), astrocytes in DREADDs animals presented hypertrophic morphology in anti-GFAP staining, which was consistent across 3 DREADDs animals. We suggest this was due to astrocytes being activated in our chemogenetic experiments, which can lead to upregulated GFAP expression. This may contribute to why the overlay of cells stained with anti-GFAP and anti-mCherry was less localised in DREADDs animals than in control animals.

Overall, using both epifluorescent and confocal imaging, we observed co-expression of anti-GFAP and anti-mCherry in cells with astrocyte-like morphology in both DREADDs and control animals, while little-to-no co-expression of anti-NeuN and anti-mCherry occurred.

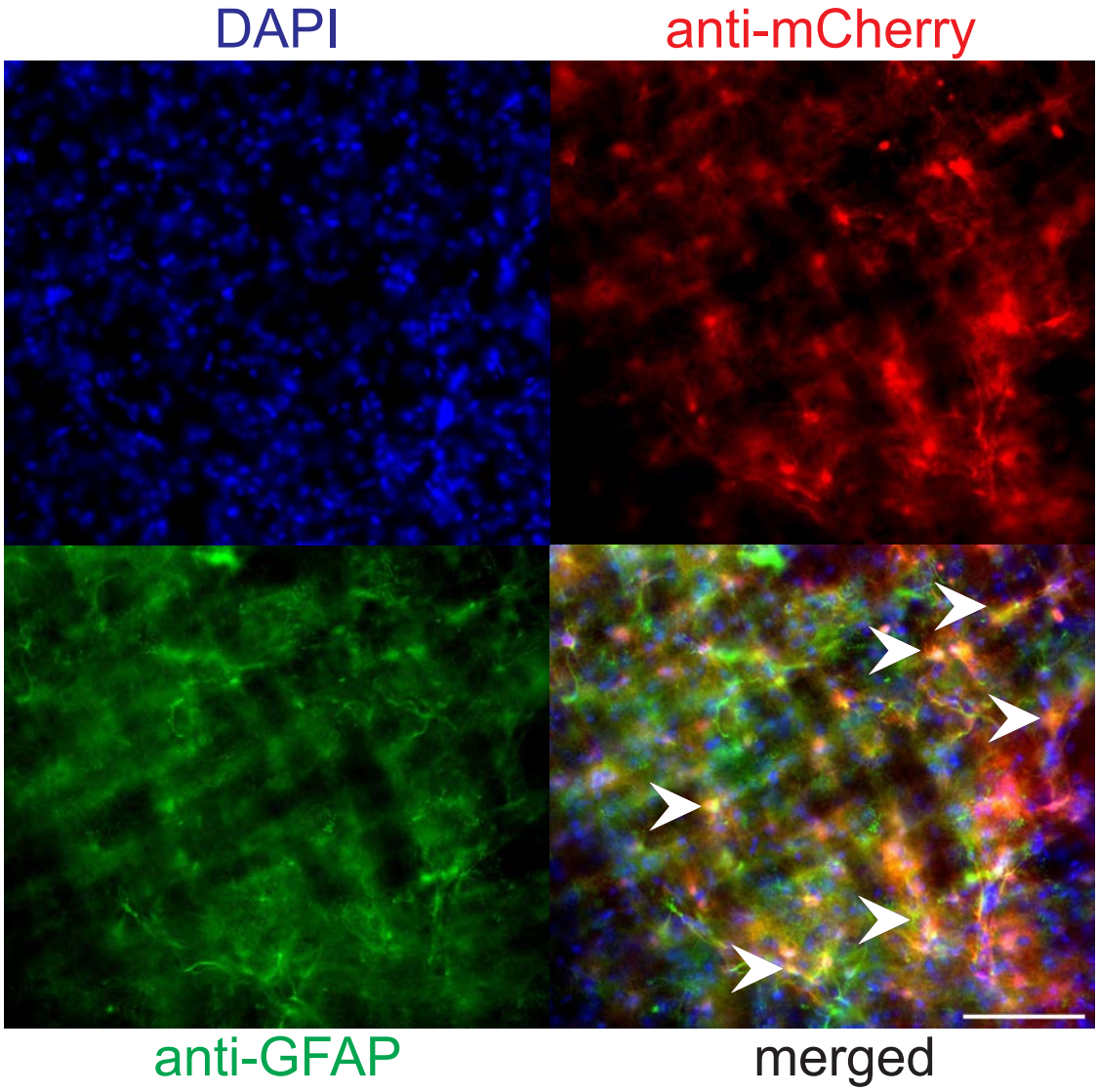

Figure 3.4. Overlap of anti-mCherry and anti-GFAP in a control animal. Examplar images of one histological section from one animal expressing control virus using epifluorescence imaging. Top left, DAPI staining. Top right, anti-mCherry staining. Bottom left, anti-GFAP staining. Bottom right, combined images of all. White arrows indicate examples of overlap. Scale bar = 100 μm.

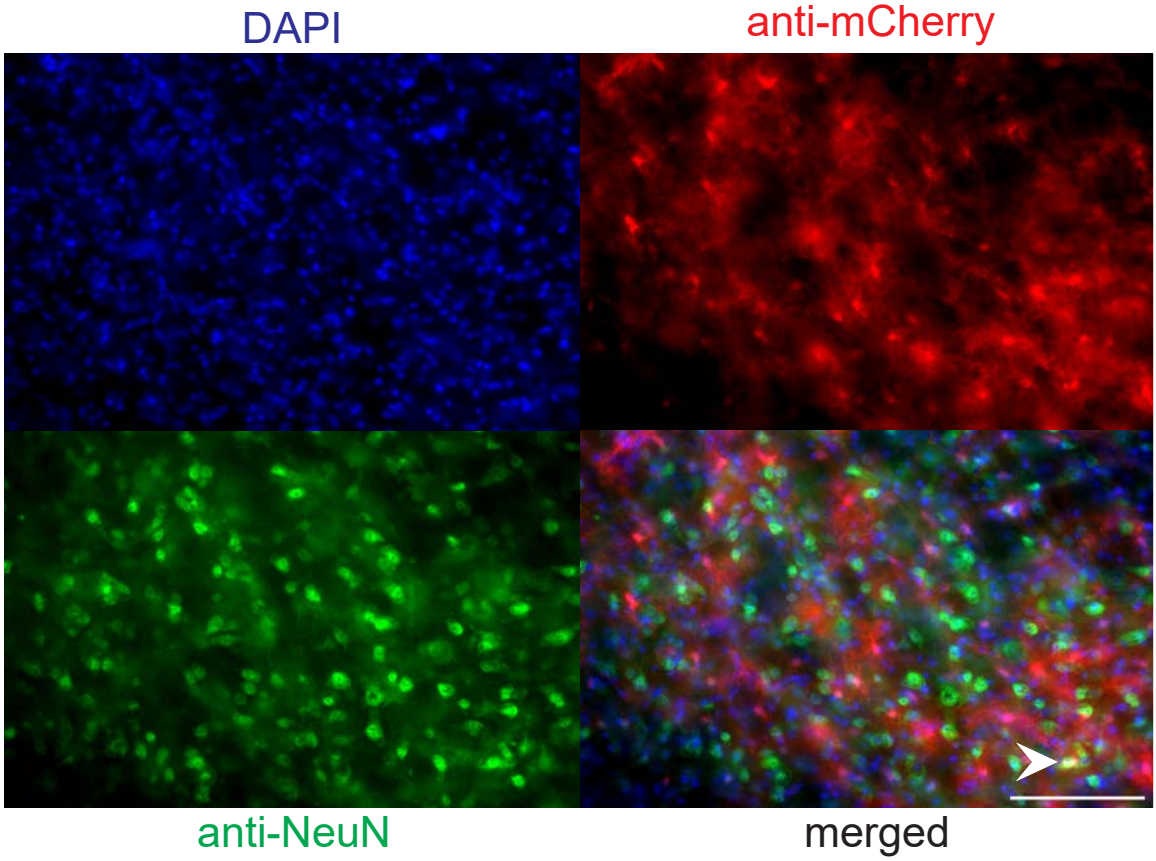

Figure 3.5. Overlap of anti-mCherry and anti-NeuN in a control animal. Examplar images of one histological section from one animal expressing control virus using epifluorescence imaging. Top left, DAPI staining. Top right, anti-mCherry staining. Bottom left, anti-NeuN staining. Bottom right, combined images of all. White arrow indicates possible co-expression. Scale bar = 100 μm.

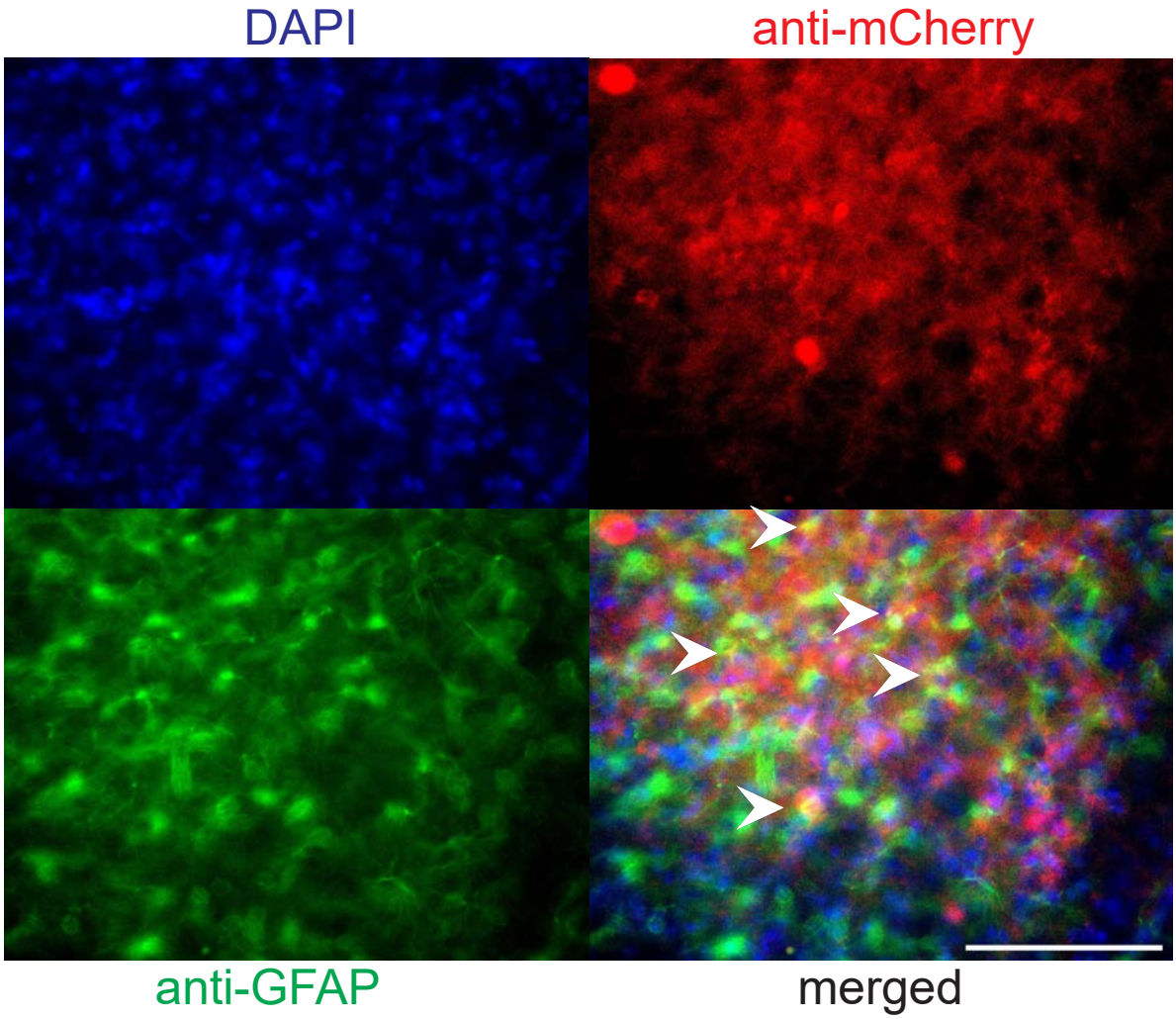

Figure 3.6. Overlap of anti-mCherry and anti-GFAP in a DREADDs animal. Examplar images of one histological section from one animal expressing hM3D virus using epifluorescence imaging. Top left, DAPI staining. Top right, anti-mCherry staining. Bottom left, anti-GFAP staining. Bottom right, combined images of all. White arrows indicate possible co-expression. Scale bar = 100 μm.

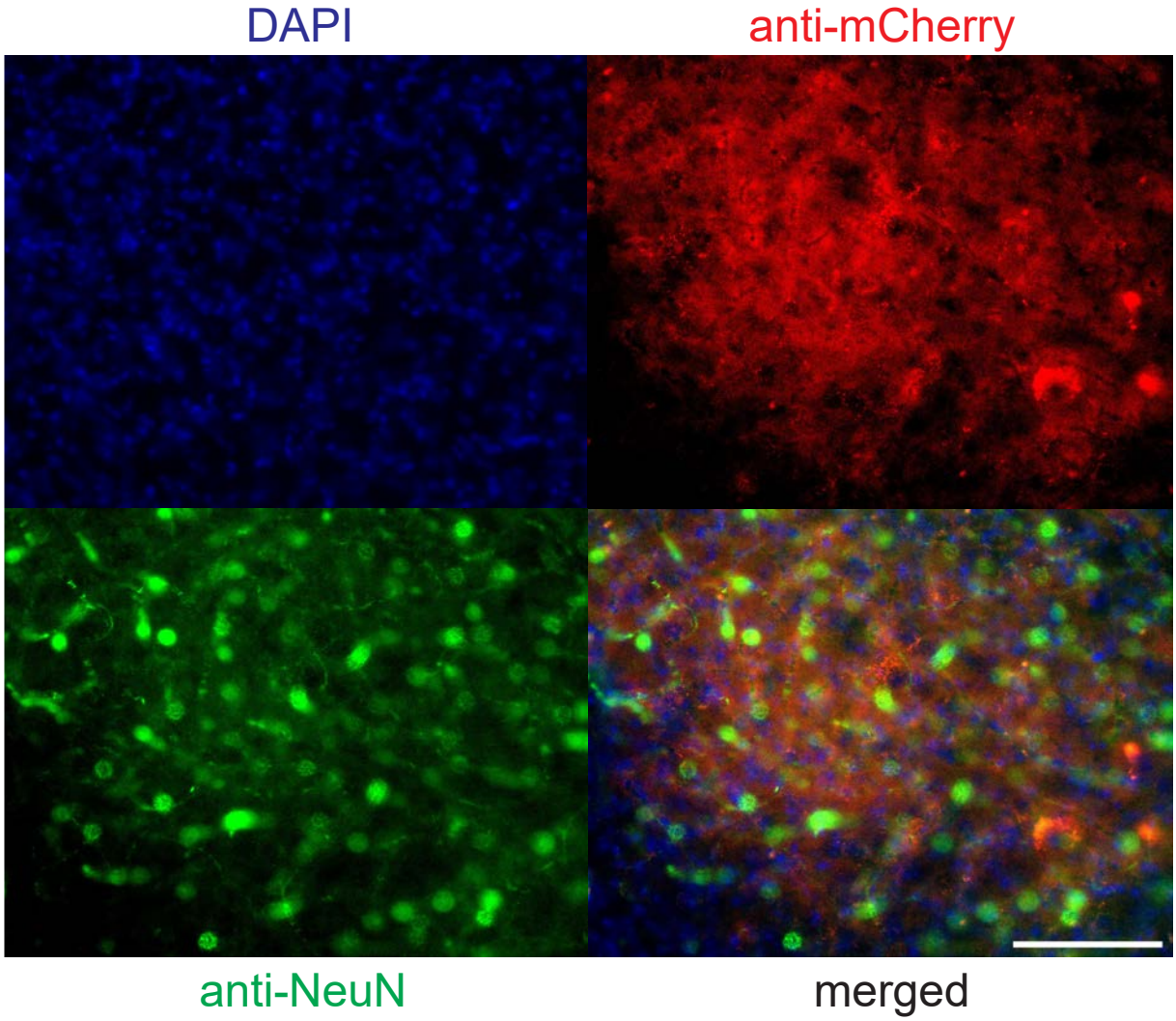

Figure 3.7. Overlap of anti-mCherry and anti-NeuN in a DREADDs animal. Examplar images of one histological section from one animal expressing hM3D virus using epifluorescence imaging. Top left, DAPI staining. Top right, anti-mCherry staining. Bottom left, anti-NeuN staining. Bottom right, combined images of all. Scale bar = 100 μm.

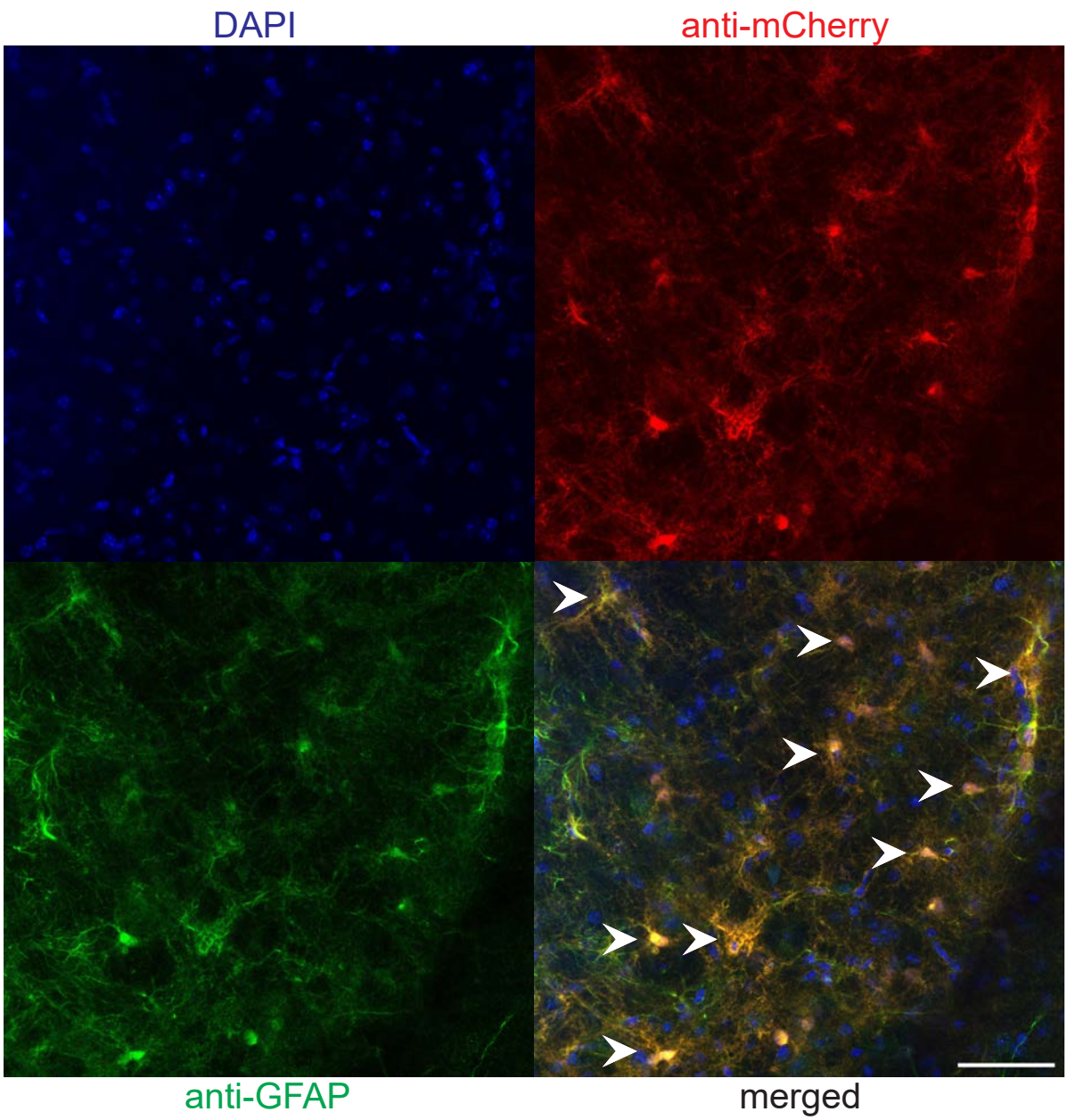

Figure 3.8. Confocal imaging of anti-mCherry and anti-GFAP in a control animal. Examplar images of one histological section from one animal expressing control virus using confocal imaging. Top left, DAPI staining. Top right, anti-mCherry staining. Bottom left, anti-GFAP staining. Bottom right, combined images of all. White arrows indicate areas of overlap. Scale bar = 50 μm.

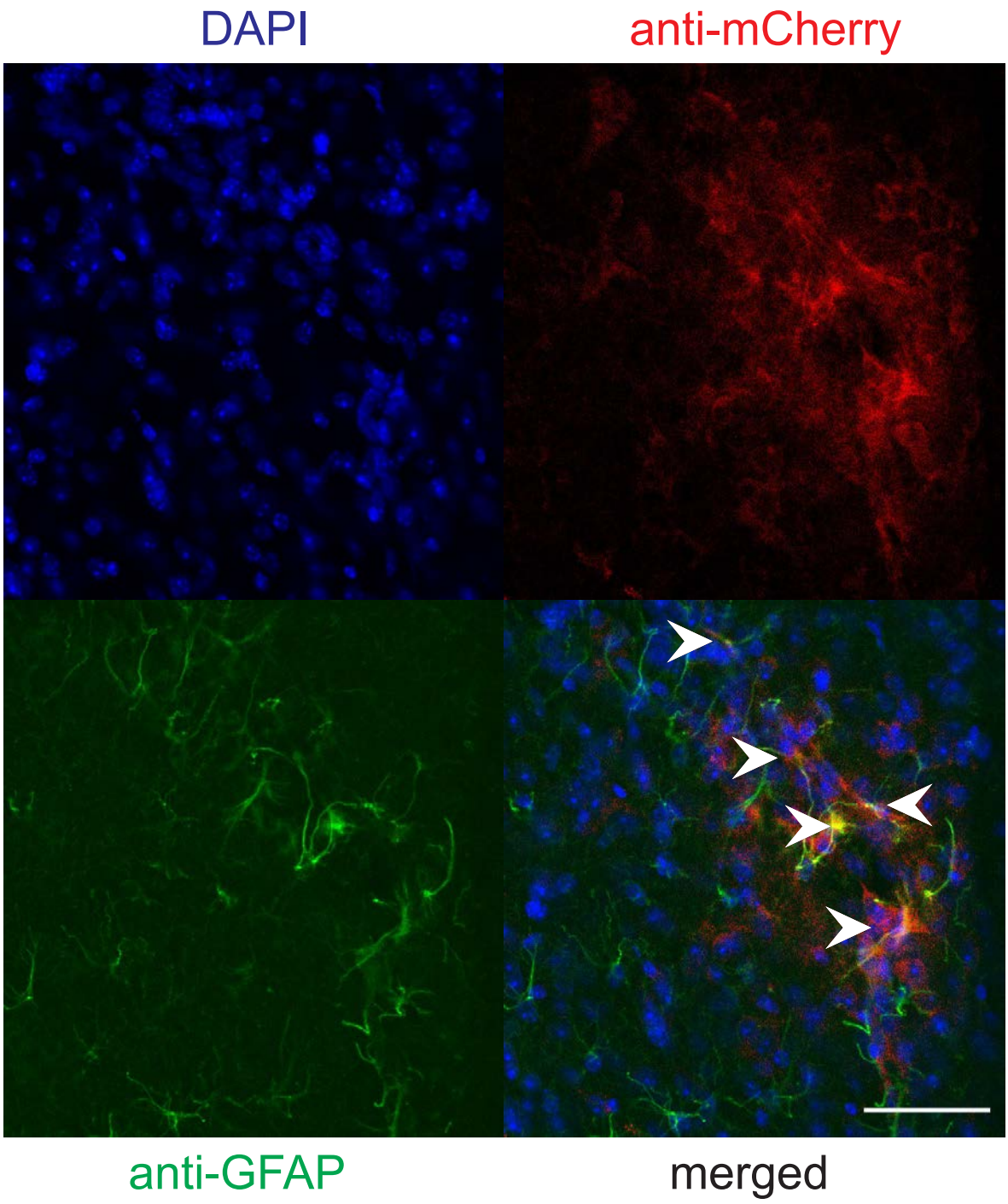

Figure 3.9. Confocal imaging of anti-mCherry and anti-GFAP in a DREADDs animal. Examplar images of one histological section from one animal expressing hM3D virus using confocal imaging. Top left, DAPI staining. Top right, anti-mCherry staining. Bottom left, anti-GFAP staining. Bottom right, combined images of all. White arrows indicate co-expression. Scale bar = 50 μm.

3.2.5. Chemogenetic activation of pontine astrocytes reduces REM sleep in a dose-dependent manner

To allow for sufficient virus expression, mice began experiments 4 weeks after viral injection surgeries. Mice were habituated to experiments by increased handling and scruffing, and being tethered to the system for short amounts of time. CNO reaches maximal plasma, brain, and CSF concentration 15 minutes post injection, and behavioural effects of CNO have been recorded up to 6 hours post injection (Jendryka *et al.*, 2019; Traut *et al.*, 2023). As such, for experiments, mice were given vehicle or CNO (1, 5 or 10 mg/kg, *i.p.* injection) immediately before tethering and beginning recordings. Initially EEG and EMG signals were recorded for 6 hours only after injection (control n=3, DREADDs n=3). Recording time was later increased to 10 hours (control n=7, DREADDs n=5) to investigate prolonged effects of CNO, or potential rebound.

During our experiments, animals displayed typical sleep-wake cycles despite being tethered to our electrophysiology system. An exemplar 10-hour sleep recording obtained from a single recording from one control mouse given a vehicle treatment prior to recording is shown in **Figure 3.10A,** this demonstrates the frequency of cortical EEG (top), sleep hypnogram (middle) and EMG activity (bottom). NREM sleep appears around 30 from the beginning of recording, while REM sleep typically initially appears after 60-90 minutes from the beginning of recordings, and steadily increases throughout the 10 hours (**Fig. 3.10A-B**). Awake episodes consist of low frequency EEG and high EMG activity, while NREM sleep is characterised by high powered low frequency EEG, particularly high delta (1-4 Hz), and low EMG power, and REM consists of high theta activity (6-8 Hz) and very low EMG power (**Fig. 3.10A & C**). This representative sleep characteristics from an individual recording shows that, as expected, animals spend a relatively large proportion of time in NREM sleep and awake, and a lower proportion of REM sleep. Animals transition through the sleep-wake cycle and have frequent episode transitions throughout the recording, while episode durations of all states can vary (**Fig. 3.10D**). Overall, this exemplar recording demonstrates that animals enter REM sleep quickly despite being tethered to our set-up, and that REM sleep occurs throughout recordings (**Fig. 3.10**).

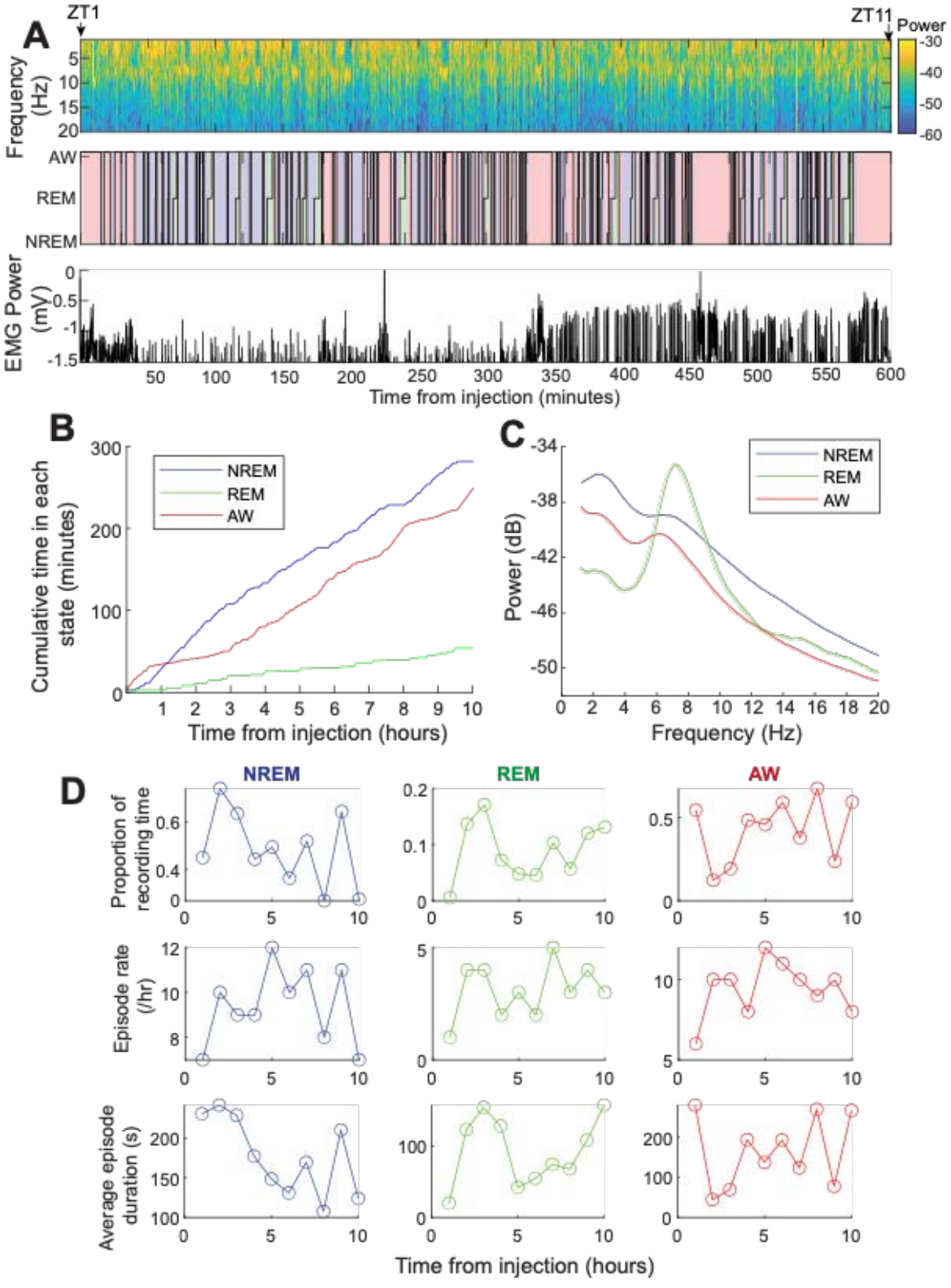

Figure 3.10. Sleep-wake cycle and sleep characteristics in individual recording across 10 hours. A. Sprectrogram (top), hypnogram (middle) and EMG power (bottom) of a single animal across 10 hours. Colourbar indicates intensity of frequency. **B.** Cumulative state duration across 10 hours. **C.** Frequency of cortical EEG in each state. **D.** Proportion (top row), number of episode per hour (middle row) and average episode duration (bottom row) of NREM (blue) REM (green) and wake (red).

To determine a cut-off point to look at effects of chemogenetic modulation and long-term rebound effects separately, we wanted to look at changes in sleep architecture across 10 hours post injection. For this we combined all 6-hour and 10-hour recordings and determined differences in total state duration, number of episodes per hour, and average episode durations between treatments (control n=10, DREADDs n=8). However, this leaves data from hours 7-10 under sampled in comparison to the first 6 hours. While examining changes between control and DREADDs animals given vehicle and a moderate dose of CNO only (1 mg/kg), the fraction of awake and NREM sleep remained relatively stable across the 10 hours, with only a difference in total NREM sleep occurring between animal groups at hour 5 ($F(1, 31) = 4.24$, $p = 0.048$, two-way ANOVA). Meanwhile, all animals given 1 mg/kg CNO had less REM sleep than animals given vehicle injections at hour 3 ($F(1, 31) = 5.40$, $p = 0.0268$, two-way ANOVA), and a significant difference was detected with animal:drug interaction at hour 5 ($F(1, 31) = 5.47$, $p = 0.0262$, two-way ANOVA) (**Fig. 3.11A**).

Similarly, while the number of episodes per hour remained relatively stable for awake and NREM, with a difference in wake episode number only occurring between animal:drug interactions at hour 7 ($F(1, 19) = 8.56$, $p = 0.0087$, two-way ANOVA), differences in rate of REM episodes occurred at hours 2, 3, and 4 between animal groups ($F(1,31) = 5.24$, $p = 0.029$; $F(1, 31) = 4.88$, $p = 0.0348$; $F(1, 31) = 5.98$, $p = 0.0203$, two-way ANOVA), at hour 6 between animal:drug interactions ($F(1, 31) = 5.23$, $p = 0.0296$, two-way ANOVA), and between drug treatments at hour 9 ($F(1, 31) = 4.75$, $p = 0.0421$, two-way ANOVA) (**Fig. 3.11B**).

In contrast, no differences in length of episodes was found in REM sleep or awake, but differences in NREM episode length were found throughout recordings (dose - hour 1 $F(1, 31) = 5.15$, $p = 0.0309$; animal group - hour 5 $F(1, 31) = 4.82$, $p = 0.036$; hour 7 $F(1, 19) = 9.17$, $p = 0.0076$; hour 8 $F(1, 19) = 6.88$, $p = 0.0173$; hour 10 $F(1, 19) = 6.82$, $p = 0.0177$, two-way ANOVA) (**Fig 3.11C**).

Due to these differences, we chose to examine the initial 6 hours post injection for direct effects of chemogenetic activation of pontine astrocytes on REM sleep and the sleep-wake cycle, and the last 4 hours to look at rebound sleep following chemogenetic modification.

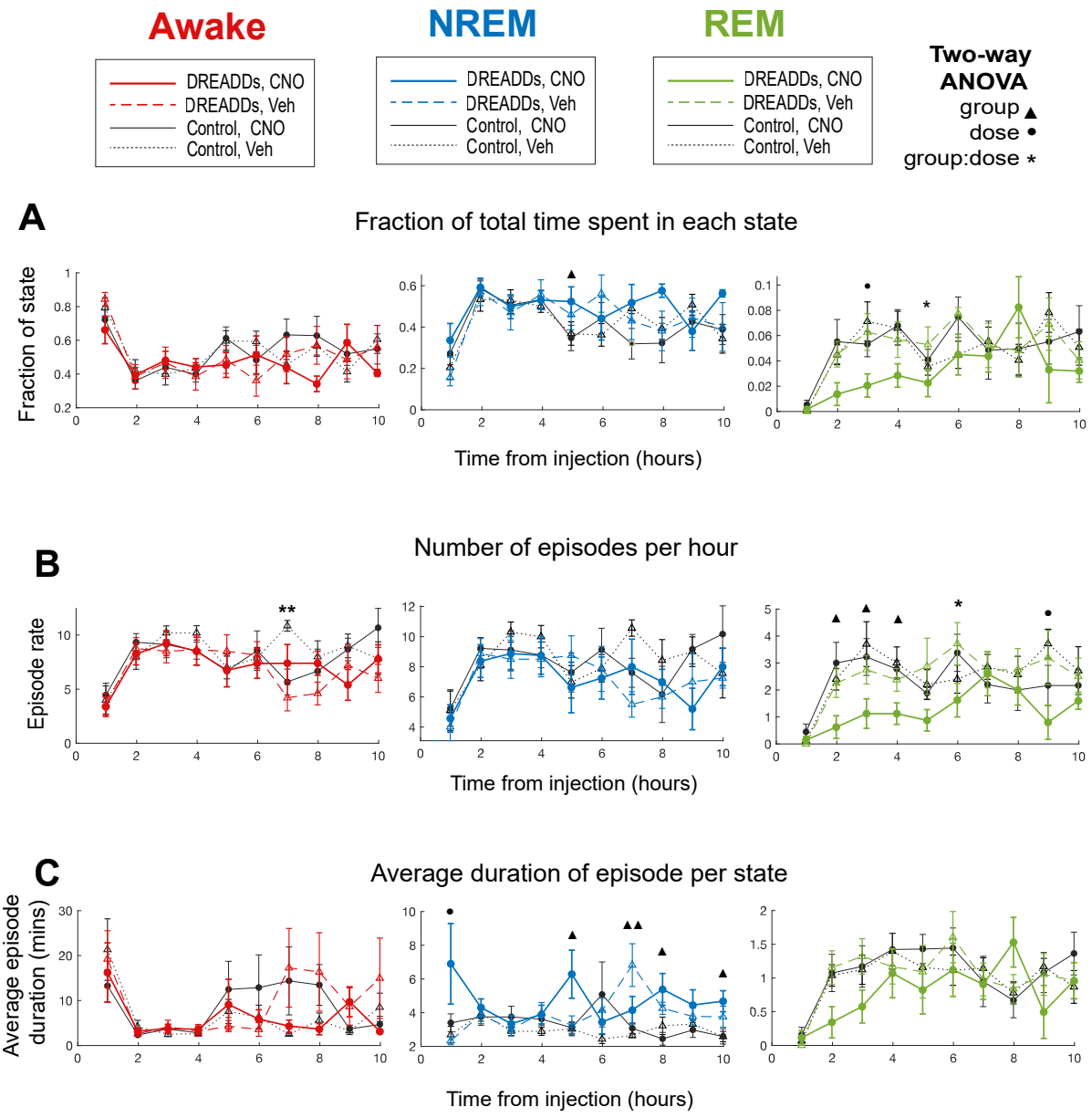

Figure 3.11. Characteristics of the sleep-wake cycle 10 hours after CNO injections (1mg/kg). Effects of *i.p.* injections of vehicle or CNO (1 mg/kg) on animals expressing a control virus or expressing DREADDs for 10 hours following injection on the total fraction of each state (**A**), number of episodes of each state per hour (**B**), and the average episode duration (**C**). Data shown as average ± SEM. Significance calculated with two-way ANOVA, Animal group sinificance represented as ▲, dose represented as ●, animal:drug interaction *. *p<0.05, **p<0.001. Hours 1-6, control n=10, DREADDs n=8; hours 7-10, control = 7, DREADDs = 5.

To demonstrate the changes in the sleep-wake cycle in these 6-hour periods following drug treatments, we show exemplar data from one DREADDs mouse. When this animal received an *i.p.* injection of vehicle, REM sleep appeared 60-90 minutes from the beginning of recording, and occurred frequently throughout the remainder of the 6 hours (**Fig. 3.12A**). Following administration of CNO (1 mg/kg), it took longer for this mouse to enter REM sleep, with REM episodes occurring less frequently (**Fig. 3.12B**). When this CNO concentration was increased to 5 mg/kg and 10 mg/kg, this effect was exaggerated with only singular REM episodes occurring (**Fig. 3.12C-D**).

This exemplar data suggests CNO reduced the occurrence of REM sleep and increased REM sleep latency in a dose-dependent manner in a DREADDs animal (**Fig. 3.12**). To look at this further, we examined group data from all mice.

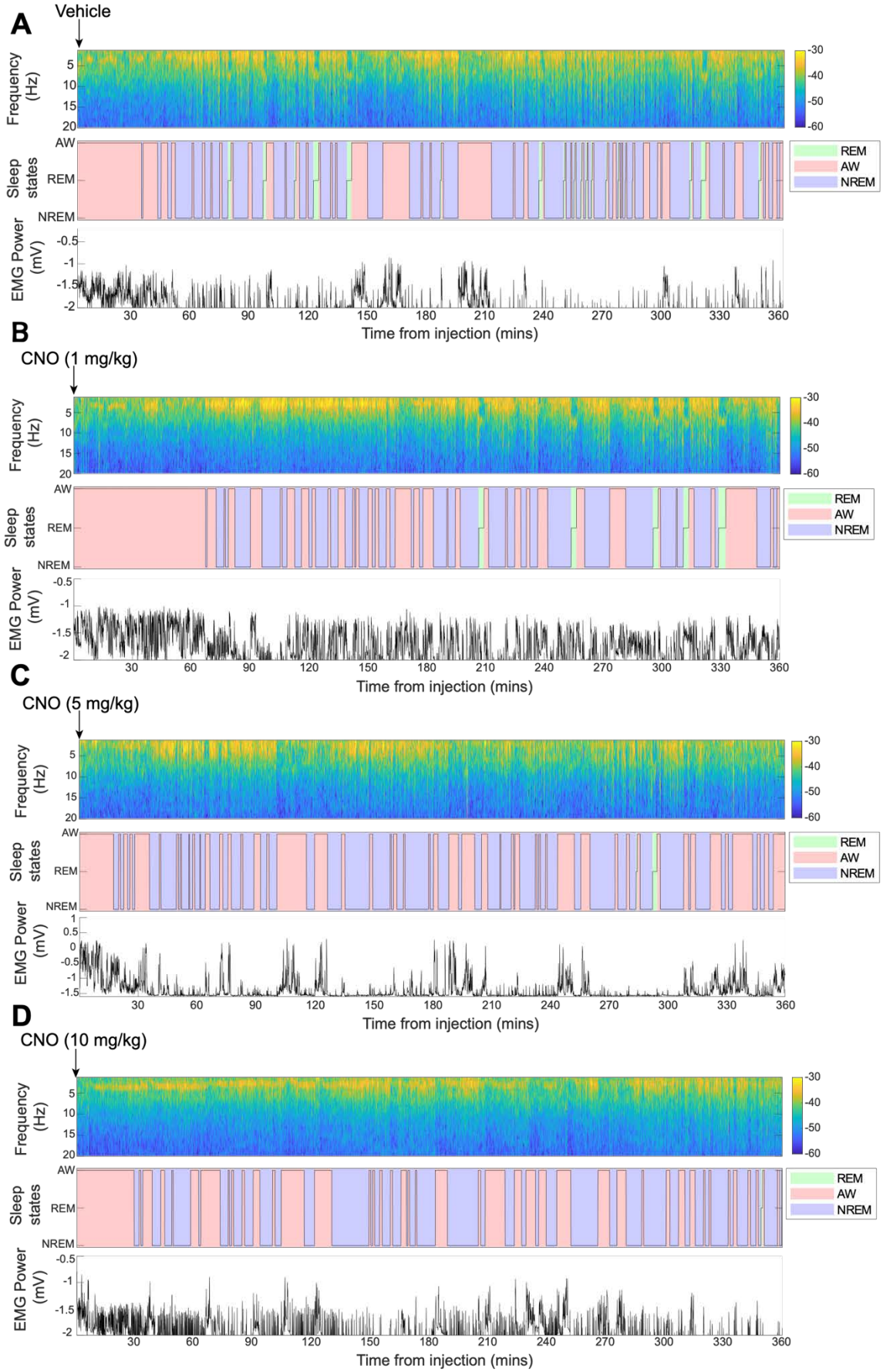

Figure 3.12. Examples of sleep-wake cycles in a single DREADDs animal with different concentrations of CNO. Features and characterisation of sleep states in one animal expressing hM3D virus 6 hours after injection of vehical **(A),** 1 mg/kg CNO **(B),** 5 mg/kg CNO **(C),** 10 mg/kg **(D).** In each image from top to bottom, top - a spectrogram showing cotrical EEG frequency (0-20 Hz), colourbar indicates intensity of frequency, middle - hypnogram showing sleep states, awake (red), REM sleep (green), NREM sleep (blue), bottom - EMG power (mV).

To quantify these differences, we looked at differences of sleep architecture between groups (control n=10, DREADDs n=8). Control animals refer to animals that bilaterally express AAV5-GfaABC$_1$D-tdTomato, while DREADDs animals refer to animals who express AAV5-GfaABC$_1$D-hM3D-mCherry, which are represented in bar graphs in lighter and darker colours, respectively. Both groups of animals received vehicle or CNO (1, 5, and 10 mg/kg) treatments, creating multiple negative control conditions.

Group data supported representative descriptions, as chemogenetic activation of pontine astrocytes reduced total percent of REM sleep between animal groups ($F(1, 62) = 51.89$, $p = 0.0001$, two-way ANOVA), drug treatment ($F(3, 62) = 7.11$, $p = 0.0004$, two-way ANOVA), and animal:drug interaction ($F(3, 62) = 8.33$, $p = 0.0001$, two-way ANOVA) (**Fig 3.13A**). Specifically, while post-hoc statistical analysis shows there were no differences in total percent time spent in REM sleep between control and DREADDs animals in the vehicle condition (4.3889 ± 0.49 vs 4.7702 ± 0.74 respectively, $p = 0.9992$, Tukey-Kramer test), compared to control animals, DREADDs animals spent a significantly less time in REM sleep when given 1 mg/kg CNO (4.9486 ± 0.39 vs 2.2014 ± 0.60, $p = 0.0052$, Tukey-Kramer test), 5 mg/kg CNO (4.8272 ± 0.54 vs 1.0648 ± 0.42, $p = 0.0001$, Tukey-Kramer test), and 10 mg/kg CNO (4.3889 ± 0.38 vs 0.5347 ± 0.22, $p = 0$, Tukey-Kramer test). Compared to DREADDs animals that received vehicle treatment, CNO reduced total percent REM sleep in a dose dependent manner (vs 1mg/kg $p = 0.0052$, vs 5 mg/kg $p = 0.0001$, vs 10 mg/kg $p = 0.0001$, Tukey-Kramer test) (**Fig 3.13A**). Two-way ANOVA statistical tests also showed significant differences in total percent spent awake and in NREM sleep between drug treatments ($F(3, 62) = 3.2$, $p = 0.0295$, two-way ANOVA; $F(3, 62) = 4.91$, $p = 0.0040$, respectively, two-way ANOVA). Post-hoc analysis found only DREADDs animals given 10 mg/kg CNO spent significantly more time in NREM when compared to control animals receiving vehicle injections (55.4560 ± 2.88 vs 41.6704 ± 2.13 respectively, $p = 0.0499$, Tukey-Kramer test) (**Fig 3.13A**). Notably, we found no difference in total REM sleep in control animals given vehicle or CNO treatments.

Similarly, differences were found between the total number of REM episodes between animal groups ($F(1, 62) = 68.13$, $p = 0$, two-way ANOVA), drug treatments ($F(3, 62) = 11.71$, $p = 0$, two-way ANOVA), and animal:drug interactions ($F(3, 62) = 7.84$, $p = 0.0002$, two-way ANOVA) (**Fig. 3.13B**). Specifically, post-hoc analysis found strong

reductions in REM episode rate in DREADDs animals compared to control animals following injections of 1 mg/kg CNO (5.5001 ± 1.88 vs 14.1111 ± 1.09, p = 0.0005, Tukey-Kramer test), 5 mg/kg CNO (2.1250 ± 0.77 vs 12.0010 ± 1.35, p = 0.0001, Tukey-Kramer test), and 10 mg/kg CNO (1.3750 ± 0.3750 vs 13.0000 ± 1.1155, p = 0.0001, Tukey-Kramer test). In comparison, there was no difference between DREADDs and control animals when given vehicle treatments (13.6250 ± 1.71 vs 13.8000 ± 1.39, p = 0.9999, Tukey-Kramer test) (**Fig. 3.13B**). Post-hoc analysis also found strong significant reductions in DREADDs animals with all CNO doses compared to vehicle (vs 1mg p = 0.0018, vs 5 mg/kg CNO p = 0.0001, vs 10 mg/kg CNO p = 0.0001, Tukey-Kramer test) (**Fig. 3.13B**). It is worth noting that although all other groups were normally distributed, the data for number of REM episodes in control mice given vehicle were not normally distributed (p = 0.0396, Shapiro-Wilk test). On the other hand, differences were found in the total number of awake and NREM sleep episodes between animals (F(3, 62) = 5.9, p = 0.0101; F(3, 62) = 6.78, p = 0.0115, respectively, two-way ANOVA) (**Fig. 3.13B**), but no post-hoc pairwise significance was found between groups.

When exploring average durations of REM sleep episodes, no significant differences were found with two-way ANOVA or pairwise comparisons (animal:drug interactions, F(3, 62) = 0.24, p = 0.8658, two-way ANOVA) (**Fig. 3.13C**). However, differences between animal groups were found in average duration of wake episodes and NREM episodes (F(3, 62) = 7.83, p = 0.0068; F(3, 62) = 12.57, p = 0.0008, respectively, two-way ANOVA), showing DREADDs animals appear to have longer episode durations, as well as fewer (**Fig. 3.13B-C**). Differences in average length of NREM episodes were also found between drug treatments (F(3, 62) = 4.5, p = 0.0064, two-way ANOVA), while posthoc pairwise differences found that compared to control animals given vehicle (192.6776 sec ± 12.42) DREADDs animals given high concentrations of CNO had longer NREM episodes on average (5 mg/kg 302.1519 sec ± 27.46, p = 0.0444, Tukey-Kramer test; 10 mg/kg 344.7023 sec ± 30.54, p = 0.0027, Tukey-Kramer test) (**Fig. 3.13C**). While all data for average REM and NREM episode duration were normally distributed, some group conditions for awake episode durations were not normally distributed (control:10 mg/kg CNO p = 0.0004, Shapiro-Wilk test).

Latency to first REM sleep episode also increased in DREADDs animals given CNO compared to control animals and/or vehicle conditions (animal, $F(1, 62) = 74.5$, $p = 0.0001$; drug, $F(3, 62) = 7.69$, $p = 0.0002$; animal:drug interaction, $F(3, 62) = 10.0$, $p = 0.0001$, two-way ANOVA) (**Fig. 3.13D**). Specifically, post-hoc analysis found DREADDs animals took longer to enter REM sleep compared to control animals when given 1 mg/kg CNO (200.9667 mins ± 49.92 vs 77.6889 mins ± 9.1504 respectively, $p = 0.0104$, Tukey-Kramer test), 5 mg/kg CNO (275.8833 mins ± 42.35 vs 57.7630 mins ± 4.67 respectively, $p = 0.0001$, Tukey-Kramer test), and 10 mg/kg CNO (305.5917 mins ± 21.25 vs 81.4733 mins ± 11.57 respectively, $p = 0.0001$, Tukey-Kramer test) while no differences were found in vehicle conditions (89.3667 mins ± 8.18 vs 85.9400 mins ± 6.19 respectively, $p = 1.00$ Tukey-Kramer test). Compared to DREADDs animals given vehicle, CNO increased latency to REM sleep in a dose-dependent manner (vs 1/mg/kg $p = 0.0369$, vs 5 mg/kg $p = 0.0001$, vs 10 mg/kg $p = 0.0001$, Tukey-Kramer test). Two-way ANOVA also detected reduced latency to NREM sleep between drug treatments ($F(3, 62) = 4.32$, $p = 0.0079$, two-way ANOVA) (**Fig. 3.13D**). The data in some conditions were not normally distributed (latency to REM, DREADDs:vehicle $p = 0.0005$; latency to NREM, control:vehicle $p = 0.0406$, control:10 mg/kg CNO $p = 0.0055$, Shapiro-Wilk test).

Overall, CNO reduced total time in REM sleep and the number of REM sleep episodes and increased latency to first REM episode in DREADDs animals. In contrast, CNO did not affect the length of REM sleep episodes. CNO also increased total NREM sleep and reduced latency to NREM sleep, while reducing total time awake, regardless of animal group, suggesting a sedative effect of CNO. Notably, all differences were observed in both male and female animals, and sex-dependent differences were not found. Interestingly, we found that no alteration to REM sleep was caused by CNO alone. DREADDs animals also had longer and fewer NREM and awake episodes, suggesting that chemogenetic modification may make sleep less fragmented, however, post-hoc analysis did not confirm this.

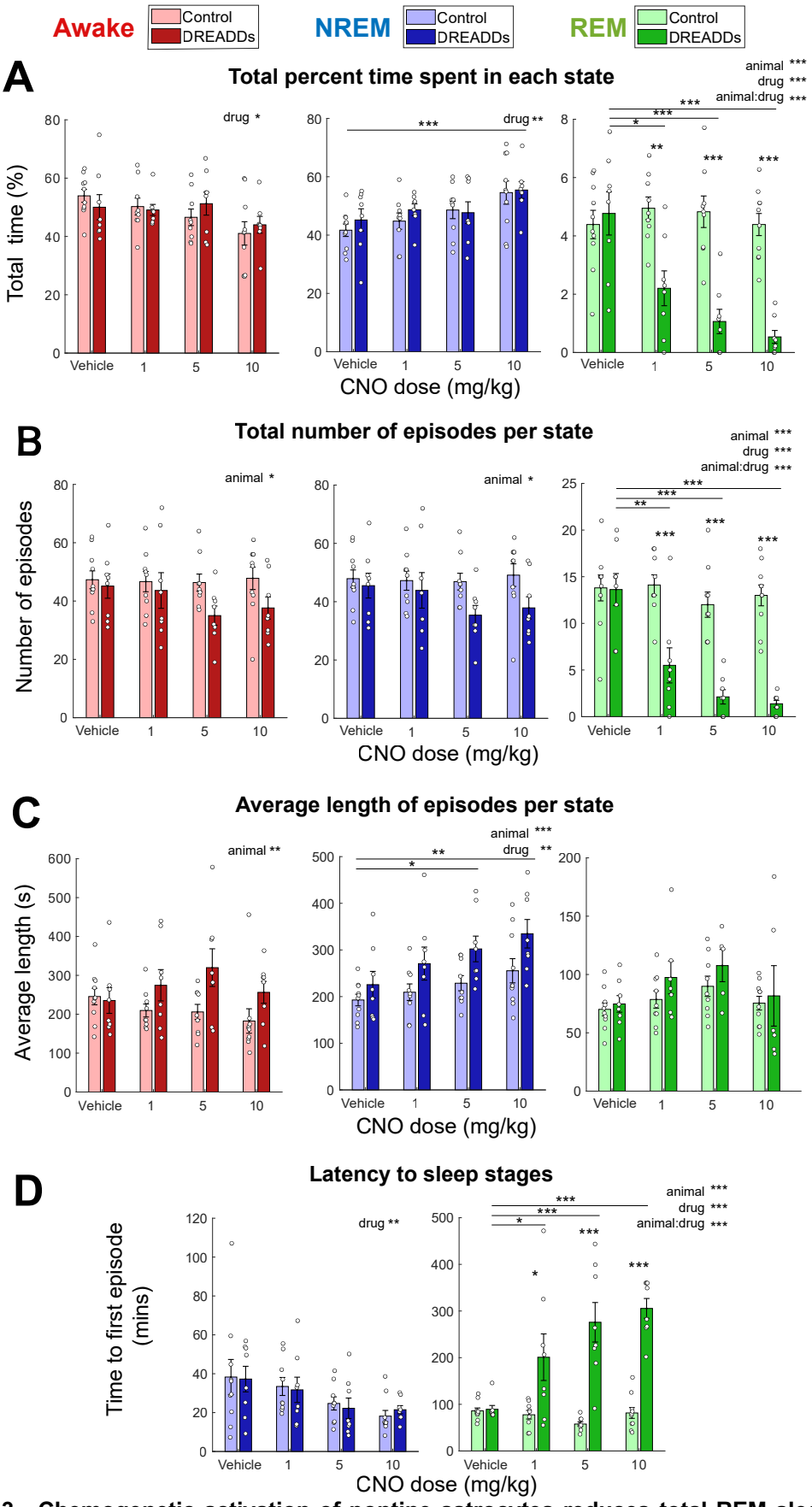

Figure 3.13. Chemogenetic activation of pontine astrocytes reduces total REM sleep and number of episodes. Effects of chemogenetic modification on total percent time in each state (**A**), total number of episodes (**B**), average episode length (**C**), and latency to sleep state (**D**). Data represented in mean ± SEM. Red = awake, blue = NREM sleep, green = REM sleep. Lighter colours indicate control group, dark colours indicate DREADDs group. Control n = 10, DREADDs n = 8. P values from two-way ANOVA comparing effects by animal group, drug treatment, and interaction shown in top right corner of each graph. P values from post-hoc analysis shown, *p<0.05, **p<0.01, ***p<0.001.

3.2.6. Effects of chemogenetics on REM sleep are diminished after 10 hours

Due to the reduction of REM sleep caused by chemogenetic activation of pontine astrocytes, we wanted to investigate if this would cause rebound REM sleep to occur in later hours. Rebound REM sleep could appear as longer or increased number of REM sleep bouts, due to increased REM sleep pressure following chemogenetic-induced deprivation. As we observed effects of CNO up to 6 hours, we extended our recording times and observed sleep-wake cycles for 10 hours following injections of vehicle or CNO.

In a single representative DREADDs animal given a vehicle injection, REM sleep occurred regularly throughout all 10 hours post injection (**Fig. 3.14A**). As illustrated before, in a DREADDs animals receiving increasing doses of CNO, REM sleep occurs less frequently and it takes longer for the animal to enter REM sleep post injection (**Fig. 3.14B-D**). However, in hours 6-10 REM sleep occurred frequently in all drug treatments (**Fig. 3.14**).

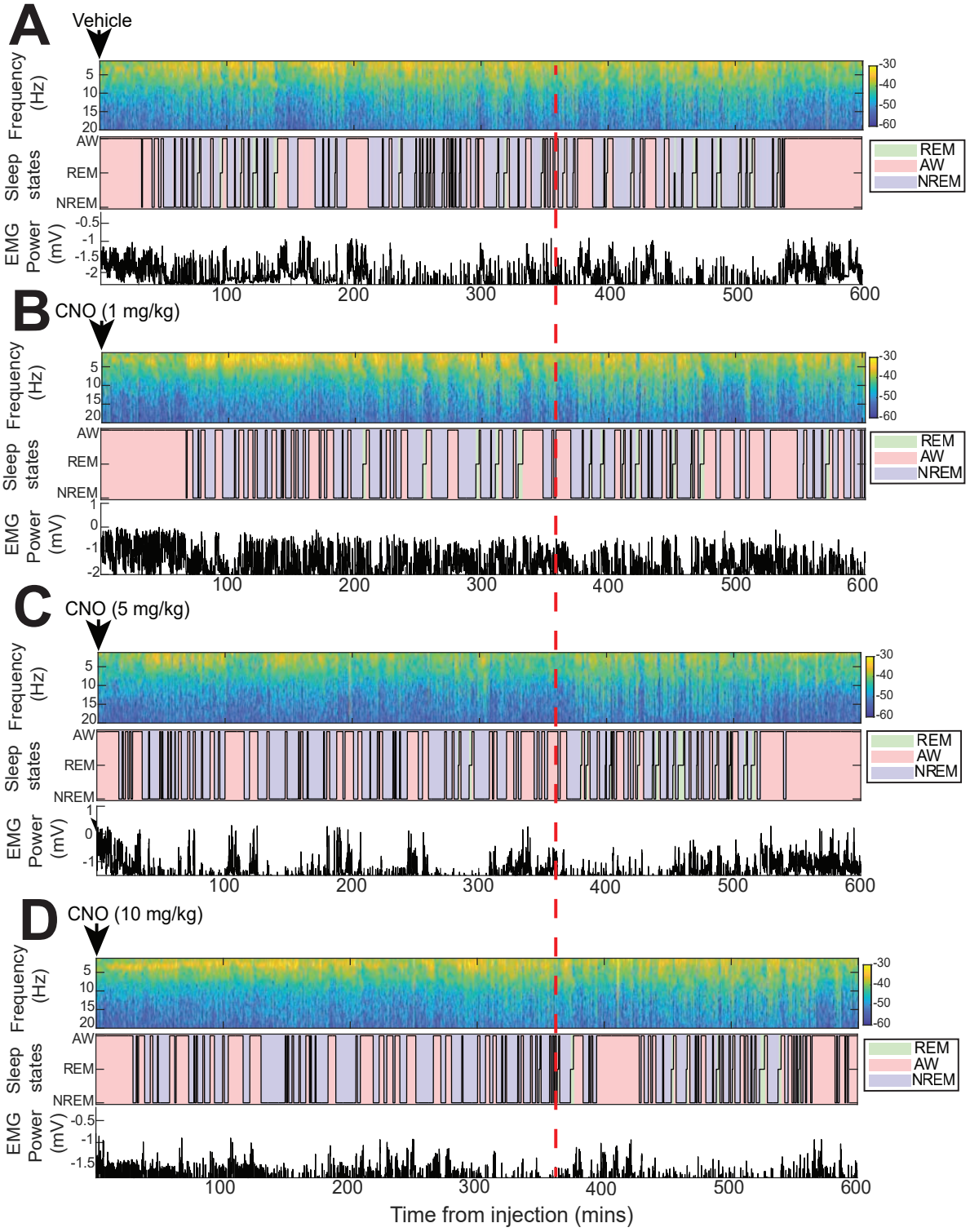

Figure 3.14. Examples of sleep-wake cycles in a single DREADDs animal with different concentrations of CNO across 10 hours. Features and characterisation of sleep states in one animal expressing hM3D virus 10 hours after injection of vehicle **(A),** 1 mg/kg CNO **(B),** 5 mg/kg CNO **(C),** 10 mg/kg **(D).** In each image from top to bottom, top - a spectrogram showing cortical EEG frequency (0-20 Hz), colourbar indicates intensity of frequency, middle - hypnogram showing sleep states, awake (red), REM sleep (green), NREM sleep (blue), bottom - EMG power (mV). Red dashed line indiactes 6 hour time point, which was used to split data into chemogenetic modification (first 6 hours) and rebound sleep data (last 4 hours).

To assess this trend across animals, we plotted sleep characteristics in all groups from different concentrations of CNO. Visually, we observed that after DREADDs animal were given CNO (1 mg/kg), NREM sleep and wakefulness remained relatively stable in proportion, number of episodes, and average episode duration across all groups. However, in DREADDs animals receiving CNO (1 mg/kg), REM sleep had a lower proportion and number of episodes until hour 6 (**Fig. 3.15**). Both proportion of REM sleep, and number of REM sleep episodes seemed to begin to increase from hour 4 (**Fig. 3.15**). In comparison, average duration of REM sleep episodes appeared lower in DREADDs animals receiving CNO (1 mg/kg) from hours 0-3, and appeared to not largely differ to other groups from hours 4 onwards (**Fig. 3.15**).

At higher concentrations, this effect was exaggerated. When DREADDs animals were administered with CNO (5 or 10 mg/kg), proportion of REM sleep and number of REM sleep episodes remained lower than all control group for 6 hours, before beginning to increase in the final 4 hours (**Fig 3.16** & **Fig. 3.17**). Average duration of REM sleep episodes seems to be reduced in DREADDs animals receiving higher doses of CNO at hours 0-2, and gradually increases from time of injection (**Fig. 3.16**). Similar to lower doses, all characteristics of NREM sleep and wake seem to remain similar across all groups, with the exception of episode rate of both NREM sleep and wake, which appear lower in DREADDs animals administered with CNO (5 mg/kg) for the first 6 hours after injection (**Fig. 3.16**).

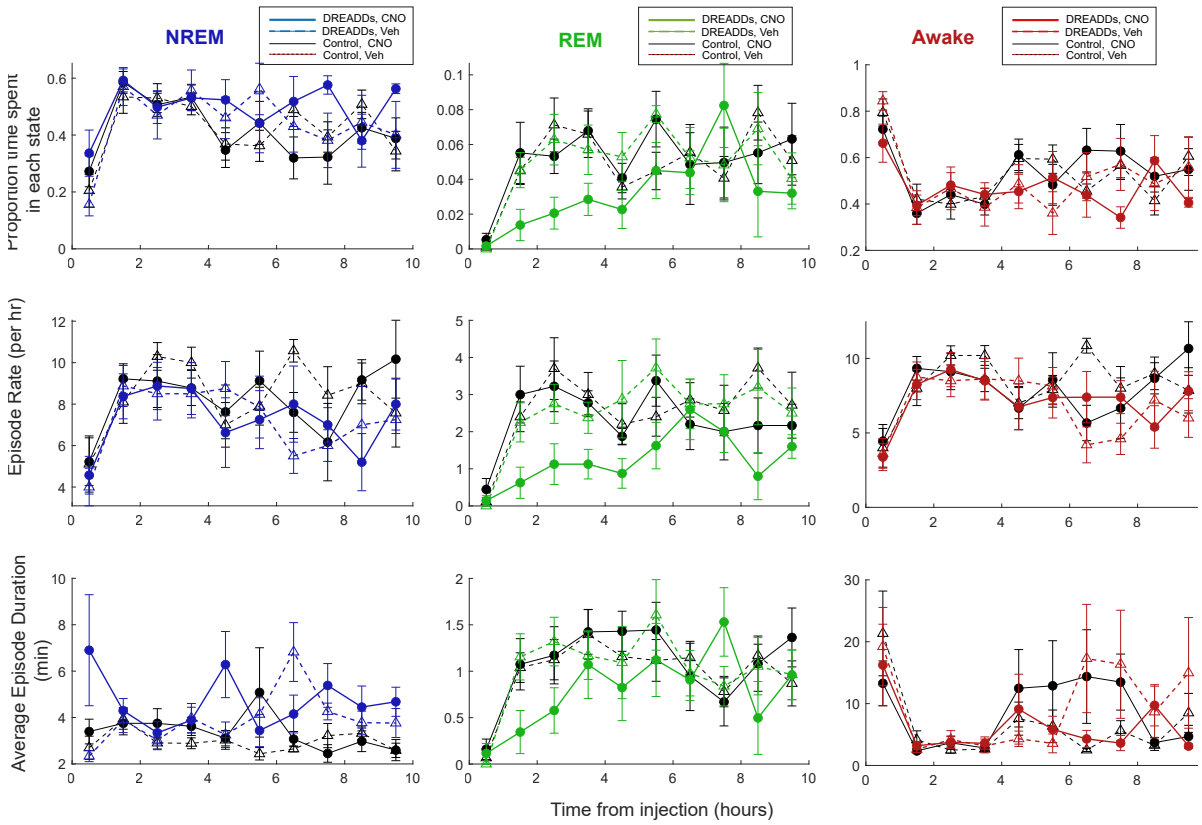

Figure 3.15. Sleep characteristics of the sleep-wake cycle 10 hours after CNO injections (1mg/kg). Effects of *i.p.* injections of vehicle (dashed lines) or CNO (1 mg/kg) (solid lines) on animals expressing a control virus (black lines) or expressing DREADDs (coloured lines) for 10 hours following injection on the total fraction of each state (top), number of episodes of each state per hour (middle), and the average episode duration (bottom). Data shown as average ± SEM.

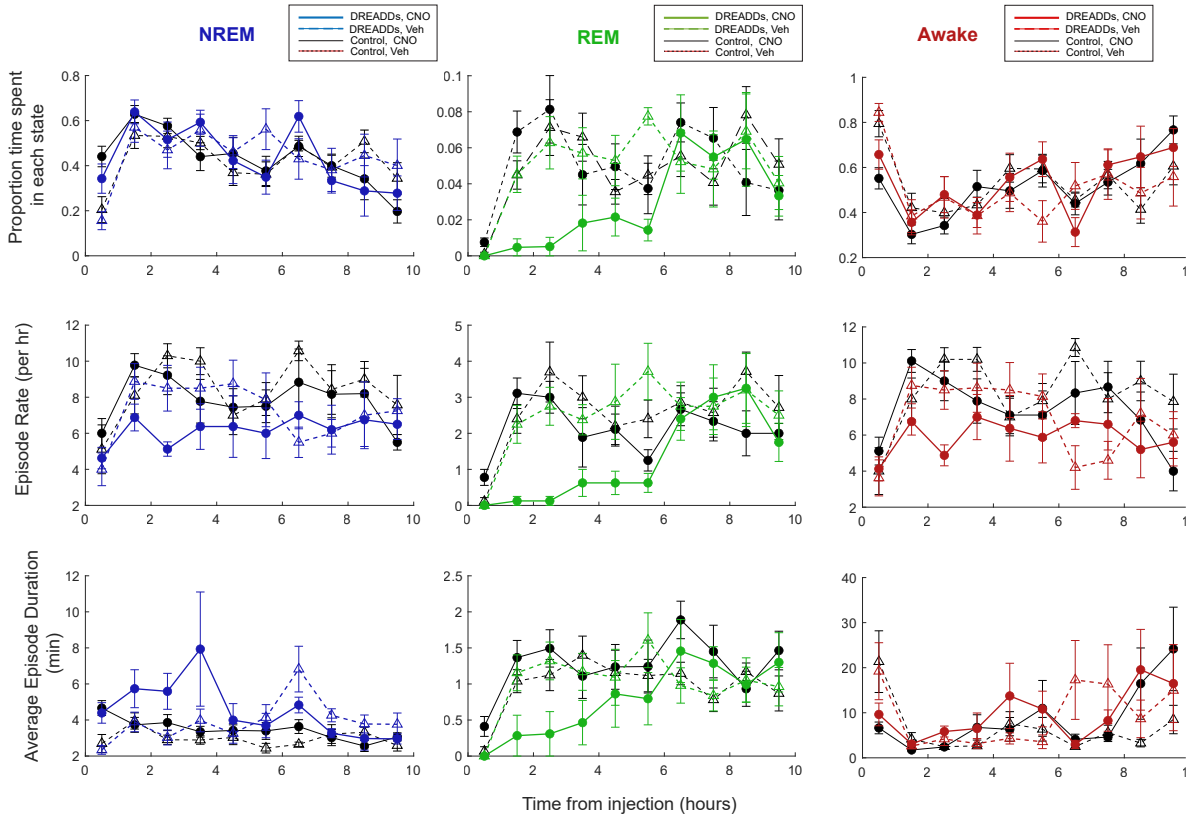

Figure 3.16. Sleep characteristics of the sleep-wake cycle 10 hours after CNO injections (5 mg/kg). Effects of *i.p.* injections of vehicle (dashed lines) or CNO (5 mg/kg) (solid lines) on animals expressing a control virus (black lines) or expressing DREADDs (coloured lines) for 10 hours following injection on the total fraction of each state (top), number of episodes of each state per hour (middle), and the average episode duration (bottom). Data shown as average ± SEM.

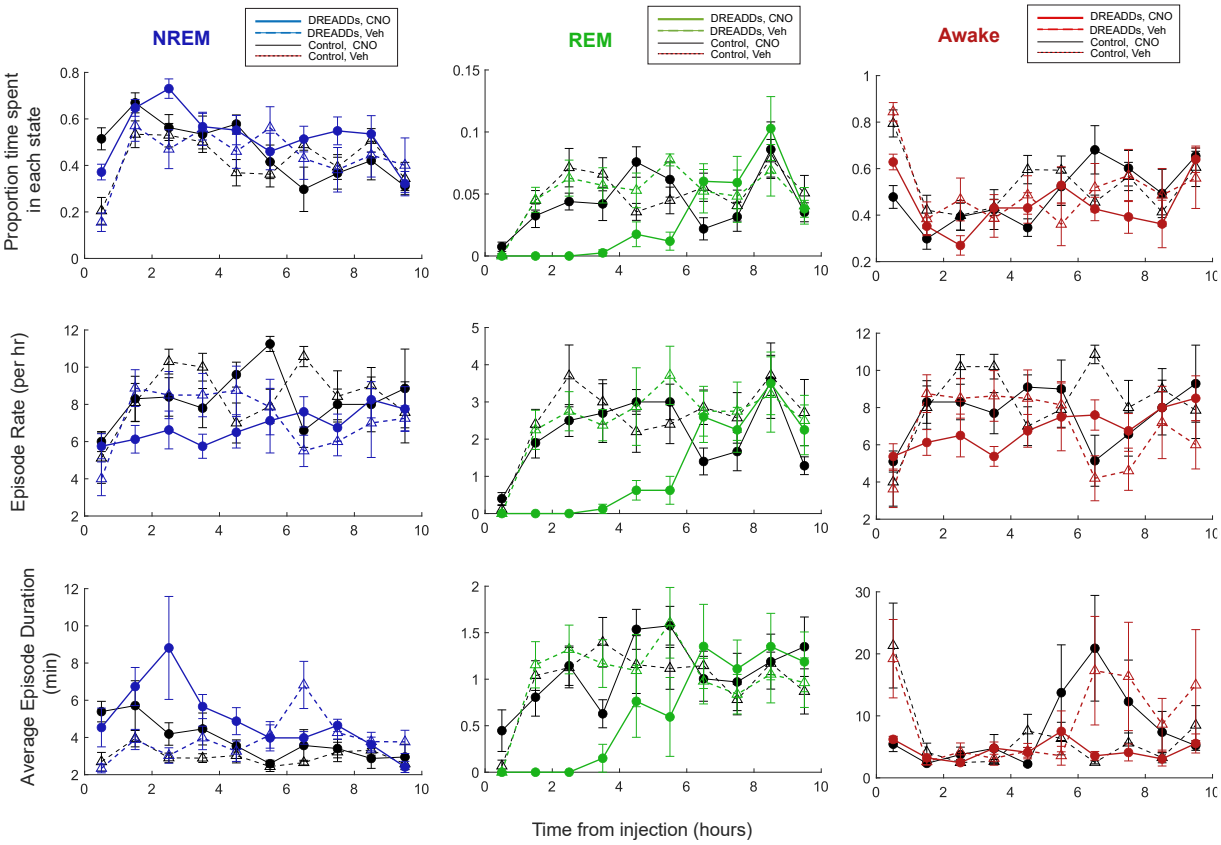

Figure 3.17. Sleep characteristics of the sleep-wake cycle 10 hours after CNO injections (10 mg/kg). Effects of *i.p.* injections of vehicle (dashed lines) or CNO (10 mg/kg) (solid lines) on animals expressing a control virus (black lines) or expressing DREADDs (coloured lines) for 10 hours following injection on the total fraction of each state (top), number of episodes of each state per hour (middle), and the average episode duration (bottom). Data shown as average ± SEM.

After visually assessing sleep characteristics across the 10-hour recording period, it appeared that REM sleep seemed to recover in the final 4 hours, when we expect activity of CNO to be diminished. Thus, we further assessed the last 4 hours (control n = 7, DREADDs n = 5). Using two-way ANOVA, and post-hoc pairwise comparisons, we found no differences in the total percent time spent in awake, NREM sleep, or REM sleep (awake, $F(3, 38) = 1.17$, $p = 0.3351$, NREM, $F(3, 38) = 1.17$, $p = 0.3349$, REM $F(3, 38) = 0.24$, $p = 0.8692$, two-way ANOVA) (**Fig. 3.18A**), or in number of episodes per hour of any of these states (awake, $F(3, 38) = 1.10$, $p = 0.3591$, NREM, $F(3, 38) = 1.57$, $p = 0.2133$, REM $F(3, 38) = 0.17$, $p = 0.9193$, two-way ANOVA) (**Fig. 3.18B**). Some data in these groups were not normally distributed (percent awake, CNTL:1 mg/kg CNO $p = 0.0401$; percent NREM, DREADDs:vehicle $p = 0.0462$; average number of REM episodes, control:vehicle $p = 0.0014$, control:5 mg/kg CNO $p = 0.0330$,

Shapiro-Wilk test). There were also no differences detected in the average length of awake or REM sleep episodes by two-way ANOVA or post-hoc pairwise comparisons (awake, $F(3, 38) = 0.87$, $p = 0.4654$, REM $F(3, 38) = 0.92$, $p = 0.92$, two-way ANOVA), however, differences in the average length of NREM episodes occurred between animal groups ($F(1, 38) = 9.81$, $p = 0.0033$, two-way ANOVA) (**Fig. 3.18C**). Again, some of the data for average length of episode did not follow normal distribution (awake, control:vehicle $p = 0.0052$, control:1 mg/kg CNO $p = 0.0290$, DREADDs:vehicle $p = 0.0135$, DREADDs:5 mg/kg CNO $p = 0.0139$, DREADDs:10 mg/kg CNO $p = 0.0260$; NREM, DREADDs:10 mg/kg CNO $p = 0.0093$; REM, DREADDs:5 mg/kg CNO $p = 0.0309$, Shapiro-Wilk test). Overall, this suggests that rebound REM sleep did not occur in the immediate hours following chemogenetic activation of pontine astrocytes.

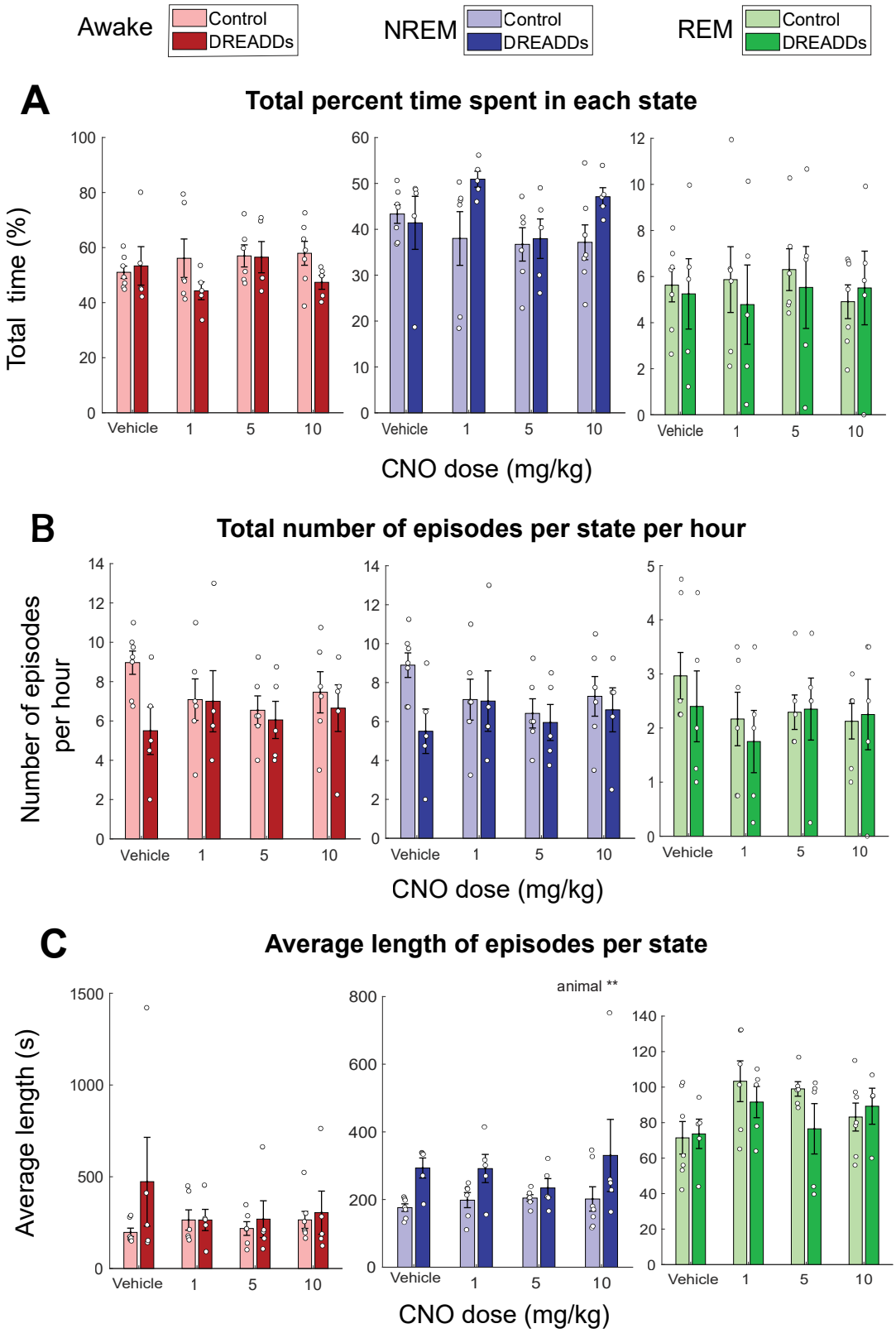

Figure 3.18. No rebound REM sleep occurs in hours 6-10 following chemogenetic modulation. Differences between control and DREADDs animal in hours 6-10 post injection of vehicle or CNO (1, 5, 10 mg/kg) of percent total time in each state (**A**), number of episodes per hour of each state (**B**), and average length of episode per state in seconds (**C**). Data represented in mean ± SEM. Red = awake, blue = NREM sleep, green = REM sleep. Lighter colours indicate control group, dark colours indicate DREADDs group. Control n = 7, DREADDs n = 5. P values from two-way ANOVA comparing effects by animal group, drug treatment, and interaction shown in top right corner of each graph. *p<0.05, **p<0.01, ***p<0.001.

We also looked at the same sleep characteristics across all 10 hours post injections. No changes in total percent of awake or NREM sleep occurred (awake, $F(3, 37) = 0.37$, $p = 0.7777$, NREM, $F(3, 37) = 0.20$, $p = 0.8937$, two-way ANOVA), however, two-way ANOVA detected a difference between animal groups for total percent REM sleep ($F(1, 37) = 9.18$, $p = 0.0044$, two-way ANOVA). Despite this, no post-hoc pairwise differences were found (**Fig. 3.19A**). All percent state data followed normal distribution except for DREADDs animals given 10 mg/kg CNO ($p = 0.0472$, Shapiro-Wilk test). Two-way ANOVA also detected differences between animal groups for average episode rate per hour for awake and NREM ($F(1, 37) = 4.17$, $p = 0.0484$; $F(1, 37) = 4.35$, $p = 0.0439$, respectively, two-way ANOVA) (**Fig. 3.19B**). Differences between both animals groups and drug treatments were also found for REM sleep episode rate ($F(1, 37) = 14.12$, $p = 0.0006$; $F(1, 37) = 4.37$, $p = 0.0099$, respectively, two-way ANOVA) (**Fig. 3.19B**). Despite these differences, post-hoc pairwise differences between animal groups receiving the same drug treatments were not found, unlike what was found for the first 6 hours only. Instead, pairwise differences were only detected between control animals receiving vehicle injections, and DREADDs animals receiving high doses of CNO (control-vehicle 2.7429 ± 0.24 vs DREADDs-CNO 5 mg/kg 1.1000 ± 0.32, $p = 0.0127$; vs DREADDs-CNO 10 mg/kg 1.0400 ± 0.30, $p = 0.0088$, Tukey-Kramer test) (**Fig 3.19B**). Some of these data did not follow normal distribution (awake, DREADDs:1 mg/kg CNO $p = 0.0247$; NREM, control:vehicle $p = 0.0495$, DREADDs:1 mg/kg CNO $p = 0.0490$; REM control:vehicle $p = 0.0228$, Shapiro-Wilk test). Finally, no differences were detected for the average length of awake or REM sleep episodes (awake, $F(3, 37) = 0.37$, $p = 0.7777$, REM $F(3, 37) = 0.83$, $p = 0.4851$, two-way ANOVA), but an animal group dependent difference was found for average length of NREM was found ($F(1, 37) = 12.48$, $p = 0.0011$, two-way ANOVA). All groups followed normal distribution for average NREM and REM episode length, while data for control animals given 10 mg/kg CNO did not ($p = 0.0042$, Shapiro-Wilk test).

Overall, while rebound REM does not seem to occur in hours 6-10 following chemogenetic activation of pontine astrocytes, total REM sleep and REM sleep episode rate over 10 hours post injection does appear to recover, as the difference is less significant in comparison to data found in following 6 hours post injection. Sedative effects of CNO that were apparent in the 6 hours post injection also appear

to recover in both the last 4 hours and total 10 hours of recording, however differences between animal groups were still significant for number of awake and NREM sleep episodes, and average length of NREM sleep episodes.

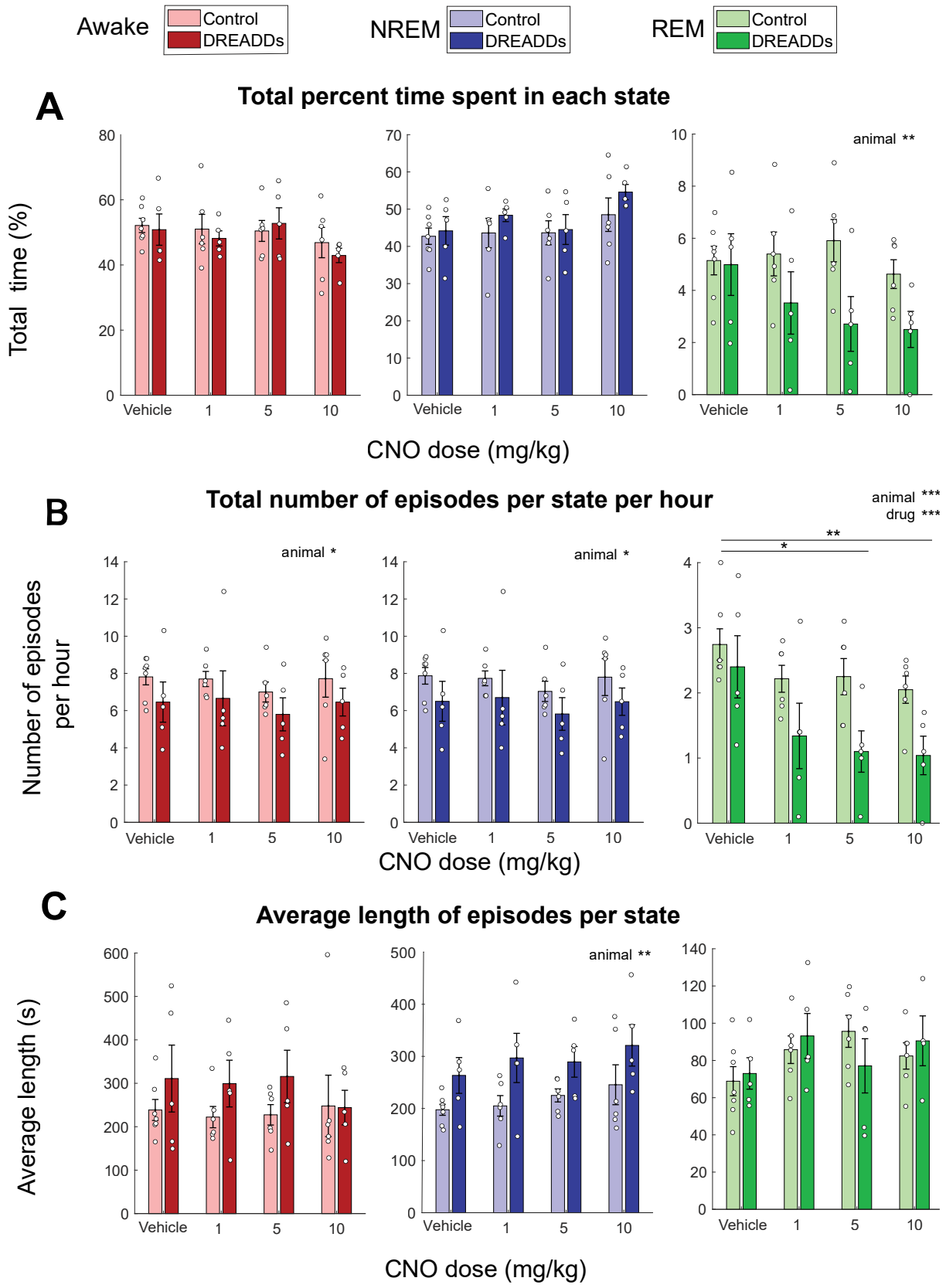

Figure 3.19. REM sleep is partially recovered but still reduced for 10 hours following chemogenetic activation of pontine astrocytes. Differences between control and DREADDs animal 10 hours post injection of vehicle or CNO (1, 5, 10 mg/kg) of percent total time in each state (**A**), number of episodes per hour of each state (**B**), and average length of episode per state in seconds (**C**). Data represented in mean ± SEM. Red = awake, blue = NREM sleep, green = REM sleep. Lighter colours indicate control group, dark colours indicate DREADDs group. Control n = 7, DREADDs n = 5. P values from two-way ANOVA comparing effects by animal group, drug treatment, and interaction shown in top right corner of each graph. P values from post-hoc analysis shown *p<0.05, **p<0.01, ***p<0.001.

3.2.7. Spectral power is not altered during chemogenetic experiments

Finally, we wanted to perform spectral analysis on all data to determine if there were any differences in power spectral density (PSD) between animal groups. Briefly, the frequency of cortical EEGs from all recordings was extracted and organised by manually-scored state, animal group, and drug condition. PSD data was then normalised to the sum of all PSD values, which transformed data into proportions in which the sum of all PSD data in each recording was equal to 1, allowing us to compare PSD amongst animal groups and drug treatments for each state.

Visually, during awake states, low frequencies occurred at the highest power in both control and DREADDs animals given vehicle treatment. During NREM and REM sleep, both control and DREADDs animals appear to have increased power at 1-4Hz and 6-8 Hz, respectively (**Fig. 3.20A**). The same patterns were also observed in animals given 1 mg/kg CNO (**Fig. 3.20B**), 5 mg/kg CNO (**Fig. 3.20C**), and 10 mg/kg CNO (**Fig. 3.20D**). To assess this further, we applied a two-way ANOVA to compare the effect of frequency bins, and animal groups (**Table 3.1**). We observed no interaction between variables ($p>0.05$) using two-way ANOVA (Table 3.1) or post-hoc comparisons. We did observe some animal group and frequency bin-dependent differences, which is likely due to the large number of frequency bins.

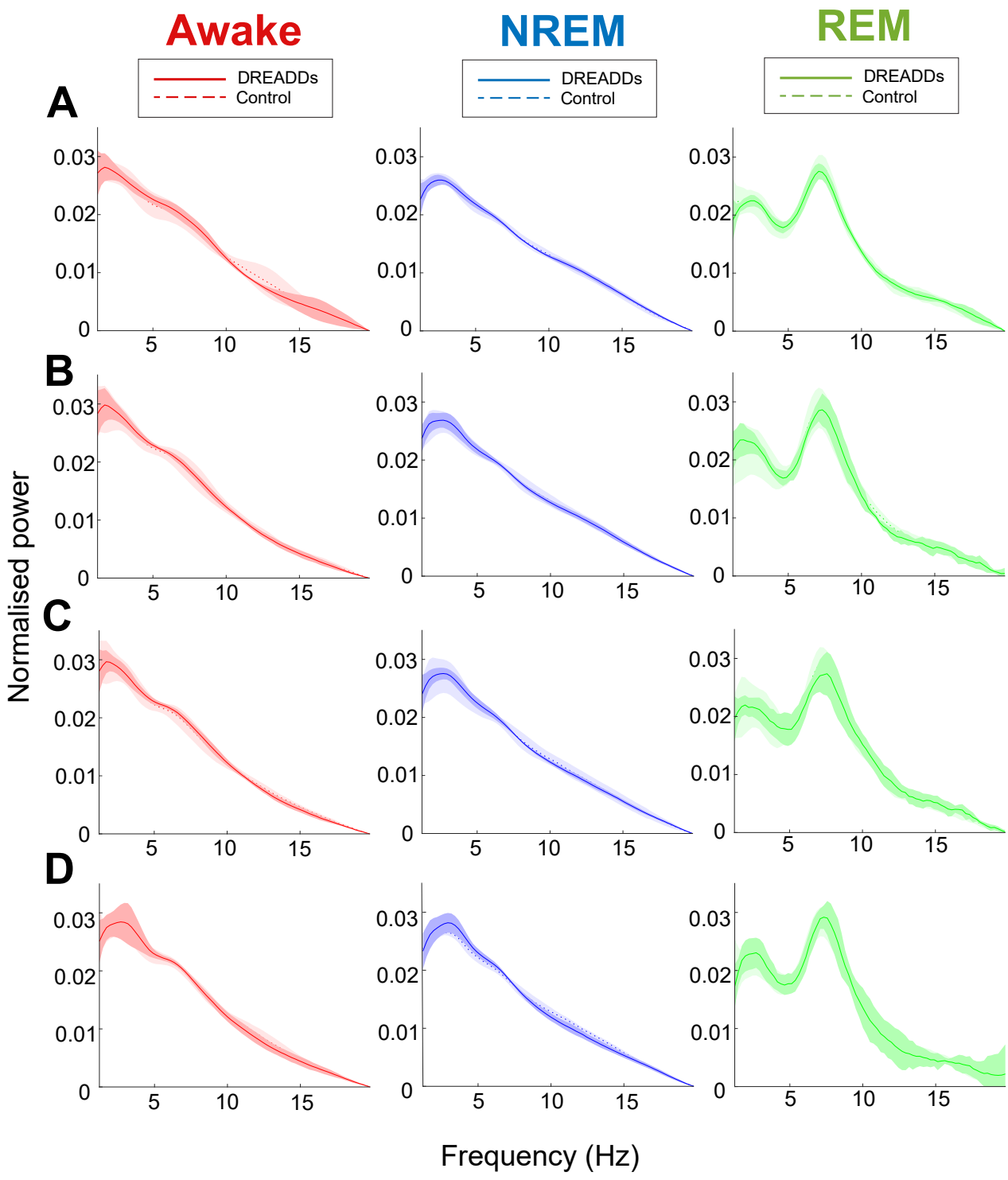

Figure 3.20. Spectral analysis of all sleep scored data. Normalised PSD for control animals and DREADDs animals in each state (Awake = red; NREM = blue; REM = green) for all sleep scored data following injections of vehicle (**A**), 1 mg/kg CNO (**B**), 5 mg/kg CNO (**C**), and 10 mg/kg CNO (**D**). Data shown as mean ± SEM. DREADDs animal data shown in dark solid line with dark shadow representing SEM, control animals are shown in dashed lines with lighter shadows representing SEM.

Table 3.1. Results from Two-way ANOVA comparing frequency bins and animal group

Dose	State	DF Animal Group	P_AnimalGroup	DF_ FrequencyBin	P_ Frequency Bin	DF_ Interac-tion	P_ Interac-tion
0	NREM	1	4.1129e-54	76	4.5499e-264	76	1
0	REM	1	3.0144e-52	76	3.8866e-201	76	1
0	WAKE	1	4.8582e-23	76	5.8676e-237	76	1
1	NREM	1	2.5005e-15	76	2.2789e-182	76	1
1	REM	1	5.6636e-09	76	3.0144e-125	76	1
1	WAKE	1	0.89299	76	5.0661e-223	76	1
5	NREM	1	0.0019763	76	4.9975e-197	76	1
5	REM	1	2.367e-05	76	5.9397e-116	76	1
5	WAKE	1	0.00050571	76	1.7902e-215	76	1
10	NREM	1	1.7119e-06	76	2.2002e-315	76	1
10	REM	1	1.7119e-06	76	5.4644e-123	76	1
10	WAKE	1	6.9365e-11	76	4.7089e-273	76	1

Dose of CNO, DF = degrees of freedom, P = p value

Next, to investigate this further, we extracted the normalised power of PSD data corresponding to 1-4 Hz and 5-8 Hz for NREM and REM sleep, respectively, to allow for statistical analysis. Using two-way ANOVA, and post-hoc pairwise comparisons, we found there were no differences in 1-4Hz power during NREM sleep in any group-drug treatment combination ($F(3, 62) = 0.83$, $p = 0.4849$, two-way ANOVA) (**Fig. 3.21A**). Similarly, there was no difference in 6-8 Hz power during REM sleep between animal group-drug treatment interactions or posthoc comparisons ($F(3, 60) = 0.47$, $p = 0.7058$) (**Fig. 21B**). Some of the extracted PSD data did not follow normal distribution (delta during NREM, control:1 mg/kg CNO $p = 0.0037$, control:5 mg/kg CNO $p = 0.0012$; theta during REM, control:5 mg/kg CNO $p = 0.0035$, DREADDs:1 mg/kg CNO $p = 0.0105$, DREADDs:5 mg/kg CNO $p = 0.0022$, Shapiro-Wilk test).

Overall, we did not observe any changes in frequency power during sleep states, suggesting that chemogenetic activation of pontine astrocytes did not affect EEG frequency.

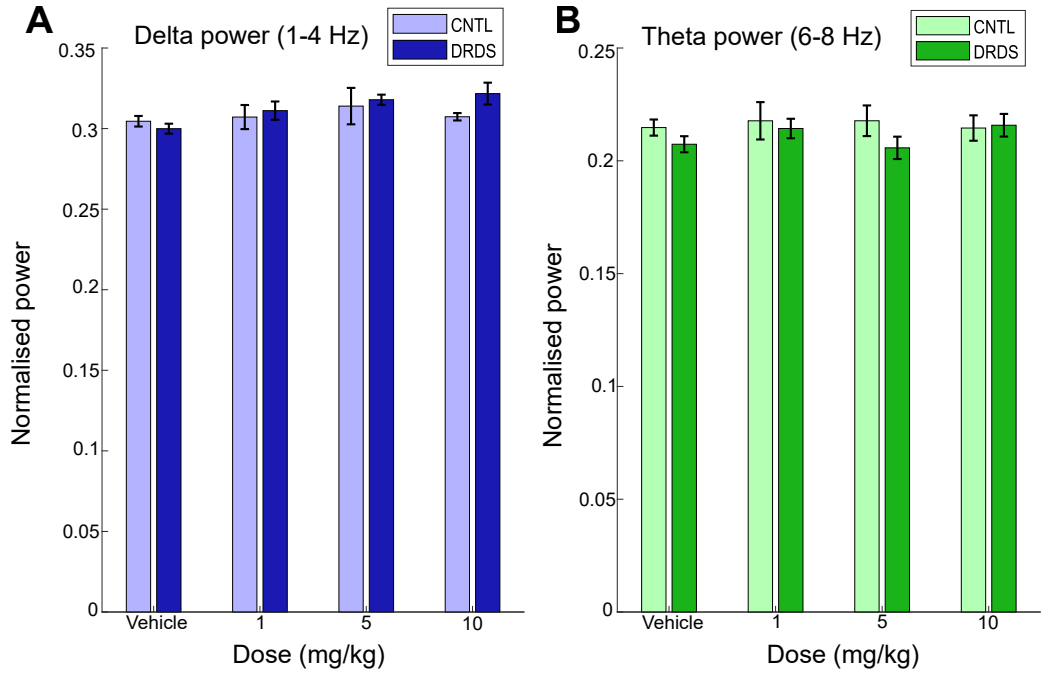

Figure 3.21. Delta power during NREM and theta power during REM sleep in all sleep scored data. A. Frequencies between 1-4 Hz during NREM was extracted from all sleep scored data, normalised power was plotted for control animals (light blue) and DREADDs animals (dark blue) for all treatment conditions. **B.** Frequency between 6-8 Hz during REM sleep was extracted from all sleep scored data, normalised power was plotted for control animals (light green) and DREADDs animals (dark green) for all treatment conditions. Data plotted as mean ± SEM. Significance was calculated using two-way ANOVA, and post-hoc pairwise analysis Tukey-Kramer tests. All data was not signficant $p>0.05$.

3.3. Discussion

3.3.1. Summary of findings

Firstly, we utilised immunohistochemistry techniques to show co-expression of anti-GFAP and anti-mCherry in both animal groups, in both epifluorescent and confocal imaging, meanwhile, little-to-no co-expression was observed between anti-NeuN and anti-mCherry (**Figs. 3.4-3.9**).

Next, and most importantly, we found that by using chemogenetics to activate astrocytes in the pons, we were able to reduce total REM sleep, REM sleep incidence,

and increase latency to first REM episode for 6 hours post injection (**Fig. 3.12**). This effect was dose-dependent, with high doses of CNO having a strong effect and in some cases completely inhibiting REM sleep for 6 hours post injection. We also found no differences in the length of REM sleep episodes between groups. Together this suggests pontine astrocytes may be involved in REM sleep initiation, and not REM sleep maintenance. We also found a sedative effect of CNO alone, with high doses of CNO increasing total NREM sleep and reducing NREM sleep latency regardless of animal group. However, in our control animals which were administered with CNO, we did not find any alteration to REM sleep caused by CNO alone, even at high concentrations (**Fig. 3.12**), which opposes previous reports (Traut *et al.*, 2023).

Next, we found that rebound REM sleep, in the form of increased total REM sleep, increased REM episodes, or longer REM sleep episode durations, did not occur immediately in the latter hours (6-10 hours after injection) of our chemogenetic experiments (**Fig. 3.14**). However, we did observe that across 10-hour recordings, effects of CNO were diminished, as reductions in REM sleep were less significant across 10-hours post injection in comparison to 6-hour recordings (**Fig 3.12** & **Fig. 3.15**).

Finally, we showed that EEG power does not change between animal groups or drug treatments (**Fig. 3.16** & **Fig. 3.17**).

3.3.2. Limitations and future work

As outlined in section 3.2.2, one limitation was using antibodies raised in a mouse for histological analysis. This can lead to non-specific binding, such as binding to endogenous IgG in the tissue, as the primary antibody was mouse-derived. This led to increased background fluorescence, and in DREADDs animals, where the virus had a lower titre, a much dimmer fluorescence of virus expression (**Fig. 3.2**). Before validating histology with a rabbit strain of anti-dsRed, many DREADDs animals were excluded due to negative histology, thus, these may have been false negatives. With this in mind, this limitation may have caused reduced sample sizes.

In addition, with our injection-based method of hM3D-containing virus expression, we observed virus expression in regions out with the pons (**Fig. 3.3**). As previously described (section 1.2.2.5.1), the pons itself has many subregions that have complex activities. Some of these regions contain neurons which are REM-on, while some are REM-off, and as astrocytes are highly involved in synaptic transmission of neurons, the activity of these regions may be influenced by local astrocytes. Thus, it would be optimal to limit expression to specific subregions, such as the SLD. However, due to the nature of the techniques, and the small size of these subregions, this remains very challenging.

Regarding our immunohistochemistry data (**Figs 3.4-3.9**), a major consideration for these findings is the differences in morphology using anti-GFAP staining between control and DREADDs groups. As we know from previous studies, GFAP is upregulated when astrocytes are in an activated state (Eng *et al.*, 2000), thus it is possible that repeatedly activating astrocytes has resulted in the increase of GFAP expression and hypertrophic morphology. To minimise the effect this could have on our results, drug treatments were randomised, and multiple control groups were used, including DREADDs animals receiving a vehicle injection. Our observation of reduced REM sleep incidence following chemogenetic manipulations was not observed in these animals, suggesting changes in astrocyte state did not cause the reduction in REM sleep. However, because of these findings, it would be interesting to further investigate the changes occurring in astrocytes. A potential means for this could be single-cell RNA sequencing, which would provide us with more detailed information about changes in astrocyte state and protein expression.

A limitation of all chemogenetic experiments is the pharmacology of CNO. CNO is readily reversed into parent compound clozapine, with both clozapine and CNO itself reported to have off-target binding properties (Jendryka *et al.*, 2019; Gomez *et al.*, 2017). Because of these effects, CNO alone has been found to cause changes to the sleep-wake cycle and exert sedative effects (Traut *et al.*, 2023). In our studies we observed increased NREM sleep and reduced NREM sleep latency with CNO alone, particularly at high doses. However, we did not observe any changes to REM sleep caused by CNO alone, as has been previously reported (Traut *et al.*, 2023). In any case, due to the known effects of CNO on the sleep-wake cycle, in our study we

carefully designed our experiments to include multiple control groups, which included animals expressing a control virus that were injected with CNO, to assess any direct effects cause by CNO alone. Alternatively, it may have been advantageous to use a different DREADDs agonist, such as DCZ, which is more potent and fast-acting, and has no reported off-target binding (Nagai *et al.*, 2020).

Additionally, in our studies, longer 10-hour recordings were under sampled comparatively to 6-hour recordings. Initially, when we began experiments, we first wanted to confirm that a reduction in REM sleep would occur and did not know how pronounced this effect would be. After obtaining our preliminary results with the first few animals in each group, and observing that a strong REM reduction was occurring, we then wanted to see if this caused effects on rebound REM in the following hours. This meant that fewer animals underwent 10-hour recordings. Additionally, due to construction work in our animal unit commencing, we had a restricted timeframe to conduct these long recordings, limiting how many animals we could include in our study. Furthermore, it would have been interesting to look at the sleep-wake cycle over a longer period of time, perhaps in 24-hour recordings to investigate if REM sleep continued to recover over this time, however, this was again restricted by the schedule of construction work, which was unavoidable.

3.3.3. Summary and next steps

Overall, in this chapter we showed that using chemogenetics to activate pontine astrocytes reduced REM sleep incidence. Since commencing these experiments, supporting findings were published (Peng *et al.*, 2023; Kurogi *et al.*, 2024). However, we show, for the first time, that this effect was dose-dependent.

Next, due to the involvement of REM sleep in memory formation (see section 1.2.2.4), we aimed to investigate if chemogenetic-induced REM sleep reduction would impair memory in mice. In particular, due to the involvement of the hippocampus in theta generation (see section 1.2.2.6.1), we aimed to examine hippocampus-dependent spatial memory following chemogenetic activation of pontine astrocytes.

4. Effects of chemogenetic activation of pontine astrocytes on memory

As we previously observed a strong reduction in REM sleep following chemogenetic activation of pontine astrocytes, we wanted to investigate if this had any effects of memory consolidation during sleep, which will be the basis of this chapter. Firstly, I will briefly describe the background, hypothesis, and aims for behaviour experiments (section 4.1). I will then discuss the results obtained including a description of our database and the exclusion criteria for animals, and then the results we obtained from the novel object location test (NOLT), and novel object recognition test (NORT) (section 4.2), and discuss these findings (section 4.3). Overall, our pilot experiments show a trend for chemogenetic activation of astrocytes to reduce spatial, but not object recognition memory.

4.1. Introduction

NREM sleep has a critical role in memory formation. In particular, hippocampal SWRs are critical for spatial memory. During SWRs, place cell activity enquired during waking exploratory behaviour, is replayed, leading to the consolidation of spatial memory (O'Keefe and Dostrovsky, 1971; O'Keefe, 1976; Morris *et al.*, 1982; Girardeau *et al.*, 2009; Ego-Stengel and Wilson, 2010; van de Ven *et al.*, 2016; Wilson and McNaughton, 1994; Ormond and O'Keefe, 2022). However, investigating the importance of REM sleep for memory consolidation is more controversial due to it being experimentally challenging to modulate REM sleep independently to NREM.

Hippocampal theta during REM sleep has been shown to be involved in replay and strengthening of place cell activity from memories which occurred during wake (Poe *et al.*, 2000; Louie and Wilson, 2001). P-waves, another oscillatory component of REM sleep, are also thought to be involved in consolidation and integration of memories, with increased P-wave activity resulting in improved avoidance learning in rats (Mavanji and Datta, 2003; Datta, 2000). Selective REM sleep deprivation has shown reduced spatial learning and memory in rats (Smith and Rose, 1996; Beaulieu and Godbout, 2000; Youngblood *et al.*, 1997). However, these studies used the flower-pot method for REM sleep deprivation, where the animal is placed on a small platform

surrounded by water, and upon loss of muscle tone they would fall into the water. This method has several limitations, for example NREM sleep can also be affected, as muscle relaxation also occurs during NREM sleep, and the animal may try to stay awake due to the stressful nature of this method. In addition, small episodes of REM sleep may still occur before the animal falls, or due to adaptation. Meanwhile, some literature has found no effects of REM sleep in spatial memory (Sloan, 1972; Holdstock and Verschoor, 1973).

More recently, there have been advancements in REM sleep deprivation techniques. Optogenetically attenuating theta during REM, without affecting sleep, impaired spatial, and fear-conditioned contextual memory (Boyce *et al.*, 2016). Optogenetic manipulations took place for 4 hours following encoding session for NOLT, and after fear conditioning session for contextual memory, suggesting consolidation of these memories are dependent on hippocampal theta during REM sleep. On the other hand, optogenetically silencing REM-on hypothalamic MCH neurons during REM sleep between encoding and retention periods of the NORT, significantly improved object recognition memory (Izawa *et al.*, 2019). Together, these studies demonstrate the complexity of the involvement of REM sleep in memory consolidation. As such, more experiments which reduce or inhibit REM sleep, such as our chemogenetic studies, are needed to further characterise the role of REM sleep in memory.

4.1.1. Hypothesis and aims

Given the reduction in REM sleep following chemogenetic modulation, and that rebound REM sleep did not occur, we hypothesised that hippocampus-dependent spatial memory would be impaired. To test this, we used NOLT and NORT, which test spatial and object recognition memory, respectively. Importantly, NOLT is a hippocampus-dependent test, which is also dependent on sleep following encoding sessions. On the other hand, NORT is not hippocampus dependent, and is unaffected by sleep deprivation immediately after encoding (Ishikawa *et al.*, 2014; Sawangjit *et al.*, 2018). For this reason, we hypothesised that NOLT, but not NORT, would be impaired by chemogenetic modulation. We aimed to modulate pontine astrocyte activity in DREADDs mice using CNO at a concentration of 1 mg/kg immediately following encoding sessions, and test consolidation of memory during retention

sessions 24-hours later. We chose this concentration of CNO as it had minimal effects on NREM sleep, while maintaining a significant reduction in REM sleep.

4.2. Results

4.2.1. Animal groups and database

As briefly discussed, (section 2.1), 44 WT mice aged 8-24 weeks upon time of surgery were used for memory tests (**Fig. 4.1**). Of these 44, 20 were bilaterally injected with a control virus, while 24 were injected with the activatory chemogenetic receptor. 1 mouse developed cataracts and blindness from natural aging during the virus incubation period, thus did not partake in behaviour experiments. Due to the nature of experiments testing memory, drug treatments were not repeated in animals, instead animals were split into 4 independent groups. In control animals, 10 were given *i.p.* injections of vehicle while 10 were given CNO (1 mg/kg). 1 control animal in each treatment group was excluded after histological analysis, and 1 control animal given vehicle was later excluded for lack of exploration, leaving a final number of 8 control animals given vehicle (4 males and 4 females) and 9 administered with CNO (5 males and 4 females). In DREADDs animals, 11 were given vehicle and 12 were administered with CNO (1 mg/kg), of which 3 DREADDs:vehicle and 4 DREADDs:CNO animals were excluded after histological analysis, and 2 animals in each drug treatment were excluded for lack of exploration. This left a final number of 6 DREADDs animals given vehicle (4 males and 2 females) and 6 administered with CNO (1 mg/kg) (3 males and 3 females).

Experiments generally begun 4 weeks after virus injection surgery following a period of virus incubation. 11 mice underwent behaviour experiments 6-8 weeks after virus injection surgery as they were also used in chemogenetic studies prior to behaviour tests. Behavioural tests were conducted over 5 consecutive days. Day 1 consisted of a 20-minute habituation to the test environment, while day 2 and 3 were encoding and retention days for NOLT, and 4 and 5 were encoding and retention days for NORT (see section 2.6 and **Fig. 2.10**). All test sessions lasted 10 minutes and occurred within the same hour every day. Drug treatments were given immediately after encoding. Several sets of objects were used, and for NOLT encoding sessions, a set of objects was allocated to an animal at random, and the same objects would be used

per mouse for NORT encoding sessions. During NOLT and NORT retention sessions novel object locations or novel objects were assigned randomly, respectively.

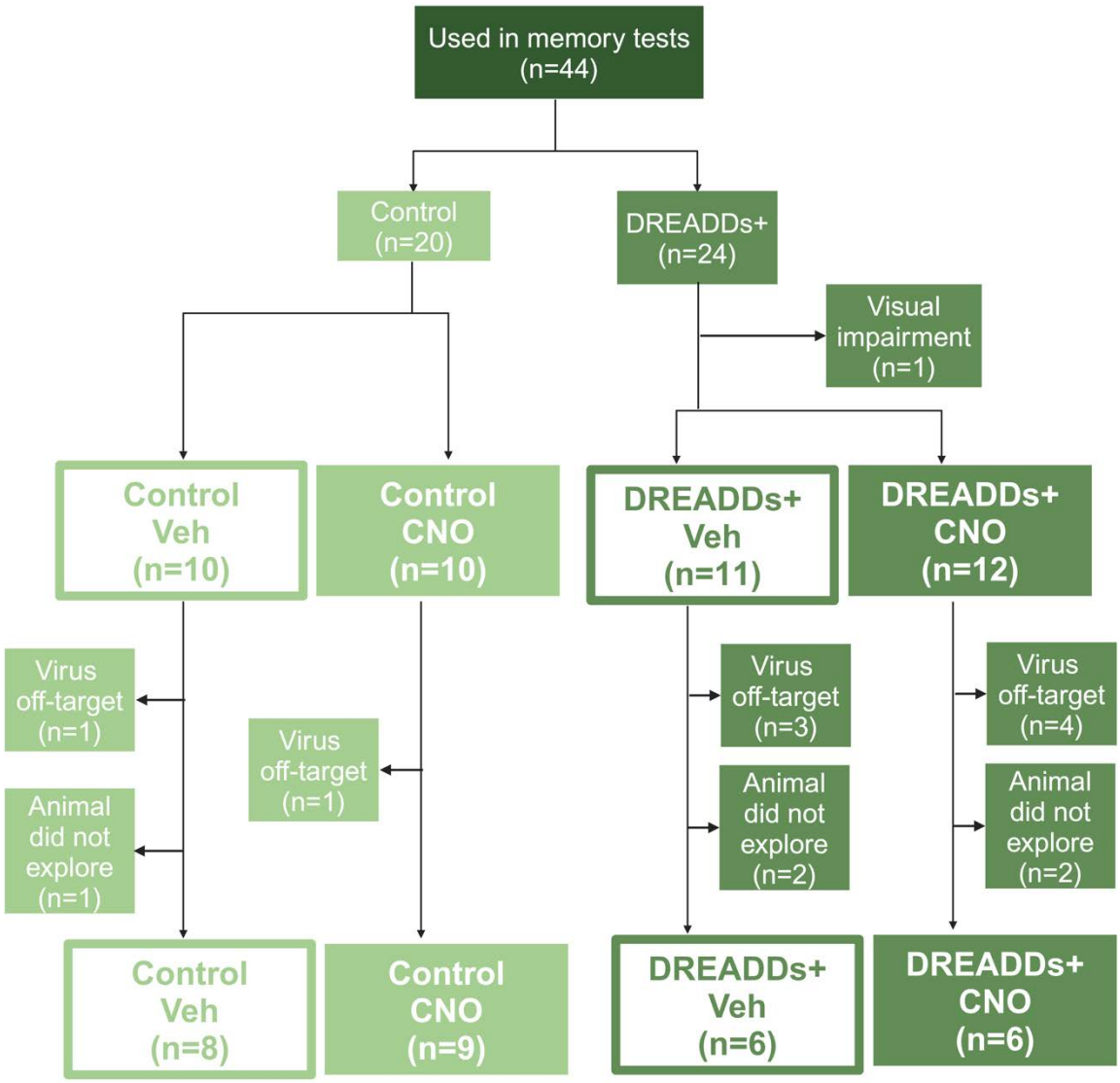

Figure 4.1. Flowchart of the animals used in memory tests.

4.2.2. Establishing inclusion and exclusion criteria

As previously described for chemogenetic studies, some animals were excluded if virus expression was off-target, or a lack of expression was found (see sections 3.2.2 and **Fig. 3.1** & **Fig. 3.2**). In memory tests, a total of 9 mice were excluded for this reason.

Another reason for exclusion in these experiments was lack of exploration. To investigate this, we explored various behaviours which would indicate exploration.

First, we extracted the trajectory of the animal throughout the entire test session by tracking the nose position. The trajectory was visualised with a colormap that reflects the time course of the recording, allowing us to see how the animal's movements evolved over the session. The location of the fixed object is indicated by a blue cross, while the location of the variable object is marked with a red cross (**Fig. 4.2 A&B,** left panel). Next, we calculated the discrimination index for each minute, across various distances from the centre of the objects (ranging from 2 to 10 cm in 0.5 cm intervals). This information is presented as a heat map, where blue represents a preference for the fixed object, and red indicates a preference for the variable object within each exploration zone for each minute of the test (**Fig. 4.2 A&B,** middle panel). Finally, we extracted the discrimination index based on cumulative exploration duration across the same range of distances from the objects centre. This allows us to visualise how the discrimination index evolves as the cumulative time spent exploring the objects increases, along with the proximity of the exploration. It shows how closely and for how long the animals explored each object, and how their preference changed as they continued to explore (**Fig. 4.2A&B,** right panel).

In animals that explored we observed a complex trajectory, and changes in discrimination index across the session. Most importantly we seen changes in discrimination index which corresponded to increases in cumulative exploration duration at distances close to the object which occurred as the animal explored objects (**Fig. 4.2A**). In contrast, animals that did not explore tended to stay in certain areas of the test environment and showed no cumulative exploratory time or preference for objects (**Fig. 4.2B**). To determine an exclusion criterion for exploration, we first calculated total exploration of both objects (within 4 cm from object centre) for all test sessions and plotted distribution of exploration (**Fig. 4.2C**). We chose to exclude animals that had any less than 13 seconds exploration for any test session, which included 6 sessions in 5 animals. This value was arbitrary, and was based on trends in exploratory data.

Overall, with the outlined exclusion criteria, results from a total of 8 control animals given vehicle and 9 given CNO treatments, and 6 DREADDs animals given vehicle and 6 given CNO will be reported in this chapter.

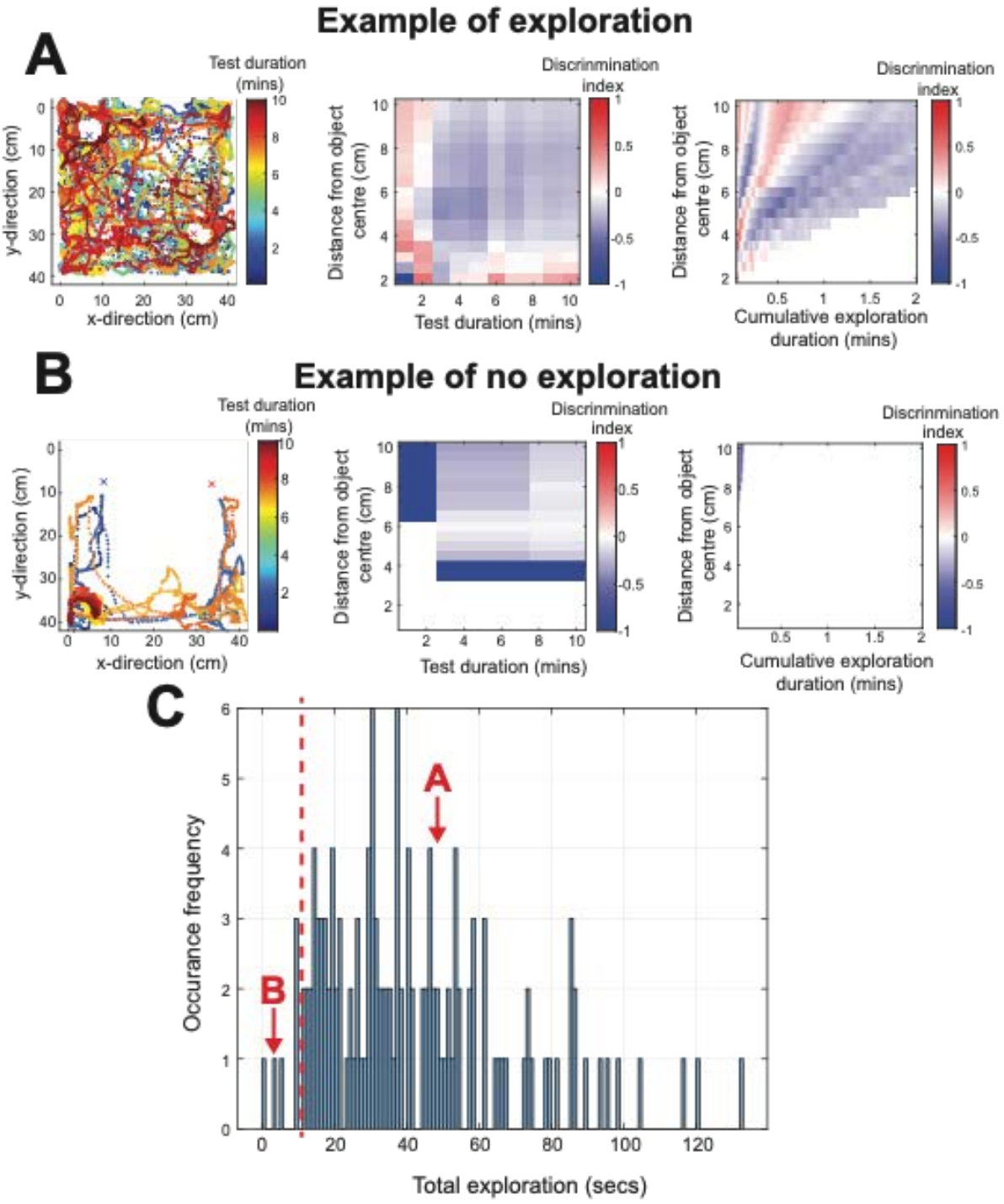

Figure 4.2. Examples of exploration and exclusion criteria. A. Left - trajectory within experimental box according to recording time. Object A (fixed) represented by blue cross, object B (variable) represented by red cross. Trajectory used nose as tracked bodypart. Colourbar indicates time of recording. Middle - cumulative discrimination index across recording depending on distance from object centre. Colourbar, positive values (red) indicate more time spent near object B, and negative values (blue) indicate more time spent near object A. Right - discrimination index based on cumulative exploration duration depending on distance from object centre. Colourbar, positive values (red) indicate more time spent near object B, and negative values (blue) indicate more time spent near object A. **B.** Same as in A but in an example of no exploration. **C.** Distribution of total exploration time for both objects at 4 cm from object centres for all experiments (n = 136). The chosen threshold is shown as a red sashed line, and the location in the distribution of examples are displayed in (A) and (B) are indicated.

4.2.3. Bilateral virus expression in the pons

Immunohistochemistry was carried out on all mice to confirm virus was expressed bilaterally in the pons. As previously (see section 3.3.1), anti-DsRed or anti-mCherry were used to amplify mCherry or tdTomato signals, the fluorescent tags which were conjugated to DREADDs and control viruses, respectively, while DAPI was used for counterstaining (**Fig. 4.3A**). To further investigate expression pattern and spread, we registered 2 histology sections per animal to the Allen Mouse Brain atlas CCFv3, and extracted virus expression for each animal group. Atlas maps were grouped according to AP axis position and aligned, and the matching virus expression segmentation was overlayed to the corresponding atlas. With this visualisation, we observed bilateral expression in a range of pontine regions, with some minimal expression also occurring in midbrain, medullar, and cerebellar regions in control mice administered with vehicle (n = 16 images for 8 animals) (**Fig. 4.3B**), control mice administered with CNO (1 mg/kg) (n = 18 images for 9 animals) (**Fig. 4.3C**), DREADDs animals administered with vehicle (n = 12 images for 6 animals) (**Fig. 4.3D**), and DREADDs animals administered with CNO (1 mg/kg) (n = 12 images for 6 animals) (**Fig. 4.3E**).

As previous, we also stained for anti-GFAP to assess co-expression of our viruses and an astrocyte-specific marker. As the same viruses were used in these experiments as in chemogenetic studies, we observed the same co-expression as previously reported (see section 3.3.2 & **Figs. 3.4-3.9**).

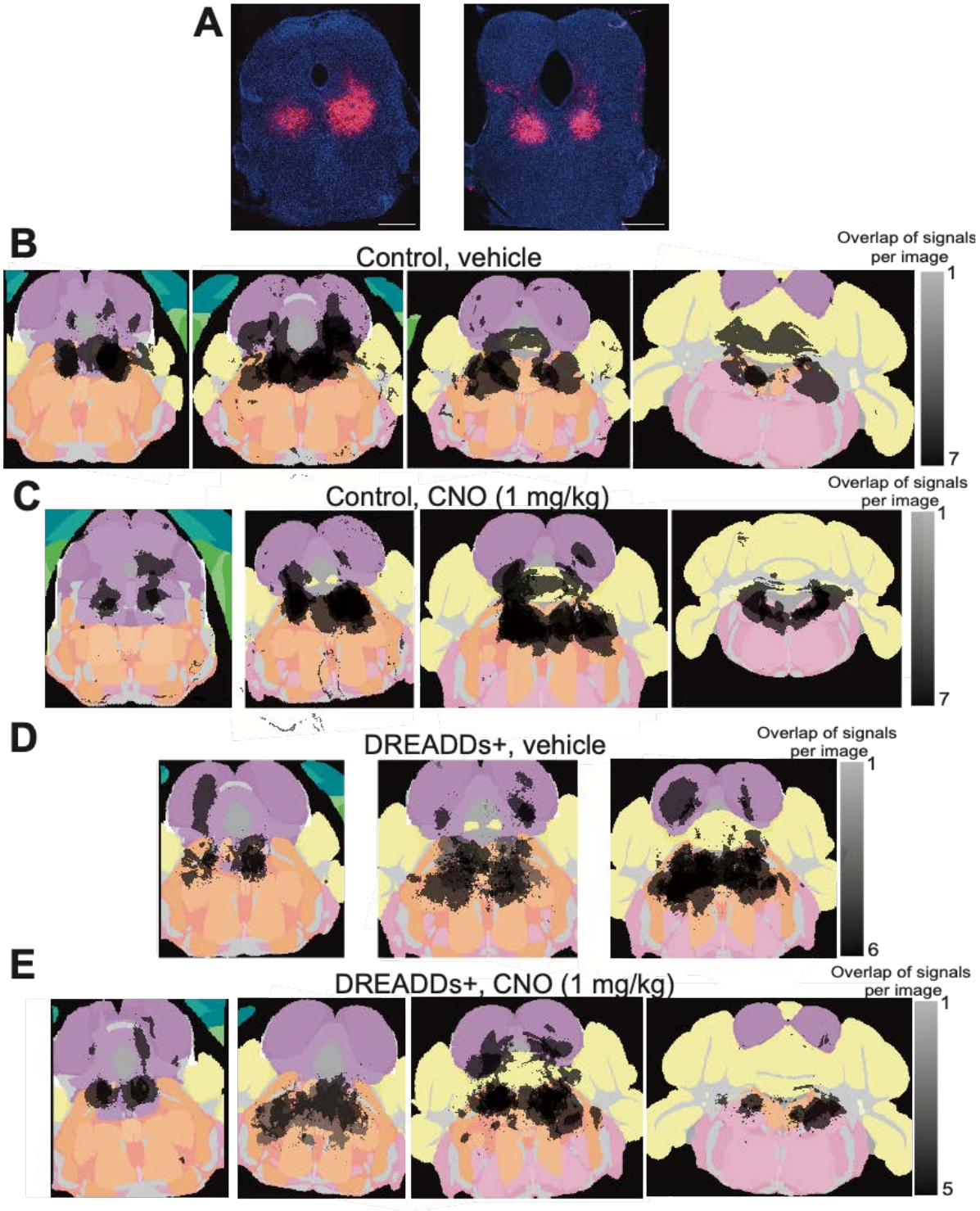

Figure 4.3. Virus expressed in pontine regions and some midbrain and medulla/cerebellar regions across animals used in behaviour studies. **A.** Examples of bilateral virus expression in the pons in two seperate animals (blue = DAPI, red = anti-DsRed). Scale bar = 1000 μm. **B.** Virus expression in control animals administered with vehicle across the anterior-posterior axis. Histological images were registered to the Allen Mouse Brain atlas CCFv3, where colours indicate wider regions. Blue/green = cortex, purple = midbrain, orange = pons, pink = medulla, yellow = cerebellum. Black indicates viral expression where darker colour indicates overlayed expression in multile sections (demonstrated in colourbar). n = 16 histological images for 8 animals, 2 images per animal. **C.** Same as in (**B**) but in control animals administered with CNO (1 mg/kg). n = 18 histological images for 9 animals, 2 images per animal. **D.** Same as in (**B**) but in DREADDs animals administered with vehicle. n = 12 histological images for 6 animals, 2 images per animal. **E.** Same as in (**B**) but in DREADDs animals administered with CNO (1 mg/kg). n = 12 histological images for 6 animals, 2 images per animal.

4.2.4. Novel object location test

During NOLT, encoding sessions lasted 10 minutes where animals explored two novel objects. Immediately after encoding, animals were given *i.p.* injections of vehicle or CNO. 24-hours after encoding sessions, animals underwent 10-minute retention sessions where they could explore both objects again after one object was moved to a novel location, in order to test spatial memory. Discrimination indices that were positive indicate a preference for novel location, while a negative discrimination index implies a preference for the fixed object. Exemplar data of a control animal shows some preference during encoding for the object that will remain in the same location, and shows that the animal explored both objects multiple times (**Fig. 4.4A,** top). During retention, the same animal showed preference for exploring the object that was moved to a new location, spending a longer exploratory time at a closer distance to the object at novel location compared to the fixed object (**Fig. 4.4A,** bottom). In comparison, while an exemplar DREADDs animal also showed little preference for either object during encoding (**Fig. 4.4B,** top), when the animal was given CNO immediately after encoding, little-to-no preference could be observed again during retention (**Fig. 4.4B,** bottom).

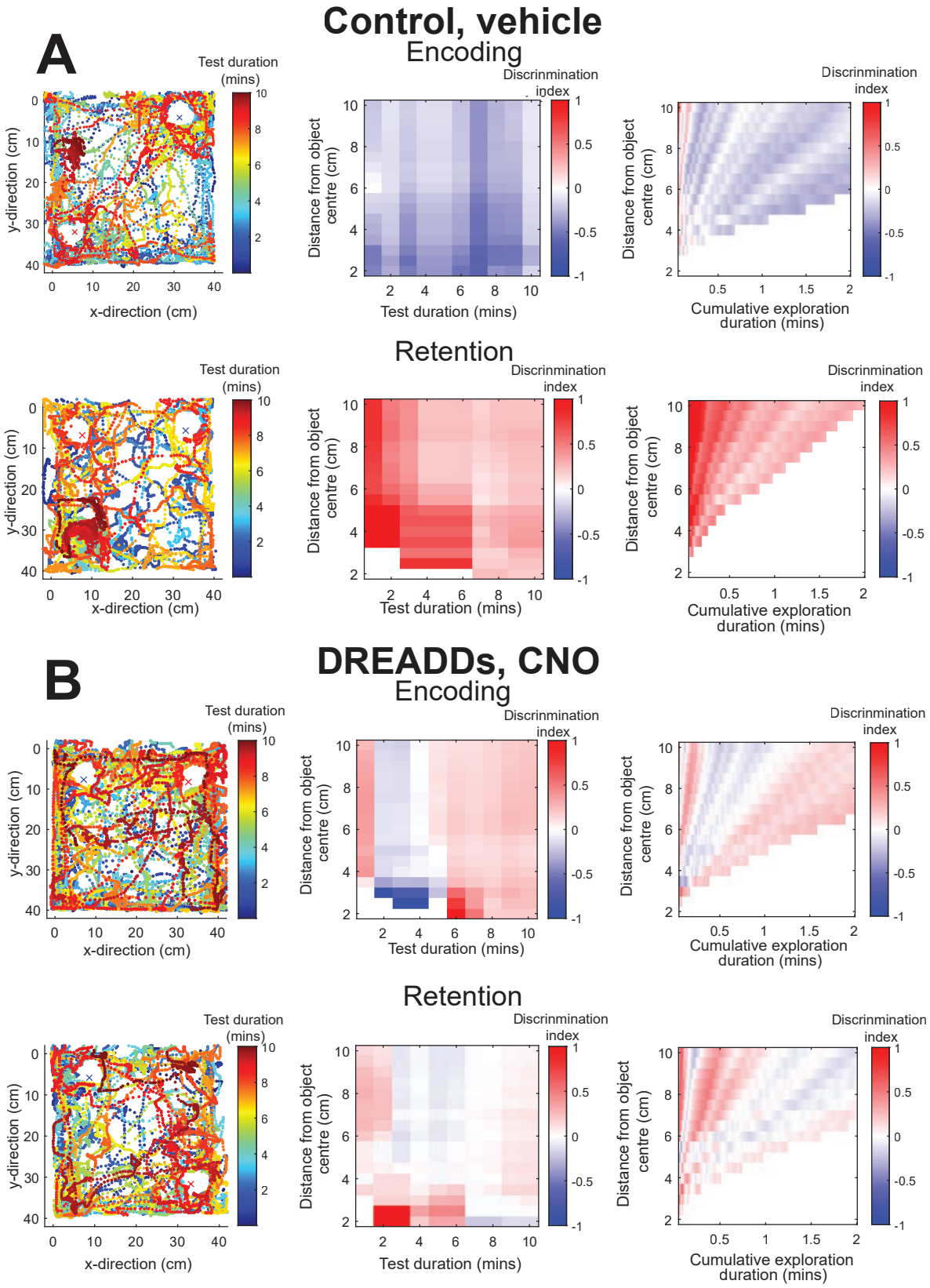

Figure 4.4. Examples of NOLT with and without chemogenetic modulation of pontine astrocytes. A. Same figure configuration as in Figure 4.2A, in a control animal during an encoding sessions (top) and a retention session (bottom). **B.** Same as in A but in a DREADDs animal given CNO after encoding session.

To explore this further, we looked at differences in discrimination indices across different animal groups, drug treatments, and test sessions. We analysed exploration 4 cm from the centre of objects, which was ~2 cm from the edge of objects. We chose this distance due to trends across all groups at this distance. All data was normally distributed ($p>0.05$ per group, Shapiro-Wilk test). Despite objects being randomly placed for every session, all animal groups appear to have a negative discrimination index during encoding, suggesting a preference for the fixed object (control:vehicle, -1.002 ± 0.0883; control:CNO, -0.1285 ± 0.0442; DREADDs:vehicle, -0.0429 ± 0.0671; DREADDs:CNO, -0.1342 ± 0.0739) (**Fig. 4.5**). In all control groups, this preference became positive in favour of the novel object during retention sessions (control:vehicle, 0.0895 ± 0.0842; control:CNO, 0.0633 ± 0.0815; DREADDs:vehicle, 0.1029 ± 0.1486). In comparison, DREADDs animals that were given CNO still had a negative discrimination index in retention sessions (-0.0281 ± 0.1248) (**Fig. 4.5)**. We observed no significant differences between encoding session and retention sessions in animals following vehicle treatments ($p = 0.2236$, paired t-test), or DREADDs animals given vehicle drug treatment ($p = 0.4228$, paired t-test), however, a significant difference was found between control animals who received CNO ($p = 0.0492$, paired t-test). DREADDs animals that received CNO treatment also did not have statistical differences in discrimination index between encoding and retention sessions ($p = 0.3371$, paired t-test). Notably, while sex-dependent changes in performance were very little, females in each group tended to perform slightly better than males of the same group, with smaller p values occurring for the former, with the exception of control animals given vehicle, in which males performed better.

Overall, we observed a trend for reduced discrimination indices during retention sessions in animals that underwent chemogenetic activation of pontine astrocytes, suggesting reduced spatial memory which may be caused by REM sleep reductions. Despite this trend, and the fact that no statistical difference was found between the encoding and retention sessions in DREADDs animals receiving CNO treatment, we also did not see significant differences in some control groups. This could be due to the large variance of data, and/or small sample sizes.

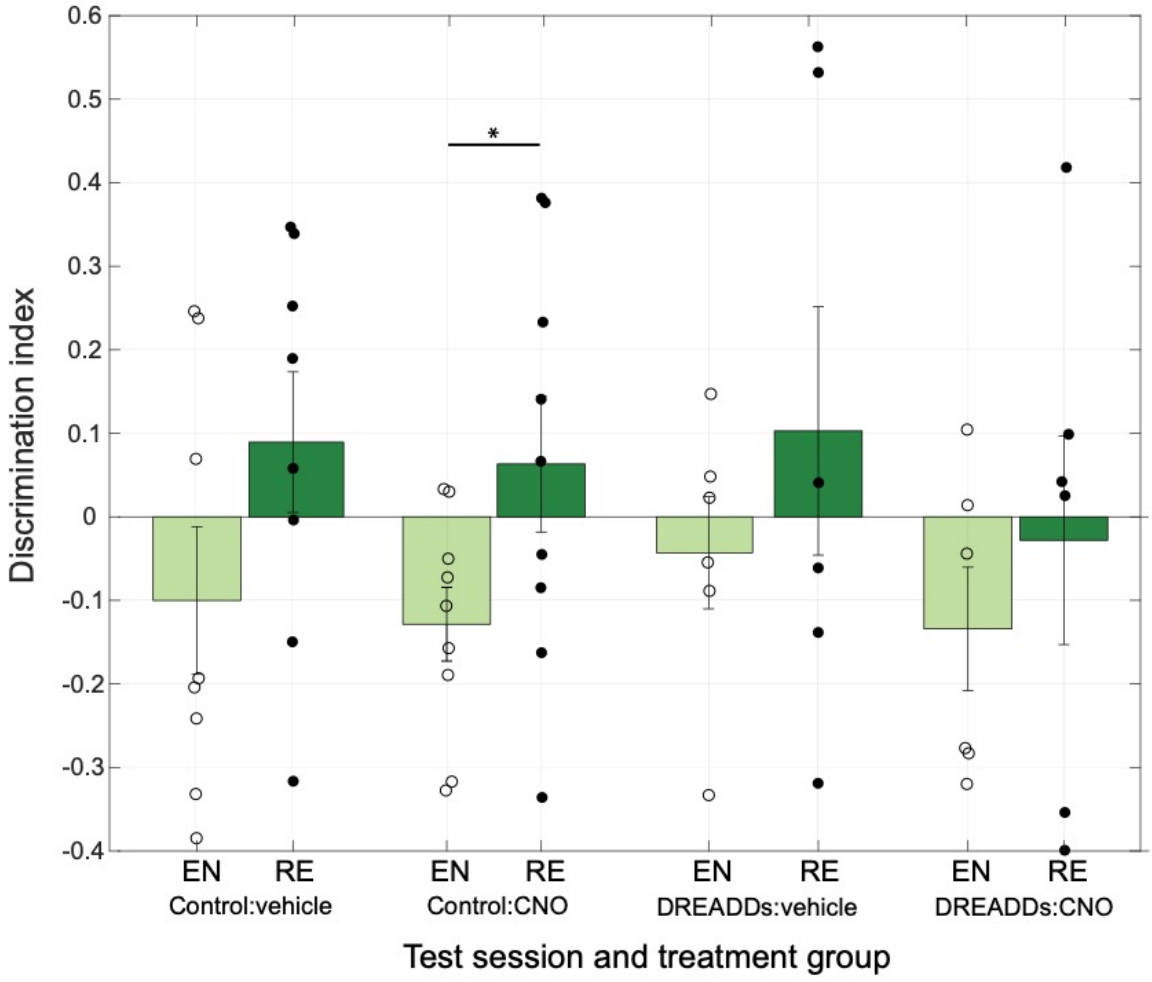

Figure 4.5. Discrimination indices for NOLT. Mean discrimination indices ± SEM for all groups including control animals given vehicle injections after encoding session, control animals given CNO (1 mg/kg) after encoding, DREADDs animals given vehicle injections after encoding session, and DREADDs animals given CNO (1 mg/kg) after encoding. All groups show discrimination indices first for encoding and then retention. All discrimination indices for distances 4 cm from oject centre. EN = encoding, RE = retention. Control:vehicle n = 8, control:CNO n = 9, DREADDs:vehicle n = 6, DREADDs:CNO n = 6. Normality calculated using Shapiro-Wilk test, significance calulated using two-way ANOVA and posthoc pairwise tests using Tukey-Kramer test, all data was not significant, $p > 0.05$.

4.2.5. Novel object recognition test

Similarly to NOLT, during NORT, 10-minute encoding sessions were done 24 hours before retention sessions. Immediately after encoding, animals were given *i.p.* injections of vehicle or CNO. In retention sessions, one object was switched to a novel object to test object recognition memory. Discrimination indices that were positive indicate a preference for novel object, while a negative discrimination index implies preference for the familiar object. Exemplar data of a control animal shows during encoding the animal explored both objects to a similar extent (**Fig. 4.6A,** top). During retention, the same animal showed a very strong positive preference for exploring the novel object, spending a longer exploratory time at a much closer distance and demonstrating extensive rearing behaviour with the novel object (**Fig. 4.6A,** bottom). Similarly, an exemplar DREADDs animal also showed little-to-no preference for either object during encoding (**Fig. 4.6B,** top), while following CNO administration immediately after encoding, a positive preference for the novel object was still observed (**Fig. 4.6B,** bottom), however, this effect seemed stronger in control animals.

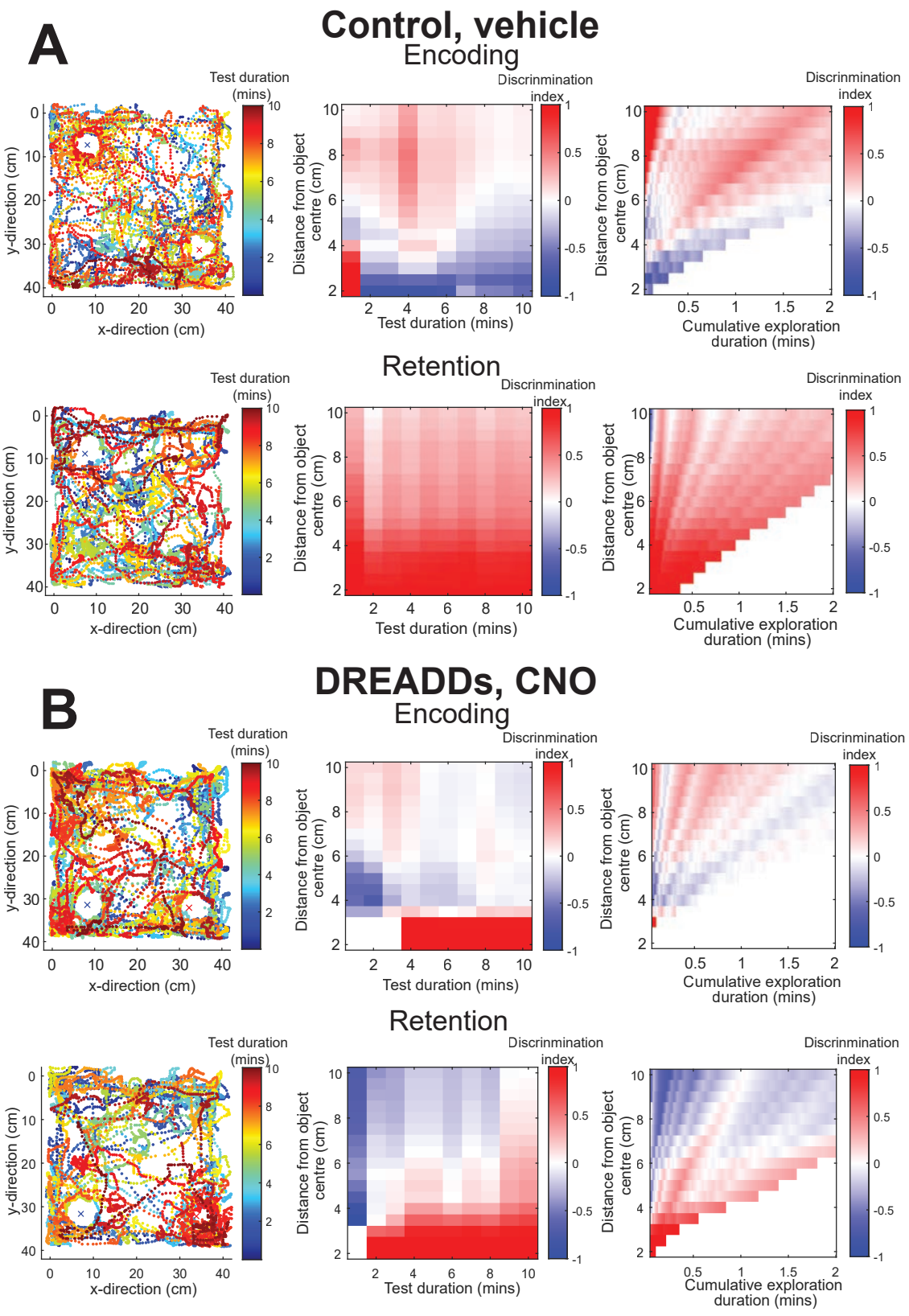

Figure 4.6. Examples of NORT with and without chemogenetic modulation of pontine astrocytes. **A.** Same figure configuration as in Figure 4.2A, in a control animal during an encoding sessions (top) and a retention session (bottom). **B.** Same as in A but in a DREADDs animal given CNO after encoding session.

Given that the strength of preference for the novel object seemed to be diminished following chemogenetic activation of pontine astrocytes in comparison to control groups in exemplar data, we wanted to look at group data and statistical analysis to explore this further. Again, we analysed discrimination indices for 4 cm distance from object centre. All data was normally distributed ($p>0.05$ per group, Shapiro-Wilk test). Discrimination was statistically lower during encoding than during retention for control animals given vehicle (0.0482 ± 0.1059 vs 0.4541 ± 0.1545, respectively, $p = 0.0303$, paired t-test) and had a tendency to be lower in control animals following CNO (0.0021 ± 0.1019 vs 0.3201 ± 0.1112, respectively, $p = 0.0684$, paired t-test), as well as DREADDs animals given vehicle (0.1821 ± 0.1447 vs 0.6141 ± 0.0689, respectively, $p = 0.0640$, paired t-test), suggesting animals preferred the novel object (**Fig. 4.7**). Despite seeing reduced effect in NORT in some DREADDs animals that received CNO, we found statistical differences between encoding and retention sessions in these animals (-0.0107 ± 0.1042 vs 0.5146 ± 0.1164, respectively, $p = 0.0014$, paired t-test) (**Fig. 4.7**). Notably, sex-dependent differences in performance were again minimal for NORT performance, with control females given vehicle and DREADDs female given CNO performing slightly better, and males performing slightly better in the other two groups.

Overall, we observed a significant difference between encoding and retention sessions in DREADDs animals that received CNO, suggesting object recognition memory was not impaired by chemogenetic activation of pontine astrocytes. Again, lack of statistical significance in control groups is likely due to the large variation in data.

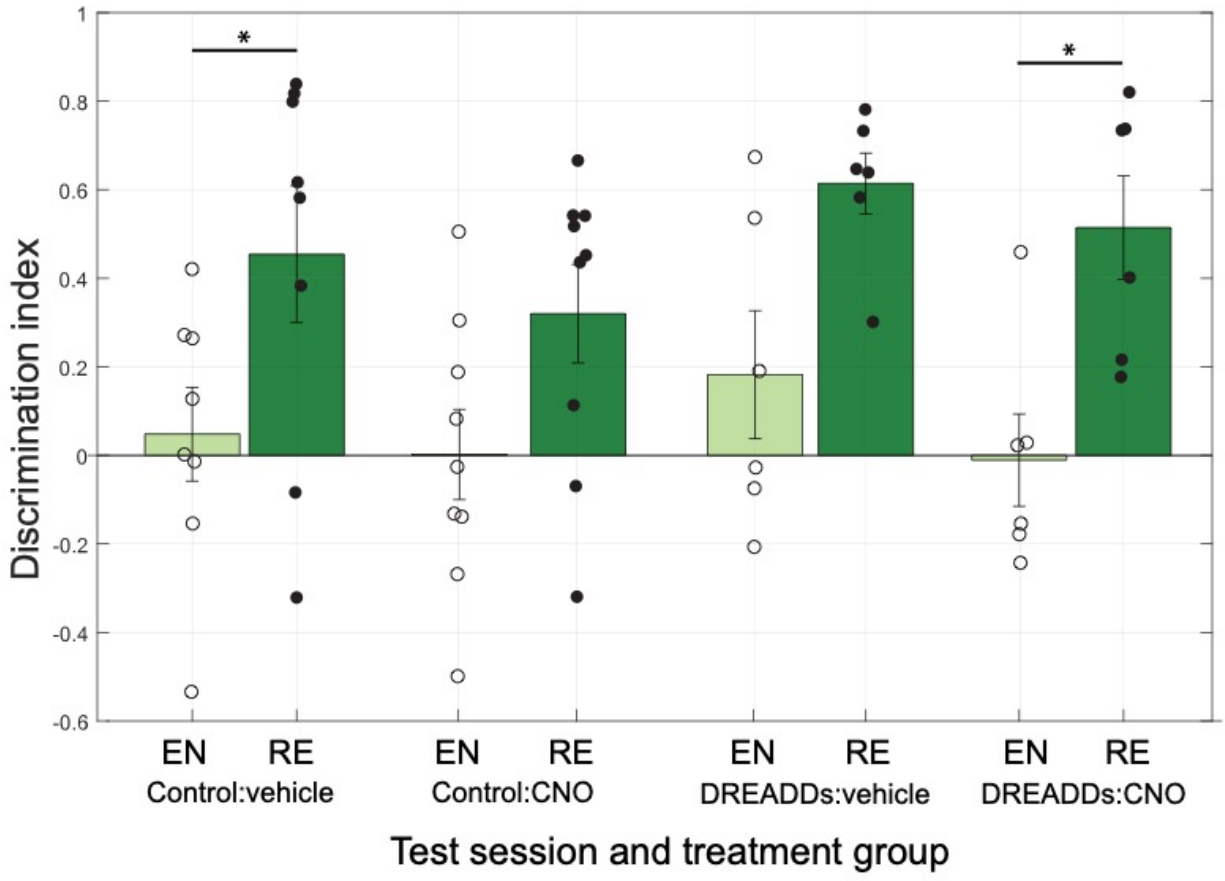

Figure 4.7. Discrimination indices for NORT. Mean discrimination indices ± SEM for all groups including control animals given vehicle injections after encoding session, control animals given CNO (1 mg/kg) after encoding, DREADDs animals given vehicle injections after encoding session, and DREADDs animals given CNO (1 mg/kg) after encoding. All groups show discrimination indices first for encoding and then retention. All discrimination indices for distances 4 cm from oject centre. EN = encoding, RE = retention. Control:vehicle n = 8, control:CNO n = 9, DREADDs:vehicle n = 6, DREADDs:CNO n = 6. Normality calculated using Shapiro-Wilk test, significance calulated using two-way ANOVA. Posthoc pairwise comparisons using Tukey-Kramer tests shown, *p<0.05.

4.3. Discussion

4.3.1. Summary of findings

In this chapter we showed that, unlike controls, following chemogenetic activation there was no positive preference for the novel object location during retention sessions for NOLT only. The difference between average discrimination index for encoding and retention sessions in animals undergoing chemogenetic modulation did not change to a level of statistical significance (**Fig. 4.4** & **Fig. 4.5**). Together, this suggests a potential effect for chemogenetic modulation to reduce spatial memory. However, as the change in discrimination index between encoding and retention sessions did not

reach significance level in all control groups, further studies and larger sample sizes are needed to confirm this effect.

Furthermore, during NORT we showed that while some animals had a reduced tendency to prefer the novel object after chemogenetic modulation, there was still a statistically significant change of discrimination indices between encoding and retention sessions in these animals, suggesting that chemogenetically activating pontine astrocytes had no effects on object recognition memory (**Fig. 4.5** & **Fig. 4.6**). However, similar to NOLT, changes in discrimination index did not reach significance in some control groups, suggesting further studies are again needed to confirm results. An additional finding was that discrimination indices had a greater increase from encoding sessions to retention sessions in control animals during NORT compared to NOLT. This could be due to NOLT being hippocampus- and sleep-dependent, while NORT is not (Ishikawa *et al.*, 2014; Sawangjit *et al.*, 2018). We also suggest that the improved performance during NORT could also be due to the animals being well acquainted with the familiar objects as the NOLT was performed prior to the NORT.

4.3.2. Limitations and future work

A main caveat for these behaviour studies is that the sleep-wake cycle was not measured in the 24-hour period between encoding and retention sessions. A main reason for this was due to conflicting schedules with ongoing construction in the animal unit, near our sleep experimental rooms, which would have disrupted natural sleep. Several animals (control n = 5, DREADDs = 2) that were included in these results also underwent chemogenetic studies in the weeks prior to behaviour tests, and were included in the results in the previous chapter. We confirmed in these DREADDs animals that REM sleep was significantly reduced for following 1 mg/kg CNO. However, another limitation to this issue is that several animals were injected with a new batch of DREADDs virus (see section 2.3.2.2), therefore it is not possible to confirm REM sleep was truly reduced in these animals. Thus, ideally memory studies would have been run concurrent with sleep monitoring, and we would show the sleep-wake cycle in the 24-hour periods between encoding and retention in all animals to confirm REM sleep was indeed reduced.

As briefly discussed, the wide deviation of data suggests technical limitations in our studies. By applying power calculations to our data, we found that 11-18 animals per group would be required for our control groups to reach statistical significance at 80% power for NORT. This was even higher for NOLT, with some control groups requiring 64 animals to reach statistical significance. This suggests that a much higher number of animals would be required for us to confirm the observed effect of reduced spatial memory following chemogenetic modulations. In addition, NOLT and NORT are simple tests that rely on natural exploratory behaviours, and does not involve punishment or reinforcement (Ennaceur and Delacour, 1988; Antunes and Biala, 2012). While this is advantageous due to being less stressful for the animals than tests that include punishment, due to the simplicity of this test, many factors can impact the outcomes. Parameters such as odour, noise, lighting, environmental cues, type of objects, analysis parameters, habituation and test durations, and length of retention interval can affect natural exploratory behaviour in mice. Stress and anxiety levels will also naturally differ between mice, which can also affect exploratory behaviour. Similarly, due to the quick experimental timeline, and the inability to repeat these tests in the same animal, rates of learning are not taken into consideration (Lueptow, 2017). To test the efficacy of the NOLT for spatial memory and avoid such limitations, alternative tests such as the Morris water maze, the Barnes maze test, or the active place avoidance test could be used to assess spatial memory (Blackmore *et al.*, 2022).

4.3.3. Summary and next steps

Overall, we show a trend for reduced spatial, but not object recognition, memory following chemogenetic activation of pontine astrocytes, which is likely due to reduction of REM sleep. With further studies, and increased sample sizes, this trend could become significant.

As we previously found that our chemogenetic studies induced strong changes in the sleep-wake cycle, specifically with reducing REM sleep incidence, and has a tendency to alter spatial memory, we wanted to confirm astrocyte activity was successfully increased following chemogenetic manipulations. To do this, we aimed to co-express DREADDs and GCaMP6f and monitor pontine astrocyte activity with and without chemogenetic manipulation using fibre photometry.

5. A pilot study on measuring astrocyte Ca^{2+} signals following chemogenetic modification

Following investigations on changes to the sleep-wake cycle and memory, we wanted to confirm that astrocyte Ca^{2+} levels were truly increased during chemogenetic manipulation. To do this, we wanted to combine our chemogenetic experiments with fibre photometry to monitor astrocyte calcium activity following injections of CNO. In this chapter I will first briefly introduce the background and hypothesis behind these experiments (section 5.1), describe the animals included in these results, and finally show some preliminary results we obtained from these studies (section 5.2). I will discuss some limitations we encountered and propose some further studies and next steps necessary to meet our aims (section 5.3).

The experiments reported in this chapter were a collaborative study with a postdoc in our lab, Dr Yuri Elias Rodrigues. All immunohistochemistry, imaging and image processing was done by myself. Fibre photometry experiments, including surgeries, recordings, and perfusions were shared equally by Dr Elias Rodrigues and myself, and data processing, including sleep scoring and fibre photometry signal reconstruction, was done by Dr Elias Rodrigues.

5.1. Introduction

Fibre photometry has been successfully used and combined with EEG/EMG recording to investigate astrocytic Ca^{2+} during the sleep-wake cycle and compare activity in different states (Tsunematsu *et al.*, 2021; Peng *et al.*, 2023; Cai *et al.*, 2022). Tsunematsu *et al.* (2021) used a transgenic mouse model, *Mlc1*-tTA; TetO-YCnano50, to express YCnano50, a genetically encoded calcium indicator consisting of YFP and CFP, exclusively in astrocytes. Following increases in intracellular Ca^{2+} in astrocytes, a conformational change between YFP and CFP occurs, leading to changes in fluorescence emission, thus the ratio between fluorescence is representative of Ca^{2+} changes. They then implanted optic fibres into mice and measured astrocyte Ca^{2+} activity in different regions during the sleep-wake cycle using fibre photometry. On the other hand, Peng *et al.* (2023), virally expressed genetically encoded Ca^{2+} sensor GCaMP6f specifically in astrocytes in target regions, and later implanted an optic fibre

into the same region to measure astrocyte Ca^{2+} levels during the sleep-wake cycle. GCaMP6f is a suitable GECI for studying astrocytes as it is more sensitive to small and fast Ca^{2+} events, compared to many other GECIs (Ye *et al.*, 2017). However, more recently, new variants with superior kinetics have been developed, such as the jGCaMP8s sensor (Zhang *et al.*, 2023). Similarly, Cai *et al.* 2022, used a viral technique to express GCaMP6m and implanted an optical fibre to measure Ca^{2+} activity in astrocytes.

As discussed, fibre photometry has been used for measuring astrocytic Ca^{2+}, with studies using these methods to characterise astrocyte activity throughout the sleep-wake cycle. Fibre photometry has also been used to demonstrate the effects of chemogenetics in astrocytes, although, this is yet to be fully characterised. GCaMP and hM3D have been co-expressed using viral based delivery of equal combinations of two viral vectors prior to implantation of optical implant. This has allowed studies to validate an increase in population astrocyte Ca^{2+} levels, or Ca^{2+} events, following administration of CNO (Cai *et al.*, 2022; Noh *et al.*, 2023). This is of particular importance for our study, as characterising astrocytic Ca^{2+} following chemogenetic manipulations would further validate our results reported in the previous two chapters.

5.1.1. Hypothesis and aims

The results in this chapter were based on the hypothesis that following chemogenetic manipulations, we would observe an increase in astrocytic Ca^{2+}. To address our hypothesis, we aimed to combine chemogenetic and fibre photometry approaches, and measure changes in pontine astrocyte fluorescence following CNO application in animals expressing DREADDs.

5.2. Results

5.2.1. Animals and dataset

A total of 14 animals were used in the experiments reported on in this chapter (**Fig. 5.1**). Animals underwent unilateral virus injection surgeries aged 8-24 weeks. 8 of these animals were injected with an equal volume cocktail of AAV5-gfaABC$_1$D-GCaMP6f and AAV5-gfaABC$_1$D-hM3D-mCherry, while 6 were injected with an equal volume cocktail of AAV5-gfaABC$_1$D-GCaMP6f and AAV5-gfaABC$_1$D-tdTomato. 3-4

weeks later, an optic fibre was implanted into the pons slightly dorsal to virus injection site, along with cortical EEG and EMG connections. 1 mouse in both the control group and DREADDs group were excluded due to the virus being off-target, and an additional DREADDs mouse was excluded for the fibre implant being off-target leaving a total of 5 control animals and 6 DREADDs animals included in the data for this chapter (**Fig. 5.1**).

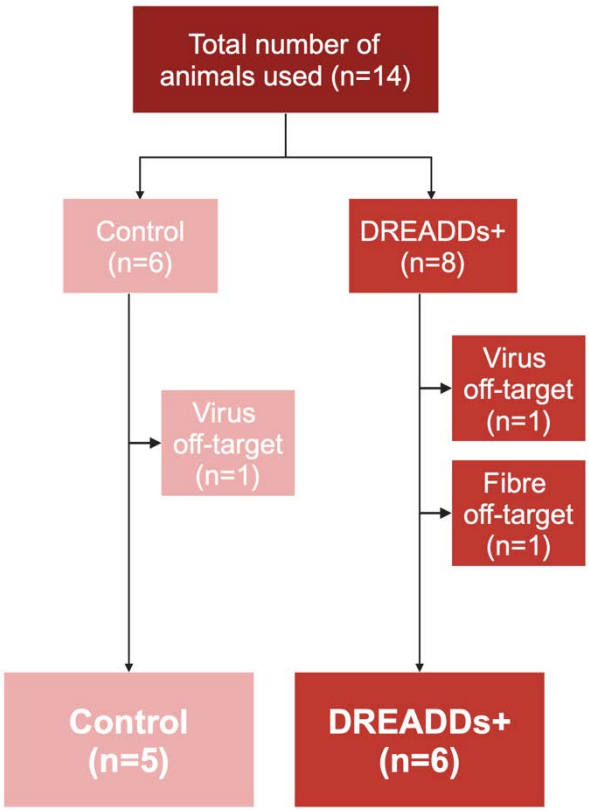

Figure 5.1. Animals used in combined fibre photometry and chemogenetic studies.

5.2.2. Virus expression and fibre implant in the pons

To visualise virus expression and the location of fibre implant in all mice, we carried out immunohistochemistry on sections from all mice. As our GCaMP virus was conjugated with fluorescent tag GFP, and control and hM3D viruses were conjugated with tdTomato and mCherry, respectively, we stained sections with anti-GFP and anti-dsRed to visualise unilateral virus expression (**Fig. 5.2A**). Damage from fibre implantation also allowed us to visualise the location of optic fibre (**Fig. 5.2A**). To visualise the spread of virus expression and fibre location, we registered 2-3 sections from each animal used in the database of this chapter to the Allen Mouse Brain atlas CCFv3 and extracted virus expression (shown in black) and damage from optic fibre

(shown in white) to visualise how this changed across the AP-axis. Our visualisation suggests that in control animals (**Fig. 5.2B**) and DREADDs animals (**Fig. 5.2C**) virus expression and location of fibre tip occurred in the pons, however some virus expression spread to midbrain, medullar and cerebellar regions (n = 12 sections from 5 control animals, n = 14 sections from 6 DREADDs animals) (**Fig. 5.2**).

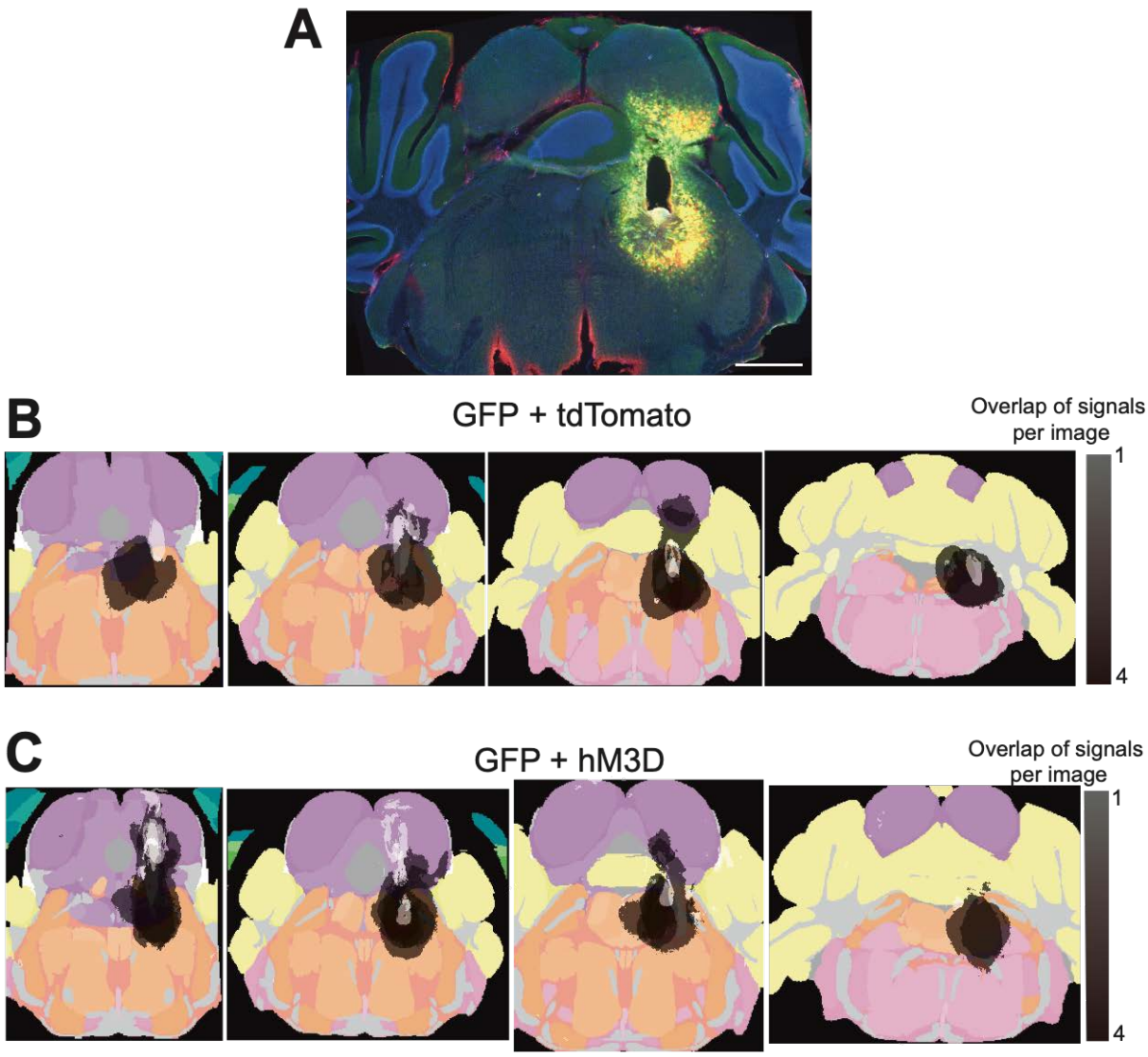

Figure 5.2. Virus expression and fibre implant location. **A.** Examplar images of histological sections stained with anti-GFP (green) and anti-dsRed (red), and counterstained with DAPI. Damage from fibre tip visable. Scale bar = 1000 μm. **B.** Virus expression (black) and damage from fibre implant (white) in control animals expressing GCaMP and tdTomato. Location registered and mapped according to the Allen Mouse Brain atlas CCFv3, blue/green = cortex, purple = midbrain, orange = pons, pink = medulla, yellow = cerebellum. Black indicates the virus where darker colour indicates overlayed expression in multiple sections (demonstrated in colourbar). n = 12 histological sections from 5 animals, n = 2-3 per animal. **C.** Same as in (B) but in DREADDs animals expressing GCaMP and hM3D. n = 14 histological images from 6 animals, n = 2-3 per animal.

5.2.3. Limited co-expression of GCaMP6f and hM3D in astrocytes

After assessing the location of virus expression and fibre implantation, we wanted to look more closely at the co-expression of anti-GFP and anti-dsRed (or anti-mCherry) in pontine astrocytes. Using epifluorescent imaging at 4X magnification, we observed good overlap of anti-GFP and anti-dsRed surrounding the fibre tip in control animals (**Fig. 5.3A**). At a higher magnification, we looked at co-expression of anti-GFP and anti-mCherry with astrocyte specific marker, anti-GFAP. We observed many cells with astrocyte-morphology co-expressing these markers (**Fig. 5.3B**).

On the other hand, at 4X magnification using epifluorescent imaging, in DREADDs animals we observed less extensive expression of anti-dsRed in regions that we observed good expression of anti-GFP (**Fig. 5.4A**). In areas where we did observe anti-dsRed expression, we looked at co-expression of anti-GFAP, anti-GFP, and anti-mCherry at a higher magnification. Although again we observed less extensive anti-mCherry expression, cells with astrocyte-like morphology that did express anti-mCherry also tended to co-express anti-GFP and/or anti-GFAP (**Fig. 5.4B**). This observed effect was consistent across the 6 animals used in this study.

Overall, we observed good co-expression of anti-GFP and anti-dsRed or anti-mCherry in cells which had astrocyte-like morphology and expressed anti-GFAP in control animals, suggesting co-expression of our viruses in these animals. However, in DREADDs animals this tended to be less extensive, suggesting the viruses were not co-expressed well, which may affect our results for fibre photometry following chemogenetic manipulations.

Across animals, we found that good co-expression of anti-dsRed and anti-GFP occurred across five control animals (**Fig. 5.5**), suggesting good co-expression of tdTomato and GCaMP6f occurred in pontine astrocytes in these animals. In comparison, we found very little labelling of anti-dsRed in DREADDs animals, resulting in poor co-expression of anti-dsRed and anti-GFP (**Fig. 5.6**). This suggests that a lack of co-expression of hM3D and GCaMP6f occurred in these animals, caused by poor hM3D expression.

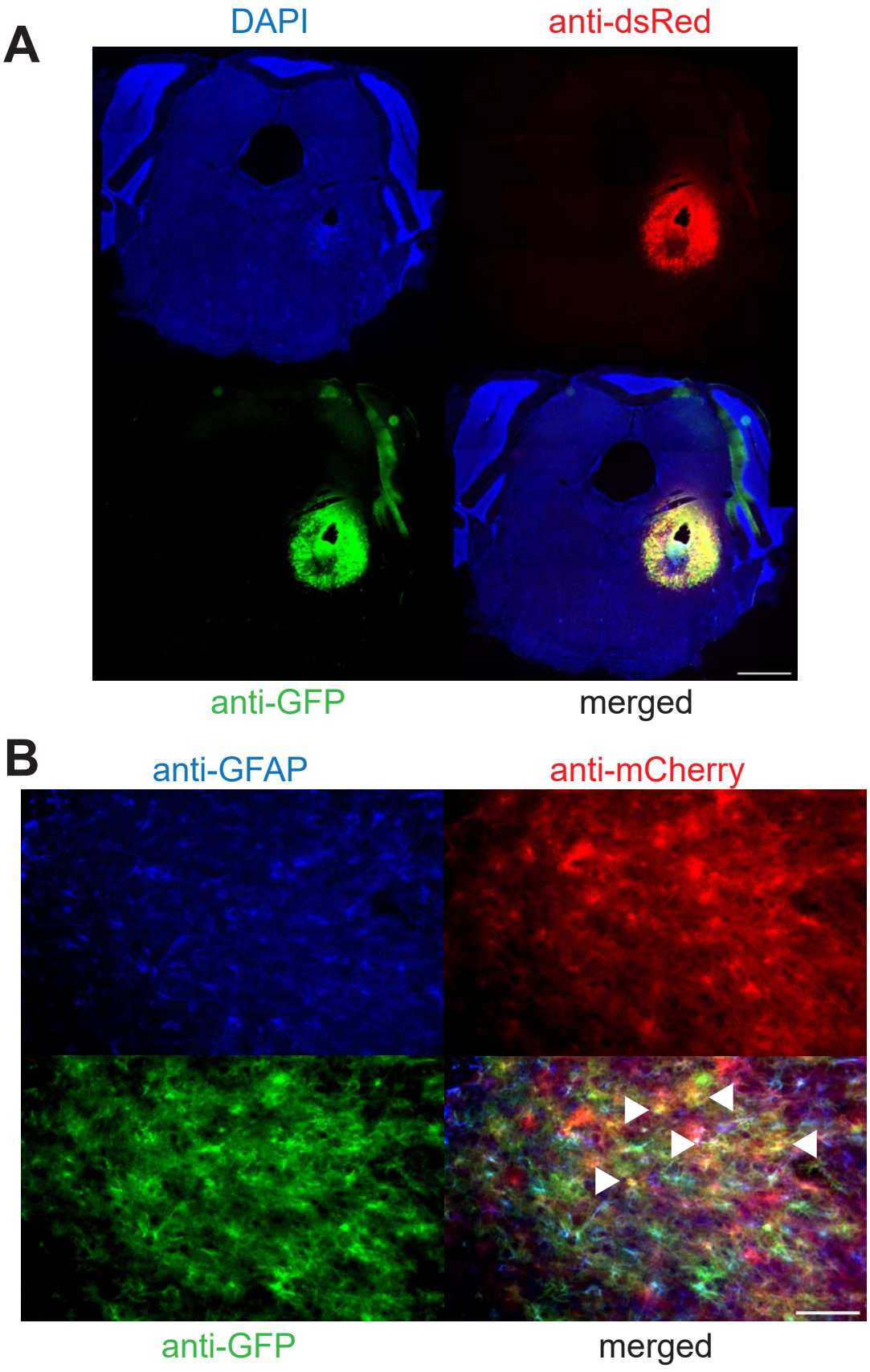

Figure 5.3. Co-expression of anti-GFP and anti-mCherry in a control animal. Examplar images of immunohistochemistry from one control animal using epifluorescence imaging. **A.** 4x magnification, DAPI counterstaining, anti-mCherry and anti-GFP signals, and merged image to illustrate overlap of signals. Scale bar = 1000 μm. **B.** 20x magnification of anti-GFAP, anti-mCherry, and anti-GFP signals, and merged image to illustrate co-expression. Scale bar = 100 μm.

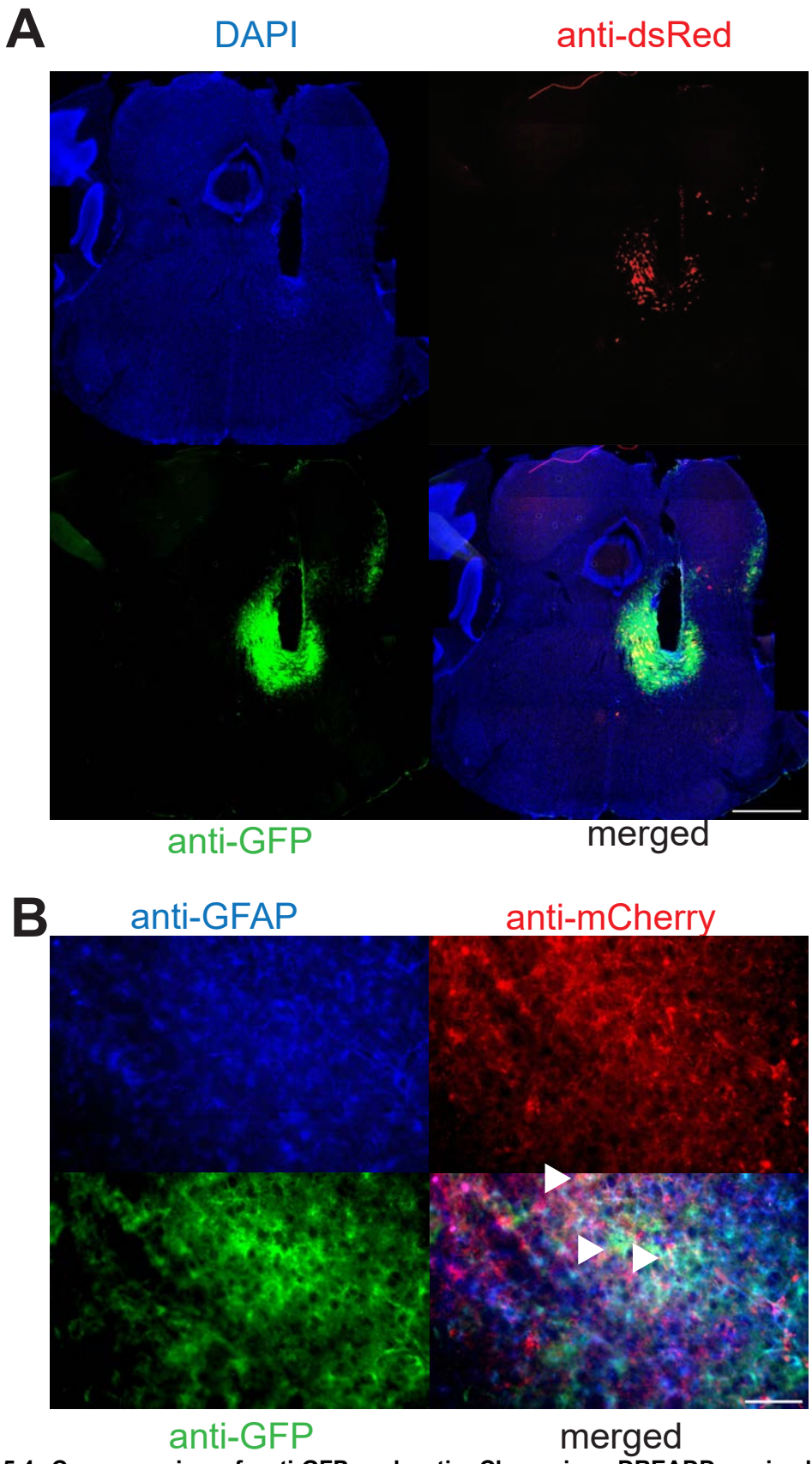

Figure 5.4. Co-expression of anti-GFP and anti-mCherry in a DREADDs animal. Examplar images of immunohistochemistry from one DREADDs animal using epifluorescence imaging. **A.** 4x magnification, DAPI counterstaining, anti-mCherry and anti-GFP signals, and merged image to illustrate overlap of signals. Scale bar = 1000 μm. **B.** 20x magnification of anti-GFAP, anti-mCherry, and anti-GFP signals, and merged image to illustrate co-expression. Scale bar = 100 μm. White arrows indicate co-expression.

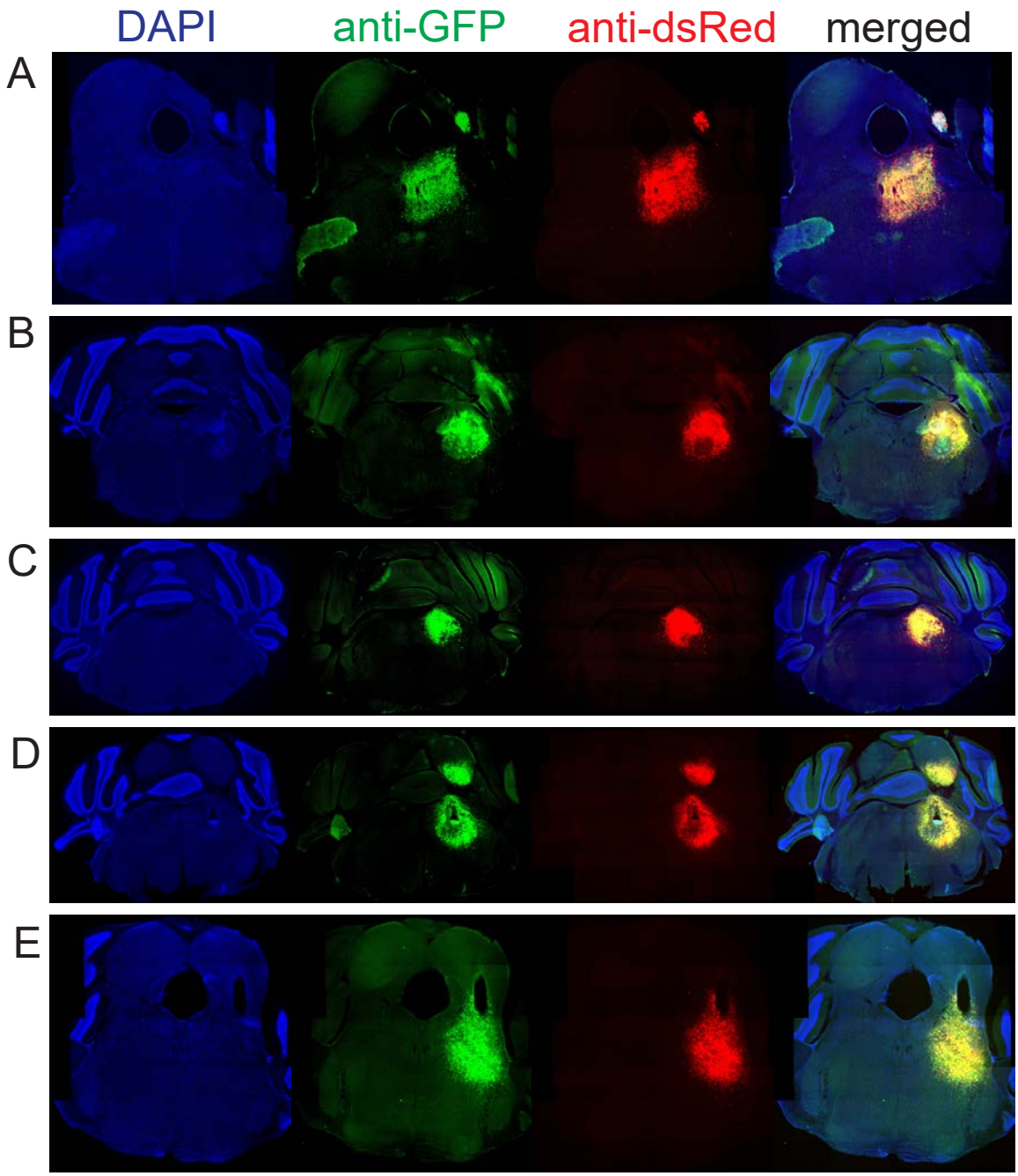

Figure 5.5. Co-expression of tdTomato and GCaMP6f in control animals. Immunostaining of control animals showing DAPI (blue), anti-dsRed (red), and and-GFP (green), and merged images to illustrate co-expression in 5 control animals (**A-E**).

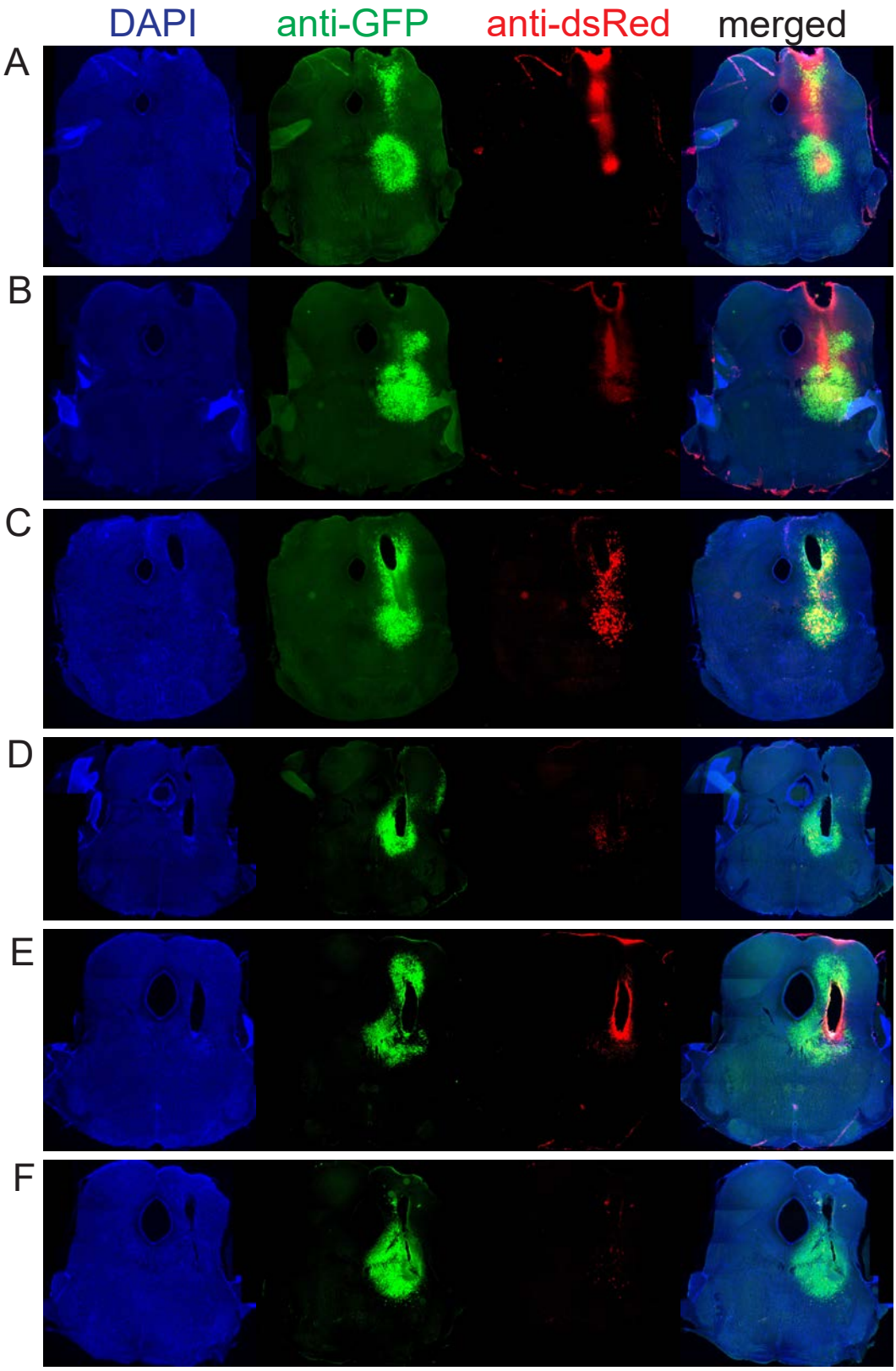

Figure 5.6. Co-expression of hM3D and GCaMP6f in DREADDs animals. Immunostaining of control animals showing DAPI (blue), anti-dsRed (red), and and-GFP (green), and merged images to illustrate co-expression in 6 DREADDs animals (**A-F**).

5.2.4. State-dependent changes in GCaMP fluorescence following chemogenetic modulation in pontine astrocytes

Following sleep-scoring of data, we looked at state-dependent changes in GCaMP fluorescence after CNO application in a control and a DREADDs animal. An animal with relatively good co-expression of hM3D and GCaMP6f was chosen as the representative DREADDs animal (**Fig 5.6C**).

In an exemplar recording from a control animal following administration of CNO (1 mg/kg), upon REM sleep we observed a drop in GCaMP fluorescence that occurred upon transitions into and throughout REM sleep (**Fig. 5.7A**). Fluorescence appeared to recover after transitioning from REM sleep into wake, and seemed relatively stable during wakefulness and NREM sleep (**Fig. 5.7A**). This effect could be observed in control animals despite different drug treatments, suggesting astrocytic Ca^{2+} is reduced during REM sleep. Changes in baseline fluorescence before and after injection of CNO (1 mg/kg) was not apparent (**Fig. 5.7A**).

On the other hand, in a DREADDs animal, following CNO administration (1 mg/kg) we did not observe a drop in GCaMP fluorescence during REM sleep **(Fig. 5.7B)**. We also observed some spontaneous transient increases in GCaMP fluorescence (**Fig. 5.7B**). In comparison with our results from chapter 3, we observed REM sleep occurrence in this animal during the 2.5 hours post CNO injection. We suggest this is due to our DREADDs virus being expressed unilaterally, in comparison to animals that were injected bilaterally for experiments shown in chapter 3.

Overall, this suggests that GCaMP fluorescence, and hence astrocytic Ca^{2+} activity, is altered, particularly during REM sleep, following chemogenetic activation. In addition, we show in control animals that astrocytic Ca^{2+} was lower during REM sleep. To confirm chemogenetic modulations were selectively activating astrocytes, we wanted to investigate changes in baseline fluorescence following CNO administration in group data, however, due to our uncertainty of co-expression of hM3D and GCaMP6f, we were unable to inspect this further.

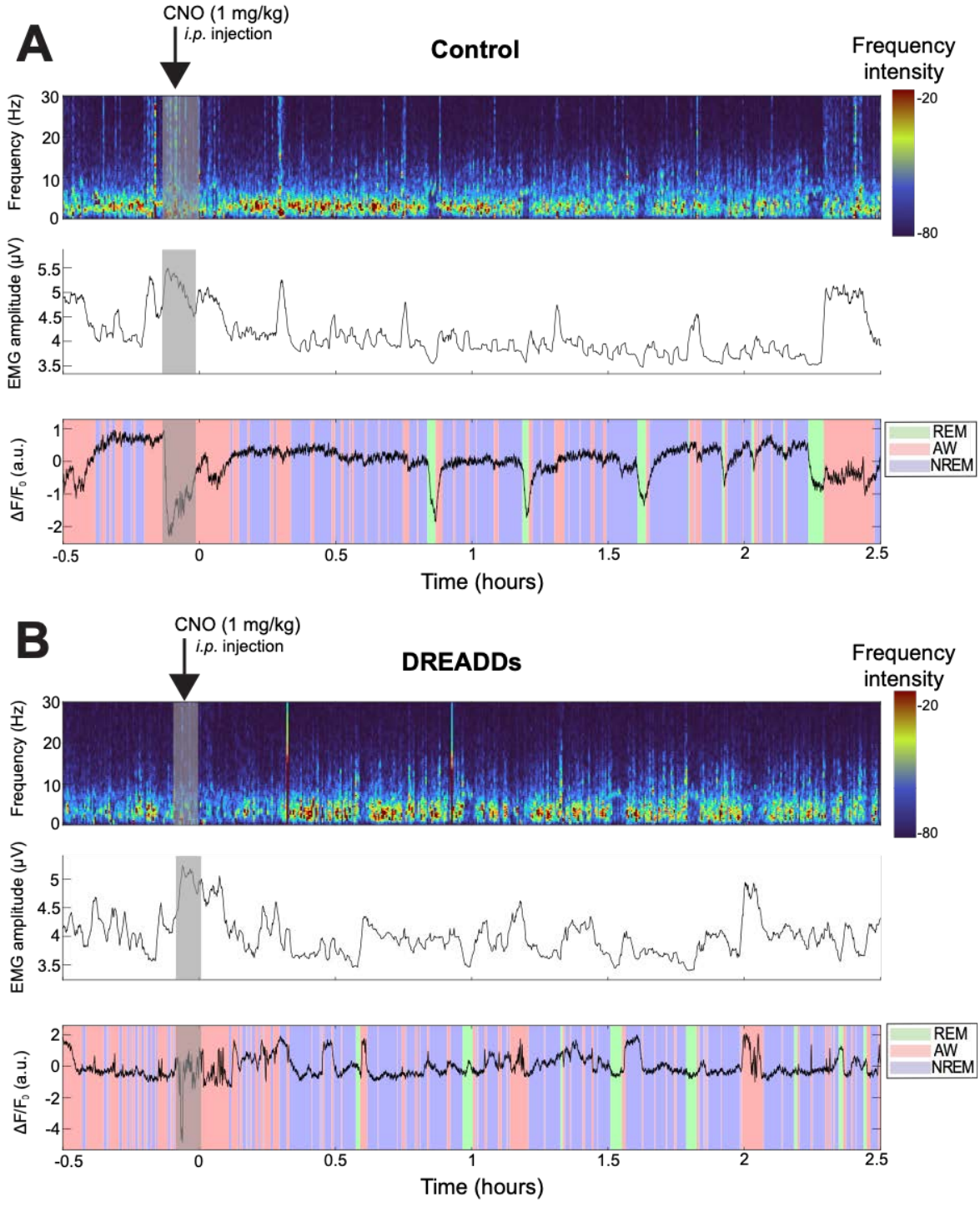

Figure 5.7. Examples of state-dependent changes in fluorescence in a control and DREADDs animal following chemogenetic modulation. A. Spectrogram of cortical EEG frequency (top), EMG amplitude (middle) and changes in GCaMP fluorescence according to state (bottom) (wake = red, NREM sleep = blue, REM sleep = green) across 4 hours, 30 minutes before injection of CNO (1 mg/kg) and 2.5 hours post-injection. **B.** Same as in (A) but in a DREADDs animal.

5.3. Discussion

5.3.1. Summary of findings

Overall, we first observed that both virus expression and location of fibre implant were mostly contained to the pons (**Fig. 5.2**). However, we observed that co-expression of anti-GFP and anti-dsRed/anti-mCherry in animals injected with a cocktail of our GCaMP- and hM3D-containing viruses was less convincing in comparison to animals injected with a cocktail of GCaMP-containing virus and our control chemogenetic virus (**Fig. 5.3 – Fig. 5.6**). This suggests that hM3D was expressed in less cells than GCaMP6f. We hypothesise that this may be due to our methods, in which we combined two viruses to inject into the brain, which can result in limited co-expression.

Next, we found in an exemplar sleep scored dataset that a reduction in GCaMP fluorescence occurred upon and throughout REM sleep episodes in a control animal following CNO administration (**Fig. 5.7**). This result occurs in agreement with results from Tsunematsu *et al.,* who found lowered astrocyte activity during REM sleep compared with other states (Tsunematsu *et al.*, 2021). In comparison, this decrease was not seen in a representative DREADDs animal, suggesting astrocytic activity during REM sleep was altered by chemogenetic activations (**Fig. 5.7**). We were unable to determine if this effect was seen across animals due to the poor co-expression of hM3D and GCaMP6f.

5.3.2. Limitations and future work

From previous work which utilise similar techniques, we expected to see an increase in baseline change in fluorescence following CNO in animals expressing GCaMP and hM3D (Cai *et al.*, 2022). As previously mentioned, we suggest this is due to lack of hM3D expression. Our viruses had different titres (AAV5-gfaABC$_1$D-tdTomato, ≥ 7×10^{12} gc/mL; AAV5-gfaABC$_1$D-hM3D-mCherry, 3x10^{12} gc/mL; AAV5-gfaABC$_1$D-GCaMP6f, ≥ 7×10^{12} vg/mL), and as our hM3D-containing virus had the lower titre, this could result in several limitations to our methods. Lower titres generally infect a lower number of cells, and when we inject a mixture of our two viruses the imbalance in titres can lead to an imbalance in expression where the virus with the higher titre dominates expression. When we utilised immunohistochemistry analysis, we found that this was the case between our GCaMP6f- and hM3D-expressing viruses, but not between

GCaMP6f- and tdTomato-expressing viruses, which had similar titres. A potential solution for this limitation could be to dilute our GCaMP virus, or increase the volume of hM3D-containing virus. Alternatively, staggering virus injections, and injecting hM3D first and allowing a brief incubation period may also help balance expression.

Additionally, our baseline recording period should be longer. Due to constraints caused by construction work in our animal unit, we had restricted time for recordings, leading to only short baseline periods (1-hour) being measured prior to CNO or vehicle treatments. Ideally, baseline recordings of 4 hours would be obtained before commencing treatments to more accurately reflect natural changes in brain activity caused by circadian fluctuations. This would allow for better comparison of brain activity caused by CNO.

Furthermore, our pilot data could be further analysed. Firstly, it would be beneficial to investigate state-dependent changes in fluorescence across animals further. This would inform us that, even at low expression of hM3D, the activity of GCaMP fluorescence was altered during REM sleep following chemogenetic modulation. Secondly, with our group data, further investigation into differences between animals and variations in raw data, as well as EMG activity to assess potential hyperactivity that could affect fluorescence could help us interpret our data, as well as determine why we do not see consistent results for baseline time periods, control animals, and vehicle conditions.

5.3.3. Overall summary

Overall, in our pilot results reported in this chapter, we found that astrocyte activity seems to reduce during REM sleep, with chemogenetic modifications altering such an effect. However, overall, we were unable to confirm such an effect across animals due to the lack of hM3D expression in astrocytes.

6. Discussion

In this final chapter, I will summarise our main findings from each results chapter (section 6.1). I will then discuss the significance of such findings, and possible interpretations (section 6.2). Next, I will discuss all experimental difficulties and limitations we encountered throughout the project (section 6.3), and potential future work which could overcome these issues, as well as future work which could lead on from our findings (section 6.4). Importantly, I will conclude with the main conclusions arising from all experiments (section 6.5).

6.1. Summary of findings

The main aims of this project were based upon the hypothesis that modulating pontine astrocyte activity would reduce REM sleep incidence. To address this hypothesis, we aimed to modulate astrocyte activity in the pons using chemogenetics and assess effects on REM sleep occurrence *in vivo* (chapter 3). This involved bilateral injection of an hM3D-containing virus which selectively targeted astrocytes in the pons (**Figs. 3.4-3.9**) and monitoring the sleep-wake cycle following CNO administration. Most importantly, we observed the 6 hours following CNO administration and found that there was a significant reduction in total REM sleep, number of REM episodes, and increased latency to REM sleep following chemogenetic modulations (**Fig. 3.13**). We then found that while rebound REM sleep did not occur, this effect was partly diminished in the hours following modulation (**Fig. 3.14-Fig. 3.19**). Subsequently we found a trend for reduced spatial memory in animals following chemogenetic modulations (**Fig. 4.4** & **Fig. 4.5**).

6.2. Interpretation and significance of results

Most significantly, we showed a reduction in REM sleep following chemogenetic activation of pontine astrocytes. At the time of commencing experiments and collecting data, these results were novel, with the motivation of the project largely based on results from Tsunematsu *et al.* which used fibre photometry to show reduced astrocytic Ca^{2+} activity in the pons during REM sleep (Tsunematsu *et al.*, 2021). However, similar results were later replicated in published and unpublished studies (**Fig. 3.13**) (Peng *et al.*, 2023; Kurogi *et al.*, 2024). Peng *et al.* published largely based

on data in the basal forebrain, but included results based on fibre photometry and chemogenetic experiments in the brainstem, specifically LC-SLD. While their chemogenetic data matches what we presented in this project (CNO 1 mg/kg), their fibre photometry data was the opposite of what is expected, and what we found in control animals during fibre photometry experiments (chapter 5), showing relatively high astrocytic Ca^{2+} during REM sleep (Peng *et al.*, 2023). On the other hand, Kurogi *et al.* presented chemogenetic activation of hippocampal and pontine astrocytes. While their results in the pons again match those in our study, their lack of control groups highlights a flaw in their experimental design. In this study they did not include a negative control group in which a control virus was used. Instead, hM3D was expressed in all mice and during experiments animals were given vehicle or CNO (1 mg/kg), meaning that the direct effects of CNO alone could not be assessed. Such a negative control is necessary to validate their results, due to the known sedative effects of CNO on the sleep-wake cycle, particularly at high concentrations of CNO (Kurogi *et al.*, 2024; Traut *et al.*, 2023). Notably, consistent with previous reports, during our experiments we also found that CNO alone caused sedative effects by promoting NREM sleep and reducing latency to NREM sleep, particularly at high concentrations (**Fig. 3.13**). However, interestingly, we found that REM sleep was not altered by CNO alone, as we observed no differences in total REM sleep, number of REM sleep episodes, average duration of REM sleep episodes, or latency to REM sleep between any of our control groups, including control animals administered with vehicle or CNO. This opposes a previous study which found a reduced proportion of REM sleep, reduced number of REM sleep episodes, increased average REM sleep episode duration, and increased latency to REM sleep, particularly at high doses of CNO (Traut *et al.*, 2023). In this study, as well as showing reduced REM sleep incidence following chemogenetic activation of pontine astrocytes, using all appropriate negative controls, we also showed that this effect was dose-dependent, with high concentration of CNO abolishing REM sleep completely in some cases (**Fig. 3.13**). We also showed that rebound REM sleep did not occur in the hours following this effect, however, over the course of 10 hours, this effect was partially diminished (**Fig. 3.14-Fig 3.19**). This is, to the best of my knowledge, the first time rebound REM sleep has been investigated following chemogenetic manipulation of pontine astrocytes.

Next, we found a trend for reduced spatial, but not object recognition, memory retention in DREADDs mice following CNO injections. However, as some control groups did not reach differences to a significant level, we cannot fully validate this claim. The sample size required to reach statistical significance with proper power has been reported to be around 15-20 per group for behaviour tests, plus those that would be excluded due to lack of exploration (Lueptow, 2017). In line with this, we found that for NORT sample sizes of 11-18 were required for control groups to reach statistical significance with a power of 80%, while higher numbers of 16-64 would be required for control groups to reach significance in NOLT, suggesting high numbers of animal would be required to confirm our trend. Previous studies have used a range of methods to reduce REM sleep and test the impact of this on memory. Optogenetically inhibiting MS GABAergic neurons during REM sleep to attenuate theta without affecting the sleep wake cycle, caused a reduction in spatial and contextual fear memory (Boyce *et al.*, 2016), while optogenetically silencing adult-born neurons in the dentate gyrus during REM also impairs contextual fear memory (Kumar *et al.*, 2020). Similarly, optogenetically inhibiting hypothalamic supramammillary nucleus projections to the CA2 during REM sleep impaired social memory (Qin *et al.*, 2022). To the best of my knowledge, this is the first time that the impact of reducing REM sleep on memory by targeting astrocytes has been assessed. However, despite the observed trend for reduced spatial memory after chemogenetic-induced REM sleep reduction, more studies would have to carried out before we could confirm this trend.

Finally, by combining fibre photometry and chemogenetic techniques we observed some changes in astrocyte fluorescence during REM sleep in exemplar data between a control animal and a DREADDs animal (**Fig. 5.7**). Interestingly, in our exemplar data of a control animal, we replicated studies from Tsunematsu *et al.,* who demonstrated that pontine astrocyte Ca^{2+} was lowered during REM sleep compared to other states, while this contrasts data from Peng *et al.* who found that pontine astrocyte Ca2+ was relatively high during REM sleep (Tsunematsu *et al.*, 2021; Peng *et al.*, 2023). In comparison, our DREADDs animal did not display such reduced activity upon and during REM sleep. However, overall, we were not able to confirm if this effect was consistent across animals, or address our hypothesis that increased baseline fluorescent would be increased upon CNO administration caused by chemogenetic activation of pontine astrocytes. We expected to see this given previous data, which

virally co-expressed GCaMP6m and hM3D and showed an increased baseline fluorescence following CNO administration (Cai *et al.*, 2022; Noh *et al.*, 2023). We suggest that we were unable to produce this finding in this project due to insufficient expression of hM3D in astrocytes expressing GCaMP6f (**Fig. 5.3**-**Fig. 5.6**).

6.3. Project limitations

Specific limitations were discussed in the relevant chapters (see section 3.3.2, 4.3.2, 5.3.2). Here, I will discuss some general limitations, one of the most significant being time. Due to the nature of the methodology, several training months were required, while several months were also required for set-up refinement. In addition, experimental timelines per animal included 4 weeks for viral incubation and several weeks of experiments, and often inclusion criteria could not be determined until histology, meaning several weeks of work were often discarded. Furthermore, the most limiting factor for time occurred due to construction work in our animal unit. This also affected daily activities due to the schedule of construction work, which restricted us to shorter sleep recordings, where ideally, we would have assessed the sleep-wake cycle for longer time frames to assess rebound sleep, and also to assess sleep behaviour between encoding and retention sessions during memory testing. This scheduling also led to many days being too loud and disruptive to perform experiments, or led to experiments being discarded due to unexpected interference, with which delayed many of our experiments. Such delays were a major reason that the number of animals were low in some experiments.

In terms of experimental limitations, several that we encountered had a substantial impact on our project. Firstly, as previously discussed, the use of mouse-derived antibodies had impacts on the final number of animals used in the study, delayed our experimental timelines, and make histology interpretation more difficult (**Fig. 3.2-Fig. 3.3**). This also led to the use of more animals, which opposes our principles of three R's (replacement, reduction and refinement) as per the UK Animals (Scientific Procedures) Act of 1986, principle we aim to adhere to as much as possible.

6.4. Future work

For potential future work, firstly, increased sample sizes and improvements to methodology would validate some of our observed trends in this project. Our behaviour experiments presented some interesting trends, suggesting spatial memory, but not object recognition memory, were impaired due to chemogenetic modulation, however, this trend could not be fully claimed, as some of our control groups did not reach differences to a significant level. This could potentially be rectified by increasing our sample size, or using alternative tests for spatial memory, which do not rely on exploratory behaviour, and result in such wide variation. However, this remains challenging as sample sizes required to reach statistical significance with proper power has been reported to be around 15-20 per group for behaviour tests (Lueptow, 2017). In addition, as previously discussed, tests for spatial memory each have their own constraints (see section 1.2.3.3.1), thus leaving a demand for novel tests with clear advantages to be designed. Similarly, our aims to use fibre photometry in combination with chemogenetic techniques to confirm increased astrocytic Ca^{2+} in the pons following administration of CNO could be validated with further experiments. As the overlap of anti-GFP and anti-dsRed was unconvincing, further experiments would need to address this issue. This could be done by balancing viral titres or using a combination of transgenic and viral approaches.

In addition, the results we report from this project raise interesting questions for future studies. Firstly, due to the clear reduction in REM sleep incidence following chemogenetic activation, it would be of benefit to determine if inhibiting astrocyte activity would induce opposite effects. This could be done using CalEx experiments (Yu *et al.*, 2018), and measuring the sleep wake cycle in a similar approach as this project. If this successfully increased REM sleep, it would be greatly interesting to carry these experiments out in animal models of disease in which REM sleep is altered. For example, $App^{NL\text{-}G\text{-}F}$ is an animal model of AD that replicates the reduced REM sleep occurrence observed in AD, along with learning and memory impairments, and accumulation of Aβ (Maezono *et al.*, 2020). Using this model, we could apply chemogenetic activation of pontine astrocytes and CalEx inhibition of astrocyte activity, and determine the outcomes on REM sleep, as well as memory performance and disease pathology for both methodologies. This would be highly beneficial to

advance our understanding of astrocyte-dependent REM sleep regulation in the disease progression of AD.

Secondly, it would be interesting to measure the sleep-wake cycle for a longer time period, such as 24-48 hours following chemogenetic manipulations, to determine if any compensatory REM sleep occurs. This could also involve simultaneously measuring astrocyte activity, using fibre photometry or imaging techniques, to determine if any changes in astrocyte activity occurs over this longer time frame. This could also involve measuring astrocyte activity following periods of total REM sleep deprivation using chemogenetics and CNO administration.

Thirdly, due to the strong effects activating astrocytes has on REM sleep, as well as the changes in morphology we observed in astrocytes after chemogenetic activation, single-cell RNA sequencing would provide us with valuable knowledge about what is driving these effects, and the state of astrocytes following chemogenetic activation. New methods for microfluid-free single-cell RNA sequencing present an opportunity for relatively quick and simple identification of cell-type, marker identification, and gene expression (Clark *et al.*, 2023; Frazel *et al.*, 2023), such methods could answer some of these questions.

Finally, it would be interesting to investigate the relationship between astrocytes and neurons during this effect. As astrocytes secrete gliotransmitters such as glutamate, GABA, and D-serine, simultaneously measuring activity of pontine astrocytes and local glutamatergic or GABAergic neurons during the sleep-wake cycle would provide us with more information about the co-activities of these cell populations. This could be achieved by dual-colour fibre photometry (Serikov *et al.*, 2024). In addition, chemogenetically modifying astrocyte activity and measuring GABAergic or glutatergic neural activity, or reversely optogenetically modifying GABAergic or glutamatergic neural activity and simultaneously measuring local astrocyte activity would greatly expand our understanding to the relationship between these cell populations during the sleep wake cycle, and what is driving the strong effects we observed in this project.

Similarly, at the same time as measuring astrocyte activity, measuring extracellular levels of various gliotransmitters would provide us with more information about how

astrocytes exert effects. Gliotransmitter levels can be measured using biological sensors, such as G-protein-coupled receptor activation-based (GRAB) sensors. Such biological sensors have been developed for a wide range of neurotransmitters and neuromodulators, such as GABA, glutamate, dopamine, histamine, and ATP (Marvin *et al.*, 2019; Marvin *et al.*, 2013; Marvin *et al.*, 2018; Sun *et al.*, 2018; Dong *et al.*, 2023; Wu *et al.*, 2022a). Alternatively, using a gliotransmitter knock-out mouse model and determining subsequent effects of chemogenetic activation of pontine astrocytes on REM sleep could address a question of if, and which, gliotransmitters are exerting such effects. Peng *et al.* (2023) utilised both of these methods, using both a biological sensor for adenosine (Peng *et al.*, 2020) and knock-out model for astrocyte-derived adenosine, and showed that effects of pontine astrocytes were adenosine-independent (Peng *et al.*, 2023). However, other gliotransmitters such as glutamate, GABA, and D-serine have yet to be investigated.

6.5. Main conclusions

Overall, we most importantly demonstrated that chemogenetic activation of pontine astrocytes *in vivo* led to a dose-dependent reduction in REM sleep, using appropriate controls to ensure the validity of our findings. These results highlight a causal role of astrocytes in REM sleep regulation and provides a basis for future studies to explore the interactions between astrocytes and neurons that drives these changes. While the methods used in this project are not directly translatable to humans, these results provide key information about the relationship between pontine astrocytes and REM sleep. Such information is essential for advancing our knowledge of REM sleep regulation and may influence the development of new treatments for sleep disorders and conditions characterised by disrupted REM sleep, including neurodegenerative diseases such as AD.

7. References

Abbott, N.J., Ronnback, L. and Hansson, E. (2006) 'Astrocyte-endothelial interactions at the blood-brain barrier'. *Nat Rev Neurosci,* **7** (1), pp. 41-53.

Abdellahi, M.E.A., Koopman, A.C.M., Treder, M.S. and Lewis, P.A. (2023) 'Targeted memory reactivation in human REM sleep elicits detectable reactivation'. *Elife,* **12**.

Adamantidis, A.R., Gutierrez Herrera, C. and Gent, T.C. (2019) 'Oscillating circuitries in the sleeping brain'. *Nat Rev Neurosci,* **20** (12), pp. 746-762.

Adamsky, A., Kol, A., Kreisel, T., Doron, A., Ozeri-Engelhard, N., Melcer, T., Refaeli, R., Horn, H., Regev, L., Groysman, M., London, M. and Goshen, I. (2018) 'Astrocytic Activation Generates De Novo Neuronal Potentiation and Memory Enhancement'. *Cell,* **174** (1), pp. 59-71 e14.

Adelsberger, H., Garaschuk, O. and Konnerth, A. (2005) 'Cortical calcium waves in resting newborn mice'. *Nat Neurosci,* **8** (8), pp. 988-990.

Agarwal, A., Wu, P.H., Hughes, E.G., Fukaya, M., Tischfield, M.A., Langseth, A.J., Wirtz, D. and Bergles, D.E. (2017) 'Transient Opening of the Mitochondrial Permeability Transition Pore Induces Microdomain Calcium Transients in Astrocyte Processes'. *Neuron,* **93** (3), pp. 587-605 e587.

Agulhon, C., Boyt, K.M., Xie, A.X., Friocourt, F., Roth, B.L. and McCarthy, K.D. (2013) 'Modulation of the autonomic nervous system and behaviour by acute glial cell Gq protein-coupled receptor activation in vivo'. *J Physiol,* **591** (22), pp. 5599-5609.

Aime, M., Calcini, N., Borsa, M., Campelo, T., Rusterholz, T., Sattin, A., Fellin, T. and Adamantidis, A. (2022) 'Paradoxical somatodendritic decoupling supports cortical plasticity during REM sleep'. *Science,* **376** (6594), pp. 724-730.

Akerboom, J., Chen, T.W., Wardill, T.J., Tian, L., Marvin, J.S., Mutlu, S., Calderon, N.C., Esposti, F., Borghuis, B.G., Sun, X.R., Gordus, A., Orger, M.B., Portugues, R., Engert, F., Macklin, J.J., Filosa, A., Aggarwal, A., Kerr, R.A., Takagi, R., Kracun, S., . . . Looger, L.L. (2012) 'Optimization of a GCaMP calcium indicator for neural activity imaging'. *J Neurosci,* **32** (40), pp. 13819-13840.

Alam, M.A., Kostin, A., Siegel, J., McGinty, D., Szymusiak, R. and Alam, M.N. (2018) 'Characteristics of sleep-active neurons in the medullary parafacial zone in rats'. *Sleep,* **41** (10), pp.

Alam, M.A., Kumar, S., McGinty, D., Alam, M.N. and Szymusiak, R. (2014) 'Neuronal activity in the preoptic hypothalamus during sleep deprivation and recovery sleep'. *J Neurophysiol,* **111** (2), pp. 287-299.

Alfonsa, H., Burman, R.J., Brodersen, P.J.N., Newey, S.E., Mahfooz, K., Yamagata, T., Panayi, M.C., Bannerman, D.M., Vyazovskiy, V.V. and Akerman, C.J. (2023) 'Intracellular chloride regulation mediates local sleep pressure in the cortex'. *Nat Neurosci,* **26** (1), pp. 64-78.

Allen, N.J. (2014) 'Astrocyte regulation of synaptic behavior'. *Annu Rev Cell Dev Biol,* **30** 439-463.

Allen, N.J., Bennett, M.L., Foo, L.C., Wang, G.X., Chakraborty, C., Smith, S.J. and Barres, B.A. (2012) 'Astrocyte glypicans 4 and 6 promote formation of excitatory synapses via GluA1 AMPA receptors'. *Nature,* **486** (7403), pp. 410-414.

Allen, N.J. and Eroglu, C. (2017) 'Cell Biology of Astrocyte-Synapse Interactions'. *Neuron,* **96** (3), pp. 697-708.

Alonso, A. and Garcia-Austt, E. (1987) 'Neuronal sources of theta rhythm in the entorhinal cortex of the rat. I. Laminar distribution of theta field potentials'. *Exp Brain Res,* **67** (3), pp. 493-501.

Amzica, F. and Massimini, M. (2002) 'Glial and neuronal interactions during slow wave and paroxysmal activities in the neocortex'. *Cereb Cortex,* **12** (10), pp. 1101-1113.

Amzica, F. and Neckelmann, D. (1999) 'Membrane capacitance of cortical neurons and glia during sleep oscillations and spike-wave seizures'. *J Neurophysiol,* **82** (5), pp. 2731-2746.

Amzica, F. and Steriade, M. (1997) 'The K-complex: its slow (<1-Hz) rhythmicity and relation to delta waves'. *Neurology,* **49** (4), pp. 952-959.

Anaclet, C., Ferrari, L., Arrigoni, E., Bass, C.E., Saper, C.B., Lu, J. and Fuller, P.M. (2014) 'The GABAergic parafacial zone is a medullary slow wave sleep-promoting center'. *Nat Neurosci,* **17** (9), pp. 1217-1224.

Anaclet, C., Lin, J.S., Vetrivelan, R., Krenzer, M., Vong, L., Fuller, P.M. and Lu, J. (2012) 'Identification and characterization of a sleep-active cell group in the rostral medullary brainstem'. *J Neurosci,* **32** (50), pp. 17970-17976.

Anaclet, C., Pedersen, N.P., Ferrari, L.L., Venner, A., Bass, C.E., Arrigoni, E. and Fuller, P.M. (2015) 'Basal forebrain control of wakefulness and cortical rhythms'. *Nat Commun,* **6** 8744.

Anafi, R.C., Kayser, M.S. and Raizen, D.M. (2019) 'Exploring phylogeny to find the function of sleep'. *Nat Rev Neurosci,* **20** (2), pp. 109-116.

Andre, C., Martineau-Dussault, M.E., Daneault, V., Blais, H., Frenette, S., Lorrain, D., Hudon, C., Bastien, C., Petit, D., Lafreniere, A., Thompson, C., Montplaisir, J., Gosselin, N. and Carrier, J. (2023) 'REM sleep is associated with the volume of the cholinergic basal forebrain in aMCI individuals'. *Alzheimers Res Ther,* **15** (1), pp. 151.

Andriezen, W.L. (1893) 'The Neuroglia Elements in the Human Brain'. *Br Med J,* **2** (1700), pp. 227-230.

Angelova, P.R., Kasymov, V., Christie, I., Sheikhbahaei, S., Turovsky, E., Marina, N., Korsak, A., Zwicker, J., Teschemacher, A.G., Ackland, G.L., Funk, G.D., Kasparov, S., Abramov, A.Y. and Gourine, A.V. (2015) 'Functional Oxygen Sensitivity of Astrocytes'. *J Neurosci,* **35** (29), pp. 10460-10473.

Antunes, M. and Biala, G. (2012) 'The novel object recognition memory: neurobiology, test procedure, and its modifications'. *Cogn Process,* **13** (2), pp. 93-110.

Araque, A., Carmignoto, G., Haydon, P.G., Oliet, S.H., Robitaille, R. and Volterra, A. (2014) 'Gliotransmitters travel in time and space'. *Neuron,* **81** (4), pp. 728-739.

Armbruster, B.N., Li, X., Pausch, M.H., Herlitze, S. and Roth, B.L. (2007) 'Evolving the lock to fit the key to create a family of G protein-coupled receptors potently activated by an inert ligand'. *Proc Natl Acad Sci U S A,* **104** (12), pp. 5163-5168.

Asaka, Y., Seager, M.A., Griffin, A.L. and Berry, S.D. (2000) 'Medial septal microinfusion of scopolamine disrupts hippocampal activity and trace jaw movement conditioning'. *Behav Neurosci,* **114** (6), pp. 1068-1077.

Aserinsky, E. and Kleitman, N. (1953) 'Regularly occurring periods of eye motility, and concomitant phenomena, during sleep'. *Science,* **118** (3062), pp. 273-274.

Aton, S.J., Seibt, J., Dumoulin, M., Jha, S.K., Steinmetz, N., Coleman, T., Naidoo, N. and Frank, M.G. (2009) 'Mechanisms of sleep-dependent consolidation of cortical plasticity'. *Neuron,* **61** (3), pp. 454-466.

Ballanyi, K., Grafe, P. and ten Bruggencate, G. (1987) 'Ion activities and potassium uptake mechanisms of glial cells in guinea-pig olfactory cortex slices'. *J Physiol,* **382** 159-174.

Bandarabadi, M., Herrera, C.G., Gent, T.C., Bassetti, C., Schindler, K. and Adamantidis, A.R. (2020) 'A role for spindles in the onset of rapid eye movement sleep'. *Nat Commun,* **11** (1), pp. 5247.

Barnes, C.A. (1979) 'Memory deficits associated with senescence: a neurophysiological and behavioral study in the rat'. *J Comp Physiol Psychol,* **93** (1), pp. 74-104.

Bartho, P., Slezia, A., Matyas, F., Faradzs-Zade, L., Ulbert, I., Harris, K.D. and Acsady, L. (2014) 'Ongoing network state controls the length of sleep spindles via inhibitory activity'. *Neuron,* **82** (6), pp. 1367-1379.

Batini, C., Moruzzi, G., Palestini, M., Rossi, G.F. and Zanchetti, A. (1958) 'Presistent patterns of wakefulness in the pretrigeminal midpontine preparation'. *Science,* **128** (3314), pp. 30-32.

Batiuk, M.Y., Martirosyan, A., Wahis, J., de Vin, F., Marneffe, C., Kusserow, C., Koeppen, J., Viana, J.F., Oliveira, J.F., Voet, T., Ponting, C.P., Belgard, T.G. and Holt, M.G. (2020) 'Identification of region-specific astrocyte subtypes at single cell resolution'. *Nat Commun,* **11** (1), pp. 1220.

Bayraktar, O.A., Bartels, T., Holmqvist, S., Kleshchevnikov, V., Martirosyan, A., Polioudakis, D., Ben Haim, L., Young, A.M.H., Batiuk, M.Y., Prakash, K., Brown, A., Roberts, K., Paredes, M.F., Kawaguchi, R., Stockley, J.H., Sabeur, K., Chang, S.M., Huang, E., Hutchinson, P., Ullian, E.M., . . . Rowitch, D.H. (2020) 'Astrocyte layers in the mammalian cerebral cortex revealed by a single-cell in situ transcriptomic map'. *Nat Neurosci,* **23** (4), pp. 500-509.

Bazhenov, M., Timofeev, I., Steriade, M. and Sejnowski, T.J. (2002) 'Model of thalamocortical slow-wave sleep oscillations and transitions to activated States'. *J Neurosci,* **22** (19), pp. 8691-8704.

Bear, M., Connors, B. and Paradiso, M.A. (2020) *Neuroscience: Exploring the Brain, Enhanced Edition: Exploring the Brain.* Jones & Bartlett Learning.

Beaulieu, I. and Godbout, R. (2000) 'Spatial learning on the Morris Water Maze Test after a short-term paradoxical sleep deprivation in the rat'. *Brain Cogn,* **43** (1-3), pp. 27-31.

Bellesi, M., de Vivo, L., Tononi, G. and Cirelli, C. (2015) 'Effects of sleep and wake on astrocytes: clues from molecular and ultrastructural studies'. *BMC Biol,* **13** 66.

Bellot-Saez, A., Cohen, G., van Schaik, A., Ooi, L., J, W.M. and Buskila, Y. (2018) 'Astrocytic modulation of cortical oscillations'. *Sci Rep,* **8** (1), pp. 11565.

Beltramo, R., D'Urso, G., Dal Maschio, M., Farisello, P., Bovetti, S., Clovis, Y., Lassi, G., Tucci, V., De Pietri Tonelli, D. and Fellin, T. (2013) 'Layer-specific excitatory circuits differentially control recurrent network dynamics in the neocortex'. *Nat Neurosci,* **16** (2), pp. 227-234.

Ben Haim, L. and Rowitch, D.H. (2017) 'Functional diversity of astrocytes in neural circuit regulation'. *Nat Rev Neurosci,* **18** (1), pp. 31-41.

Berg, S., Kutra, D., Kroeger, T., Straehle, C.N., Kausler, B.X., Haubold, C., Schiegg, M., Ales, J., Beier, T., Rudy, M., Eren, K., Cervantes, J.I., Xu, B., Beuttenmueller, F.,

Wolny, A., Zhang, C., Koethe, U., Hamprecht, F.A. and Kreshuk, A. (2019) 'ilastik: interactive machine learning for (bio)image analysis'. *Nat Methods,* **16** (12), pp. 1226-1232.

Binder, S., Molle, M., Lippert, M., Bruder, R., Aksamaz, S., Ohl, F., Wiegert, J.S. and Marshall, L. (2019) 'Monosynaptic Hippocampal-Prefrontal Projections Contribute to Spatial Memory Consolidation in Mice'. *J Neurosci,* **39** (35), pp. 6978-6991.

Bindocci, E., Savtchouk, I., Liaudet, N., Becker, D., Carriero, G. and Volterra, A. (2017) 'Three-dimensional Ca(2+) imaging advances understanding of astrocyte biology'. *Science,* **356** (6339), pp.

Blackmore, D.G., Brici, D. and Walker, T.L. (2022) 'Protocol for three alternative paradigms to test spatial learning and memory in mice'. *STAR Protoc,* **3** (3), pp. 101500.

Blanco-Centurion, C., Luo, S., Vidal-Ortiz, A., Swank, C. and Shiromani, P.J. (2021) 'Activity of a subset of vesicular GABA-transporter neurons in the ventral zona incerta anticipates sleep onset'. *Sleep,* **44** (6), pp.

Blanco-Suarez, E., Liu, T.F., Kopelevich, A. and Allen, N.J. (2018) 'Astrocyte-Secreted Chordin-like 1 Drives Synapse Maturation and Limits Plasticity by Increasing Synaptic GluA2 AMPA Receptors'. *Neuron,* **100** (5), pp. 1116-1132 e1113.

Blasiak, T., Zawadzki, A. and Lewandowski, M.H. (2013) 'Infra-slow oscillation (ISO) of the pupil size of urethane-anaesthetised rats'. *PLoS One,* **8** (4), pp. e62430.

Blum, I.D., Keles, M.F., Baz, E.S., Han, E., Park, K., Luu, S., Issa, H., Brown, M., Ho, M.C.W., Tabuchi, M., Liu, S. and Wu, M.N. (2021) 'Astroglial Calcium Signaling Encodes Sleep Need in Drosophila'. *Curr Biol,* **31** (1), pp. 150-162 e157.

Blume, C., Del Giudice, R., Wislowska, M., Lechinger, J. and Schabus, M. (2015) 'Across the consciousness continuum-from unresponsive wakefulness to sleep'. *Front Hum Neurosci,* **9** 105.

Boissard, R., Gervasoni, D., Schmidt, M.H., Barbagli, B., Fort, P. and Luppi, P.H. (2002) 'The rat ponto-medullary network responsible for paradoxical sleep onset and maintenance: a combined microinjection and functional neuroanatomical study'. *Eur J Neurosci,* **16** (10), pp. 1959-1973.

Bojarskaite, L., Bjornstad, D.M., Pettersen, K.H., Cunen, C., Hermansen, G.H., Abjorsbraten, K.S., Chambers, A.R., Sprengel, R., Vervaeke, K., Tang, W., Enger, R. and Nagelhus, E.A. (2020a) 'Astrocytic Ca(2+) signaling is reduced during sleep and is involved in the regulation of slow wave sleep'. *Nat Commun,* **11** (1), pp. 3240.

Bojarskaite, L., Bjørnstad, D.M., Pettersen, K.H., Cunen, C., Hermansen, G.H., Åbjørsbråten, K.S., Chambers, A.R., Sprengel, R., Vervaeke, K., Tang, W., Enger, R. and Nagelhus, E.A. (2020b) 'Astrocytic Ca'. *Nat Commun,* **11** (1), pp. 3240.

Bonjean, M., Baker, T., Bazhenov, M., Cash, S., Halgren, E. and Sejnowski, T. (2012) 'Interactions between core and matrix thalamocortical projections in human sleep spindle synchronization'. *J Neurosci,* **32** (15), pp. 5250-5263.

Bonjean, M., Baker, T., Lemieux, M., Timofeev, I., Sejnowski, T. and Bazhenov, M. (2011) 'Corticothalamic feedback controls sleep spindle duration in vivo'. *J Neurosci,* **31** (25), pp. 9124-9134.

Borbely, A.A. (1982) 'A two process model of sleep regulation'. *Hum Neurobiol,* **1** (3), pp. 195-204.

Borbely, A.A. and Achermann, P. (1992) 'Concepts and models of sleep regulation: an overview'. *J Sleep Res,* **1** (2), pp. 63-79.

Borbely, A.A. and Achermann, P. (1999) 'Sleep homeostasis and models of sleep regulation'. *J Biol Rhythms,* **14** (6), pp. 557-568.

Borbely, A.A., Daan, S., Wirz-Justice, A. and Deboer, T. (2016) 'The two-process model of sleep regulation: a reappraisal'. *J Sleep Res,* **25** (2), pp. 131-143.

Bowser, D.N. and Khakh, B.S. (2004) 'ATP excites interneurons and astrocytes to increase synaptic inhibition in neuronal networks'. *J Neurosci,* **24** (39), pp. 8606-8620.

Boyce, R., Glasgow, S.D., Williams, S. and Adamantidis, A. (2016) 'Causal evidence for the role of REM sleep theta rhythm in contextual memory consolidation'. *Science,* **352** (6287), pp. 812-816.

Brockett, A.T., Kane, G.A., Monari, P.K., Briones, B.A., Vigneron, P.A., Barber, G.A., Bermudez, A., Dieffenbach, U., Kloth, A.D., Buschman, T.J. and Gould, E. (2018) 'Evidence supporting a role for astrocytes in the regulation of cognitive flexibility and neuronal oscillations through the Ca2+ binding protein S100beta'. *PLoS One,* **13** (4), pp. e0195726.

Brodt, S., Inostroza, M., Niethard, N. and Born, J. (2023) 'Sleep-A brain-state serving systems memory consolidation'. *Neuron,* **111** (7), pp. 1050-1075.

Brooks, D.C. and Bizzi, E. (1963) 'Brain Stem Electrical Activity during Deep Sleep'. *Arch Ital Biol,* **101** 648-665.

Brown, R.E., Basheer, R., McKenna, J.T., Strecker, R.E. and McCarley, R.W. (2012) 'Control of sleep and wakefulness'. *Physiol Rev,* **92** (3), pp. 1087-1187.

Bullock, T.H., Buzsaki, G. and McClune, M.C. (1990) 'Coherence of compound field potentials reveals discontinuities in the CA1-subiculum of the hippocampus in freely-moving rats'. *Neuroscience,* **38** (3), pp. 609-619.

Burton, A., Obaid, S.N., Vazquez-Guardado, A., Schmit, M.B., Stuart, T., Cai, L., Chen, Z., Kandela, I., Haney, C.R., Waters, E.A., Cai, H., Rogers, J.A., Lu, L. and Gutruf, P. (2020) 'Wireless, battery-free subdermally implantable photometry systems for chronic recording of neural dynamics'. *Proc Natl Acad Sci U S A,* **117** (6), pp. 2835-2845.

Bushong, E.A., Martone, M.E., Jones, Y.Z. and Ellisman, M.H. (2002) 'Protoplasmic astrocytes in CA1 stratum radiatum occupy separate anatomical domains'. *J Neurosci,* **22** (1), pp. 183-192.

Buzsaki, G. (1986) 'Hippocampal sharp waves: their origin and significance'. *Brain Res,* **398** (2), pp. 242-252.

Buzsaki, G. (1989) 'Two-stage model of memory trace formation: a role for "noisy" brain states'. *Neuroscience,* **31** (3), pp. 551-570.

Buzsaki, G. (2002) 'Theta oscillations in the hippocampus'. *Neuron,* **33** (3), pp. 325-340.

Buzsaki, G. (2015) 'Hippocampal sharp wave-ripple: A cognitive biomarker for episodic memory and planning'. *Hippocampus,* **25** (10), pp. 1073-1188.

Buzsaki, G., Anastassiou, C.A. and Koch, C. (2012) 'The origin of extracellular fields and currents--EEG, ECoG, LFP and spikes'. *Nat Rev Neurosci,* **13** (6), pp. 407-420.

Buzsaki, G., Leung, L.W. and Vanderwolf, C.H. (1983) 'Cellular bases of hippocampal EEG in the behaving rat'. *Brain Res,* **287** (2), pp. 139-171.

Buzsaki, G. and Wang, X.J. (2012) 'Mechanisms of gamma oscillations'. *Annu Rev Neurosci,* **35** 203-225.

Byron, N. and Sakata, S. (2024) 'Fiber photometry-based investigation of brain function and dysfunction'. *Neurophotonics,* **11** (Suppl 1), pp. S11502.

Cai, P., Huang, S.N., Lin, Z.H., Wang, Z., Liu, R.F., Xiao, W.H., Li, Z.S., Zhu, Z.H., Yao, J., Yan, X.B., Wang, F.D., Zeng, S.X., Chen, G.Q., Yang, L.Y., Sun, Y.K., Yu, C., Chen, L. and Wang, W.X. (2022) 'Regulation of wakefulness by astrocytes in the lateral hypothalamus'. *Neuropharmacology,* 109275.

Callaway, C.W., Lydic, R., Baghdoyan, H.A. and Hobson, J.A. (1987) 'Pontogeniculooccipital waves: spontaneous visual system activity during rapid eye movement sleep'. *Cell Mol Neurobiol,* **7** (2), pp. 105-149.

Cantero, J.L., Atienza, M., Stickgold, R., Kahana, M.J., Madsen, J.R. and Kocsis, B. (2003) 'Sleep-dependent theta oscillations in the human hippocampus and neocortex'. *J Neurosci,* **23** (34), pp. 10897-10903.

Cao, J., Herman, A.B., West, G.B., Poe, G. and Savage, V.M. (2020) 'Unraveling why we sleep: Quantitative analysis reveals abrupt transition from neural reorganization to repair in early development'. *Sci Adv,* **6** (38), pp.

Caravagna, C., Soliz, J. and Seaborn, T. (2013) 'Brain-derived neurotrophic factor interacts with astrocytes and neurons to control respiration'. *Eur J Neurosci,* **38** (9), pp. 3261-3269.

Cash, S.S., Halgren, E., Dehghani, N., Rossetti, A.O., Thesen, T., Wang, C., Devinsky, O., Kuzniecky, R., Doyle, W., Madsen, J.R., Bromfield, E., Eross, L., Halasz, P., Karmos, G., Csercsa, R., Wittner, L. and Ulbert, I. (2009) 'The human K-complex represents an isolated cortical down-state'. *Science,* **324** (5930), pp. 1084-1087.

Caton, R. (1875) 'Electrical Currents of the Brain'. *The Journal of Nervous and Mental Disease,* **2** (4), pp. 610.

Chai, H., Diaz-Castro, B., Shigetomi, E., Monte, E., Octeau, J.C., Yu, X., Cohn, W., Rajendran, P.S., Vondriska, T.M., Whitelegge, J.P., Coppola, G. and Khakh, B.S. (2017) 'Neural Circuit-Specialized Astrocytes: Transcriptomic, Proteomic, Morphological, and Functional Evidence'. *Neuron,* **95** (3), pp. 531-549 e539.

Chan, K.Y., Jang, M.J., Yoo, B.B., Greenbaum, A., Ravi, N., Wu, W.L., Sanchez-Guardado, L., Lois, C., Mazmanian, S.K., Deverman, B.E. and Gradinaru, V. (2017) 'Engineered AAVs for efficient noninvasive gene delivery to the central and peripheral nervous systems'. *Nat Neurosci,* **20** (8), pp. 1172-1179.

Charles, A.C., Merrill, J.E., Dirksen, E.R. and Sanderson, M.J. (1991) 'Intercellular signaling in glial cells: calcium waves and oscillations in response to mechanical stimulation and glutamate'. *Neuron,* **6** (6), pp. 983-992.

Chen, C., Jiang, Z., Fu, X., Yu, D., Huang, H. and Tasker, J.G. (2019) 'Astrocytes Amplify Neuronal Dendritic Volume Transmission Stimulated by Norepinephrine'. *Cell Rep,* **29** (13), pp. 4349-4361 e4344.

Chen, J., Tan, Z., Zeng, L., Zhang, X., He, Y., Gao, W., Wu, X., Li, Y., Bu, B., Wang, W. and Duan, S. (2013a) 'Heterosynaptic long-term depression mediated by ATP released from astrocytes'. *Glia,* **61** (2), pp. 178-191.

Chen, K.S., Xu, M., Zhang, Z., Chang, W.C., Gaj, T., Schaffer, D.V. and Dan, Y. (2018) 'A Hypothalamic Switch for REM and Non-REM Sleep'. *Neuron,* **97** (5), pp. 1168-1176 e1164.

Chen, T.W., Wardill, T.J., Sun, Y., Pulver, S.R., Renninger, S.L., Baohan, A., Schreiter, E.R., Kerr, R.A., Orger, M.B., Jayaraman, V., Looger, L.L., Svoboda, K. and Kim, D.S. (2013b) 'Ultrasensitive fluorescent proteins for imaging neuronal activity'. *Nature,* **499** (7458), pp. 295-300.

Chen, X., Choo, H., Huang, X.P., Yang, X., Stone, O., Roth, B.L. and Jin, J. (2015) 'The first structure-activity relationship studies for designer receptors exclusively activated by designer drugs'. *ACS Chem Neurosci,* **6** (3), pp. 476-484.

Cho, W.H., Noh, K., Lee, B.H., Barcelon, E., Jun, S.B., Park, H.Y. and Lee, S.J. (2022) 'Hippocampal astrocytes modulate anxiety-like behavior'. *Nat Commun,* **13** (1), pp. 6536.

Chowdhury, B., Abhilash, L., Ortega, A., Liu, S. and Shafer, O. (2023) 'Homeostatic control of deep sleep and molecular correlates of sleep pressure in Drosophila'. *Elife,* **12**.

Chung, S., Weber, F., Zhong, P., Tan, C.L., Nguyen, T.N., Beier, K.T., Hormann, N., Chang, W.C., Zhang, Z., Do, J.P., Yao, S., Krashes, M.J., Tasic, B., Cetin, A., Zeng, H., Knight, Z.A., Luo, L. and Dan, Y. (2017) 'Identification of preoptic sleep neurons using retrograde labelling and gene profiling'. *Nature,* **545** (7655), pp. 477-481.

Chung, W.S., Clarke, L.E., Wang, G.X., Stafford, B.K., Sher, A., Chakraborty, C., Joung, J., Foo, L.C., Thompson, A., Chen, C., Smith, S.J. and Barres, B.A. (2013) 'Astrocytes mediate synapse elimination through MEGF10 and MERTK pathways'. *Nature,* **504** (7480), pp. 394-400.

Cimadevilla, J.M., Fenton, A.A. and Bures, J. (2000) 'Functional inactivation of dorsal hippocampus impairs active place avoidance in rats'. *Neurosci Lett,* **285** (1), pp. 53-56.

Clark, I.C., Fontanez, K.M., Meltzer, R.H., Xue, Y., Hayford, C., May-Zhang, A., D'Amato, C., Osman, A., Zhang, J.Q., Hettige, P., Ishibashi, J.S.A., Delley, C.L., Weisgerber, D.W., Replogle, J.M., Jost, M., Phong, K.T., Kennedy, V.E., Peretz, C.A.C., Kim, E.A., Song, S., . . . Abate, A.R. (2023) 'Microfluidics-free single-cell genomics with templated emulsification'. *Nat Biotechnol,* **41** (11), pp. 1557-1566.

Clement, O., Sapin, E., Libourel, P.A., Arthaud, S., Brischoux, F., Fort, P. and Luppi, P.H. (2012) 'The lateral hypothalamic area controls paradoxical (REM) sleep by means of descending projections to brainstem GABAergic neurons'. *J Neurosci,* **32** (47), pp. 16763-16774.

Cole, S.L. and Vassar, R. (2007) 'The Alzheimer's disease beta-secretase enzyme, BACE1'. *Mol Neurodegener,* **2** 22.

Colgin, L.L. (2016) 'Rhythms of the hippocampal network'. *Nat Rev Neurosci,* **17** (4), pp. 239-249.

Contreras, D., Destexhe, A., Sejnowski, T.J. and Steriade, M. (1997) 'Spatiotemporal patterns of spindle oscillations in cortex and thalamus'. *J Neurosci,* **17** (3), pp. 1179-1196.

Contreras, D. and Steriade, M. (1995) 'Cellular basis of EEG slow rhythms: a study of dynamic corticothalamic relationships'. *J Neurosci,* **15** (1 Pt 2), pp. 604-622.

Corkrum, M., Covelo, A., Lines, J., Bellocchio, L., Pisansky, M., Loke, K., Quintana, R., Rothwell, P.E., Lujan, R., Marsicano, G., Martin, E.D., Thomas, M.J., Kofuji, P. and Araque, A. (2020) 'Dopamine-Evoked Synaptic Regulation in the Nucleus Accumbens Requires Astrocyte Activity'. *Neuron,* **105** (6), pp. 1036-1047 e1035.

Cornell-Bell, A.H., Finkbeiner, S.M., Cooper, M.S. and Smith, S.J. (1990) 'Glutamate induces calcium waves in cultured astrocytes: long-range glial signaling'. *Science,* **247** (4941), pp. 470-473.

Cox, J., Pinto, L. and Dan, Y. (2016) 'Calcium imaging of sleep-wake related neuronal activity in the dorsal pons'. *Nat Commun,* **7** 10763.

Csercsa, R., Dombovari, B., Fabo, D., Wittner, L., Eross, L., Entz, L., Solyom, A., Rasonyi, G., Szucs, A., Kelemen, A., Jakus, R., Juhos, V., Grand, L., Magony, A., Halasz, P., Freund, T.F., Magloczky, Z., Cash, S.S., Papp, L., Karmos, G., . . . Ulbert, I. (2010) 'Laminar analysis of slow wave activity in humans'. *Brain,* **133** (9), pp. 2814-2829.

Csicsvari, J., Hirase, H., Mamiya, A. and Buzsaki, G. (2000) 'Ensemble patterns of hippocampal CA3-CA1 neurons during sharp wave-associated population events'. *Neuron,* **28** (2), pp. 585-594.

Cui, W., Allen, N.D., Skynner, M., Gusterson, B. and Clark, A.J. (2001) 'Inducible ablation of astrocytes shows that these cells are required for neuronal survival in the adult brain'. *Glia,* **34** (4), pp. 272-282.

Daan, S., Beersma, D.G. and Borbely, A.A. (1984) 'Timing of human sleep: recovery process gated by a circadian pacemaker'. *Am J Physiol,* **246** (2 Pt 2), pp. R161-183.

Dahan, L., Astier, B., Vautrelle, N., Urbain, N., Kocsis, B. and Chouvet, G. (2007) 'Prominent burst firing of dopaminergic neurons in the ventral tegmental area during paradoxical sleep'. *Neuropsychopharmacology,* **32** (6), pp. 1232-1241.

Dana, H., Sun, Y., Mohar, B., Hulse, B.K., Kerlin, A.M., Hasseman, J.P., Tsegaye, G., Tsang, A., Wong, A., Patel, R., Macklin, J.J., Chen, Y., Konnerth, A., Jayaraman, V., Looger, L.L., Schreiter, E.R., Svoboda, K. and Kim, D.S. (2019) 'High-performance calcium sensors for imaging activity in neuronal populations and microcompartments'. *Nat Methods,* **16** (7), pp. 649-657.

Datta, S. (1997) 'Cellular basis of pontine ponto-geniculo-occipital wave generation and modulation'. *Cell Mol Neurobiol,* **17** (3), pp. 341-365.

Datta, S. (2000) 'Avoidance task training potentiates phasic pontine-wave density in the rat: A mechanism for sleep-dependent plasticity'. *J Neurosci,* **20** (22), pp. 8607-8613.

Dauvilliers, Y., Schenck, C.H., Postuma, R.B., Iranzo, A., Luppi, P.H., Plazzi, G., Montplaisir, J. and Boeve, B. (2018) 'REM sleep behaviour disorder'. *Nat Rev Dis Primers,* **4** (1), pp. 19.

David, F., Schmiedt, J.T., Taylor, H.L., Orban, G., Di Giovanni, G., Uebele, V.N., Renger, J.J., Lambert, R.C., Leresche, N. and Crunelli, V. (2013) 'Essential thalamic contribution to slow waves of natural sleep'. *J Neurosci,* **33** (50), pp. 19599-19610.

De Gennaro, L., Gorgoni, M., Reda, F., Lauri, G., Truglia, I., Cordone, S., Scarpelli, S., Mangiaruga, A., D'Atri, A., Lacidogna, G., Ferrara, M., Marra, C. and Rossini, P.M. (2017) 'The Fall of Sleep K-Complex in Alzheimer Disease'. *Sci Rep,* **7** 39688.

de Vivo, L., Melone, M., Rothstein, J.D. and Conti, F. (2010) 'GLT-1 Promoter Activity in Astrocytes and Neurons of Mouse Hippocampus and Somatic Sensory Cortex'. *Front Neuroanat,* **3** 31.

Dement, W. (1958) 'The occurrence of low voltage, fast, electroencephalogram patterns during behavioral sleep in the cat'. *Electroencephalogr Clin Neurophysiol,* **10** (2), pp. 291-296.

Dement, W. and Kleitman, N. (1957) 'Cyclic variations in EEG during sleep and their relation to eye movements, body motility, and dreaming'. *Electroencephalogr Clin Neurophysiol,* **9** (4), pp. 673-690.

Dergacheva, O., Wang, X., Lovett-Barr, M.R., Jameson, H. and Mendelowitz, D. (2010) 'The lateral paragigantocellular nucleus modulates parasympathetic cardiac neurons: a mechanism for rapid eye movement sleep-dependent changes in heart rate'. *J Neurophysiol,* **104** (2), pp. 685-694.

Di Castro, M.A., Chuquet, J., Liaudet, N., Bhaukaurally, K., Santello, M., Bouvier, D., Tiret, P. and Volterra, A. (2011) 'Local Ca2+ detection and modulation of synaptic release by astrocytes'. *Nat Neurosci,* **14** (10), pp. 1276-1284.

Dijk, D.J. and von Schantz, M. (2005) 'Timing and consolidation of human sleep, wakefulness, and performance by a symphony of oscillators'. *J Biol Rhythms,* **20** (4), pp. 279-290.

Ding, F., O'Donnell, J., Thrane, A.S., Zeppenfeld, D., Kang, H., Xie, L., Wang, F. and Nedergaard, M. (2013) 'alpha1-Adrenergic receptors mediate coordinated Ca2+

signaling of cortical astrocytes in awake, behaving mice'. *Cell Calcium,* **54** (6), pp. 387-394.

Dispersyn, G., Sauvet, F., Gomez-Merino, D., Ciret, S., Drogou, C., Leger, D., Gallopin, T. and Chennaoui, M. (2017) 'The homeostatic and circadian sleep recovery responses after total sleep deprivation in mice'. *J Sleep Res,* **26** (5), pp. 531-538.

Dong, H., Li, M., Yan, Y., Qian, T., Lin, Y., Ma, X., Vischer, H.F., Liu, C., Li, G., Wang, H., Leurs, R. and Li, Y. (2023) 'Genetically encoded sensors for measuring histamine release both in vitro and in vivo'. *Neuron,* **111** (10), pp. 1564-1576 e1566.

Dong, Y., Li, J., Zhou, M., Du, Y. and Liu, D. (2022) 'Cortical regulation of two-stage rapid eye movement sleep'. *Nat Neurosci,* **25** (12), pp. 1675-1682.

Dopp, J., Ortega, A., Davie, K., Poovathingal, S., Baz, E.S. and Liu, S. (2024) 'Single-cell transcriptomics reveals that glial cells integrate homeostatic and circadian processes to drive sleep-wake cycles'. *Nat Neurosci,* **27** (2), pp. 359-372.

Drieu, C., Todorova, R. and Zugaro, M. (2018) 'Nested sequences of hippocampal assemblies during behavior support subsequent sleep replay'. *Science,* **362** (6415), pp. 675-679.

Du, Z., Song, Y., Chen, X., Zhang, W., Zhang, G., Li, H., Chang, L. and Wu, Y. (2021) 'Knockdown of astrocytic Grin2a aggravates beta-amyloid-induced memory and cognitive deficits through regulating nerve growth factor'. *Aging Cell,* **20** (8), pp. e13437.

Duffy, S. and MacVicar, B.A. (1995) 'Adrenergic calcium signaling in astrocyte networks within the hippocampal slice'. *J Neurosci,* **15** (8), pp. 5535-5550.

Dumoulin Bridi, M.C., Aton, S.J., Seibt, J., Renouard, L., Coleman, T. and Frank, M.G. (2015) 'Rapid eye movement sleep promotes cortical plasticity in the developing brain'. *Sci Adv,* **1** (6), pp. e1500105.

Durkee, C.A., Covelo, A., Lines, J., Kofuji, P., Aguilar, J. and Araque, A. (2019) 'Gi/o protein-coupled receptors inhibit neurons but activate astrocytes and stimulate gliotransmission'. *Glia,* **67** (6), pp. 1076-1093.

Dutt, M., Redhu, S., Goodwin, M. and Omlin, C.W. (2023) 'SleepXAI: An explainable deep learning approach for multi-class sleep stage identification'. *Applied Intelligence,* **53** (13), pp. 16830-16843.

Dvorzhak, A., Vagner, T., Kirmse, K. and Grantyn, R. (2016) 'Functional Indicators of Glutamate Transport in Single Striatal Astrocytes and the Influence of Kir4.1 in Normal and Huntington Mice'. *J Neurosci,* **36** (18), pp. 4959-4975.

Ego-Stengel, V. and Wilson, M.A. (2010) 'Disruption of ripple-associated hippocampal activity during rest impairs spatial learning in the rat'. *Hippocampus,* **20** (1), pp. 1-10.

Endo, F., Kasai, A., Soto, J.S., Yu, X., Qu, Z., Hashimoto, H., Gradinaru, V., Kawaguchi, R. and Khakh, B.S. (2022) 'Molecular basis of astrocyte diversity and morphology across the CNS in health and disease'. *Science,* **378** (6619), pp. eadc9020.

Eng, L.F., Ghirnikar, R.S. and Lee, Y.L. (2000) 'Glial fibrillary acidic protein: GFAP-thirty-one years (1969-2000)'. *Neurochem Res,* **25** (9-10), pp. 1439-1451.

Ennaceur, A. (2010) 'One-trial object recognition in rats and mice: methodological and theoretical issues'. *Behav Brain Res,* **215** (2), pp. 244-254.

Ennaceur, A. and Delacour, J. (1988) 'A new one-trial test for neurobiological studies of memory in rats. 1: Behavioral data'. *Behav Brain Res,* **31** (1), pp. 47-59.

Ennis, M. and Aston-Jones, G. (1989) 'GABA-mediated inhibition of locus coeruleus from the dorsomedial rostral medulla'. *J Neurosci,* **9** (8), pp. 2973-2981.

Escartin, C., Galea, E., Lakatos, A., O'Callaghan, J.P., Petzold, G.C., Serrano-Pozo, A., Steinhauser, C., Volterra, A., Carmignoto, G., Agarwal, A., Allen, N.J., Araque, A., Barbeito, L., Barzilai, A., Bergles, D.E., Bonvento, G., Butt, A.M., Chen, W.T., Cohen-Salmon, M., Cunningham, C., . . . Verkhratsky, A. (2021) 'Reactive astrocyte nomenclature, definitions, and future directions'. *Nat Neurosci,* **24** (3), pp. 312-325.

Eugenin Leon, J., Olivares, M.J. and Beltran-Castillo, S. (2016) 'Role of Astrocytes in Central Respiratory Chemoreception'. *Adv Exp Med Biol,* **949** 109-145.

Falcon-Moya, R., Perez-Rodriguez, M., Prius-Mengual, J., Andrade-Talavera, Y., Arroyo-Garcia, L.E., Perez-Artes, R., Mateos-Aparicio, P., Guerra-Gomes, S., Oliveira, J.F., Flores, G. and Rodriguez-Moreno, A. (2020) 'Astrocyte-mediated switch in spike timing-dependent plasticity during hippocampal development'. *Nat Commun,* **11** (1), pp. 4388.

Farmer, W.T., Abrahamsson, T., Chierzi, S., Lui, C., Zaelzer, C., Jones, E.V., Bally, B.P., Chen, G.G., Theroux, J.F., Peng, J., Bourque, C.W., Charron, F., Ernst, C., Sjostrom, P.J. and Murai, K.K. (2016) 'Neurons diversify astrocytes in the adult brain through sonic hedgehog signaling'. *Science,* **351** (6275), pp. 849-854.

Fellin, T., Halassa, M.M., Terunuma, M., Succol, F., Takano, H., Frank, M., Moss, S.J. and Haydon, P.G. (2009) 'Endogenous nonneuronal modulators of synaptic transmission control cortical slow oscillations in vivo'. *Proc Natl Acad Sci U S A,* **106** (35), pp. 15037-15042.

Feng, H., Wen, S.Y., Qiao, Q.C., Pang, Y.J., Wang, S.Y., Li, H.Y., Cai, J., Zhang, K.X., Chen, J., Hu, Z.A., Luo, F.L., Wang, G.Z., Yang, N. and Zhang, J. (2020) 'Orexin signaling modulates synchronized excitation in the sublaterodorsal tegmental nucleus to stabilize REM sleep'. *Nat Commun,* **11** (1), pp. 3661.

Fernandez, L.M.J. and Luthi, A. (2020) 'Sleep Spindles: Mechanisms and Functions'. *Physiol Rev,* **100** (2), pp. 805-868.

Fernandez-Mendoza, J., Lozano, B., Seijo, F., Santamarta-Liebana, E., Ramos-Platon, M.J., Vela-Bueno, A. and Fernandez-Gonzalez, F. (2009) 'Evidence of subthalamic PGO-like waves during REM sleep in humans: a deep brain polysomnographic study'. *Sleep,* **32** (9), pp. 1117-1126.

Fernandez-Ruiz, A., Oliva, A., Fermino de Oliveira, E., Rocha-Almeida, F., Tingley, D. and Buzsaki, G. (2019) 'Long-duration hippocampal sharp wave ripples improve memory'. *Science,* **364** (6445), pp. 1082-1086.

Fiacco, T.A. and McCarthy, K.D. (2018) 'Multiple Lines of Evidence Indicate That Gliotransmission Does Not Occur under Physiological Conditions'. *J Neurosci,* **38** (1), pp. 3-13.

Foo, L.C., Allen, N.J., Bushong, E.A., Ventura, P.B., Chung, W.S., Zhou, L., Cahoy, J.D., Daneman, R., Zong, H., Ellisman, M.H. and Barres, B.A. (2011) 'Development of a method for the purification and culture of rodent astrocytes'. *Neuron,* **71** (5), pp. 799-811.

Fraigne, J.J., Luppi, P.H., Mahoney, C.E., De Luca, R., Shiromani, P.J., Weber, F., Adamantidis, A. and Peever, J. (2023) 'Dopamine neurons in the ventral tegmental area modulate rapid eye movement sleep'. *Sleep,* **46** (8), pp.

Frank, M.G. (2013) 'Astroglial regulation of sleep homeostasis'. *Curr Opin Neurobiol,* **23** (5), pp. 812-818.

Frank, M.G. (2019) 'The Role of Glia in Sleep Regulation and Function'. *Handb Exp Pharmacol,* **253** 83-96.

Frank, M.G., Issa, N.P. and Stryker, M.P. (2001) 'Sleep enhances plasticity in the developing visual cortex'. *Neuron,* **30** (1), pp. 275-287.

Franks, N.P. and Wisden, W. (2021) 'The inescapable drive to sleep: Overlapping mechanisms of sleep and sedation'. *Science,* **374** (6567), pp. 556-559.

Frazel, P.W., Fricano-Kugler, K., May-Zhang, A.A., O'Dea, M.R., Prakash, P., Desmet, N.M., Lee, H., Meltzer, R.H., Fontanez, K.M., Hettige, P., Agam, Y., Lithwick-Yanai, G., Lipson, D., Luikart, B.W., Dasen, J.D. and Liddelow, S.A. (2023) 'Single-cell analysis of the nervous system at small and large scales with instant partitions'. *bioRxiv*.

Friedrich, M., Molle, M., Friederici, A.D. and Born, J. (2020) 'Sleep-dependent memory consolidation in infants protects new episodic memories from existing semantic memories'. *Nat Commun,* **11** (1), pp. 1298.

Friedrich, M., Wilhelm, I., Born, J. and Friederici, A.D. (2015) 'Generalization of word meanings during infant sleep'. *Nat Commun,* **6** 6004.

Fritz, E.M., Kreuzer, M., Altunkaya, A., Singewald, N. and Fenzl, T. (2021) 'Altered sleep behavior in a genetic mouse model of impaired fear extinction'. *Sci Rep,* **11** (1), pp. 8978.

Funk, C.M., Peelman, K., Bellesi, M., Marshall, W., Cirelli, C. and Tononi, G. (2017) 'Role of Somatostatin-Positive Cortical Interneurons in the Generation of Sleep Slow Waves'. *J Neurosci,* **37** (38), pp. 9132-9148.

Garcia-Marin, V., Garcia-Lopez, P. and Freire, M. (2007) 'Cajal's contributions to glia research'. *Trends Neurosci,* **30** (9), pp. 479-487.

Ge, W.P., Miyawaki, A., Gage, F.H., Jan, Y.N. and Jan, L.Y. (2012) 'Local generation of glia is a major astrocyte source in postnatal cortex'. *Nature,* **484** (7394), pp. 376-380.

Gedankien, T., Tan, R.J., Qasim, S.E., Moore, H., McDonagh, D., Jacobs, J. and Lega, B. (2023) 'Acetylcholine modulates the temporal dynamics of human theta oscillations during memory'. *Nat Commun,* **14** (1), pp. 5283.

Gent, T.C., Bandarabadi, M., Herrera, C.G. and Adamantidis, A.R. (2018) 'Thalamic dual control of sleep and wakefulness'. *Nat Neurosci,* **21** (7), pp. 974-984.

George, R., Haslett, W.L. and Jenden, D.J. (1964) 'A Cholinergic Mechanism in the Brainstem Reticular Formation: Induction of Paradoxical Sleep'. *Int J Neuropharmacol,* **3** 541-552.

Gervasoni, D., Peyron, C., Rampon, C., Barbagli, B., Chouvet, G., Urbain, N., Fort, P. and Luppi, P.H. (2000) 'Role and origin of the GABAergic innervation of dorsal raphe serotonergic neurons'. *J Neurosci,* **20** (11), pp. 4217-4225.

Geva-Sagiv, M., Mankin, E.A., Eliashiv, D., Epstein, S., Cherry, N., Kalender, G., Tchemodanov, N., Nir, Y. and Fried, I. (2023) 'Augmenting hippocampal-prefrontal neuronal synchrony during sleep enhances memory consolidation in humans'. *Nat Neurosci,* **26** (6), pp. 1100-1110.

Ghandour, K., Ohkawa, N., Fung, C.C.A., Asai, H., Saitoh, Y., Takekawa, T., Okubo-Suzuki, R., Soya, S., Nishizono, H., Matsuo, M., Osanai, M., Sato, M., Ohkura, M., Nakai, J., Hayashi, Y., Sakurai, T., Kitamura, T., Fukai, T. and Inokuchi, K. (2019) 'Orchestrated ensemble activities constitute a hippocampal memory engram'. *Nat Commun,* **10** (1), pp. 2637.

Girardeau, G., Benchenane, K., Wiener, S.I., Buzsaki, G. and Zugaro, M.B. (2009) 'Selective suppression of hippocampal ripples impairs spatial memory'. *Nat Neurosci,* **12** (10), pp. 1222-1223.

Girardeau, G. and Lopes-Dos-Santos, V. (2021) 'Brain neural patterns and the memory function of sleep'. *Science,* **374** (6567), pp. 560-564.

Gleichman, A.J., Kawaguchi, R., Sofroniew, M.V. and Carmichael, S.T. (2023) 'A toolbox of astrocyte-specific, serotype-independent adeno-associated viral vectors using microRNA targeting sequences'. *Nat Commun,* **14** (1), pp. 7426.

Golgi, C. (1873) 'On the structure of the brain grey matter'. *Gazzetta Medica Italiana. Lombardia,* **33** 244-246.

Golgi, C. (1903) *Opera omnia.* Hoepli.

Gomez, J.L., Bonaventura, J., Lesniak, W., Mathews, W.B., Sysa-Shah, P., Rodriguez, L.A., Ellis, R.J., Richie, C.T., Harvey, B.K., Dannals, R.F., Pomper, M.G., Bonci, A. and Michaelides, M. (2017) 'Chemogenetics revealed: DREADD occupancy and activation via converted clozapine'. *Science,* **357** (6350), pp. 503-507.

Gomez-Arboledas, A., Davila, J.C., Sanchez-Mejias, E., Navarro, V., Nunez-Diaz, C., Sanchez-Varo, R., Sanchez-Mico, M.V., Trujillo-Estrada, L., Fernandez-Valenzuela, J.J., Vizuete, M., Comella, J.X., Galea, E., Vitorica, J. and Gutierrez, A. (2018) 'Phagocytic clearance of presynaptic dystrophies by reactive astrocytes in Alzheimer's disease'. *Glia,* **66** (3), pp. 637-653.

Goodpaster, T. and Randolph-Habecker, J. (2014) 'A flexible mouse-on-mouse immunohistochemical staining technique adaptable to biotin-free reagents, immunofluorescence, and multiple antibody staining'. *J Histochem Cytochem,* **62** (3), pp. 197-204.

Goubard, V., Fino, E. and Venance, L. (2011) 'Contribution of astrocytic glutamate and GABA uptake to corticostriatal information processing'. *J Physiol,* **589** (Pt 9), pp. 2301-2319.

Gourine, A.V. and Kasparov, S. (2011) 'Astrocytes as brain interoceptors'. *Exp Physiol,* **96** (4), pp. 411-416.

Gourine, A.V., Kasymov, V., Marina, N., Tang, F., Figueiredo, M.F., Lane, S., Teschemacher, A.G., Spyer, K.M., Deisseroth, K. and Kasparov, S. (2010) 'Astrocytes control breathing through pH-dependent release of ATP'. *Science,* **329** (5991), pp. 571-575.

Grandner, M.A. and Fernandez, F.X. (2021) 'The translational neuroscience of sleep: A contextual framework'. *Science,* **374** (6567), pp. 568-573.

Gutierrez Herrera, C., Girard, F., Bilella, A., Gent, T.C., Roccaro-Waldmeyer, D.M., Adamantidis, A. and Celio, M.R. (2019) 'Neurons in the Nucleus papilio contribute to the control of eye movements during REM sleep'. *Nat Commun,* **10** (1), pp. 5225.

Halassa, M.M., Florian, C., Fellin, T., Munoz, J.R., Lee, S.Y., Abel, T., Haydon, P.G. and Frank, M.G. (2009) 'Astrocytic modulation of sleep homeostasis and cognitive consequences of sleep loss'. *Neuron,* **61** (2), pp. 213-219.

Halassa, M.M., Siegle, J.H., Ritt, J.T., Ting, J.T., Feng, G. and Moore, C.I. (2011) 'Selective optical drive of thalamic reticular nucleus generates thalamic bursts and cortical spindles'. *Nat Neurosci,* **14** (9), pp. 1118-1120.

Halasz, P. (2005) 'K-complex, a reactive EEG graphoelement of NREM sleep: an old chap in a new garment'. *Sleep Med Rev,* **9** (5), pp. 391-412.

Han, Z., Luo, N., Ma, W., Liu, X., Cai, Y., Kou, J., Wang, J., Li, L., Peng, S., Xu, Z., Zhang, W., Qiu, Y., Wu, Y., Ye, C., Lin, K. and Xu, F. (2023) 'AAV11 enables efficient retrograde targeting of projection neurons and enhances astrocyte-directed transduction'. *Nat Commun,* **14** (1), pp. 3792.

Harrison, F.E., Hosseini, A.H. and McDonald, M.P. (2009) 'Endogenous anxiety and stress responses in water maze and Barnes maze spatial memory tasks'. *Behav Brain Res,* **198** (1), pp. 247-251.

Hars, B. and Hennevin, E. (1983) 'Reminder abolishes impairment of learning induced by paradoxical sleep retardation'. *Physiol Behav,* **30** (6), pp. 831-836.

Hasegawa, E., Miyasaka, A., Sakurai, K., Cherasse, Y., Li, Y. and Sakurai, T. (2022) 'Rapid eye movement sleep is initiated by basolateral amygdala dopamine signaling in mice'. *Science,* **375** (6584), pp. 994-1000.

Hassainia, F., Petit, D., Nielsen, T., Gauthier, S. and Montplaisir, J. (1997) 'Quantitative EEG and statistical mapping of wakefulness and REM sleep in the evaluation of mild to moderate Alzheimer's disease'. *Eur Neurol,* **37** (4), pp. 219-224.

Hassani, O.K., Henny, P., Lee, M.G. and Jones, B.E. (2010) 'GABAergic neurons intermingled with orexin and MCH neurons in the lateral hypothalamus discharge maximally during sleep'. *Eur J Neurosci,* **32** (3), pp. 448-457.

Hassani, O.K., Lee, M.G. and Jones, B.E. (2009) 'Melanin-concentrating hormone neurons discharge in a reciprocal manner to orexin neurons across the sleep-wake cycle'. *Proc Natl Acad Sci U S A,* **106** (7), pp. 2418-2422.

Hayashi, Y., Kashiwagi, M., Yasuda, K., Ando, R., Kanuka, M., Sakai, K. and Itohara, S. (2015) 'Cells of a common developmental origin regulate REM/non-REM sleep and wakefulness in mice'. *Science,* **350** (6263), pp. 957-961.

Haydon, P.G. and Carmignoto, G. (2006) 'Astrocyte control of synaptic transmission and neurovascular coupling'. *Physiol Rev,* **86** (3), pp. 1009-1031.

Hefendehl, J.K., LeDue, J., Ko, R.W., Mahler, J., Murphy, T.H. and MacVicar, B.A. (2016) 'Mapping synaptic glutamate transporter dysfunction in vivo to regions surrounding Abeta plaques by iGluSnFR two-photon imaging'. *Nat Commun,* **7** 13441.

Heffernan, K.S., Rahman, K., Smith, Y. and Galvan, A. (2022) 'Characterization of the GfaABC1D promoter to selectively target astrocytes in the rhesus macaque brain'. *J Neurosci Methods,* **372** 109530.

Heine, R. (1914) *über Wiedererkennen und rückwirkende Hemmung.* Johann Ambrosius Barth.

Henley, K. and Morrison, A.R. (1974) 'A re-evaluation of the effects of lesions of the pontine tegmentum and locus coeruleus on phenomena of paradoxical sleep in the cat'. *Acta Neurobiol Exp (Wars),* **34** (2), pp. 215-232.

Henneberger, C., Papouin, T., Oliet, S.H. and Rusakov, D.A. (2010) 'Long-term potentiation depends on release of D-serine from astrocytes'. *Nature,* **463** (7278), pp. 232-236.

Hennevin, E. and Leconte, P. (1977) '[Study of the relations between paradoxical sleep and learning processes (author's transl)]'. *Physiol Behav,* **18** (2), pp. 307-319.

Herice, C., Patel, A.A. and Sakata, S. (2019) 'Circuit mechanisms and computational models of REM sleep'. *Neurosci Res,* **140** 77-92.

Herrera, C.G., Cadavieco, M.C., Jego, S., Ponomarenko, A., Korotkova, T. and Adamantidis, A. (2016) 'Hypothalamic feedforward inhibition of thalamocortical network controls arousal and consciousness'. *Nat Neurosci,* **19** (2), pp. 290-298.

Hirase, H., Qian, L., Bartho, P. and Buzsaki, G. (2004) 'Calcium dynamics of cortical astrocytic networks in vivo'. *PLoS Biol,* **2** (4), pp. E96.

Hobson, J.A. (2009) 'REM sleep and dreaming: towards a theory of protoconsciousness'. *Nat Rev Neurosci,* **10** (11), pp. 803-813.

Hobson, J.A., McCarley, R.W. and Wyzinski, P.W. (1975) 'Sleep cycle oscillation: reciprocal discharge by two brainstem neuronal groups'. *Science,* **189** (4196), pp. 55-58.

Holdstock, T.L. and Verschoor, G.J. (1973) 'Retention of maze learning following paradoxical sleep deprivation in rats'. *Physiological Psychology,* **1** (1), pp. 29-32.

Hong, J., Lozano, D.E., Beier, K.T., Chung, S. and Weber, F. (2023) 'Prefrontal cortical regulation of REM sleep'. *Nat Neurosci,* **26** (10), pp. 1820-1832.

Honjoh, S., Sasai, S., Schiereck, S.S., Nagai, H., Tononi, G. and Cirelli, C. (2018) 'Regulation of cortical activity and arousal by the matrix cells of the ventromedial thalamic nucleus'. *Nat Commun,* **9** (1), pp. 2100.

Horikawa, K., Yamada, Y., Matsuda, T., Kobayashi, K., Hashimoto, M., Matsu-ura, T., Miyawaki, A., Michikawa, T., Mikoshiba, K. and Nagai, T. (2010) 'Spontaneous network activity visualized by ultrasensitive Ca(2+) indicators, yellow Cameleon-Nano'. *Nat Methods,* **7** (9), pp. 729-732.

Huang, A.Y., Woo, J., Sardar, D., Lozzi, B., Bosquez Huerta, N.A., Lin, C.J., Felice, D., Jain, A., Paulucci-Holthauzen, A. and Deneen, B. (2020) 'Region-Specific Transcriptional Control of Astrocyte Function Oversees Local Circuit Activities'. *Neuron,* **106** (6), pp. 992-1008 e1009.

Huber, R., Ghilardi, M.F., Massimini, M. and Tononi, G. (2004) 'Local sleep and learning'. *Nature,* **430** (6995), pp. 78-81.

Huerta, P.T. and Lisman, J.E. (1993) 'Heightened synaptic plasticity of hippocampal CA1 neurons during a cholinergically induced rhythmic state'. *Nature,* **364** (6439), pp. 723-725.

Hughes, E.G., Elmariah, S.B. and Balice-Gordon, R.J. (2010) 'Astrocyte secreted proteins selectively increase hippocampal GABAergic axon length, branching, and synaptogenesis'. *Mol Cell Neurosci,* **43** (1), pp. 136-145.

Hughes, S.W., Lorincz, M.L., Parri, H.R. and Crunelli, V. (2011) 'Infraslow (<0.1 Hz) oscillations in thalamic relay nuclei basic mechanisms and significance to health and disease states'. *Prog Brain Res,* **193** 145-162.

Huh, C.Y., Goutagny, R. and Williams, S. (2010) 'Glutamatergic neurons of the mouse medial septum and diagonal band of Broca synaptically drive hippocampal pyramidal cells: relevance for hippocampal theta rhythm'. *J Neurosci,* **30** (47), pp. 15951-15961.

Huitron-Resendiz, S., Sanchez-Alavez, M. and Criado, J.R. (2005) 'Sleep-wake states in transgenic mouse models overexpressing the human beta-amyloid precursor protein'. *Am J Alzheimers Dis Other Demen,* **20** (2), pp. 87-90.

Huntington, T.E. and Srinivasan, R. (2021) 'Astrocytic mitochondria in adult mouse brain slices show spontaneous calcium influx events with unique properties'. *Cell Calcium,* **96** 102383.

Hyden, H. and Lange, P.W. (1965) 'Rhythmic Enzyme Changes in Neurons and Glia during Sleep'. *Science,* **149** (3684), pp. 654-656.

Iber, C., Ancoli-Israel, S., Chesson, A. and Quan, S.F. (2007a) '*The AASM Manual for the Score of Sleep and Associated Events: Rules, Terminology, and Technical Specifications* '. 1st ed ed. American Academy of Sleep Medicine, Westchester, IL.

Iber, C., Ancoli-Israel, S., Chesson, A.L. and Quan, S. (2007b) 'The AASM Manual for the Scoring of Sleep and Associated Events: Rules, Terminology and Technical Specifications'. *Westchester, IL: American Academy of Sleep Medicine*.

Iliff, J.J., Wang, M., Liao, Y., Plogg, B.A., Peng, W., Gundersen, G.A., Benveniste, H., Vates, G.E., Deane, R., Goldman, S.A., Nagelhus, E.A. and Nedergaard, M. (2012) 'A paravascular pathway facilitates CSF flow through the brain parenchyma and the clearance of interstitial solutes, including amyloid β'. *Sci Transl Med,* **4** (147), pp. 147ra111.

Iliff, J.J., Wang, M., Zeppenfeld, D.M., Venkataraman, A., Plog, B.A., Liao, Y., Deane, R. and Nedergaard, M. (2013) 'Cerebral arterial pulsation drives paravascular CSF-interstitial fluid exchange in the murine brain'. *J Neurosci,* **33** (46), pp. 18190-18199.

Ingiosi, A.M. and Frank, M.G. (2022) 'Goodnight, astrocyte: waking up to astroglial mechanisms in sleep'. *FEBS J*.

Ingiosi, A.M. and Frank, M.G. (2023) 'Goodnight, astrocyte: waking up to astroglial mechanisms in sleep'. *FEBS J,* **290** (10), pp. 2553-2564.

Ingiosi, A.M., Hayworth, C.R. and Frank, M.G. (2023) 'Activation of Basal Forebrain Astrocytes Induces Wakefulness without Compensatory Changes in Sleep Drive'. *J Neurosci,* **43** (32), pp. 5792-5809.

Ingiosi, A.M., Hayworth, C.R., Harvey, D.O., Singletary, K.G., Rempe, M.J., Wisor, J.P. and Frank, M.G. (2020) 'A Role for Astroglial Calcium in Mammalian Sleep and Sleep Regulation'. *Curr Biol,* **30** (22), pp. 4373-4383 e4377.

Ishikawa, H., Yamada, K., Pavlides, C. and Ichitani, Y. (2014) 'Sleep deprivation impairs spontaneous object-place but not novel-object recognition in rats'. *Neurosci Lett,* **580** 114-118.

Isomura, Y., Sirota, A., Ozen, S., Montgomery, S., Mizuseki, K., Henze, D.A. and Buzsaki, G. (2006) 'Integration and segregation of activity in entorhinal-hippocampal subregions by neocortical slow oscillations'. *Neuron,* **52** (5), pp. 871-882.

Izawa, S., Chowdhury, S., Miyazaki, T., Mukai, Y., Ono, D., Inoue, R., Ohmura, Y., Mizoguchi, H., Kimura, K., Yoshioka, M., Terao, A., Kilduff, T.S. and Yamanaka, A. (2019) 'REM sleep-active MCH neurons are involved in forgetting hippocampus-dependent memories'. *Science,* **365** (6459), pp. 1308-1313.

Jack, C.R., Jr., Bennett, D.A., Blennow, K., Carrillo, M.C., Dunn, B., Haeberlein, S.B., Holtzman, D.M., Jagust, W., Jessen, F., Karlawish, J., Liu, E., Molinuevo, J.L.,

Montine, T., Phelps, C., Rankin, K.P., Rowe, C.C., Scheltens, P., Siemers, E., Snyder, H.M., Sperling, R., . . . Contributors (2018) 'NIA-AA Research Framework: Toward a biological definition of Alzheimer's disease'. *Alzheimers Dement,* **14** (4), pp. 535-562.

Jego, S., Glasgow, S.D., Herrera, C.G., Ekstrand, M., Reed, S.J., Boyce, R., Friedman, J., Burdakov, D. and Adamantidis, A.R. (2013) 'Optogenetic identification of a rapid eye movement sleep modulatory circuit in the hypothalamus'. *Nat Neurosci,* **16** (11), pp. 1637-1643.

Jendryka, M., Palchaudhuri, M., Ursu, D., van der Veen, B., Liss, B., Katzel, D., Nissen, W. and Pekcec, A. (2019) 'Pharmacokinetic and pharmacodynamic actions of clozapine-N-oxide, clozapine, and compound 21 in DREADD-based chemogenetics in mice'. *Sci Rep,* **9** (1), pp. 4522.

Jo, S., Yarishkin, O., Hwang, Y.J., Chun, Y.E., Park, M., Woo, D.H., Bae, J.Y., Kim, T., Lee, J., Chun, H., Park, H.J., Lee, D.Y., Hong, J., Kim, H.Y., Oh, S.J., Park, S.J., Lee, H., Yoon, B.E., Kim, Y., Jeong, Y., . . . Lee, C.J. (2014) 'GABA from reactive astrocytes impairs memory in mouse models of Alzheimer's disease'. *Nat Med,* **20** (8), pp. 886-896.

John Lin, C.C., Yu, K., Hatcher, A., Huang, T.W., Lee, H.K., Carlson, J., Weston, M.C., Chen, F., Zhang, Y., Zhu, W., Mohila, C.A., Ahmed, N., Patel, A.J., Arenkiel, B.R., Noebels, J.L., Creighton, C.J. and Deneen, B. (2017) 'Identification of diverse astrocyte populations and their malignant analogs'. *Nat Neurosci,* **20** (3), pp. 396-405.

Jones, B.E. and Yang, T.Z. (1985) 'The efferent projections from the reticular formation and the locus coeruleus studied by anterograde and retrograde axonal transport in the rat'. *J Comp Neurol,* **242** (1), pp. 56-92.

Jouvet, M. (1962) '[Research on the neural structures and responsible mechanisms in different phases of physiological sleep]'. *Arch Ital Biol,* **100** 125-206.

Jouvet, M. (1965) 'Paradoxical Sleep--a Study of Its Nature and Mechanisms'. *Prog Brain Res,* **18** 20-62.

Jouvet, M. and Michel, F. (1959) '[Electromyographic correlations of sleep in the chronic decorticate & mesencephalic cat]'. *C R Seances Soc Biol Fil,* **153** (3), pp. 422-425.

Jouvet-Mounier, D., Astic, L. and Lacote, D. (1970) 'Ontogenesis of the states of sleep in rat, cat, and guinea pig during the first postnatal month'. *Dev Psychobiol,* **2** (4), pp. 216-239.

Kang, J., Jiang, L., Goldman, S.A. and Nedergaard, M. (1998) 'Astrocyte-mediated potentiation of inhibitory synaptic transmission'. *Nat Neurosci,* **1** (8), pp. 683-692.

Karashima, A., Nakamura, K., Sato, N., Nakao, M., Katayama, N. and Yamamoto, M. (2002) 'Phase-locking of spontaneous and elicited ponto-geniculo-occipital waves is associated with acceleration of hippocampal theta waves during rapid eye movement sleep in cats'. *Brain Res,* **958** (2), pp. 347-358.

Karna, B. and Gupta, V. (2022) 'Sleep Disorder'. *StatPearls.* Treasure Island (FL): pp.

Kashiwagi, M., Kanuka, M., Tatsuzawa, C., Suzuki, H., Morita, M., Tanaka, K., Kawano, T., Shin, J.W., Suzuki, H., Itohara, S., Yanagisawa, M. and Hayashi, Y. (2020) 'Widely Distributed Neurotensinergic Neurons in the Brainstem Regulate NREM Sleep in Mice'. *Curr Biol,* **30** (6), pp. 1002-1010 e1004.

Kawamura, H. and Sawyer, C.H. (1965) 'Elevation in brain temperature during paradoxical sleep'. *Science,* **150** (3698), pp. 912-913.

Khakh, B.S. and Sofroniew, M.V. (2015) 'Diversity of astrocyte functions and phenotypes in neural circuits'. *Nat Neurosci,* **18** (7), pp. 942-952.

Kim, C.K., Yang, S.J., Pichamoorthy, N., Young, N.P., Kauvar, I., Jennings, J.H., Lerner, T.N., Berndt, A., Lee, S.Y., Ramakrishnan, C., Davidson, T.J., Inoue, M., Bito, H. and Deisseroth, K. (2016) 'Simultaneous fast measurement of circuit dynamics at multiple sites across the mammalian brain'. *Nat Methods,* **13** (4), pp. 325-328.

Kim, J.H., Choi, I.S., Jeong, J.Y., Jang, I.S., Lee, M.G. and Suk, K. (2020) 'Astrocytes in the Ventrolateral Preoptic Area Promote Sleep'. *J Neurosci,* **40** (47), pp. 8994-9011.

Kirov, R. and Moyanova, S. (2002) 'Distinct sleep-wake stages in rats depend differentially on age'. *Neurosci Lett,* **322** (2), pp. 134-136.

Klinzing, J.G., Niethard, N. and Born, J. (2019) 'Mechanisms of systems memory consolidation during sleep'. *Nat Neurosci,* **22** (10), pp. 1598-1610.

Knoop, M.S., de Groot, E.R. and Dudink, J. (2021) 'Current ideas about the roles of rapid eye movement and non-rapid eye movement sleep in brain development'. *Acta Paediatr,* **110** (1), pp. 36-44.

Kofuji, P. and Araque, A. (2021) 'G-Protein-Coupled Receptors in Astrocyte-Neuron Communication'. *Neuroscience,* **456** 71-84.

Kofuji, P. and Newman, E.A. (2004) 'Potassium buffering in the central nervous system'. *Neuroscience,* **129** (4), pp. 1045-1056.

Koh, W., Park, Y.M., Lee, S.E. and Lee, C.J. (2017) 'AAV-Mediated Astrocyte-Specific Gene Expression under Human ALDH1L1 Promoter in Mouse Thalamus'. *Exp Neurobiol,* **26** (6), pp. 350-361.

Kohro, Y., Matsuda, T., Yoshihara, K., Kohno, K., Koga, K., Katsuragi, R., Oka, T., Tashima, R., Muneta, S., Yamane, T., Okada, S., Momokino, K., Furusho, A., Hamase, K., Oti, T., Sakamoto, H., Hayashida, K., Kobayashi, R., Horii, T., Hatada, I., . . . Tsuda, M. (2020) 'Spinal astrocytes in superficial laminae gate brainstem descending control of mechanosensory hypersensitivity'. *Nat Neurosci,* **23** (11), pp. 1376-1387.

Koike, B.D.V., Farias, K.S., Billwiller, F., Almeida-Filho, D., Libourel, P.A., Tiran-Cappello, A., Parmentier, R., Blanco, W., Ribeiro, S., Luppi, P.H. and Queiroz, C.M. (2017) 'Electrophysiological Evidence That the Retrosplenial Cortex Displays a Strong and Specific Activation Phased with Hippocampal Theta during Paradoxical (REM) Sleep'. *J Neurosci,* **37** (33), pp. 8003-8013.

Konopacki, J., MacIver, M.B., Bland, B.H. and Roth, S.H. (1987) 'Carbachol-induced EEG 'theta' activity in hippocampal brain slices'. *Brain Res,* **405** (1), pp. 196-198.

Kragel, J.E., VanHaerents, S., Templer, J.W., Schuele, S., Rosenow, J.M., Nilakantan, A.S. and Bridge, D.J. (2020) 'Hippocampal theta coordinates memory processing during visual exploration'. *Elife,* **9**.

Krause, A.J., Simon, E.B., Mander, B.A., Greer, S.M., Saletin, J.M., Goldstein-Piekarski, A.N. and Walker, M.P. (2017) 'The sleep-deprived human brain'. *Nat Rev Neurosci,* **18** (7), pp. 404-418.

Krenzer, M., Anaclet, C., Vetrivelan, R., Wang, N., Vong, L., Lowell, B.B., Fuller, P.M. and Lu, J. (2011) 'Brainstem and spinal cord circuitry regulating REM sleep and muscle atonia'. *PLoS One,* **6** (10), pp. e24998.

Kroeger, D., Bandaru, S.S., Madara, J.C. and Vetrivelan, R. (2019) 'Ventrolateral periaqueductal gray mediates rapid eye movement sleep regulation by melanin-concentrating hormone neurons'. *Neuroscience,* **406** 314-324.

Kroeger, D., Ferrari, L.L., Petit, G., Mahoney, C.E., Fuller, P.M., Arrigoni, E. and Scammell, T.E. (2017) 'Cholinergic, Glutamatergic, and GABAergic Neurons of the Pedunculopontine Tegmental Nucleus Have Distinct Effects on Sleep/Wake Behavior in Mice'. *J Neurosci,* **37** (5), pp. 1352-1366.

Krohn, L., Heilbron, K., Blauwendraat, C., Reynolds, R.H., Yu, E., Senkevich, K., Rudakou, U., Estiar, M.A., Gustavsson, E.K., Brolin, K., Ruskey, J.A., Freeman, K., Asayesh, F., Chia, R., Arnulf, I., Hu, M.T.M., Montplaisir, J.Y., Gagnon, J.F., Desautels, A., Dauvilliers, Y., . . . Gan-Or, Z. (2022) 'Genome-wide association study of REM sleep behavior disorder identifies polygenic risk and brain expression effects'. *Nat Commun,* **13** (1), pp. 7496.

Krone, L.B., Yamagata, T., Blanco-Duque, C., Guillaumin, M.C.C., Kahn, M.C., van der Vinne, V., McKillop, L.E., Tam, S.K.E., Peirson, S.N., Akerman, C.J., Hoerder-Suabedissen, A., Molnar, Z. and Vyazovskiy, V.V. (2021) 'A role for the cortex in sleep-wake regulation'. *Nat Neurosci,* **24** (9), pp. 1210-1215.

Kucukdereli, H., Allen, N.J., Lee, A.T., Feng, A., Ozlu, M.I., Conatser, L.M., Chakraborty, C., Workman, G., Weaver, M., Sage, E.H., Barres, B.A. and Eroglu, C. (2011) 'Control of excitatory CNS synaptogenesis by astrocyte-secreted proteins Hevin and SPARC'. *Proc Natl Acad Sci U S A,* **108** (32), pp. E440-449.

Kumar, D., Koyanagi, I., Carrier-Ruiz, A., Vergara, P., Srinivasan, S., Sugaya, Y., Kasuya, M., Yu, T.S., Vogt, K.E., Muratani, M., Ohnishi, T., Singh, S., Teixeira, C.M., Cherasse, Y., Naoi, T., Wang, S.H., Nondhalee, P., Osman, B.A.H., Kaneko, N., Sawamoto, K., . . . Sakaguchi, M. (2020) 'Sparse Activity of Hippocampal Adult-Born Neurons during REM Sleep Is Necessary for Memory Consolidation'. *Neuron,* **107** (3), pp. 552-565 e510.

Kurdziel, L., Duclos, K. and Spencer, R.M. (2013) 'Sleep spindles in midday naps enhance learning in preschool children'. *Proc Natl Acad Sci U S A,* **110** (43), pp. 17267-17272.

Kurogi, Y., Sanagi, T., Ono, D. and Tsunematsu, T. (2024) 'Chemogenetic activation of astrocytes modulates sleep/wakefulness states in a brain region-dependent manner'. *bioRxiv,* 2024.2006.2003.597103.

Kwak, H., Koh, W., Kim, S., Song, K., Shin, J.I., Lee, J.M., Lee, E.H., Bae, J.Y., Ha, G.E., Oh, J.E., Park, Y.M., Kim, S., Feng, J., Lee, S.E., Choi, J.W., Kim, K.H., Kim, Y.S., Woo, J., Lee, D., Son, T., . . . Cheong, E. (2020) 'Astrocytes Control Sensory Acuity via Tonic Inhibition in the Thalamus'. *Neuron,* **108** (4), pp. 691-706 e610.

Lacroix, M.M., de Lavilléon, G., Lefort, J., El Kanbi, K., Bagur, S., Laventure, S., Dauvilliers, Y., Peyron, C. and Benchenane, K. (2018) 'Improved sleep scoring in mice reveals human-like stages'. *bioRxiv,* 489005.

Lai, Y.Y., Shalita, T., Hajnik, T., Wu, J.P., Kuo, J.S., Chia, L.G. and Siegel, J.M. (1999) 'Neurotoxic N-methyl-D-aspartate lesion of the ventral midbrain and mesopontine junction alters sleep-wake organization'. *Neuroscience,* **90** (2), pp. 469-483.

Lambert, J.C., Ibrahim-Verbaas, C.A., Harold, D., Naj, A.C., Sims, R., Bellenguez, C., DeStafano, A.L., Bis, J.C., Beecham, G.W., Grenier-Boley, B., Russo, G., Thorton-Wells, T.A., Jones, N., Smith, A.V., Chouraki, V., Thomas, C., Ikram, M.A., Zelenika, D., Vardarajan, B.N., Kamatani, Y., . . . Epidemiology, C.f.H.a.A.R.i.G. (2013) 'Meta-analysis of 74,046 individuals identifies 11 new susceptibility loci for Alzheimer's disease'. *Nat Genet,* **45** (12), pp. 1452-1458.

Latchoumane, C.V., Ngo, H.V., Born, J. and Shin, H.S. (2017) 'Thalamic Spindles Promote Memory Formation during Sleep through Triple Phase-Locking of Cortical, Thalamic, and Hippocampal Rhythms'. *Neuron,* **95** (2), pp. 424-435 e426.

Le Bon, O. (2020) 'Relationships between REM and NREM in the NREM-REM sleep cycle: a review on competing concepts'. *Sleep Med,* **70** 6-16.

Le Bon, O., Popa, D., Streel, E., Alexandre, C., Lena, C., Linkowski, P. and Adrien, J. (2007) 'Ultradian cycles in mice: definitions and links with REMS and NREMS'. *J Comp Physiol A Neuroethol Sens Neural Behav Physiol,* **193** (10), pp. 1021-1032.

Lecci, S., Fernandez, L.M., Weber, F.D., Cardis, R., Chatton, J.Y., Born, J. and Luthi, A. (2017) 'Coordinated infraslow neural and cardiac oscillations mark fragility and offline periods in mammalian sleep'. *Sci Adv,* **3** (2), pp. e1602026.

Leconte, P., Hennevin, E. and Bloch, V. (1973) '[Analysis of the effects of learning and the level of acquisition on consecutive paradoxical sleep]'. *Brain Res,* **49** (2), pp. 367-379.

Lee, H.G., Wheeler, M.A. and Quintana, F.J. (2022) 'Function and therapeutic value of astrocytes in neurological diseases'. *Nat Rev Drug Discov,* **21** (5), pp. 339-358.

Lee, H.S., Ghetti, A., Pinto-Duarte, A., Wang, X., Dziewczapolski, G., Galimi, F., Huitron-Resendiz, S., Pina-Crespo, J.C., Roberts, A.J., Verma, I.M., Sejnowski, T.J. and Heinemann, S.F. (2014) 'Astrocytes contribute to gamma oscillations and recognition memory'. *Proc Natl Acad Sci U S A,* **111** (32), pp. E3343-3352.

Lee, M.G., Hassani, O.K. and Jones, B.E. (2005) 'Discharge of identified orexin/hypocretin neurons across the sleep-waking cycle'. *J Neurosci,* **25** (28), pp. 6716-6720.

Lee, S., Yoon, B.E., Berglund, K., Oh, S.J., Park, H., Shin, H.S., Augustine, G.J. and Lee, C.J. (2010) 'Channel-mediated tonic GABA release from glia'. *Science,* **330** (6005), pp. 790-796.

Lee, Y., Messing, A., Su, M. and Brenner, M. (2008) 'GFAP promoter elements required for region-specific and astrocyte-specific expression'. *Glia,* **56** (5), pp. 481-493.

Lemieux, M., Chen, J.Y., Lonjers, P., Bazhenov, M. and Timofeev, I. (2014) 'The impact of cortical deafferentation on the neocortical slow oscillation'. *J Neurosci,* **34** (16), pp. 5689-5703.

Leung, L.C., Wang, G.X., Madelaine, R., Skariah, G., Kawakami, K., Deisseroth, K., Urban, A.E. and Mourrain, P. (2019) 'Neural signatures of sleep in zebrafish'. *Nature,* **571** (7764), pp. 198-204.

Leung, L.W. and Borst, J.G. (1987) 'Electrical activity of the cingulate cortex. I. Generating mechanisms and relations to behavior'. *Brain Res,* **407** (1), pp. 68-80.

Levenstein, D., Buzsaki, G. and Rinzel, J. (2019) 'NREM sleep in the rodent neocortex and hippocampus reflects excitable dynamics'. *Nat Commun,* **10** (1), pp. 2478.

Lewis, L.D. (2021) 'The interconnected causes and consequences of sleep in the brain'. *Science,* **374** (6567), pp. 564-568.

Lezmy, J., Arancibia-Carcamo, I.L., Quintela-Lopez, T., Sherman, D.L., Brophy, P.J. and Attwell, D. (2021) 'Astrocyte Ca(2+)-evoked ATP release regulates myelinated axon excitability and conduction speed'. *Science,* **374** (6565), pp. eabh2858.

Li, R., Wang, Y.Q., Liu, W.Y., Zhang, M.Q., Li, L., Cherasse, Y., Schiffmann, S.N., de Kerchove d'Exaerde, A., Lazarus, M., Qu, W.M. and Huang, Z.L. (2020a) 'Activation of adenosine A(2A) receptors in the olfactory tubercle promotes sleep in rodents'. *Neuropharmacology,* **168** 107923.

Li, W., Ma, L., Yang, G. and Gan, W.B. (2017) 'REM sleep selectively prunes and maintains new synapses in development and learning'. *Nat Neurosci,* **20** (3), pp. 427-437.

Li, Y., Li, L., Wu, J., Zhu, Z., Feng, X., Qin, L., Zhu, Y., Sun, L., Liu, Y., Qiu, Z., Duan, S. and Yu, Y.Q. (2020b) 'Activation of astrocytes in hippocampus decreases fear memory through adenosine A(1) receptors'. *Elife,* **9**.

Li, Y., Wang, S., Pan, C., Xue, F., Xian, J., Huang, Y., Wang, X., Li, T. and He, H. (2018) 'Comparison of NREM sleep and intravenous sedation through local information processing and whole brain network to explore the mechanism of general anesthesia'. *PLoS One,* **13** (2), pp. e0192358.

Liang, Y., Shi, W., Xiang, A., Hu, D., Wang, L. and Zhang, L. (2021) 'The NAergic locus coeruleus-ventrolateral preoptic area neural circuit mediates rapid arousal from sleep'. *Curr Biol,* **31** (17), pp. 3729-3742 e3725.

Lines, J., Martin, E.D., Kofuji, P., Aguilar, J. and Araque, A. (2020) 'Astrocytes modulate sensory-evoked neuronal network activity'. *Nat Commun,* **11** (1), pp. 3689.

Liu, D., Li, W., Ma, C., Zheng, W., Yao, Y., Tso, C.F., Zhong, P., Chen, X., Song, J.H., Choi, W., Paik, S.B., Han, H. and Dan, Y. (2020) 'A common hub for sleep and motor control in the substantia nigra'. *Science,* **367** (6476), pp. 440-445.

Liu, K., Kim, J., Kim, D.W., Zhang, Y.S., Bao, H., Denaxa, M., Lim, S.A., Kim, E., Liu, C., Wickersham, I.R., Pachnis, V., Hattar, S., Song, J., Brown, S.P. and Blackshaw, S. (2017) 'Lhx6-positive GABA-releasing neurons of the zona incerta promote sleep'. *Nature,* **548** (7669), pp. 582-587.

Liu, Y., Shen, X., Zhang, Y., Zheng, X., Cepeda, C., Wang, Y., Duan, S. and Tong, X. (2023) 'Interactions of glial cells with neuronal synapses, from astrocytes to microglia and oligodendrocyte lineage cells'. *Glia,* **71** (6), pp. 1383-1401.

Logothetis, N.K., Eschenko, O., Murayama, Y., Augath, M., Steudel, T., Evrard, H.C., Besserve, M. and Oeltermann, A. (2012) 'Hippocampal-cortical interaction during periods of subcortical silence'. *Nature,* **491** (7425), pp. 547-553.

Lorincz, M.L., Gunner, D., Bao, Y., Connelly, W.M., Isaac, J.T., Hughes, S.W. and Crunelli, V. (2015) 'A distinct class of slow (~0.2-2 Hz) intrinsically bursting layer 5 pyramidal neurons determines UP/DOWN state dynamics in the neocortex'. *J Neurosci,* **35** (14), pp. 5442-5458.

Louie, K. and Wilson, M.A. (2001) 'Temporally structured replay of awake hippocampal ensemble activity during rapid eye movement sleep'. *Neuron,* **29** (1), pp. 145-156.

Lu, J., Bjorkum, A.A., Xu, M., Gaus, S.E., Shiromani, P.J. and Saper, C.B. (2002) 'Selective activation of the extended ventrolateral preoptic nucleus during rapid eye movement sleep'. *J Neurosci,* **22** (11), pp. 4568-4576.

Lu, J., Greco, M.A., Shiromani, P. and Saper, C.B. (2000) 'Effect of lesions of the ventrolateral preoptic nucleus on NREM and REM sleep'. *J Neurosci,* **20** (10), pp. 3830-3842.

Lu, J., Jhou, T.C. and Saper, C.B. (2006a) 'Identification of wake-active dopaminergic neurons in the ventral periaqueductal gray matter'. *J Neurosci,* **26** (1), pp. 193-202.

Lu, J., Sherman, D., Devor, M. and Saper, C.B. (2006b) 'A putative flip-flop switch for control of REM sleep'. *Nature,* **441** (7093), pp. 589-594.

Lueptow, L.M. (2017) 'Novel Object Recognition Test for the Investigation of Learning and Memory in Mice'. *J Vis Exp,* (126), pp.

Luo, J., Phan, T.X., Yang, Y., Garelick, M.G. and Storm, D.R. (2013) 'Increases in cAMP, MAPK activity, and CREB phosphorylation during REM sleep: implications for REM sleep and memory consolidation'. *J Neurosci,* **33** (15), pp. 6460-6468.

Luppi, P.H., Aston-Jones, G., Akaoka, H., Chouvet, G. and Jouvet, M. (1995) 'Afferent projections to the rat locus coeruleus demonstrated by retrograde and anterograde tracing with cholera-toxin B subunit and Phaseolus vulgaris leucoagglutinin'. *Neuroscience,* **65** (1), pp. 119-160.

Luppi, P.H., Clement, O. and Fort, P. (2013) 'Paradoxical (REM) sleep genesis by the brainstem is under hypothalamic control'. *Curr Opin Neurobiol,* **23** (5), pp. 786-792.

Luppi, P.H., Clement, O., Sapin, E., Peyron, C., Gervasoni, D., Leger, L. and Fort, P. (2012) 'Brainstem mechanisms of paradoxical (REM) sleep generation'. *Pflugers Arch,* **463** (1), pp. 43-52.

Luppi, P.H., Gervasoni, D., Verret, L., Goutagny, R., Peyron, C., Salvert, D., Leger, L. and Fort, P. (2006) 'Paradoxical (REM) sleep genesis: the switch from an aminergic-cholinergic to a GABAergic-glutamatergic hypothesis'. *J Physiol Paris,* **100** (5-6), pp. 271-283.

Luppi, P.H., Peyron, C. and Fort, P. (2017) 'Not a single but multiple populations of GABAergic neurons control sleep'. *Sleep Med Rev,* **32** 85-94.

Ma, C., Zhong, P., Liu, D., Barger, Z.K., Zhou, L., Chang, W.C., Kim, B. and Dan, Y. (2019) 'Sleep Regulation by Neurotensinergic Neurons in a Thalamo-Amygdala Circuit'. *Neuron,* **103** (2), pp. 323-334 e327.

MacDonald, A.J., Holmes, F.E., Beall, C., Pickering, A.E. and Ellacott, K.L.J. (2020) 'Regulation of food intake by astrocytes in the brainstem dorsal vagal complex'. *Glia,* **68** (6), pp. 1241-1254.

Maezono, S.E.B., Kanuka, M., Tatsuzawa, C., Morita, M., Kawano, T., Kashiwagi, M., Nondhalee, P., Sakaguchi, M., Saito, T., Saido, T.C. and Hayashi, Y. (2020) 'Progressive Changes in Sleep and Its Relations to Amyloid-beta Distribution and Learning in Single App Knock-In Mice'. *eNeuro,* **7** (2), pp.

Maingret, N., Girardeau, G., Todorova, R., Goutierre, M. and Zugaro, M. (2016) 'Hippocampo-cortical coupling mediates memory consolidation during sleep'. *Nat Neurosci,* **19** (7), pp. 959-964.

Mak-McCully, R.A., Rolland, M., Sargsyan, A., Gonzalez, C., Magnin, M., Chauvel, P., Rey, M., Bastuji, H. and Halgren, E. (2017) 'Coordination of cortical and thalamic activity during non-REM sleep in humans'. *Nat Commun,* **8** 15499.

Mander, B.A., Reid, K.J., Baron, K.G., Tjoa, T., Parrish, T.B., Paller, K.A., Gitelman, D.R. and Zee, P.C. (2010) 'EEG measures index neural and cognitive recovery from sleep deprivation'. *J Neurosci,* **30** (7), pp. 2686-2693.

Marina, N., Christie, I.N., Korsak, A., Doronin, M., Brazhe, A., Hosford, P.S., Wells, J.A., Sheikhbahaei, S., Humoud, I., Paton, J.F.R., Lythgoe, M.F., Semyanov, A., Kasparov, S. and Gourine, A.V. (2020) 'Astrocytes monitor cerebral perfusion and control systemic circulation to maintain brain blood flow'. *Nat Commun,* **11** (1), pp. 131.

Martin-Fernandez, M., Jamison, S., Robin, L.M., Zhao, Z., Martin, E.D., Aguilar, J., Benneyworth, M.A., Marsicano, G. and Araque, A. (2017) 'Synapse-specific astrocyte gating of amygdala-related behavior'. *Nat Neurosci,* **20** (11), pp. 1540-1548.

Martinez-Gonzalez, C., Bolam, J.P. and Mena-Segovia, J. (2011) 'Topographical organization of the pedunculopontine nucleus'. *Front Neuroanat,* **5** 22.

Marvin, J.S., Borghuis, B.G., Tian, L., Cichon, J., Harnett, M.T., Akerboom, J., Gordus, A., Renninger, S.L., Chen, T.W., Bargmann, C.I., Orger, M.B., Schreiter, E.R., Demb, J.B., Gan, W.B., Hires, S.A. and Looger, L.L. (2013) 'An optimized fluorescent probe for visualizing glutamate neurotransmission'. *Nat Methods,* **10** (2), pp. 162-170.

Marvin, J.S., Scholl, B., Wilson, D.E., Podgorski, K., Kazemipour, A., Muller, J.A., Schoch, S., Quiroz, F.J.U., Rebola, N., Bao, H., Little, J.P., Tkachuk, A.N., Cai, E., Hantman, A.W., Wang, S.S., DePiero, V.J., Borghuis, B.G., Chapman, E.R., Dietrich, D., DiGregorio, D.A., . . . Looger, L.L. (2018) 'Stability, affinity, and chromatic variants of the glutamate sensor iGluSnFR'. *Nat Methods,* **15** (11), pp. 936-939.

Marvin, J.S., Shimoda, Y., Magloire, V., Leite, M., Kawashima, T., Jensen, T.P., Kolb, I., Knott, E.L., Novak, O., Podgorski, K., Leidenheimer, N.J., Rusakov, D.A., Ahrens, M.B., Kullmann, D.M. and Looger, L.L. (2019) 'A genetically encoded fluorescent sensor for in vivo imaging of GABA'. *Nat Methods,* **16** (8), pp. 763-770.

Masamoto, K., Unekawa, M., Watanabe, T., Toriumi, H., Takuwa, H., Kawaguchi, H., Kanno, I., Matsui, K., Tanaka, K.F., Tomita, Y. and Suzuki, N. (2015) 'Unveiling astrocytic control of cerebral blood flow with optogenetics'. *Sci Rep,* **5** 11455.

Mascadri, F., Ciccimarra, R., Bolognesi, M.M., Stellari, F., Ravanetti, F. and Cattoretti, G. (2021) 'Background-free Detection of Mouse Antibodies on Mouse Tissue by Anti-isotype Secondary Antibodies'. *J Histochem Cytochem,* **69** (8), pp. 535-541.

Mathis, A., Mamidanna, P., Cury, K.M., Abe, T., Murthy, V.N., Mathis, M.W. and Bethge, M. (2018) 'DeepLabCut: markerless pose estimation of user-defined body parts with deep learning'. *Nat Neurosci,* **21** (9), pp. 1281-1289.

Mathis, J. (1995) '[The history of sleep research in the 20th century]'. *Praxis (Bern 1994),* **84** (50), pp. 1479-1485.

Mavanji, V. and Datta, S. (2003) 'Activation of the phasic pontine-wave generator enhances improvement of learning performance: a mechanism for sleep-dependent plasticity'. *Eur J Neurosci,* **17** (2), pp. 359-370.

McCarley, R.W. and Hobson, J.A. (1971) 'Single neuron activity in cat gigantocellular tegmental field: selectivity of discharge in desynchronized sleep'. *Science,* **174** (4015), pp. 1250-1252.

McGinty, D.J., Stevenson, M., Hoppenbrouwers, T., Harper, R.M., Sterman, M.B. and Hodgman, J. (1977) 'Polygraphic studies of kitten development: sleep state patterns'. *Dev Psychobiol,* **10** (5), pp. 455-469.

Mederos, S., Sanchez-Puelles, C., Esparza, J., Valero, M., Ponomarenko, A. and Perea, G. (2021) 'GABAergic signaling to astrocytes in the prefrontal cortex sustains goal-directed behaviors'. *Nat Neurosci,* **24** (1), pp. 82-92.

Merkle, F.T., Fuentealba, L.C., Sanders, T.A., Magno, L., Kessaris, N. and Alvarez-Buylla, A. (2014) 'Adult neural stem cells in distinct microdomains generate previously unknown interneuron types'. *Nat Neurosci,* **17** (2), pp. 207-214.

Merkle, F.T., Mirzadeh, Z. and Alvarez-Buylla, A. (2007) 'Mosaic organization of neural stem cells in the adult brain'. *Science,* **317** (5836), pp. 381-384.

Miao, A., Luo, T., Hsieh, B., Edge, C.J., Gridley, M., Wong, R.T.C., Constandinou, T.G., Wisden, W. and Franks, N.P. (2024) 'Brain clearance is reduced during sleep and anesthesia'. *Nat Neurosci,* **27** (6), pp. 1046-1050.

Mileykovskiy, B.Y., Kiyashchenko, L.I. and Siegel, J.M. (2005) 'Behavioral correlates of activity in identified hypocretin/orexin neurons'. *Neuron,* **46** (5), pp. 787-798.

Mitchell, S.J. and Ranck, J.B., Jr. (1980) 'Generation of theta rhythm in medial entorhinal cortex of freely moving rats'. *Brain Res,* **189** (1), pp. 49-66.

Mitler, M.M., Lund, R., Sokolove, P.G., Pittendrigh, C.S. and Dement, W.C. (1977) 'Sleep and activity rhythms in mice: a description of circadian patterns and unexpected disruptions in sleep'. *Brain Res,* **131** (1), pp. 129-145.

Montgomery, S.M., Sirota, A. and Buzsaki, G. (2008) 'Theta and gamma coordination of hippocampal networks during waking and rapid eye movement sleep'. *J Neurosci,* **28** (26), pp. 6731-6741.

Morairty, S.R., Dittrich, L., Pasumarthi, R.K., Valladao, D., Heiss, J.E., Gerashchenko, D. and Kilduff, T.S. (2013) 'A role for cortical nNOS/NK1 neurons in coupling homeostatic sleep drive to EEG slow wave activity'. *Proc Natl Acad Sci U S A,* **110** (50), pp. 20272-20277.

Morison, R.S. and Bassett, D.L. (1945) 'ELECTRICAL ACTIVITY OF THE THALAMUS AND BASAL GANGLIA IN DECORTICATE CATS'. *Journal of Neurophysiology,* **8** (5), pp. 309-314.

Morris, R. (1984) 'Developments of a water-maze procedure for studying spatial learning in the rat'. *J Neurosci Methods,* **11** (1), pp. 47-60.

Morris, R.G., Garrud, P., Rawlins, J.N. and O'Keefe, J. (1982) 'Place navigation impaired in rats with hippocampal lesions'. *Nature,* **297** (5868), pp. 681-683.

Morris, R.G.M. (1981) 'Spatial localization does not require the presence of local cues'. *Learning and Motivation,* **12** (2), pp. 239-260.

Mu, Y., Bennett, D.V., Rubinov, M., Narayan, S., Yang, C.T., Tanimoto, M., Mensh, B.D., Looger, L.L. and Ahrens, M.B. (2019) 'Glia Accumulate Evidence that Actions Are Futile and Suppress Unsuccessful Behavior'. *Cell,* **178** (1), pp. 27-43 e19.

Mudannayake, J.M., Mouravlev, A., Fong, D.M. and Young, D. (2016) 'Transcriptional activity of novel ALDH1L1 promoters in the rat brain following AAV vector-mediated gene transfer'. *Mol Ther Methods Clin Dev,* **3** 16075.

Müller, G.E. and Pilzecker, A. (1900) *Experimentelle beiträge zur lehre vom gedächtniss.* JA Barth.

Murdock, M.H., Yang, C.Y., Sun, N., Pao, P.C., Blanco-Duque, C., Kahn, M.C., Kim, T., Lavoie, N.S., Victor, M.B., Islam, M.R., Galiana, F., Leary, N., Wang, S., Bubnys, A., Ma, E., Akay, L.A., Sneve, M., Qian, Y., Lai, C., McCarthy, M.M., . . . Tsai, L.H. (2024) 'Multisensory gamma stimulation promotes glymphatic clearance of amyloid'. *Nature,* **627** (8002), pp. 149-156.

Muthukumar, A.K., Stork, T. and Freeman, M.R. (2014) 'Activity-dependent regulation of astrocyte GAT levels during synaptogenesis'. *Nat Neurosci,* **17** (10), pp. 1340-1350.

Nagai, J., Rajbhandari, A.K., Gangwani, M.R., Hachisuka, A., Coppola, G., Masmanidis, S.C., Fanselow, M.S. and Khakh, B.S. (2019) 'Hyperactivity with Disrupted Attention by Activation of an Astrocyte Synaptogenic Cue'. *Cell,* **177** (5), pp. 1280-1292 e1220.

Nagai, J., Yu, X., Papouin, T., Cheong, E., Freeman, M.R., Monk, K.R., Hastings, M.H., Haydon, P.G., Rowitch, D., Shaham, S. and Khakh, B.S. (2021) 'Behaviorally consequential astrocytic regulation of neural circuits'. *Neuron,* **109** (4), pp. 576-596.

Nagai, Y., Miyakawa, N., Takuwa, H., Hori, Y., Oyama, K., Ji, B., Takahashi, M., Huang, X.P., Slocum, S.T., DiBerto, J.F., Xiong, Y., Urushihata, T., Hirabayashi, T., Fujimoto, A., Mimura, K., English, J.G., Liu, J., Inoue, K.I., Kumata, K., Seki, C., . . . Minamimoto, T. (2020) 'Deschloroclozapine, a potent and selective chemogenetic actuator enables rapid neuronal and behavioral modulations in mice and monkeys'. *Nat Neurosci,* **23** (9), pp. 1157-1167.

Nakai, J., Ohkura, M. and Imoto, K. (2001) 'A high signal-to-noise Ca(2+) probe composed of a single green fluorescent protein'. *Nat Biotechnol,* **19** (2), pp. 137-141.

Nedergaard, M. and Goldman, S.A. (2020) 'Glymphatic failure as a final common pathway to dementia'. *Science,* **370** (6512), pp. 50-56.

Ni, K.M., Hou, X.J., Yang, C.H., Dong, P., Li, Y., Zhang, Y., Jiang, P., Berg, D.K., Duan, S. and Li, X.M. (2016) 'Selectively driving cholinergic fibers optically in the thalamic reticular nucleus promotes sleep'. *Elife,* **5**.

Nimmerjahn, A., Mukamel, E.A. and Schnitzer, M.J. (2009) 'Motor behavior activates Bergmann glial networks'. *Neuron,* **62** (3), pp. 400-412.

Nofzinger, E.A., Mintun, M.A., Wiseman, M., Kupfer, D.J. and Moore, R.Y. (1997) 'Forebrain activation in REM sleep: an FDG PET study'. *Brain Res,* **770** (1-2), pp. 192-201.

Noh, K., Cho, W.H., Lee, B.H., Kim, D.W., Kim, Y.S., Park, K., Hwang, M., Barcelon, E., Cho, Y.K., Lee, C.J., Yoon, B.E., Choi, S.Y., Park, H.Y., Jun, S.B. and Lee, S.J. (2023) 'Cortical astrocytes modulate dominance behavior in male mice by regulating synaptic excitatory and inhibitory balance'. *Nat Neurosci,* **26** (9), pp. 1541-1554.

Norimoto, H., Fenk, L.A., Li, H.H., Tosches, M.A., Gallego-Flores, T., Hain, D., Reiter, S., Kobayashi, R., Macias, A., Arends, A., Klinkmann, M. and Laurent, G. (2020) 'A claustrum in reptiles and its role in slow-wave sleep'. *Nature,* **578** (7795), pp. 413-418.

Norimoto, H., Makino, K., Gao, M., Shikano, Y., Okamoto, K., Ishikawa, T., Sasaki, T., Hioki, H., Fujisawa, S. and Ikegaya, Y. (2018) 'Hippocampal ripples down-regulate synapses'. *Science,* **359** (6383), pp. 1524-1527.

Norman, Y., Yeagle, E.M., Khuvis, S., Harel, M., Mehta, A.D. and Malach, R. (2019) 'Hippocampal sharp-wave ripples linked to visual episodic recollection in humans'. *Science,* **365** (6454), pp.

O'Keefe, J. (1976) 'Place units in the hippocampus of the freely moving rat'. *Exp Neurol,* **51** (1), pp. 78-109.

O'Keefe, J. and Dostrovsky, J. (1971) 'The hippocampus as a spatial map. Preliminary evidence from unit activity in the freely-moving rat'. *Brain Res,* **34** (1), pp. 171-175.

Oberheim, N.A., Takano, T., Han, X., He, W., Lin, J.H., Wang, F., Xu, Q., Wyatt, J.D., Pilcher, W., Ojemann, J.G., Ransom, B.R., Goldman, S.A. and Nedergaard, M. (2009) 'Uniquely hominid features of adult human astrocytes'. *J Neurosci,* **29** (10), pp. 3276-3287.

Octeau, J.C., Gangwani, M.R., Allam, S.L., Tran, D., Huang, S., Hoang-Trong, T.M., Golshani, P., Rumbell, T.H., Kozloski, J.R. and Khakh, B.S. (2019) 'Transient, Consequential Increases in Extracellular Potassium Ions Accompany Channelrhodopsin2 Excitation'. *Cell Rep,* **27** (8), pp. 2249-2261 e2247.

Oe, Y., Wang, X., Patriarchi, T., Konno, A., Ozawa, K., Yahagi, K., Hirai, H., Tsuboi, T., Kitaguchi, T., Tian, L., McHugh, T.J. and Hirase, H. (2020) 'Distinct temporal integration of noradrenaline signaling by astrocytic second messengers during vigilance'. *Nat Commun,* **11** (1), pp. 471.

Oishi, Y., Xu, Q., Wang, L., Zhang, B.J., Takahashi, K., Takata, Y., Luo, Y.J., Cherasse, Y., Schiffmann, S.N., de Kerchove d'Exaerde, A., Urade, Y., Qu, W.M., Huang, Z.L. and Lazarus, M. (2017) 'Slow-wave sleep is controlled by a subset of nucleus accumbens core neurons in mice'. *Nat Commun,* **8** (1), pp. 734.

Oliva, A., Fernandez-Ruiz, A., Leroy, F. and Siegelbaum, S.A. (2020) 'Hippocampal CA2 sharp-wave ripples reactivate and promote social memory'. *Nature,* **587** (7833), pp. 264-269.

Oliveira, J.F. and Araque, A. (2022) 'Astrocyte regulation of neural circuit activity and network states'. *Glia,* **70** (8), pp. 1455-1466.

Olsen, M.L., Khakh, B.S., Skatchkov, S.N., Zhou, M., Lee, C.J. and Rouach, N. (2015) 'New Insights on Astrocyte Ion Channels: Critical for Homeostasis and Neuron-Glia Signaling'. *J Neurosci,* **35** (41), pp. 13827-13835.

Olton, D.S. and Samuelson, R.J. (1976) 'Remembrance of places passed: Spatial memory in rats'. *Journal of Experimental Psychology: Animal Behavior Processes,* **2** (2), pp. 97-116.

Ormond, J. and O'Keefe, J. (2022) 'Hippocampal place cells have goal-oriented vector fields during navigation'. *Nature,* **607** (7920), pp. 741-746.

Osorio-Forero, A., Cardis, R., Vantomme, G., Guillaume-Gentil, A., Katsioudi, G., Devenoges, C., Fernandez, L.M.J. and Luthi, A. (2021) 'Noradrenergic circuit control of non-REM sleep substates'. *Curr Biol,* **31** (22), pp. 5009-5023 e5007.

Othman, M.Z., Hassan, Z. and Che Has, A.T. (2022) 'Morris water maze: a versatile and pertinent tool for assessing spatial learning and memory'. *Exp Anim,* **71** (3), pp. 264-280.

Panatier, A., Theodosis, D.T., Mothet, J.P., Touquet, B., Pollegioni, L., Poulain, D.A. and Oliet, S.H. (2006) 'Glia-derived D-serine controls NMDA receptor activity and synaptic memory'. *Cell,* **125** (4), pp. 775-784.

Panatier, A., Vallee, J., Haber, M., Murai, K.K., Lacaille, J.C. and Robitaille, R. (2011) 'Astrocytes are endogenous regulators of basal transmission at central synapses'. *Cell,* **146** (5), pp. 785-798.

Papouin, T., Dunphy, J.M., Tolman, M., Dineley, K.T. and Haydon, P.G. (2017) 'Septal Cholinergic Neuromodulation Tunes the Astrocyte-Dependent Gating of Hippocampal NMDA Receptors to Wakefulness'. *Neuron,* **94** (4), pp. 840-854 e847.

Park, J.H., Ju, Y.H., Choi, J.W., Song, H.J., Jang, B.K., Woo, J., Chun, H., Kim, H.J., Shin, S.J., Yarishkin, O., Jo, S., Park, M., Yeon, S.K., Kim, S., Kim, J., Nam, M.H., Londhe, A.M., Kim, J., Cho, S.J., Cho, S., . . . Park, K.D. (2019) 'Newly developed

reversible MAO-B inhibitor circumvents the shortcomings of irreversible inhibitors in Alzheimer's disease'. *Sci Adv,* **5** (3), pp. eaav0316.

Parpura, V. and Verkhratsky, A. (2012a) 'Astrocytes revisited: concise historic outlook on glutamate homeostasis and signaling'. *Croat Med J,* **53** (6), pp. 518-528.

Parpura, V. and Verkhratsky, A. (2012b) 'Neuroglia at the crossroads of homoeostasis, metabolism and signalling: evolution of the concept'. *ASN Neuro,* **4** (4), pp. 201-205.

Pase, M.P., Himali, J.J., Grima, N.A., Beiser, A.S., Satizabal, C.L., Aparicio, H.J., Thomas, R.J., Gottlieb, D.J., Auerbach, S.H. and Seshadri, S. (2017) 'Sleep architecture and the risk of incident dementia in the community'. *Neurology,* **89** (12), pp. 1244-1250.

Pasti, L., Volterra, A., Pozzan, T. and Carmignoto, G. (1997) 'Intracellular calcium oscillations in astrocytes: a highly plastic, bidirectional form of communication between neurons and astrocytes in situ'. *J Neurosci,* **17** (20), pp. 7817-7830.

Patel, A.A., McAlinden, N., Mathieson, K. and Sakata, S. (2020) 'Simultaneous Electrophysiology and Fiber Photometry in Freely Behaving Mice'. *Front Neurosci,* **14** 148.

Paukert, M., Agarwal, A., Cha, J., Doze, V.A., Kang, J.U. and Bergles, D.E. (2014) 'Norepinephrine controls astroglial responsiveness to local circuit activity'. *Neuron,* **82** (6), pp. 1263-1270.

Peever, J. and Fuller, P.M. (2017) 'The Biology of REM Sleep'. *Curr Biol,* **27** (22), pp. R1237-R1248.

Pelluru, D., Konadhode, R.R., Bhat, N.R. and Shiromani, P.J. (2016) 'Optogenetic stimulation of astrocytes in the posterior hypothalamus increases sleep at night in C57BL/6J mice'. *Eur J Neurosci,* **43** (10), pp. 1298-1306.

Peng, W., Liu, X., Ma, G., Wu, Z., Wang, Z., Fei, X., Qin, M., Wang, L., Li, Y., Zhang, S. and Xu, M. (2023) 'Adenosine-independent regulation of the sleep-wake cycle by astrocyte activity'. *Cell Discov,* **9** (1), pp. 16.

Peng, W., Wu, Z., Song, K., Zhang, S., Li, Y. and Xu, M. (2020) 'Regulation of sleep homeostasis mediator adenosine by basal forebrain glutamatergic neurons'. *Science,* **369** (6508), pp.

Perea, G., Yang, A., Boyden, E.S. and Sur, M. (2014) 'Optogenetic astrocyte activation modulates response selectivity of visual cortex neurons in vivo'. *Nat Commun,* **5** 3262.

Perez-Alvarez, A., Navarrete, M., Covelo, A., Martin, E.D. and Araque, A. (2014) 'Structural and functional plasticity of astrocyte processes and dendritic spine interactions'. *J Neurosci,* **34** (38), pp. 12738-12744.

Petersen, P.C. and Buzsaki, G. (2020) 'Cooling of Medial Septum Reveals Theta Phase Lag Coordination of Hippocampal Cell Assemblies'. *Neuron,* **107** (4), pp. 731-744 e733.

Petit, D., Montplaisir, J., Lorrain, D. and Gauthier, S. (1992) 'Spectral analysis of the rapid eye movement sleep electroencephalogram in right and left temporal regions: a biological marker of Alzheimer's disease'. *Ann Neurol,* **32** (2), pp. 172-176.

Petitjean, F., Sakai, K., Blondaux, C. and Jouvet, M. (1975) '[Hypersomnia by isthmic lesion in cat. II. Neurophysiological and pharmacological study]'. *Brain Res,* **88** (3), pp. 439-453.

Peyrache, A., Khamassi, M., Benchenane, K., Wiener, S.I. and Battaglia, F.P. (2009) 'Replay of rule-learning related neural patterns in the prefrontal cortex during sleep'. *Nat Neurosci,* **12** (7), pp. 919-926.

Peyrache, A. and Seibt, J. (2020) 'A mechanism for learning with sleep spindles'. *Philos Trans R Soc Lond B Biol Sci,* **375** (1799), pp. 20190230.

Peyron, C., Tighe, D.K., van den Pol, A.N., de Lecea, L., Heller, H.C., Sutcliffe, J.G. and Kilduff, T.S. (1998) 'Neurons containing hypocretin (orexin) project to multiple neuronal systems'. *J Neurosci,* **18** (23), pp. 9996-10015.

Pisanello, F., Sileo, L., Oldenburg, I.A., Pisanello, M., Martiradonna, L., Assad, J.A., Sabatini, B.L. and De Vittorio, M. (2014) 'Multipoint-emitting optical fibers for spatially addressable in vivo optogenetics'. *Neuron,* **82** (6), pp. 1245-1254.

Pisano, F., Pisanello, M., Lee, S.J., Lee, J., Maglie, E., Balena, A., Sileo, L., Spagnolo, B., Bianco, M., Hyun, M., De Vittorio, M., Sabatini, B.L. and Pisanello, F. (2019) 'Depth-resolved fiber photometry with a single tapered optical fiber implant'. *Nat Methods,* **16** (11), pp. 1185-1192.

Poe, G.R., Nitz, D.A., McNaughton, B.L. and Barnes, C.A. (2000) 'Experience-dependent phase-reversal of hippocampal neuron firing during REM sleep'. *Brain Res,* **855** (1), pp. 176-180.

Popa, D., Duvarci, S., Popescu, A.T., Lena, C. and Pare, D. (2010) 'Coherent amygdalocortical theta promotes fear memory consolidation during paradoxical sleep'. *Proc Natl Acad Sci U S A,* **107** (14), pp. 6516-6519.

Porter, J.T. and McCarthy, K.D. (1995a) 'Adenosine receptors modulate [Ca2+]i in hippocampal astrocytes in situ'. *J Neurochem,* **65** (4), pp. 1515-1523.

Porter, J.T. and McCarthy, K.D. (1995b) 'GFAP-positive hippocampal astrocytes in situ respond to glutamatergic neuroligands with increases in [Ca2+]i'. *Glia,* **13** (2), pp. 101-112.

Porter, J.T. and McCarthy, K.D. (1996) 'Hippocampal astrocytes in situ respond to glutamate released from synaptic terminals'. *J Neurosci,* **16** (16), pp. 5073-5081.

Poskanzer, K.E. and Yuste, R. (2011) 'Astrocytic regulation of cortical UP states'. *Proc Natl Acad Sci U S A,* **108** (45), pp. 18453-18458.

Poskanzer, K.E. and Yuste, R. (2016) 'Astrocytes regulate cortical state switching in vivo'. *Proc Natl Acad Sci U S A,* **113** (19), pp. E2675-2684.

Postuma, R.B., Gagnon, J.F., Vendette, M., Fantini, M.L., Massicotte-Marquez, J. and Montplaisir, J. (2009) 'Quantifying the risk of neurodegenerative disease in idiopathic REM sleep behavior disorder'. *Neurology,* **72** (15), pp. 1296-1300.

Postuma, R.B., Iranzo, A., Hu, M., Hogl, B., Boeve, B.F., Manni, R., Oertel, W.H., Arnulf, I., Ferini-Strambi, L., Puligheddu, M., Antelmi, E., Cochen De Cock, V., Arnaldi, D., Mollenhauer, B., Videnovic, A., Sonka, K., Jung, K.Y., Kunz, D., Dauvilliers, Y., Provini, F., . . . Pelletier, A. (2019) 'Risk and predictors of dementia and parkinsonism in idiopathic REM sleep behaviour disorder: a multicentre study'. *Brain,* **142** (3), pp. 744-759.

Prinz, P.N., Larsen, L.H., Moe, K.E. and Vitiello, M.V. (1992) 'EEG markers of early Alzheimer's disease in computer selected tonic REM sleep'. *Electroencephalogr Clin Neurophysiol,* **83** (1), pp. 36-43.

Puchades, M.A., Csucs, G., Ledergerber, D., Leergaard, T.B. and Bjaalie, J.G. (2019) 'Spatial registration of serial microscopic brain images to three-dimensional reference atlases with the QuickNII tool'. *PLoS One,* **14** (5), pp. e0216796.

Qin, H., Fu, L., Jian, T., Jin, W., Liang, M., Li, J., Chen, Q., Yang, X., Du, H., Liao, X., Zhang, K., Wang, R., Liang, S., Yao, J., Hu, B., Ren, S., Zhang, C., Wang, Y., Hu, Z., Jia, H., . . . Chen, X. (2022) 'REM sleep-active hypothalamic neurons may contribute to hippocampal social-memory consolidation'. *Neuron,* **110** (23), pp. 4000-4014 e4006.

Radulovacki, M., Virus, R.M., Djuricic-Nedelson, M. and Green, R.D. (1984) 'Adenosine analogs and sleep in rats'. *J Pharmacol Exp Ther,* **228** (2), pp. 268-274.

Rakic, P. (2003) 'Developmental and evolutionary adaptations of cortical radial glia'. *Cereb Cortex,* **13** (6), pp. 541-549.

Ramirez-Villegas, J.F., Besserve, M., Murayama, Y., Evrard, H.C., Oeltermann, A. and Logothetis, N.K. (2021) 'Coupling of hippocampal theta and ripples with pontogeniculooccipital waves'. *Nature,* **589** (7840), pp. 96-102.

Rasch, B. and Born, J. (2013) 'About sleep's role in memory'. *Physiol Rev,* **93** (2), pp. 681-766.

Rayan, A., Agarwal, A., Samanta, A., Severijnen, E., van der Meij, J. and Genzel, L. (2024) 'Sleep scoring in rodents: Criteria, automatic approaches and outstanding issues'. *Eur J Neurosci,* **59** (4), pp. 526-553.

Public Health Service, U.G.P.O., Washington DC (1968) *A Manual of Standardized Terminology, Techniques and Scoring System for Sleep Stages of Human Subjects. .*

Reeves, A.M., Shigetomi, E. and Khakh, B.S. (2011) 'Bulk loading of calcium indicator dyes to study astrocyte physiology: key limitations and improvements using morphological maps'. *J Neurosci,* **31** (25), pp. 9353-9358.

Reitman, M.E., Tse, V., Mi, X., Willoughby, D.D., Peinado, A., Aivazidis, A., Myagmar, B.E., Simpson, P.C., Bayraktar, O.A., Yu, G. and Poskanzer, K.E. (2023) 'Norepinephrine links astrocytic activity to regulation of cortical state'. *Nat Neurosci,* **26** (4), pp. 579-593.

Renouard, L., Billwiller, F., Ogawa, K., Clement, O., Camargo, N., Abdelkarim, M., Gay, N., Scote-Blachon, C., Toure, R., Libourel, P.A., Ravassard, P., Salvert, D., Peyron, C., Claustrat, B., Leger, L., Salin, P., Malleret, G., Fort, P. and Luppi, P.H. (2015) 'The supramammillary nucleus and the claustrum activate the cortex during REM sleep'. *Sci Adv,* **1** (3), pp. e1400177.

Robinson, J., Manseau, F., Ducharme, G., Amilhon, B., Vigneault, E., El Mestikawy, S. and Williams, S. (2016) 'Optogenetic Activation of Septal Glutamatergic Neurons Drive Hippocampal Theta Rhythms'. *J Neurosci,* **36** (10), pp. 3016-3023.

Roffwarg, H.P., Muzio, J.N. and Dement, W.C. (1966) 'Ontogenetic development of the human sleep-dream cycle'. *Science,* **152** (3722), pp. 604-619.

Roland, J.J., Stewart, A.L., Janke, K.L., Gielow, M.R., Kostek, J.A., Savage, L.M., Servatius, R.J. and Pang, K.C. (2014) 'Medial septum-diagonal band of Broca (MSDB) GABAergic regulation of hippocampal acetylcholine efflux is dependent on cognitive demands'. *J Neurosci,* **34** (2), pp. 506-514.

Rose, C.R. and Verkhratsky, A. (2016) 'Principles of sodium homeostasis and sodium signalling in astroglia'. *Glia,* **64** (10), pp. 1611-1627.

Roth, B.L. (2016) 'DREADDs for Neuroscientists'. *Neuron,* **89** (4), pp. 683-694.

Sabia, S., Fayosse, A., Dumurgier, J., van Hees, V.T., Paquet, C., Sommerlad, A., Kivimaki, M., Dugravot, A. and Singh-Manoux, A. (2021) 'Association of sleep duration in middle and old age with incidence of dementia'. *Nat Commun,* **12** (1), pp. 2289.

Sadowski, J.H., Jones, M.W. and Mellor, J.R. (2016) 'Sharp-Wave Ripples Orchestrate the Induction of Synaptic Plasticity during Reactivation of Place Cell Firing Patterns in the Hippocampus'. *Cell Rep,* **14** (8), pp. 1916-1929.

Sagales, T. and Domino, E.F. (1973) 'Effects of stress and REM sleep deprivation on the patterns of avoidance learning and brain acetylcholine in the mouse'. *Psychopharmacologia,* **29** (4), pp. 307-315.

Sakata, S. and Harris, K.D. (2009) 'Laminar structure of spontaneous and sensory-evoked population activity in auditory cortex'. *Neuron,* **64** (3), pp. 404-418.

Sakatani, S., Seto-Ohshima, A., Shinohara, Y., Yamamoto, Y., Yamamoto, H., Itohara, S. and Hirase, H. (2008) 'Neural-activity-dependent release of S100B from astrocytes enhances kainate-induced gamma oscillations in vivo'. *J Neurosci,* **28** (43), pp. 10928-10936.

Sakurai, T., Nagata, R., Yamanaka, A., Kawamura, H., Tsujino, N., Muraki, Y., Kageyama, H., Kunita, S., Takahashi, S., Goto, K., Koyama, Y., Shioda, S. and Yanagisawa, M. (2005) 'Input of orexin/hypocretin neurons revealed by a genetically encoded tracer in mice'. *Neuron,* **46** (2), pp. 297-308.

Sanchez-Vives, M.V. and McCormick, D.A. (2000) 'Cellular and network mechanisms of rhythmic recurrent activity in neocortex'. *Nat Neurosci,* **3** (10), pp. 1027-1034.

Saper, C.B., Chou, T.C. and Scammell, T.E. (2001) 'The sleep switch: hypothalamic control of sleep and wakefulness'. *Trends Neurosci,* **24** (12), pp. 726-731.

Saper, C.B., Fuller, P.M., Pedersen, N.P., Lu, J. and Scammell, T.E. (2010) 'Sleep state switching'. *Neuron,* **68** (6), pp. 1023-1042.

Sapin, E., Lapray, D., Berod, A., Goutagny, R., Leger, L., Ravassard, P., Clement, O., Hanriot, L., Fort, P. and Luppi, P.H. (2009) 'Localization of the brainstem GABAergic neurons controlling paradoxical (REM) sleep'. *PLoS One,* **4** (1), pp. e4272.

Sasaki, T., Beppu, K., Tanaka, K.F., Fukazawa, Y., Shigemoto, R. and Matsui, K. (2012) 'Application of an optogenetic byway for perturbing neuronal activity via glial photostimulation'. *Proc Natl Acad Sci U S A,* **109** (50), pp. 20720-20725.

Savtchouk, I. and Volterra, A. (2018) 'Gliotransmission: Beyond Black-and-White'. *J Neurosci,* **38** (1), pp. 14-25.

Sawangjit, A., Oyanedel, C.N., Niethard, N., Salazar, C., Born, J. and Inostroza, M. (2018) 'The hippocampus is crucial for forming non-hippocampal long-term memory during sleep'. *Nature,* **564** (7734), pp. 109-113.

Scammell, T.E., Arrigoni, E. and Lipton, J.O. (2017) 'Neural Circuitry of Wakefulness and Sleep'. *Neuron,* **93** (4), pp. 747-765.

Schabus, M., Gruber, G., Parapatics, S., Sauter, C., Klosch, G., Anderer, P., Klimesch, W., Saletu, B. and Zeitlhofer, J. (2004) 'Sleep spindles and their significance for declarative memory consolidation'. *Sleep,* **27** (8), pp. 1479-1485.

Scheffzuk, C., Kukushka, V.I., Vyssotski, A.L., Draguhn, A., Tort, A.B. and Brankack, J. (2011) 'Selective coupling between theta phase and neocortical fast gamma oscillations during REM-sleep in mice'. *PLoS One,* **6** (12), pp. e28489.

Schott, A.L., Baik, J., Chung, S. and Weber, F. (2023) 'A medullary hub for controlling REM sleep and pontine waves'. *Nat Commun,* **14** (1), pp. 3922.

Schwarz, L.A., Miyamichi, K., Gao, X.J., Beier, K.T., Weissbourd, B., DeLoach, K.E., Ren, J., Ibanes, S., Malenka, R.C., Kremer, E.J. and Luo, L. (2015) 'Viral-genetic tracing of the input-output organization of a central noradrenaline circuit'. *Nature,* **524** (7563), pp. 88-92.

Schwarz, Y., Zhao, N., Kirchhoff, F. and Bruns, D. (2017) 'Astrocytes control synaptic strength by two distinct v-SNARE-dependent release pathways'. *Nat Neurosci,* **20** (11), pp. 1529-1539.

Seehagen, S., Konrad, C., Herbert, J.S. and Schneider, S. (2015) 'Timely sleep facilitates declarative memory consolidation in infants'. *Proc Natl Acad Sci U S A,* **112** (5), pp. 1625-1629.

Seibt, J., Dumoulin, M.C., Aton, S.J., Coleman, T., Watson, A., Naidoo, N. and Frank, M.G. (2012) 'Protein synthesis during sleep consolidates cortical plasticity in vivo'. *Curr Biol,* **22** (8), pp. 676-682.

Sekiguchi, K.J., Shekhtmeyster, P., Merten, K., Arena, A., Cook, D., Hoffman, E., Ngo, A. and Nimmerjahn, A. (2016) 'Imaging large-scale cellular activity in spinal cord of freely behaving mice'. *Nat Commun,* **7** 11450.

Semba, K. and Fibiger, H.C. (1992) 'Afferent connections of the laterodorsal and the pedunculopontine tegmental nuclei in the rat: a retro- and antero-grade transport and immunohistochemical study'. *J Comp Neurol,* **323** (3), pp. 387-410.

Serikov, A., Martsishevska, I., Shin, W. and Kim, J. (2024) 'Protocol for in vivo dual-color fiber photometry in the mouse thalamus'. *STAR Protoc,* **5** (2), pp. 102931.

Sharma, S., Rakoczy, S. and Brown-Borg, H. (2010) 'Assessment of spatial memory in mice'. *Life Sci,* **87** (17-18), pp. 521-536.

Shaw, P.J., Cirelli, C., Greenspan, R.J. and Tononi, G. (2000) 'Correlates of sleep and waking in Drosophila melanogaster'. *Science,* **287** (5459), pp. 1834-1837.

Sheikhbahaei, S., Turovsky, E.A., Hosford, P.S., Hadjihambi, A., Theparambil, S.M., Liu, B., Marina, N., Teschemacher, A.G., Kasparov, S., Smith, J.C. and Gourine, A.V. (2018) 'Astrocytes modulate brainstem respiratory rhythm-generating circuits and determine exercise capacity'. *Nat Commun,* **9** (1), pp. 370.

Shein-Idelson, M., Ondracek, J.M., Liaw, H.P., Reiter, S. and Laurent, G. (2016) 'Slow waves, sharp waves, ripples, and REM in sleeping dragons'. *Science,* **352** (6285), pp. 590-595.

Shelton, M.K. and McCarthy, K.D. (2000) 'Hippocampal astrocytes exhibit Ca2+-elevating muscarinic cholinergic and histaminergic receptors in situ'. *J Neurochem,* **74** (2), pp. 555-563.

Shen, W., Chen, S., Liu, Y., Han, P., Ma, T. and Zeng, L.H. (2021) 'Chemogenetic manipulation of astrocytic activity: Is it possible to reveal the roles of astrocytes?'. *Biochem Pharmacol,* **186** 114457.

Sherin, J.E., Shiromani, P.J., McCarley, R.W. and Saper, C.B. (1996) 'Activation of ventrolateral preoptic neurons during sleep'. *Science,* **271** (5246), pp. 216-219.

Sheroziya, M. and Timofeev, I. (2014) 'Global intracellular slow-wave dynamics of the thalamocortical system'. *J Neurosci,* **34** (26), pp. 8875-8893.

Shigetomi, E., Tong, X., Kwan, K.Y., Corey, D.P. and Khakh, B.S. (2011) 'TRPA1 channels regulate astrocyte resting calcium and inhibitory synapse efficacy through GAT-3'. *Nat Neurosci,* **15** (1), pp. 70-80.

Shiromani, P., Gutwein, B.M. and Fishbein, W. (1979) 'Development of learning and memory in mice after brief paradoxical sleep deprivation'. *Physiol Behav,* **22** (5), pp. 971-978.

Shouse, M.N. and Siegel, J.M. (1992) 'Pontine regulation of REM sleep components in cats: integrity of the pedunculopontine tegmentum (PPT) is important for phasic events but unnecessary for atonia during REM sleep'. *Brain Res,* **571** (1), pp. 50-63.

Siapas, A.G. and Wilson, M.A. (1998) 'Coordinated interactions between hippocampal ripples and cortical spindles during slow-wave sleep'. *Neuron,* **21** (5), pp. 1123-1128.

Siegel, J.M. (2009) 'The neurobiology of sleep'. *Semin Neurol,* **29** (4), pp. 277-296.

Siegel, J.M., Nienhuis, R. and Tomaszewski, K.S. (1984) 'REM sleep signs rostral to chronic transections at the pontomedullary junction'. *Neurosci Lett,* **45** (3), pp. 241-246.

Silvers, J.M., Harrod, S.B., Mactutus, C.F. and Booze, R.M. (2007) 'Automation of the novel object recognition task for use in adolescent rats'. *J Neurosci Methods,* **166** (1), pp. 99-103.

Simasko, S.M. and Mukherjee, S. (2009) 'Novel analysis of sleep patterns in rats separates periods of vigilance cycling from long-duration wake events'. *Behav Brain Res,* **196** (2), pp. 228-236.

Simpson, E.H., Akam, T., Patriarchi, T., Blanco-Pozo, M., Burgeno, L.M., Mohebi, A., Cragg, S.J. and Walton, M.E. (2023) 'Lights, fiber, action! A primer on in vivo fiber photometry'. *Neuron*.

Simpson, E.H., Akam, T., Patriarchi, T., Blanco-Pozo, M., Burgeno, L.M., Mohebi, A., Cragg, S.J. and Walton, M.E. (2024) 'Lights, fiber, action! A primer on in vivo fiber photometry'. *Neuron,* **112** (5), pp. 718-739.

Simpson, J.E., Ince, P.G., Lace, G., Forster, G., Shaw, P.J., Matthews, F., Savva, G., Brayne, C., Wharton, S.B., Function, M.R.C.C. and Ageing Neuropathology Study, G. (2010) 'Astrocyte phenotype in relation to Alzheimer-type pathology in the ageing brain'. *Neurobiol Aging,* **31** (4), pp. 578-590.

Sirieix, C., Gervasoni, D., Luppi, P.H. and Leger, L. (2012) 'Role of the lateral paragigantocellular nucleus in the network of paradoxical (REM) sleep: an electrophysiological and anatomical study in the rat'. *PLoS One,* **7** (1), pp. e28724.

Sirota, A., Csicsvari, J., Buhl, D. and Buzsaki, G. (2003) 'Communication between neocortex and hippocampus during sleep in rodents'. *Proc Natl Acad Sci U S A,* **100** (4), pp. 2065-2069.

Skucas, V.A., Mathews, I.B., Yang, J., Cheng, Q., Treister, A., Duffy, A.M., Verkman, A.S., Hempstead, B.L., Wood, M.A., Binder, D.K. and Scharfman, H.E. (2011) 'Impairment of select forms of spatial memory and neurotrophin-dependent synaptic plasticity by deletion of glial aquaporin-4'. *J Neurosci,* **31** (17), pp. 6392-6397.

Slezak, M., Kandler, S., Van Veldhoven, P.P., Van den Haute, C., Bonin, V. and Holt, M.G. (2019) 'Distinct Mechanisms for Visual and Motor-Related Astrocyte Responses in Mouse Visual Cortex'. *Curr Biol,* **29** (18), pp. 3120-3127 e3125.

Sloan, M.A. (1972) 'The effects of deprivation of rapid eye movement (REM) sleep on maze learning and aggression in the albino rat'. *J Psychiatr Res,* **9** (2), pp. 101-111.

Smith, C. and Rose, G.M. (1996) 'Evidence for a paradoxical sleep window for place learning in the Morris water maze'. *Physiol Behav,* **59** (1), pp. 93-97.

Smith, C., Young, J. and Young, W. (1980) 'Prolonged increases in paradoxical sleep during and after avoidance-task acquisition'. *Sleep,* **3** (1), pp. 67-81.

Sofroniew, M.V. (2012) 'Transgenic techniques for cell ablation or molecular deletion to investigate functions of astrocytes and other GFAP-expressing cell types'. *Methods Mol Biol,* **814** 531-544.

Sofroniew, M.V. and Vinters, H.V. (2010) 'Astrocytes: biology and pathology'. *Acta Neuropathol,* **119** (1), pp. 7-35.

Somjen, G.G. (1988) 'Nervenkitt: notes on the history of the concept of neuroglia'. *Glia,* **1** (1), pp. 2-9.

Srinivasan, R., Huang, B.S., Venugopal, S., Johnston, A.D., Chai, H., Zeng, H., Golshani, P. and Khakh, B.S. (2015) 'Ca(2+) signaling in astrocytes from Ip3r2(-/-) mice in brain slices and during startle responses in vivo'. *Nat Neurosci,* **18** (5), pp. 708-717.

Srinivasan, R., Lu, T.Y., Chai, H., Xu, J., Huang, B.S., Golshani, P., Coppola, G. and Khakh, B.S. (2016) 'New Transgenic Mouse Lines for Selectively Targeting Astrocytes and Studying Calcium Signals in Astrocyte Processes In Situ and In Vivo'. *Neuron,* **92** (6), pp. 1181-1195.

Stark, E., Roux, L., Eichler, R., Senzai, Y., Royer, S. and Buzsaki, G. (2014) 'Pyramidal cell-interneuron interactions underlie hippocampal ripple oscillations'. *Neuron,* **83** (2), pp. 467-480.

Steriade, M., Contreras, D., Curro Dossi, R. and Nunez, A. (1993a) 'The slow (< 1 Hz) oscillation in reticular thalamic and thalamocortical neurons: scenario of sleep rhythm generation in interacting thalamic and neocortical networks'. *J Neurosci,* **13** (8), pp. 3284-3299.

Steriade, M., Deschenes, M., Domich, L. and Mulle, C. (1985) 'Abolition of spindle oscillations in thalamic neurons disconnected from nucleus reticularis thalami'. *J Neurophysiol,* **54** (6), pp. 1473-1497.

Steriade, M., Domich, L., Oakson, G. and Deschenes, M. (1987) 'The deafferented reticular thalamic nucleus generates spindle rhythmicity'. *J Neurophysiol,* **57** (1), pp. 260-273.

Steriade, M., Dossi, R.C. and Nunez, A. (1991) 'Network modulation of a slow intrinsic oscillation of cat thalamocortical neurons implicated in sleep delta waves: cortically induced synchronization and brainstem cholinergic suppression'. *J Neurosci,* **11** (10), pp. 3200-3217.

Steriade, M., McCormick, D.A. and Sejnowski, T.J. (1993b) 'Thalamocortical oscillations in the sleeping and aroused brain'. *Science,* **262** (5134), pp. 679-685.

Steriade, M., Nunez, A. and Amzica, F. (1993c) 'Intracellular analysis of relations between the slow (< 1 Hz) neocortical oscillation and other sleep rhythms of the electroencephalogram'. *J Neurosci,* **13** (8), pp. 3266-3283.

Steriade, M., Nunez, A. and Amzica, F. (1993d) 'A novel slow (< 1 Hz) oscillation of neocortical neurons in vivo: depolarizing and hyperpolarizing components'. *J Neurosci,* **13** (8), pp. 3252-3265.

Steriade, M. and Timofeev, I. (2003) 'Neuronal plasticity in thalamocortical networks during sleep and waking oscillations'. *Neuron,* **37** (4), pp. 563-576.

Stickgold, R., Hobson, J.A., Fosse, R. and Fosse, M. (2001) 'Sleep, learning, and dreams: off-line memory reprocessing'. *Science,* **294** (5544), pp. 1052-1057.

Stobart, J.L., Ferrari, K.D., Barrett, M.J.P., Gluck, C., Stobart, M.J., Zuend, M. and Weber, B. (2018) 'Cortical Circuit Activity Evokes Rapid Astrocyte Calcium Signals on a Similar Timescale to Neurons'. *Neuron,* **98** (4), pp. 726-735 e724.

Stowell, R.D., Sipe, G.O., Dawes, R.P., Batchelor, H.N., Lordy, K.A., Whitelaw, B.S., Stoessel, M.B., Bidlack, J.M., Brown, E., Sur, M. and Majewska, A.K. (2019) 'Noradrenergic signaling in the wakeful state inhibits microglial surveillance and synaptic plasticity in the mouse visual cortex'. *Nat Neurosci,* **22** (11), pp. 1782-1792.

Stucynski, J.A., Schott, A.L., Baik, J., Chung, S. and Weber, F. (2022) 'Regulation of REM sleep by inhibitory neurons in the dorsomedial medulla'. *Curr Biol,* **32** (1), pp. 37-50 e36.

Sulaman, B.A., Wang, S., Tyan, J. and Eban-Rothschild, A. (2023) 'Neuro-orchestration of sleep and wakefulness'. *Nat Neurosci,* **26** (2), pp. 196-212.

Sultan, S., Li, L., Moss, J., Petrelli, F., Casse, F., Gebara, E., Lopatar, J., Pfrieger, F.W., Bezzi, P., Bischofberger, J. and Toni, N. (2015) 'Synaptic Integration of Adult-Born Hippocampal Neurons Is Locally Controlled by Astrocytes'. *Neuron,* **88** (5), pp. 957-972.

Sun, F., Zeng, J., Jing, M., Zhou, J., Feng, J., Owen, S.F., Luo, Y., Li, F., Wang, H., Yamaguchi, T., Yong, Z., Gao, Y., Peng, W., Wang, L., Zhang, S., Du, J., Lin, D., Xu, M., Kreitzer, A.C., Cui, G., . . . Li, Y. (2018) 'A Genetically Encoded Fluorescent Sensor Enables Rapid and Specific Detection of Dopamine in Flies, Fish, and Mice'. *Cell,* **174** (2), pp. 481-496 e419.

Suthard, R.L., Senne, R.A., Buzharsky, M.D., Pyo, A.Y., Dorst, K.E., Diep, A.H., Cole, R.H. and Ramirez, S. (2023) 'Basolateral Amygdala Astrocytes Are Engaged by the

Acquisition and Expression of a Contextual Fear Memory'. *J Neurosci,* **43** (27), pp. 4997-5013.

Swanson, L. (1998) 'Brain maps: structure of the rat brain: a laboratory guide with printed and electronic templates for data, models, and schematics Amsterdam'. *The Netherlands: Elsevier Science Ltd [Google Scholar]*.

Sylantyev, S. and Rusakov, D.A. (2013) 'Sub-millisecond ligand probing of cell receptors with multiple solution exchange'. *Nat Protoc,* **8** (7), pp. 1299-1306.

Szabo, Z., Heja, L., Szalay, G., Kekesi, O., Furedi, A., Szebenyi, K., Dobolyi, A., Orban, T.I., Kolacsek, O., Tompa, T., Miskolczy, Z., Biczok, L., Rozsa, B., Sarkadi, B. and Kardos, J. (2017) 'Extensive astrocyte synchronization advances neuronal coupling in slow wave activity in vivo'. *Sci Rep,* **7** (1), pp. 6018.

Szymczak, J.T. (1987) 'Distribution of sleep and wakefulness in 24-h light-dark cycles in the juvenile and adult magpie, Pica pica'. *Chronobiologia,* **14** (3), pp. 277-287.

Takata, Y., Oishi, Y., Zhou, X.Z., Hasegawa, E., Takahashi, K., Cherasse, Y., Sakurai, T. and Lazarus, M. (2018) 'Sleep and Wakefulness Are Controlled by Ventral Medial Midbrain/Pons GABAergic Neurons in Mice'. *J Neurosci,* **38** (47), pp. 10080-10092.

Tan, Z., Liu, Y., Xi, W., Lou, H.F., Zhu, L., Guo, Z., Mei, L. and Duan, S. (2017) 'Glia-derived ATP inversely regulates excitability of pyramidal and CCK-positive neurons'. *Nat Commun,* **8** 13772.

Tanaka, M., Shih, P.Y., Gomi, H., Yoshida, T., Nakai, J., Ando, R., Furuichi, T., Mikoshiba, K., Semyanov, A. and Itohara, S. (2013) 'Astrocytic Ca2+ signals are required for the functional integrity of tripartite synapses'. *Mol Brain,* **6** 6.

Tarun, A., Wainstein-Andriano, D., Sterpenich, V., Bayer, L., Perogamvros, L., Solms, M., Axmacher, N., Schwartz, S. and Van De Ville, D. (2021) 'NREM sleep stages specifically alter dynamical integration of large-scale brain networks'. *iScience,* **24** (1), pp. 101923.

Teitelbaum, H., Lee, J.F. and Johannessen, J.N. (1975) 'Behaviorally evoked hippocampal theta waves: a cholinergic response'. *Science,* **188** (4193), pp. 1114-1116.

Teschemacher, A.G., Gourine, A.V. and Kasparov, S. (2015) 'A Role for Astrocytes in Sensing the Brain Microenvironment and Neuro-Metabolic Integration'. *Neurochem Res,* **40** (12), pp. 2386-2393.

Testen, A., Kim, R. and Reissner, K.J. (2020) 'High-Resolution Three-Dimensional Imaging of Individual Astrocytes Using Confocal Microscopy'. *Curr Protoc Neurosci,* **91** (1), pp. e92.

Thakkar, M., Portas, C. and McCarley, R.W. (1996) 'Chronic low-amplitude electrical stimulation of the laterodorsal tegmental nucleus of freely moving cats increases REM sleep'. *Brain Res,* **723** (1-2), pp. 223-227.

Thompson, K.J., Khajehali, E., Bradley, S.J., Navarrete, J.S., Huang, X.P., Slocum, S., Jin, J., Liu, J., Xiong, Y., Olsen, R.H.J., Diberto, J.F., Boyt, K.M., Pina, M.M., Pati, D., Molloy, C., Bundgaard, C., Sexton, P.M., Kash, T.L., Krashes, M.J., Christopoulos, A., . . . Tobin, A.B. (2018) 'DREADD Agonist 21 Is an Effective Agonist for Muscarinic-Based DREADDs in Vitro and in Vivo'. *ACS Pharmacol Transl Sci,* **1** (1), pp. 61-72.

Tiesinga, P. and Sejnowski, T.J. (2009) 'Cortical enlightenment: are attentional gamma oscillations driven by ING or PING?'. *Neuron,* **63** (6), pp. 727-732.

Tobler, I. and Borbely, A.A. (1986) 'Sleep EEG in the rat as a function of prior waking'. *Electroencephalogr Clin Neurophysiol,* **64** (1), pp. 74-76.

Tobler, I., Deboer, T. and Fischer, M. (1997) 'Sleep and sleep regulation in normal and prion protein-deficient mice'. *J Neurosci,* **17** (5), pp. 1869-1879.

Tong, X., Ao, Y., Faas, G.C., Nwaobi, S.E., Xu, J., Haustein, M.D., Anderson, M.A., Mody, I., Olsen, M.L., Sofroniew, M.V. and Khakh, B.S. (2014) 'Astrocyte Kir4.1 ion channel deficits contribute to neuronal dysfunction in Huntington's disease model mice'. *Nat Neurosci,* **17** (5), pp. 694-703.

Tononi, G. and Cirelli, C. (2003) 'Sleep and synaptic homeostasis: a hypothesis'. *Brain Res Bull,* **62** (2), pp. 143-150.

Tononi, G. and Cirelli, C. (2014) 'Sleep and the price of plasticity: from synaptic and cellular homeostasis to memory consolidation and integration'. *Neuron,* **81** (1), pp. 12-34.

Tossell, K., Yu, X., Giannos, P., Anuncibay Soto, B., Nollet, M., Yustos, R., Miracca, G., Vicente, M., Miao, A., Hsieh, B., Ma, Y., Vyssotski, A.L., Constandinou, T., Franks, N.P. and Wisden, W. (2023) 'Somatostatin neurons in prefrontal cortex initiate sleep-preparatory behavior and sleep via the preoptic and lateral hypothalamus'. *Nat Neurosci,* **26** (10), pp. 1805-1819.

Traut, J., Mengual, J.P., Meijer, E.J., McKillop, L.E., Alfonsa, H., Hoerder-Suabedissen, A., Song, S.H., Feher, K.D., Riemann, D., Molnar, Z., Akerman, C.J., Vyazovskiy, V.V. and Krone, L.B. (2023) 'Effects of clozapine-N-oxide and compound 21 on sleep in laboratory mice'. *Elife,* **12**.

Tso, M.C. and Herzog, E.D. (2015) 'Was Cajal right about sleep?'. *BMC Biol,* **13** 67.

Tsunematsu, T., Matsumoto, S., Merkler, M. and Sakata, S. (2023) 'Pontine waves accompanied by short hippocampal sharp wave-ripples during non-rapid eye movement sleep'. *Sleep*.

Tsunematsu, T., Patel, A.A., Onken, A. and Sakata, S. (2020) 'State-dependent brainstem ensemble dynamics and their interactions with hippocampus across sleep states'. *Elife,* **9**.

Tsunematsu, T., Sakata, S., Sanagi, T., Tanaka, K.F. and Matsui, K. (2021) 'Region-Specific and State-Dependent Astrocyte Ca(2+) Dynamics during the Sleep-Wake Cycle in Mice'. *J Neurosci,* **41** (25), pp. 5440-5452.

Tsunematsu, T., Ueno, T., Tabuchi, S., Inutsuka, A., Tanaka, K.F., Hasuwa, H., Kilduff, T.S., Terao, A. and Yamanaka, A. (2014) 'Optogenetic manipulation of activity and temporally controlled cell-specific ablation reveal a role for MCH neurons in sleep/wake regulation'. *J Neurosci,* **34** (20), pp. 6896-6909.

Turovsky, E.A., Braga, A., Yu, Y., Esteras, N., Korsak, A., Theparambil, S.M., Hadjihambi, A., Hosford, P.S., Teschemacher, A.G., Marina, N., Lythgoe, M.F., Haydon, P.G. and Gourine, A.V. (2020) 'Mechanosensory Signaling in Astrocytes'. *J Neurosci,* **40** (49), pp. 9364-9371.

Uchida, S., Soya, S., Saito, Y.C., Hirano, A., Koga, K., Tsuda, M., Abe, M., Sakimura, K. and Sakurai, T. (2021) 'A Discrete Glycinergic Neuronal Population in the Ventromedial Medulla That Induces Muscle Atonia during REM Sleep and Cataplexy in Mice'. *J Neurosci,* **41** (7), pp. 1582-1596.

Uchiyama, T., Yoshikawa, F., Hishida, A., Furuichi, T. and Mikoshiba, K. (2002) 'A novel recombinant hyperaffinity inositol 1,4,5-trisphosphate (IP(3)) absorbent traps IP(3), resulting in specific inhibition of IP(3)-mediated calcium signaling'. *J Biol Chem,* **277** (10), pp. 8106-8113.

Ullian, E.M., Sapperstein, S.K., Christopherson, K.S. and Barres, B.A. (2001) 'Control of synapse number by glia'. *Science,* **291** (5504), pp. 657-661.

Untiet, V., Beinlich, F.R.M., Kusk, P., Kang, N., Ladron-de-Guevara, A., Song, W., Kjaerby, C., Andersen, M., Hauglund, N., Bojarowska, Z., Sigurdsson, B., Deng, S., Hirase, H., Petersen, N.C., Verkhratsky, A. and Nedergaard, M. (2023) 'Astrocytic chloride is brain state dependent and modulates inhibitory neurotransmission in mice'. *Nat Commun,* **14** (1), pp. 1871.

Urban, D.J. and Roth, B.L. (2015) 'DREADDs (designer receptors exclusively activated by designer drugs): chemogenetic tools with therapeutic utility'. *Annu Rev Pharmacol Toxicol,* **55** 399-417.

Vaidyanathan, T.V., Collard, M., Yokoyama, S., Reitman, M.E. and Poskanzer, K.E. (2021) 'Cortical astrocytes independently regulate sleep depth and duration via separate GPCR pathways'. *Elife,* **10**.

Valencia Garcia, S., Brischoux, F., Clement, O., Libourel, P.A., Arthaud, S., Lazarus, M., Luppi, P.H. and Fort, P. (2018) 'Ventromedial medulla inhibitory neuron inactivation induces REM sleep without atonia and REM sleep behavior disorder'. *Nat Commun,* **9** (1), pp. 504.

Valtcheva, S. and Venance, L. (2016) 'Astrocytes gate Hebbian synaptic plasticity in the striatum'. *Nat Commun,* **7** 13845.

van de Ven, G.M., Trouche, S., McNamara, C.G., Allen, K. and Dupret, D. (2016) 'Hippocampal Offline Reactivation Consolidates Recently Formed Cell Assembly Patterns during Sharp Wave-Ripples'. *Neuron,* **92** (5), pp. 968-974.

Van Den Herrewegen, Y., Sanderson, T.M., Sahu, S., De Bundel, D., Bortolotto, Z.A. and Smolders, I. (2021) 'Side-by-side comparison of the effects of Gq- and Gi-DREADD-mediated astrocyte modulation on intracellular calcium dynamics and synaptic plasticity in the hippocampal CA1'. *Mol Brain,* **14** (1), pp. 144.

Van Dort, C.J., Zachs, D.P., Kenny, J.D., Zheng, S., Goldblum, R.R., Gelwan, N.A., Ramos, D.M., Nolan, M.A., Wang, K., Weng, F.J., Lin, Y., Wilson, M.A. and Brown, E.N. (2015) 'Optogenetic activation of cholinergic neurons in the PPT or LDT induces REM sleep'. *Proc Natl Acad Sci U S A,* **112** (2), pp. 584-589.

Van Horn, M.R., Benfey, N.J., Shikany, C., Severs, L.J. and Deemyad, T. (2021) 'Neuron-astrocyte networking: astrocytes orchestrate and respond to changes in neuronal network activity across brain states and behaviors'. *J Neurophysiol,* **126** (2), pp. 627-636.

Vandecasteele, M., Varga, V., Berenyi, A., Papp, E., Bartho, P., Venance, L., Freund, T.F. and Buzsaki, G. (2014) 'Optogenetic activation of septal cholinergic neurons suppresses sharp wave ripples and enhances theta oscillations in the hippocampus'. *Proc Natl Acad Sci U S A,* **111** (37), pp. 13535-13540.

Vanni-Mercier, G., Sakai, K., Lin, J.S. and Jouvet, M. (1991) 'Carbachol microinjections in the mediodorsal pontine tegmentum are unable to induce paradoxical sleep after caudal pontine and prebulbar transections in the cat'. *Neurosci Lett,* **130** (1), pp. 41-45.

Varin, C., Luppi, P.H. and Fort, P. (2018) 'Melanin-concentrating hormone-expressing neurons adjust slow-wave sleep dynamics to catalyze paradoxical (REM) sleep'. *Sleep,* **41** (6), pp.

Vasciaveo, V., Iadarola, A., Casile, A., Dante, D., Morello, G., Minotta, L., Tamagno, E., Cicolin, A. and Guglielmotto, M. (2023) 'Sleep fragmentation affects glymphatic

system through the different expression of AQP4 in wild type and 5xFAD mouse models'. *Acta Neuropathol Commun,* **11** (1), pp. 16.

Venkatraman, V., Chuah, Y.M., Huettel, S.A. and Chee, M.W. (2007) 'Sleep deprivation elevates expectation of gains and attenuates response to losses following risky decisions'. *Sleep,* **30** (5), pp. 603-609.

Venner, A., De Luca, R., Sohn, L.T., Bandaru, S.S., Verstegen, A.M.J., Arrigoni, E. and Fuller, P.M. (2019) 'An Inhibitory Lateral Hypothalamic-Preoptic Circuit Mediates Rapid Arousals from Sleep'. *Curr Biol,* **29** (24), pp. 4155-4168 e4155.

Verkhratsky, A. and Nedergaard, M. (2018) 'Physiology of Astroglia'. *Physiol Rev,* **98** (1), pp. 239-389.

Verkhratsky, A., Untiet, V. and Rose, C.R. (2020) 'Ionic signalling in astroglia beyond calcium'. *J Physiol,* **598** (9), pp. 1655-1670.

Verret, L., Goutagny, R., Fort, P., Cagnon, L., Salvert, D., Leger, L., Boissard, R., Salin, P., Peyron, C. and Luppi, P.H. (2003) 'A role of melanin-concentrating hormone producing neurons in the central regulation of paradoxical sleep'. *BMC Neurosci,* **4** 19.

Vertes, R.P. (1991) 'A PHA-L analysis of ascending projections of the dorsal raphe nucleus in the rat'. *J Comp Neurol,* **313** (4), pp. 643-668.

Vetrivelan, R., Kong, D., Ferrari, L.L., Arrigoni, E., Madara, J.C., Bandaru, S.S., Lowell, B.B., Lu, J. and Saper, C.B. (2016) 'Melanin-concentrating hormone neurons specifically promote rapid eye movement sleep in mice'. *Neuroscience,* **336** 102-113.

Virchow, R. (1856) *Gesammelte abhandlungen zur wissenschaftlichen medizin.* Meidinger.

Vogel-Ciernia, A. and Wood, M.A. (2014) 'Examining object location and object recognition memory in mice'. *Curr Protoc Neurosci,* **69** 8 31 31-17.

Volterra, A., Liaudet, N. and Savtchouk, I. (2014) 'Astrocyte Ca(2)(+) signalling: an unexpected complexity'. *Nat Rev Neurosci,* **15** (5), pp. 327-335.

Volterra, A. and Meldolesi, J. (2005) 'Astrocytes, from brain glue to communication elements: the revolution continues'. *Nat Rev Neurosci,* **6** (8), pp. 626-640.

von Lenhossék, M. (1891) *Zur Kenntnis der Neuroglia des menschlichen Rückenmarkes.*

Voutsinos-Porche, B., Bonvento, G., Tanaka, K., Steiner, P., Welker, E., Chatton, J.Y., Magistretti, P.J. and Pellerin, L. (2003) 'Glial glutamate transporters mediate a

functional metabolic crosstalk between neurons and astrocytes in the mouse developing cortex'. *Neuron,* **37** (2), pp. 275-286.

Vyazovskiy, V.V., Faraguna, U., Cirelli, C. and Tononi, G. (2009) 'Triggering slow waves during NREM sleep in the rat by intracortical electrical stimulation: effects of sleep/wake history and background activity'. *J Neurophysiol,* **101** (4), pp. 1921-1931.

Wagner, B., Natarajan, A., Grunaug, S., Kroismayr, R., Wagner, E.F. and Sibilia, M. (2006) 'Neuronal survival depends on EGFR signaling in cortical but not midbrain astrocytes'. *EMBO J,* **25** (4), pp. 752-762.

Wahis, J. and Holt, M.G. (2021) 'Astrocytes, Noradrenaline, alpha1-Adrenoreceptors, and Neuromodulation: Evidence and Unanswered Questions'. *Front Cell Neurosci,* **15** 645691.

Walker, M.P. and Stickgold, R. (2004) 'Sleep-dependent learning and memory consolidation'. *Neuron,* **44** (1), pp. 121-133.

Wang, Q., Ding, S.L., Li, Y., Royall, J., Feng, D., Lesnar, P., Graddis, N., Naeemi, M., Facer, B., Ho, A., Dolbeare, T., Blanchard, B., Dee, N., Wakeman, W., Hirokawa, K.E., Szafer, A., Sunkin, S.M., Oh, S.W., Bernard, A., Phillips, J.W., . . . Ng, L. (2020) 'The Allen Mouse Brain Common Coordinate Framework: A 3D Reference Atlas'. *Cell,* **181** (4), pp. 936-953 e920.

Wang, X., Lou, N., Xu, Q., Tian, G.F., Peng, W.G., Han, X., Kang, J., Takano, T. and Nedergaard, M. (2006) 'Astrocytic Ca2+ signaling evoked by sensory stimulation in vivo'. *Nat Neurosci,* **9** (6), pp. 816-823.

Wang, Z., Fei, X., Liu, X., Wang, Y., Hu, Y., Peng, W., Wang, Y.W., Zhang, S. and Xu, M. (2022) 'REM sleep is associated with distinct global cortical dynamics and controlled by occipital cortex'. *Nat Commun,* **13** (1), pp. 6896.

Warby, S.C., Wendt, S.L., Welinder, P., Munk, E.G., Carrillo, O., Sorensen, H.B., Jennum, P., Peppard, P.E., Perona, P. and Mignot, E. (2014) 'Sleep-spindle detection: crowdsourcing and evaluating performance of experts, non-experts and automated methods'. *Nat Methods,* **11** (4), pp. 385-392.

Weber, F., Chung, S., Beier, K.T., Xu, M., Luo, L. and Dan, Y. (2015) 'Control of REM sleep by ventral medulla GABAergic neurons'. *Nature,* **526** (7573), pp. 435-438.

Weber, F., Hoang Do, J.P., Chung, S., Beier, K.T., Bikov, M., Saffari Doost, M. and Dan, Y. (2018) 'Regulation of REM and Non-REM Sleep by Periaqueductal GABAergic Neurons'. *Nat Commun,* **9** (1), pp. 354.

Wilson, M.A. and McNaughton, B.L. (1994) 'Reactivation of hippocampal ensemble memories during sleep'. *Science,* **265** (5172), pp. 676-679.

Winchenbach, J., Duking, T., Berghoff, S.A., Stumpf, S.K., Hulsmann, S., Nave, K.A. and Saher, G. (2016) 'Inducible targeting of CNS astrocytes in Aldh1l1-CreERT2 BAC transgenic mice'. *F1000Res,* **5** 2934.

Winson, J. (1978) 'Loss of hippocampal theta rhythm results in spatial memory deficit in the rat'. *Science,* **201** (4351), pp. 160-163.

Woo, J., Min, J.O., Kang, D.S., Kim, Y.S., Jung, G.H., Park, H.J., Kim, S., An, H., Kwon, J., Kim, J., Shim, I., Kim, H.G., Lee, C.J. and Yoon, B.E. (2018) 'Control of motor coordination by astrocytic tonic GABA release through modulation of excitation/inhibition balance in cerebellum'. *Proc Natl Acad Sci U S A,* **115** (19), pp. 5004-5009.

Wu, Z., He, K., Chen, Y., Li, H., Pan, S., Li, B., Liu, T., Xi, F., Deng, F., Wang, H., Du, J., Jing, M. and Li, Y. (2022a) 'A sensitive GRAB sensor for detecting extracellular ATP in vitro and in vivo'. *Neuron,* **110** (5), pp. 770-782 e775.

Wu, Z., Lin, D. and Li, Y. (2022b) 'Pushing the frontiers: tools for monitoring neurotransmitters and neuromodulators'. *Nat Rev Neurosci,* **23** (5), pp. 257-274.

Xie, L., Kang, H., Xu, Q., Chen, M.J., Liao, Y., Thiyagarajan, M., O'Donnell, J., Christensen, D.J., Nicholson, C., Iliff, J.J., Takano, T., Deane, R. and Nedergaard, M. (2013) 'Sleep drives metabolite clearance from the adult brain'. *Science,* **342** (6156), pp. 373-377.

Xie, Y., Kuan, A.T., Wang, W., Herbert, Z.T., Mosto, O., Olukoya, O., Adam, M., Vu, S., Kim, M., Tran, D., Gomez, N., Charpentier, C., Sorour, I., Lacey, T.E., Tolstorukov, M.Y., Sabatini, B.L., Lee, W.A. and Harwell, C.C. (2022) 'Astrocyte-neuron crosstalk through Hedgehog signaling mediates cortical synapse development'. *Cell Rep,* **38** (8), pp. 110416.

Xie, Y., Wang, T., Sun, G.Y. and Ding, S. (2010) 'Specific disruption of astrocytic Ca2+ signaling pathway in vivo by adeno-associated viral transduction'. *Neuroscience,* **170** (4), pp. 992-1003.

Xu, M., Chung, S., Zhang, S., Zhong, P., Ma, C., Chang, W.C., Weissbourd, B., Sakai, N., Luo, L., Nishino, S. and Dan, Y. (2015) 'Basal forebrain circuit for sleep-wake control'. *Nat Neurosci,* **18** (11), pp. 1641-1647.

Xu, W., de Carvalho, F. and Jackson, A. (2019) 'Sequential Neural Activity in Primary Motor Cortex during Sleep'. *J Neurosci,* **39** (19), pp. 3698-3712.

Xu, Y., Schneider, A., Wessel, R. and Hengen, K.B. (2024) 'Sleep restores an optimal computational regime in cortical networks'. *Nat Neurosci,* **27** (2), pp. 328-338.

y Cajal, S.R. (1895) *Algunas conjeturas sobre el mecanismo anatómico de la ideación, asociación y atención.*

y Cajal, S.R. (1913) *Un nuevo proceder para la impregnación de la neuroglía.*

Yamashita, A., Hamada, A., Suhara, Y., Kawabe, R., Yanase, M., Kuzumaki, N., Narita, M., Matsui, R., Okano, H. and Narita, M. (2014) 'Astrocytic activation in the anterior cingulate cortex is critical for sleep disorder under neuropathic pain'. *Synapse,* **68** (6), pp. 235-247.

Yang, J., Vitery, M.D.C., Chen, J., Osei-Owusu, J., Chu, J. and Qiu, Z. (2019) 'Glutamate-Releasing SWELL1 Channel in Astrocytes Modulates Synaptic Transmission and Promotes Brain Damage in Stroke'. *Neuron,* **102** (4), pp. 813-827 e816.

Yang, Y., Ge, W., Chen, Y., Zhang, Z., Shen, W., Wu, C., Poo, M. and Duan, S. (2003) 'Contribution of astrocytes to hippocampal long-term potentiation through release of D-serine'. *Proc Natl Acad Sci U S A,* **100** (25), pp. 15194-15199.

Yang, Y., Liu, N., He, Y., Liu, Y., Ge, L., Zou, L., Song, S., Xiong, W. and Liu, X. (2018) 'Improved calcium sensor GCaMP-X overcomes the calcium channel perturbations induced by the calmodulin in GCaMP'. *Nat Commun,* **9** (1), pp. 1504.

Ye, L., Haroon, M.A., Salinas, A. and Paukert, M. (2017) 'Comparison of GCaMP3 and GCaMP6f for studying astrocyte Ca2+ dynamics in the awake mouse brain'. *PLoS One,* **12** (7), pp. e0181113.

Yoshida, K., McCormack, S., Espana, R.A., Crocker, A. and Scammell, T.E. (2006) 'Afferents to the orexin neurons of the rat brain'. *J Comp Neurol,* **494** (5), pp. 845-861.

Youngblood, B.D., Zhou, J., Smagin, G.N., Ryan, D.H. and Harris, R.B. (1997) 'Sleep deprivation by the "flower pot" technique and spatial reference memory'. *Physiol Behav,* **61** (2), pp. 249-256.

Yu, X., Moye, S.L. and Khakh, B.S. (2021) 'Local and CNS-Wide Astrocyte Intracellular Calcium Signaling Attenuation In Vivo with CalEx(flox) Mice'. *J Neurosci,* **41** (21), pp. 4556-4574.

Yu, X., Nagai, J. and Khakh, B.S. (2020) 'Improved tools to study astrocytes'. *Nat Rev Neurosci,* **21** (3), pp. 121-138.

Yu, X., Taylor, A.M.W., Nagai, J., Golshani, P., Evans, C.J., Coppola, G. and Khakh, B.S. (2018) 'Reducing Astrocyte Calcium Signaling In Vivo Alters Striatal Microcircuits and Causes Repetitive Behavior'. *Neuron,* **99** (6), pp. 1170-1187 e1179.

Yuan, X.S., Wang, L., Dong, H., Qu, W.M., Yang, S.R., Cherasse, Y., Lazarus, M., Schiffmann, S.N., d'Exaerde, A.K., Li, R.X. and Huang, Z.L. (2017) 'Striatal adenosine A(2A) receptor neurons control active-period sleep via parvalbumin neurons in external globus pallidus'. *Elife,* **6**.

Zeisel, A., Hochgerner, H., Lonnerberg, P., Johnsson, A., Memic, F., van der Zwan, J., Haring, M., Braun, E., Borm, L.E., La Manno, G., Codeluppi, S., Furlan, A., Lee, K., Skene, N., Harris, K.D., Hjerling-Leffler, J., Arenas, E., Ernfors, P., Marklund, U. and Linnarsson, S. (2018) 'Molecular Architecture of the Mouse Nervous System'. *Cell,* **174** (4), pp. 999-1014 e1022.

Zhang, K., Forster, R., He, W., Liao, X., Li, J., Yang, C., Qin, H., Wang, M., Ding, R., Li, R., Jian, T., Wang, Y., Zhang, J., Yang, Z., Jin, W., Zhang, Y., Qin, S., Lu, Y., Chen, T., Stobart, J., . . . Chen, X. (2021a) 'Fear learning induces alpha7-nicotinic acetylcholine receptor-mediated astrocytic responsiveness that is required for memory persistence'. *Nat Neurosci,* **24** (12), pp. 1686-1698.

Zhang, N., Zhang, Z., Ozden, I. and Ding, S. (2022a) 'Imaging Mitochondrial Ca2+ Uptake in Astrocytes and Neurons using Genetically Encoded Ca2+ Indicators (GECIs)'. *J Vis Exp,* (179), pp.

Zhang, Y., Cao, L., Varga, V., Jing, M., Karadas, M., Li, Y. and Buzsaki, G. (2021b) 'Cholinergic suppression of hippocampal sharp-wave ripples impairs working memory'. *Proc Natl Acad Sci U S A,* **118** (15), pp.

Zhang, Y., Ren, R., Yang, L., Zhang, H., Shi, Y., Okhravi, H.R., Vitiello, M.V., Sanford, L.D. and Tang, X. (2022b) 'Sleep in Alzheimer's disease: a systematic review and meta-analysis of polysomnographic findings'. *Transl Psychiatry,* **12** (1), pp. 136.

Zhang, Y., Rozsa, M., Liang, Y., Bushey, D., Wei, Z., Zheng, J., Reep, D., Broussard, G.J., Tsang, A., Tsegaye, G., Narayan, S., Obara, C.J., Lim, J.X., Patel, R., Zhang, R., Ahrens, M.B., Turner, G.C., Wang, S.S., Korff, W.L., Schreiter, E.R., . . . Looger, L.L. (2023) 'Fast and sensitive GCaMP calcium indicators for imaging neural populations'. *Nature,* **615** (7954), pp. 884-891.

Zhang, Z., Zhong, P., Hu, F., Barger, Z., Ren, Y., Ding, X., Li, S., Weber, F., Chung, S., Palmiter, R.D. and Dan, Y. (2019) 'An Excitatory Circuit in the Perioculomotor Midbrain for Non-REM Sleep Control'. *Cell,* **177** (5), pp. 1293-1307 e1216.

Zheng, K., Bard, L., Reynolds, J.P., King, C., Jensen, T.P., Gourine, A.V. and Rusakov, D.A. (2015) 'Time-Resolved Imaging Reveals Heterogeneous Landscapes of Nanomolar Ca(2+) in Neurons and Astroglia'. *Neuron,* **88** (2), pp. 277-288.

Zhong, P., Zhang, Z., Barger, Z., Ma, C., Liu, D., Ding, X. and Dan, Y. (2019) 'Control of Non-REM Sleep by Midbrain Neurotensinergic Neurons'. *Neuron,* **104** (4), pp. 795-809 e796.

Zucca, S., D'Urso, G., Pasquale, V., Vecchia, D., Pica, G., Bovetti, S., Moretti, C., Varani, S., Molano-Mazon, M., Chiappalone, M., Panzeri, S. and Fellin, T. (2017) 'An inhibitory gate for state transition in cortex'. *Elife,* **6**.

Zutshi, I., Valero, M., Fernandez-Ruiz, A. and Buzsaki, G. (2022) 'Extrinsic control and intrinsic computation in the hippocampal CA1 circuit'. *Neuron,* **110** (4), pp. 658-673 e655.